Theses and dissertations

1-1-2010

Generalized SDOF system for dynamic analysis of concrete rectangular liquid storage tanks

Jun Zheng Chen
Ryerson University

Follow this and additional works at: http://digitalcommons.ryerson.ca/dissertations

Part of the Civil Engineering Commons

GENERALIZED SDOF SYSTEM FOR DYNAMIC ANALYSIS OF CONCRETE RECTANGULAR LIQUID STORAGE TANKS

by

Jun Zheng Chen, P.Eng.

B.Eng., Tongji University, Shanghai, China, 1995

M.A.Sc., Ryerson University, Toronto, Ontario, Canada, 2003

A thesis

presented to Ryerson University

in partial fulfillment of the

requirement for the degree of

Doctor of Philosophy

in the program of

Civil Engineering

Toronto, Ontario, Canada, 2010

© Jun Zheng Chen 2010

AUTHOR'S DECLARATION

I hereby declare that I am the sole author of this thesis.

I authorize Ryerson University to lend this thesis to other institutions or individuals for

the purpose of scholarly research.

Jun Zheng Chen, P.Eng.

Department of Civil Engineering

Ryerson University

I further authorize Ryerson University to reproduce this thesis by photocopying or by

other means, in total or in part, at the request of other institutions or individuals for the

purpose of scholarly research.

Jun Zheng Chen, P.Eng.

Department of Civil Engineering

Ryerson University

BORROWER'S PAGE

Ryerson University requires the signatures of all persons using or photocopying this thesis. Please sign below, and give address and date.

Name of Borrowers	Date	Address	Signature

GENERALIZED SDOF SYSTEM FOR DYNAMIC ANALYSIS OF CONCRETE RECTANGULAR LIQUID STORAGE TANKS

Jun Zheng Chen, P.Eng.
Doctor of Philosophy, 2010
Department of Civil Engineering
Ryerson University

ABSTRACT

Liquid storage tanks are essential facilities in lifeline and industrial systems. To ensure liquid tightness, serviceability is the prime design concern for these structures. While there have been major studies on the behavior of steel tanks, little attention has been paid to the behavior of rectangular concrete tanks. In this study, the dynamic response of concrete rectangular liquid storage tanks is investigated.

In the current design practice, the response of liquid and tank structure is determined based on rigid tank wall and the lumped mass approach. However, the results of analysis show that the flexibility of tank wall increases the hydrodynamic pressures as compared to the rigid wall assumption. Also, recent studies show that the lumped added mass method leads to overly conservative results in terms of base shear and base moment. In addition, in spite of advanced analysis techniques available for dynamic analysis of liquid storage tanks such as finite element method and sequential coupling analysis procedure, there is a need to develop a simplified analysis method for practical applications.

In this thesis, a simplified method using the generalized single degree of freedom (SDOF) system is proposed for seismic analysis of concrete rectangular liquid containing structures (LCS). Only the impulsive hydrodynamic pressure is considered. In the proposed method, the consistent mass approach and the effect of flexibility of tank wall on hydrodynamic pressures are considered. Different analytical models are used to verify the proposed model in this study. The comparison of results based on the current design practice, the analytical-finite element models and full finite element model using ANSYS® shows that the proposed method is fairly accurate which can be used in the

structural design of liquid containing structures.

Parametric studies on seismic analysis of concrete rectangular LCS using the generalized SDOF system are carried out. Five prescribed vibration shape functions representing the first mode shape of fluid structure interaction system are used to study the effect of flexibility of tank wall and the boundary conditions. The effect of flexibility of tank wall, the amplitude of hydrodynamic pressure, the added mass of liquid due to hydrodynamic pressure, the effective heights for liquid containing system and the effect of higher modes on dynamic response of LCS are investigated. In addition, the effect of variable size of tanks and liquid depth are studied. The contribution of higher modes to the dynamic response of LCS is included in the proposed model.

A design procedure based on the structural model using the generalized SDOF system is proposed in this study. Design charts and tables for the added mass of liquid due to impulsive hydrodynamic pressure and the corresponding effective heights are presented. The proposed design procedure can be used for engineering design applications.

ACKNOWLEDGEMENTS

Foremost, I would like to express my sincere gratitude to Professor M. Reza Kianoush for his continuous support of my Ph.D. study and research. His encouragement, patience, guidance and supervision of my research work led me to this achievement.

I would like to thank the rest of my thesis committee: Dr. Lau, Dr. Hashemi, Dr. Sennah, and Dr. Yuan for their encouragement, insightful comments, and suggestions.

Finally, I am forever indebted to my parents for giving me the support throughout my life. They gave me the support that I needed whenever I asked for. Also deep gratitude is expressed to wife for her patience and encouragement. I am also grateful to my son Michael for giving me the happiness.

TABLE OF CONTENTS

LIST OF FIGURES

LIST OF SYMBOLS

A_a = pseudo-acceleration

$\tilde{c}$ = generalized damping of system

d = displacement

E = modulus of elasticity of material

E_c = modulus of elasticity of concrete

g = acceleration due to gravity

h_i = height above the base of the wall to the center of the gravity of the impulsive lateral force

h_c = height above the base of the wall to the center of the gravity of the convective lateral force

h_w = height from the base of the wall to the center of gravity of tank wall

H_L = height of liquid

H_w = height of tank wall

I = moment of inertia

$\tilde{k}$ = generalized stiffness of system

L_x, L_z = half clear inside dimensions of a rectangular tank in the directions of x and z

m = effective mass of system

m_L = effective added mass of hydrodynamic pressure

m_W = effective inertial mass of tank wall

$\tilde{m}$ = generalized mass of system

$\tilde{m}_L$ = generalized added mass of hydrodynamic pressure

$\tilde{m}_W$ = generalized inertial mass of tank wall

M_B = base moment

M_c	=	convective mass of contained liquid per unit width of a rectangular tank wall
M_i	=	impulsive mass of contained liquid per unit width of a rectangular tank wall
M_L	=	total effective added mass of hydrodynamic pressure per unit width of a rectangular tank wall
$\tilde{M}_L$	=	total generalized added mass of hydrodynamic pressure per unit width of a rectangular tank wall
M_w	=	total effective inertial mass of tank wall per unit width of a rectangular tank wall
$\tilde{M}_W$	=	total generalized inertial mass of tank wall per unit width of a rectangular tank wall
p	=	hydrodynamic pressure
$\tilde{p}$	=	generalized force of system
$\hat{p}$	=	effective mass of liquid-tank system
P	=	hydrodynamic force
P_i	=	hydrodynamic force due to impulsive component
$\hat{q}$	=	the factor of external load applied
t	=	time
t_w	=	thickness of tank wall
T_n	=	period of vibration in the n-th mode.
$u, \dot{u}, \ddot{u}$	=	displacement, velocity and acceleration, respectively
$u_g, \dot{u}_g, \ddot{u}_g$	=	ground displacement, velocity and acceleration, respectively
v	=	Poisson's ratio
v_x, v_y	=	velocity component in the directions of x, y
V_B	=	base shear of tank wall
x, y, z	=	Cartesian coordinates
W_I	=	internal work

W_E =   external work

ϕ =   velocity potential function for liquid

ψ_n =   shape function for n-th mode

$\lambda_{i,n}$ =   wavelength for impulsive pressure for the n-th mode

ρ_l =   mass density of liquid

ρ_w =   mass density of tank wall

ω_n =   natural frequency of the n-th mode of vibration

ζ =   damping ratio

CHAPTER 1 INTRODUCTION

1.1 Introduction

Liquid containing structures (LCS), as part of environmental engineering facilities, are primarily used for water and sewage treatment plants and other industrial wastes. It is important that utility facilities remain operational following an earthquake to meet the emergency requirements such as firefighting water or meet the public demands as a source of water supply. Also, the containment of hazardous waste is important to meet the public safety after a seismic event. For these reasons, serviceability becomes the prime design consideration in most of these structures. A good understanding of the seismic behaviour of these structures is necessary in order to ensure safe design while keeping construction and maintenance costs at an acceptable level.

Extensive studies on the seismic behavior of LCS have been conducted in the past. However, most of them are related to circular liquid storage tanks, especially steel tanks. Little attention has been focused on the dynamic response of concrete rectangular tanks. In this study, the dynamic response of concrete rectangular liquid storage tanks is investigated.

Concrete rectangular liquid storage tanks are commonly used in water and wastewater treatment plants. Concrete tanks are efficient structural systems since they can be easily formed in different sizes to meet the process requirements. Also, rectangular tanks are more efficient and easier to be separated into sub-tanks for different process purposes within a limited space than circular tanks. In addition, concrete rectangular tanks are often used in nuclear power plants to store the radioactive material such as spent fuel storage pools. Due to the criticality of radioactive material to the public safety, the seismic performance of such tanks is a major concern in nuclear industry.

Housner (1957 and 1963) has developed the most commonly used model for dynamic analysis of liquid storage tanks. In Housner's model, hydrodynamic pressures induced by earthquake were separated into two parts, namely impulsive pressure and convective pressure. The portion of the liquid accelerating with the tank is called impulsive pressure. The portion of the liquid sloshing in the tank is called convective pressure. For dynamic analysis, the impulsive and convective pressures can be approximated by using added masses, which are attached to the tank wall using rigid and spring connections, respectively.

There are currently few guidelines and standards available in North America for seismic design of LCS. Also, a great deal of inconsistency exists among these guidelines and standards for this important class of structures. For concrete rectangular LCS, the American Concrete Institute (ACI) has published the ACI 350.3 (2006) in the form of a mandatory document for seismic design of ground-supported reinforced concrete tanks. In most current design guidelines and standards, Housner's model (1957 and 1963) has been used for seismic design of LCS. The response of liquid and tank structure is determined using rigid tank wall and the lumped mass approach. However, the results of analysis show that the flexibility of tank wall increases the hydrodynamic pressures as compared to the rigid wall assumption (Yang, 1976 and Veletsos 1984). Also, the recent studies show that the lumped added mass method leads to overly conservative results in terms of base shear and base moment (Chen and Kianoush, 2005, Ghaemian et al. 2005 and Kianoush et al. 2006). In addition, recently many advanced analysis techniques, such as finite element method and sequential coupling analysis procedure (Chen, 2005), have been used in dynamic analysis of liquid storage tanks. However, these techniques are not appropriate for practical design applications due to complexity and time consuming. Also, the trends of response cannot be easily identified in terms of variable size of tanks and liquid depth. As a result, there is a need to develop a simplified analysis method to

overcome the deficiencies in the current design practice. Also, there is a need to improve the understanding of the response of tank structures from a designer's point of view in terms of the effect of different size of tanks and liquid condition.

In this research, a simplified method based on the generalized single degree of freedom (SDOF) system is proposed for seismic analysis of concrete rectangular LCS. In the proposed method, the consistent mass approach and the effect of flexibility of tank wall on hydrodynamic pressure are considered. The verification and validation of the proposed method is performed. Parametric studies on seismic analysis of concrete rectangular LCS using the generalized SDOF system are carried out. A design procedure based on the structural model using the generalized SDOF system is proposed.

The major challenge in studying the dynamic response of LCS is the accurate modeling of fluid structure interaction (FSI) effects. For seismic analysis of LCS, FSI includes solid and fluid dynamic analyses and coupling analysis between these two fields. In this study, the different analysis techniques are applied for dynamic analysis of liquid storage tanks. It is noted that the techniques used for FSI problems can also be applied to other liquid containing structures in civil engineering. In this regards, this research can provide references for future studies related to the dynamic analysis of liquid containing structures.

1.2 Objectives and Scope of the Study

The main purpose of this research is to develop a simplified method for dynamic analysis of rectangular LCS. As stated in Eurocode 8 (2006) Part 4, the studies on the seismic response of flexible rectangular tanks are few and their results are not in the form suitable for direct use in design. In this study, a structural model based on the generalized SDOF system is proposed in which the consistent mass approach and the effect of flexibility of

tank wall on hydrodynamic pressures are considered. It is expected that the proposed model using the generalized SDOF system can provide fairly accurate results and be used in structural design of LCS.

Different analytical models are used to verify the proposed model in this study. Two analytical-finite element models and one full finite element model using the general-purpose finite element analysis program ANSYS® are used to validate the proposed simplified method. Extensive parametric studies are carried out based on the proposed generalized SDOF system. The effects of different tank parameters on the dynamic response of rectangular concrete liquid storage tanks are then investigated. Based on the results of parametric studies, design tables and charts are developed which can be used for design application. This study also intends to investigate different techniques used for dynamic analysis of LCS to solve the fluid structural interaction problem. Other objectives include evaluating the current guidelines and standards for seismic design of LCS and developing design procedure for practical applications.

In summary, the objectives of this study are as follows:

(1) Investigate the effect of flexibility of tank wall on hydrodynamic pressure distribution.

(2) Evaluate different coupling analysis techniques for liquid structure interaction and apply these techniques in dynamic analysis of LCS for comparison.

(3) Develop a simplified method using the generalized SDOF system for dynamic analysis of concrete rectangular liquid storage tanks.

(4) Carry out extensive parametric studies on the dynamic response of concrete rectangular liquid storage tanks based on the proposed simplified method.

(5) Verify the proposed generalized SDOF system using different analytical models including the analytical-finite element models and full finite element model using the

4

general-purpose finite element analysis software ANSYS®.

(6) Develop a design procedure, including design charts and tables, to be used by practicing engineers.

The scope of this study is summarized as follows:

(1) The dynamic analysis is based on the two-dimensional tank model. The effect of the two sidewalls which are parallel to the direction of ground motion is not considered.

(2) Only the impulsive hydrodynamic pressure is considered in this study. It is worth noting that the main objective of this investigation is to study the effect flexibility of tank wall on dynamic response of rectangular liquid storage tanks which is ignored in the current design practice. Since the flexibility of tank wall does not affect the convective component, the effect of convective hydrodynamic pressure is ignored in this investigation.

(3) In this study, only above ground, open top concrete rectangular liquid storage tanks are considered. However, the proposed analytical model can also be applied with some modifications to tanks having other configurations.

(4) Only the horizontal ground motions are considered in the current study and the effect of vertical acceleration is ignored.

(5) The tanks are assumed to be fixed to rigid foundation and soil structure interaction effect is ignored.

1.3 Thesis Layout

The thesis is divided into nine chapters. In Chapter 1, the objectives and the scope of research are described.

The previous research work on seismic response of liquid storage tanks is presented in Chapter 2. Damages and failures of liquid storage tanks resulting from actual past

earthquakes are described. The failure mechanisms associated with concrete liquid storage tanks are summarized. An extensive literature review on dynamic analysis of liquid storage tanks is presented. The contributions and significance of past studies on seismic analysis of LCS are summarized. The procedure for design of LCS based on different design codes and standards are discussed and compared in this chapter.

Chapter 3 presents the dynamic analysis of concrete rectangular LCS using the analytical - finite element models. The tank wall is modeled using the finite element method, while the analytical method is used to calculate the hydrodynamic pressure in liquid domain. The theories for calculation of impulsive hydrodynamic pressure using the lamina fluid theory and the velocity potential theory are discussed. The sequential coupling analysis procedure is used to consider fluid structure interaction. The efficiency of the sequential coupling analysis procedure is demonstrated using different modeling approaches. Based on a two-dimensional model of the tank wall, a tall tank and a shallow tank are used for verification. The results of analysis are compared with those obtained based on other research and the current design codes and standards. It is worth noting that this chapter provides the basis for the proposed simplified method described in the following chapters.

In order to further verify the different models used for dynamic analysis of liquid storage tanks, the full finite element method is used in this study as described in Chapter 4. The general purpose finite element analysis software ANSYS® is used for dynamic analysis. The tank wall is modeled using transient structural analysis system. The hydrodynamic pressure is calculated based on the fluid flow theory using computational fluid dynamic (CFD) analysis techniques. The coupling analysis method for fluid structure interaction is described. Finally, the dynamic response of a tall tank is presented.

In Chapter 5, a simplified method using the generalized single degree of freedom (SDOF) system for dynamic analysis of concrete rectangular LCS is proposed. The consistent mass approach based on the analytical method is used in the proposed model. The effect of flexibility of tank wall on hydrodynamic pressure is considered. The theories and application of the generalized SDOF system in dynamic analysis of concrete rectangular LCS are presented in this chapter. The results are compared with those obtained using the analytical - finite element models and full finite element model as presented in Chapters 3 and 4, respectively.

The parametric studies on seismic response of concrete rectangular LCS using the generalized SDOF system are presented in Chapters 6 and 7. The effect of flexibility of tank wall, the amplitude of hydrodynamic pressure, the added mass of liquid due to hydrodynamic pressure, the effective heights for liquid containing system and the effect of higher modes on dynamic response of LCS are investigated in Chapter 6. The effects of tank dimensions and liquid height are studied in Chapter 7.

The application of proposed analytical model using the generalized SDOF system for design purpose is presented in Chapter 8. The design charts and tables for the added mass of liquid due to impulsive hydrodynamic pressure and the corresponding effective heights are presented and compared with those adopted in the current design codes and standards. Two sets of calculations for a tall and a shallow tank are presented and compared with the results obtained using the current practice as well as the model proposed in Chapter 3.

A summary and the major conclusions reached in this study are described in Chapter 9. Some recommendations for further study are also given in this chapter.

CHAPTER 2 LITERATURE REVIEW

2.1 Introduction

In this chapter, a literature review on seismic response of liquid storage tanks is presented. Section 2.2 describes the performance of liquid storage tanks under actual earthquakes and the resulting failure mechanisms are summarized. An extensive literature review on dynamic analysis of liquid storage tanks is presented in Section 2.3. The contributions and significance of previous studies are summarized. Sections 2.4 presents design guidelines based on current codes and standards for seismic design of liquid storage tanks. Overall, the intention for this chapter is to provide an overview of dynamic behavior of liquid storage tanks under earthquakes. Also, previous research studies and current design practice for liquid storage tanks are discussed.

2.2 Damage to Liquid Containing Structures under Historical Earthquakes

Some major earthquakes that have occurred in different parts of the world can be regarded as significant to seismic design of liquid containing structures as described in this section. The dynamic behavior of liquid containing structures under earthquakes and the influence of such events on engineering research and practice is of particular interest which is discussed. The failure mechanisms under the effect of earthquakes are also summarized and discussed.

2.2.1 North America

In North America, most devastating earthquakes usually occurred on the west coast of US and Canada around the Pacific Ocean. The major historical earthquakes which caused significant damage to liquid containing structures and consequently led to developments in design codes and standards for seismic design of liquid containing structures are presented herein.

1906 San Francisco California Earthquake

The California earthquake of April 18, 1906 ranks as one of the most significant earthquakes of all time. One lesson learned from this earthquake is the importance of water supply for firefighting and drinking water. Because one pipeline that carried water from San Andreas Lake to San Francisco was broken, the fires due to earthquake quickly raged through the city. A large part of San Francisco was destroyed because of the lack of water to control the fires. The 1906 earthquake marked the dawn of modern scientific study of earthquake engineering in North America. Further details on the effect of the above earthquake can be found at U.S. Geological Survey (USGS) website as follows: http://earthquake.usgs.gov/earthquakes/eqarchives/.

1964 Great Alaska Earthquake

On March 27, 1964, a great earthquake of magnitude 9.2 (moment magnitude) occurred in Prince William Sound region of Alaska. The oil storage tanks were damaged significantly during the earthquake. Many fuel storage tanks in the Union Oil Corporation and U.S. Army tank farm area were damaged by a combination of fire, seismic shaking and waves (Kachadoorian, 1965).

The 1964 Great Alaska Earthquake along with the Niigata Earthquake which occurred in the same year in Japan caused significant loss in the oil storage tanks. Both of these two earthquakes brought the attention to the earthquake engineering society to improve the seismic design of liquid storage tank, especially for the petroleum storage tanks.

1971 San Fernando Earthquake

On February 9, 1971 a destructive earthquake with magnitude 6.6 occurred in a sparsely populated area of the San Gabriel Mountains, near San Fernando, California. The earthquake caused considerable damage to the facilities of water and wastewater

treatment systems in the Sylmar and Granada Hills areas of the north San Fernando Valley (Murphy, 1973). Notable structural failures occurred to storage facilities at Sesnon and Granada High Tanks and Maclay Reservoir. The damage to Sesnon Tank, a welded steel water tank consisted of a horizontal buckle in the shell plate on the south side of the tank due to overloaded stress caused by foundation failure and differential settlement. Also the sloshing caused the roof damage of Sesnon Tank and roof collapses of Granada High Tank and Maclay Reservoir.

The earthquake caused damage to two storage facilities at the Joseph Jensen Filtration Plant in Sylmar area. The steel washwater tank had significant movement caused by the earthquake induced sloshing of the water inside, which resulted in rocking of the tank.

Another underground concrete water reservoir in Joseph Jensen Flirtation Plant also suffered severe damage to the roof, column and wall systems due to the excess inertial forces in the fill-covered roof as shown in Figures 2.1 and 2.2.

Figure 2.1 Joseph Jensen Filtration Plant -Collapse of Concrete Wall of Underground Reservoir, 1971 San Fernando, California, Earthquake.

Figure 2.2 Joseph Jensen Filtration Plant - Damage of Column of Concrete Underground Reservoir 1971 San Fernando, California, Earthquake.

It is worth noting that the reservoir which was just completed after construction was still empty during the earthquake. However, the backfill on roof commonly used for underground concrete reservoir to prevent floatation resulted in significant inertial forces on the structure.

The damage suffered from 1971 San Fernando earthquake led to the adoption of more stringent seismic design requirements of many lifeline facilities in California. In 1994, an earthquake of similar magnitude occurred in the City of Northridge, in the same area of San Fernando Valley caused only minor damage to liquid storage tanks. This can be attributed to better design and detailing of such facilities after the San Fernando earthquake.

1989 Loma Prieta Earthquake

On October 18, 1989, a magnitude 6.9 earthquake occurred in the Santa Cruz Mountains in the forest of Nisene Marks State Park, California. The earthquake significantly affected

water and wastewater (sewage) lifeline systems. The damage was concentrated in the San Francisco and Oakland areas adjacent to San Francisco Bay that underwent liquefaction, and in the Santa Cruz area along the San Lorenzo River (Schiff, 1998).

Several water tanks were damaged in the Los Gatos-San Jose area. An unanchored 1000,000 gal bolted tank built in 1966 had an "elephant's foot" buckle. Damaged steel tanks were based on old designs without seismic consideration. The earthquake induced ground and water motion significantly damaged a concrete tank in the Purisima Hills Water District. This wire-wound post-tensioned concrete tank was constructed in 1964 by alternate pours of the vertical panels. The earthquake caused the collapse of the column supporting the roof slab and the rupture of a panel joint. The entire 1.1 million gal of water in the tank was lost. The submerged and attached equipment in tanks, including floating tank roofs, were significantly damaged at some water- and wastewater-treatment plants. Repair costs were as high as $1.7 million at one treatment plant.

An inventory of the earthquake damage to water and wastewater treatment plants in the San Francisco Bay region revealed that basin and tank structures using reinforced and/or prestressed concrete were not significantly damaged. Steel water storage tanks built to American Water Works Association (AWWA) seismic specification D100 also performed well.

1994 Northridge Earthquake

On January 17, 1994, an earthquake with a magnitude of 6.6 occurred about 30 km northwest of Los Angeles. In the San Fernando Valley area, the earthquake caused damage to five steel water storage tanks located in the San Susan Mountains and Santa Monica Mountains. Much of the observed damage was attributed to the uplift of the tanks during the earthquake. The roof of several tanks collapsed owing to impact of the

sloshing water waves and raised serious concerns about the stability of these structures in case of major aftershocks. The damage caused by the earthquake left more than two-thirds of the San Fernando Valley without water services. However, due to the seismic upgrades carried out after 1971 San Fernando earthquake, the performance of the liquid storage tanks during Northridge earthquake was much better than that during the San Fernando earthquake which was just centered 25km north of the Northridge. The damage suffered to major installations and critical facilities were only minor and repaired soon after the earthquake (Lau, 1995).

2.2.2 Other Countries

There are many other records of damage to liquid storage tanks in the historical earthquakes around the world.

The Great Chilean Earthquake of 22 May 1960 is the most powerful earthquake ever recorded to date, with the moment magtitude of 9.5. The Tsunami due to the earthquake even affected many countries on the western side of Pacific Ocean. Many elevated tanks were damaged significantly during this earthquake. Further details on the effect of the above earthquake can be found at U.S. Geological Survey (USGS) website as follows: http://earthquake.usgs.gov/earthquakes/eqarchives/.

On January 17, 1995, the Kobe earthquake occurred with 6.8 on the moment magnitude scale. The heavy damage to the Nippon Gatx tank farm, about 10km east of epicenter and on the waterfront resulted in loss of properties. The damage consisted principally of tank tilting and loss of foundation supports in pipe support. Liquefaction was the principle cause of damage at this waterfront location. Further details on the effect of the above earthquake can be found at U.S. Geological Survey (USGS) website as follows: http://earthquake.usgs.gov/earthquakes/eqarchives/.

The August 17, 1999, Kocaeli (Izmit) earthquake with moment magnitude of 7.4 occurred on the North Anatolian fault in northwestern Turkey. Many liquid storage tanks in tank farm of the Tüpras refinery and the Petkim petrochemical plant were damaged due to the fires as an indirect consequence of the earthquake shaking. In the Habas plant, the major damage was the collapse of two of the three liquid gas storage tanks (Sezen et al., 2000).

In the Bhuj, Indian earthquake of January 26, 2001 with moment magnitude of 7.7, many elevated water tanks suffered damage to their staging (support structure). The investigation revealed that the majority of these tanks supported on cylindrical shaft type staging developed circumferential flexural cracks near the base. Two reinforced concrete (RC) framed staging tanks located in regions of the highest intensity of shaking collapsed while a few developed cracking near brace-column joint regions. (Dutta et al., 2009)

2.2.3 Failure Mechanism

There are different failure mechanisms involved in liquid storage tanks under seismic loads. Such failures depend on type of tanks, configuration of the tank, the material of construction and supporting method. The content of liquid storage tanks can be oil, water, chemicals or any types of liquid material. The configuration of a tank is often affected by the purpose of its usage. It may be circular, rectangular, cone or other shapes. Concrete and carbon steel are the most common materials used for construction. Other materials include high alloy steel and fiberglass. Steel tanks can be either anchored into the foundation or unanchored. Concrete tanks can be cast-in-place, prestressed with tendons or post-tensioned with wrapped wire/strands. Tanks can be supported on grade, below grade or elevated using steel or concrete frames or concrete pedestals.

There are not many reports available in the literature on failure of concrete liquid storage

tanks due to earthquakes. This is due to that many liquid storage tanks built were made of steel. Many concrete liquid storage tanks are built underground and the surrounding soil provides restraint on the movement of tank. In addition, the elements for concrete tanks are normally in large dimensions in terms of size of column and thickness of wall and slab. It is noted that the design criteria for concrete tanks are based on crack control. As a result, the failure of concrete tank normally is due to leakage rather than collapse. Therefore, concrete tanks may have sufficient strength to resist seismic loads when subjected to a major earthquake. However, it may fail to meet serviceability requirements which are also considered as a type of failure.

Based on past performance and observations, the possible failure modes in concrete liquid containing structures under the effects of earthquakes are categorized as follows:

(1) Collapse of concrete structures due to large inertial force: As compared to steel tanks, the self-weight of concrete tanks contributes significantly to inertial forces in overall seismic loads. This is even worse when concrete tanks have backfill on top as evidenced by damage around the supporting columns of a roof of a liquid storage tank during the 1971 San Fernando Earthquake.

(2) Failure of concrete support: Damage due to earthquakes shows that elevated concrete tanks are very vulnerable under seismic excitations due to the heavy mass on top of a concrete frame or pedestal. The concrete frame may crack severely or even collapse as a result of lateral forces due to earthquakes. The overturning moment can result in large tension forces on one side of concrete pedestal. Because insufficient reinforcements were provided in concrete pedestals and the openings may even weaken the pedestal, many elevated tanks collapsed during 1960 Great Chilean and 2001 Bhuj, Indian earthquakes.

(3) Shear failure of concrete columns: The concrete columns placed inside a reservoir to support the roof or placed as short columns below the tanks to support tank itself could fail due to shear. The main concern is the weak connections between the concrete column that could lead to the failure of the structure and the supporting structures with inadequate ties or stirrups.

(4) Loss of stress in prestressed or post-tensioned concrete tank in reinforcing tendons or wrapped wire/strands: The loss of stress in strands was recorded in 1989 Loma Prieta Earthquake for a concrete tank in the Purisima Hills Water District which was ruptured at a vertical panel joint.

It is worth noting that the failure modes discussed in this section are focused on concrete tanks. Some failure modes which are common for all types of liquid storage tanks such as failure of foundation and connections between tank and piping or other accessory systems also occur in concrete tanks. Also it is possible that different construction materials may be used for a storage facility such as elevated tank made of a concrete pedestal and a steel tank on top. The failure of the concrete pedestal may cause the overall failure of the system under an earthquake.

2.3 Previous Research

Intensive research work on dynamic response of liquid storage tanks commenced in the late 1940's, but originally was related to the study of dynamic response of fuel tanks in aerospace engineering. The main difference on the behavior of dynamic response of fuel tanks in aerospace engineering and those in civil earthquake engineering is that the latter is more concerned with response in the lower frequency range. Since the size of such tanks are so much lager, dynamic response resulting from lower frequencies especially in steel tanks dominates critical stresses and deformations.

In this section, previous research studies on dynamic response of liquid storage tanks are reviewed. The literature review is focused on the topic of dynamic analysis. However, references are also provided for other related areas such as soil structure interaction, base isolation, elevated tanks, sloshing, uplifting and anchoring, and filled material in tank. The research significance, major contributions and conclusions for these studies are summarized in this section.

2.3.1 Dynamic Analysis

Housner (1957 and 1963) developed the most commonly used model for dynamic analysis of liquid storage tanks as indicated in Figure 2.3. He assumed the incompressible liquid underwent small displacement. Hydrodynamic pressures induced by earthquake were separated into two parts: impulsive pressure - the portion of the liquid accelerating with the tank, and convective pressure - the portion of the liquid sloshing in the tank. On this basis, he developed simplified expressions to approximate these pressures by added masses. The added mass in terms of impulsive pressure is assumed rigidly connected with the tank wall and the added mass in terms of convective pressure is assumed connected to the tank wall using springs. The boundary condition in calculation of hydrodynamic pressures was treated as rigid in the model.

(a) Fluid Motion in Tank   (b) Dynamic Model for Rigid Wall Tank
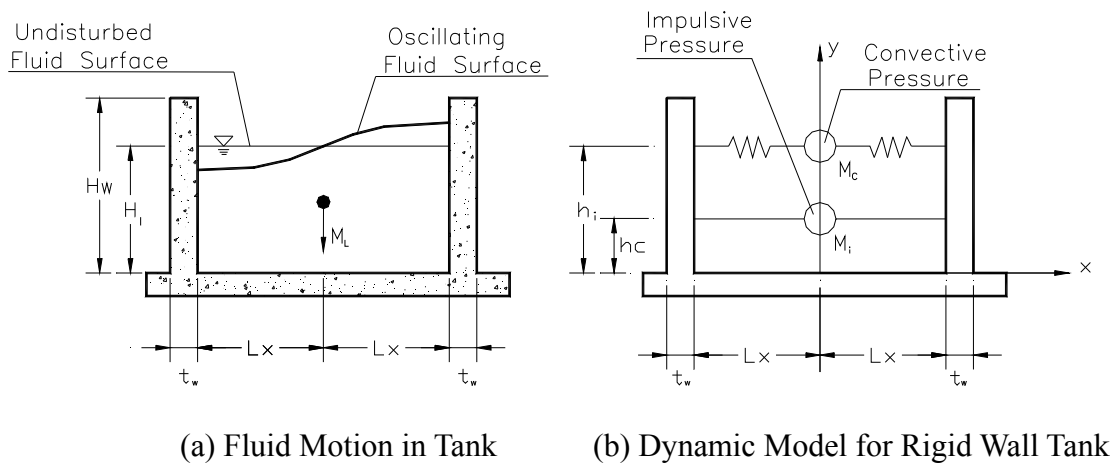
Figure 2.3 Hounser's Model

Later, Epstein (1976) presented the design charts according to Housner's model for estimating the bending and overturning moment induced by the hydrodynamic pressures for both cylindrical and rectangular tanks.

Yang (1976) and Veletsos (1984) considered the effect of wall flexibility on the magnitude and distribution of the hydrodynamic pressures and associated tank forces. They assumed that the tank-fluid system behaved like a single degree of freedom system and the base shear and moment were evaluated for several prescribed modes of vibration. They used Flügge's shell theory (Flügge, 1960) to analyze the dynamic response of tank. The displacement component of the arbitrary point on the shell were expressed in terms of natural modes of the vibration of a uniform cantilever beam with shear and bending flexibilities, and the effect of the container liquid was approximated by assuming that a portion of the mass of liquid was attached to the shell. It was found that for tanks with realistic flexibility, the impulsive forces were considerably higher than those in rigid tanks.

Veletsos and Tang (1986) presented a simple practical procedure for evaluating the dynamic response of an upright circular cylindrical liquid storage tank to a vertical component of ground shaking, considering the flexibility of the supporting medium. Galerkin's method considering the tank-liquid system to respond as a single-degree-of-freedom system was used for dynamic analysis. It was shown that soil-structure interaction reduces the hydrodynamic effects and that the consequences of such interaction may be approximated with good accuracy by a change in the natural frequency of the tank-liquid system and by an increase in damping. The maximum hydrodynamic effects were related simply to the corresponding hydrostatic effects.

Veletsos and Tang (1987) also studied the dynamic response of liquid containing, upright

circular cylindrical tanks to a rocking base motion of arbitrary temporal variation. Both rigid and flexible tanks were examined. The interrelationship of the responses of the system to rocking and lateral base motions of the same temporal variation was established. It was shown that some of the effects of base rocking may be determined from available data concerning the response of laterally excited tanks.

Balendra and Nash (1975) used the Finite Element Method to discretize the tank wall and considered it to be a thin elastic shell element. The effect of sloshing was neglected. Thus, the problem was reduced to an empty cylindrical tank with mass matrix augmented by an "added mass" representing the effect of the contained liquid. The program "EXDOMTANK" based on the reference (Balendra and Nash, 1975) gave the time history of displacement and stress in the shell due to impulsive forces.

Later, Yu and Nash (1986) used Finite Element-Perturbation method which was based on the perturbation technique to study the non-linear sloshing of liquid and the stability. The response of solid tank was solved by nonlinear finite element method. The technique, which was called sequential method, was used to simulate the interaction between fluid and wall. But no time history response associated with earthquake engineering was demonstrated in their study. The commercial finite element software ANSYS$^{\circledR}$ was used in their study.

Kana (1979) carried out experimental work on liquid slosh and tank wall flexural vibrations in a flexible model storage tank subjected to simulated earthquake environments. The influence of wall flexural vibrations on induced stresses was determined. Then, a series of scale model experiments were conducted to evaluate the formulation of an approximate analytical model for prediction of seismically induced stress. Validity range for the model was established by comparison of various predicted

responses with observed results.

Kana (1982) also reviewed the methods available for seismic design of liquid storage tanks to establish the needs for future research. A transfer function and response spectrum method was used for prediction of slosh response and impulsive loading. The method was applicable to operating transient loads that occur in nuclear power plants. Direct applicability was noted for much of the available design data that had previously been developed for aerospace launch vehicles.

Haroun carried out extensive theoretical and experimental investigations of dynamic behavior of fluid storage tanks. Haroun (1981) used liquid-shell system in which the shell wall was discretized by using cylindrical finite element and the fluid region was treated as a continuum by the boundary solution techniques.

Later, Haroun (1984) presented a very detailed analytical method in the typical systems of loadings in the rectangular tanks. The hydrodynamic pressures were calculated by classical potential flow approach. The formulas of hydrodynamic pressures only considered the rigid wall boundary condition.

In addition, Haroun (1983) carried out theoretical and experimental investigations on dynamic behavior of ground-supported, deformable, cylindrical liquid storage tanks. In the first phase, a detailed theoretical treatment of the coupled liquid-shell system for tanks rigidly anchored to their foundation was studied. Then, a series of ambient and forced vibration tests of three, full scale water storage tanks were conducted to determine the natural frequencies and the mode shapes of vibration. Two tanks were selected in which permanent instruments were installed to record the possible future earthquakes. This research work significantly improved the understanding of dynamic response of

fluid storage tanks and provided practicing engineers with simple and sufficiently accurate tools to estimate such response.

Haroun and Tayel (1985A and 1985B) presented both analytical and numerical methods for the computation of the axisymmetrical dynamic characteristics of partly-filled cylindrical tanks. For analytical method, two coupled partial differential equations governed the vibrations of the shell considering the liquid structure interaction. For numerical method, natural frequencies and mode shapes were evaluated by means of a discretization scheme in which the shell was modeled by finite elements and the liquid region was treated analytically. The distribution of the hydrodynamic pressure along the inner surface of the shell as well as the distribution of shell stresses was displayed. For practical applications, a simplified formula was developed to calculate the fundamental natural frequency of full tanks. The effect of vertical ground acceleration was considered.

Liu (1981) used a nonlinear finite element method to study the structural behavior of tanks in conjunction with fluid, including the dynamics and buckling. The mixed Lagrangian-Eulerian kinematical description was used for modeling fluid subdomains in fluid-structure interaction problems. The nonlinear methodologies were integrated into a finite element computer code FLUSTR.

Later, Liu and Lam (1983) applied this numerical tank model to dynamic analysis of cylindrical liquid storage tanks. The results show that the tank model collapses at a critical load 20% lower than the classical prediction using linear theory. It also shows that higher order modes are significant in the hoop stress profile which is nonlinear in character. The observed "elephant-foot buckling" and the "ovalling" response of liquid storage tanks in many tank failures during earthquakes can be predicted with these nonlinear methodologies.

Liu and Uras (1989A and 1989B) derived the governing equations which consider dynamic fluid-structure interaction, modal coupling in both axial and circumferential directions, and dynamic buckling. The various pressure components acting on the shell wall due to a seismic event were analyzed. The matrix equation of motion for liquid-filled shells was obtained through a Galerkin/Finite Element discretization procedure. The modal coupling among the various combinations of axial and circumferential modes was identified with a particular reference to the fluid-structure system under seismic excitation. The theory was applied to study the effects of various types of ground motion on the dynamic stability of the fluid-structure system. The stability criteria of liquid-filled shells subjected to horizontal and rocking excitation, shear loading, bending/shear combined loading, and vertically applied load were established.

In addition, Chang et al. (1998) applied FLUSTR-ANL for seismic analysis of Liquid Metal Reactor (LMR) tanks in nuclear industry. The efficiency of the numerical algorithm was demonstrated.

Luft (1984) presented a normal mode solution for a neoprene pad supported, cylindrical, prestressed concrete tank subjected to vertical accelerations. The solution, which gives the natural modes and frequencies and the load participation factors, was used to compute the hoop forces caused by the hydrodynamic fluid pressure.

Kennedy and Kassawara (1990) presented a procedure for evaluating the seismic capacity of flat-bottom fluid storage tanks. This procedure can be conservatively applied in seismic analysis and design of liquid storage tank for nuclear industry. The predicted capacity represents a High Confidence Low Probability of Failure (HCLPF) capacity consistent with earthquake experience.

Park et al. (1990) performed research studies on dynamic response of rectangular tanks. They used the boundary element method to calculate the hydrodynamic pressures and finite element method to analyze the solid wall. The governing equation for the coupled system was given. The time history analysis was used to obtain the dynamic response of fluid storage tanks. Both impulsive and convective effects were considered.

Later, Kim et al. (1996) used an analytical method to solve this problem. They presented formulas for the 3-D hydrodynamic pressures calculation and applied the Rayleigh-Ritz method using assumed vibration modes of rectangular plate with suitable boundary conditions as admissible functions for dynamic analysis. The results obtained from the analytical solution agreed well with those from the coupled boundary element – finite element method.

Gupta and Hutchinson (1991) studied the effects of wall flexibility on the dynamic response of liquid storage tanks. Variation principles were used to obtain a functional describing coupled oscillation between a linear elastic body and a liquid of small wave heights. A complementary Rayleigh's quotient was introduced to obtain coupled natural frequencies and the dynamic pressure distribution in the axisymmetric natural modes of vibration. Both low frequencies (liquid sloshing mode) and high frequencies (tank bulging mode) were included in the study.

Gupta (1995) investigated the coupled free vibration characteristics of partially or completely liquid-filled ground supported circular cylindrical tanks. Flugge's exact equations of motion were applied to study the vibrations of the container itself. The radial liquid dynamic pressure was obtained using the liquid velocity potential method. The results were found to be in good agreement with those obtained by Haroun and Housner model. The coupled natural frequencies in bulging modes were also studied.

Lay (1993) developed a numerical model for the seismic analysis of tanks with single and double curvatures such as cylindrical tanks and spherical tanks using a combined finite element-boundary element numerical procedure. The boundary element equations for the liquid region were used to obtain an equivalent finite element fluid mass matrix. Free-surface sloshing of liquid and tank-wall flexibility was included in the model.

Dogangun et al. (1996) developed the formulation of three-dimensional Lagrangian fluid finite element which includes the effects of compressibility and surface sloshing motion. The finite element was incorporated into a general purpose structural analysis program SAPIV and used for the static and dynamic behavior of rectangular liquid storage tanks.

Peek and El-Bkaily (1997) considered the P-Δ effect for dynamic analysis of tall tanks. A general approach to obtain the properties of the equivalent mechanical model for a container of any shape was described.

Nachtigall et al. (2003) argued the common assumption adopted from Haroun-Housner and Veletsos that a circular cylindrical tank containing liquid behaves like a cantilever beam. Instead, the shell modal was used in order to generate a refined model. The fundamental frequencies for the tank-liquid-system were calculated based on Galerkin's approximations for cylindrical shells.

Virella et al. (2003) studied the influence of a fixed roof on the natural periods of vibrations of thin-walled above ground steel tanks with clamped boundary conditions at the base. It was found that the vibration of empty tanks with a fixed roof is dictated either by cylinder modes or roof modes of vibrations. For self-supported roofs, predominant roof modes for tanks with roofs supported by rafters, cylinder modes dominate the dynamic behavior of the tank. Roof dominant modes had natural periods that remain

constant regardless of the aspect ratio considered. Cylinder modes, on the other hand, were characterized by natural periods that show a linear dependence with the aspect ratio of the tank.

In response to the concern of Nachtigall et al. (2003), Virella et al. (2006) studied the fundamental impulsive modes of vibration of cylindrical tank-liquid systems anchored to the foundation under horizontal motion. The analyses were performed using a general purpose finite element (FE) program ANSYS, The roof and walls were represented with shell elements and the liquid was modeled using two techniques: the added mass formulation and acoustic finite elements. It was concluded that the fundamental modes of tank models with aspect ratios (H/D) larger than 0.63 were very similar to the first mode of a cantilever beam. For the shortest tank (H/D = 0.40), the fundamental mode was a bending mode with a circumferential wave n = 1 and an axial half-wave (m) characterized by a bulge formed near the mid-height of the cylinder.

Virella et al. (2008) evaluated the elastic buckling of above-ground steel tanks anchored to the foundation due to seismic shaking. The proposed nonlinear static procedure was based on the capacity spectrum method (CSM) utilized for the seismic evaluation of buildings. Rather than the base shear and the maximum displacement of a characteristic point of the structure used for the standard CSM, the results of minimum value of the horizontal peak ground acceleration (PGA) that produces buckling in the tank shell are used in their study.

Kruntcheva (2007) carried out a theoretical and experimental study on the effect of different parameters on the coupled modal characteristics of circular cylindrical tanks. The clamped-free tanks resting on rigid foundations were investigated by using finite-element (FE) modeling and holographic experiments. The research showed a good

agreement between experimental and numerical results. The effects of a flexible foundation and axial compression were also investigated using holographic interferometry. The modal responses of this shell–liquid system were found to be different from those of the existing theoretical models.

Li et al. (2007) investigated the seismic response and performance of a water-filled, prestressed concrete egg-shaped digester (ESD) subjected to various earthquake inputs by shaking table test. The natural frequency, seismic responses including the amplification factor of acceleration (AFA), the relative displacement and the strain and stress were investigated based on the test results. Finite-element modeling computations were conducted. Comparison with the test counterparts showed a fair agreement.

Chen and Kianoush (2005) developed a procedure referred to as the sequential method for computing hydrodynamic pressures based on a two-dimensional model for rectangular tanks in which the effect of flexibility of tank wall was taken into consideration. The sequential method is a coupling technique in which the two fields of fluid and structure are coupled by applying results from the first analysis as loads or boundary conditions for the second analysis. Compared to the Housner's model, it was shown that the lumped mass approach overestimates the base shear and base moment significantly.

In addition, Kianoush and Chen (2006) investigated the response of concrete rectangular liquid storage tanks subjected to vertical ground acceleration in which the importance of the vertical component of ground motion on the overall seismic behavior of liquid storage tanks was evaluated. It was concluded that the response of tank due to vertical ground acceleration can be significant and should be considered in design.

Chen and Kianoush (2004) also studied the effect of different ground motions on the dynamic response of LCS. The study on the convective pressure can be found in the Master thesis (Chen, 2003).

Later, Kianoush et al. (2006) and Ghaemian et al. (2005) applied the staggered method to solve the coupled liquid storage tank problems in three-dimensional space. The staggered method is a partitioned solution procedure that can be organized in terms of sequential execution of a single-field analyser. The scheme of staggered method is to find the displacement and hydrodynamic pressure at the end of the time increment $i + 1$, given the displacement and hydrodynamic pressure at time i. Compared to Housner's model, these results show that in most cases the lumped mass approach overestimates the base shear and base moment significantly.

2.3.2 Other Related Studies

Veletsos and Tang (1990), Veletsos et al. (1992), Haroun and Abou-Izzeddine (1992A and 1992B), Malhotra (1997), Chatterjee and Basu (2001 and 2004), Livaoglu and Dogangun (2006), and Dutta et al. (2009) conducted studies on the effects of soil structure interaction (SSI) on the response of liquid containing tanks.

Kim and Lee (1995), Malhotra (1997A), Shenton and Hampton (1999), Park et al. (2000), Wang et al. (2001), Shrimali and Jangid (2002A and 2002B), Panchal and Jangid (2008), Almazan et al. (2007), Mordini and Strauss (2008) and Shekari et al. (2009) studied the effects of base-isolation on the seismic response of liquid storage tanks.

Tung and Kiremidjian (1991), El Damatty et al. (1997A and 1997B), Shenton and Hampton (1999), Sweedan and El Damatty (2003 and 2005), Livaoglu and Dogangun (2006) and Sezen et al. (2008) conducted studies on elevated water tanks.

Ma et al. (1982), Lepelletier and Raichlen (1988), Amano et al. (1993), Chen et al. (1996), Choun and Yun (1996 and 1998), Warnitchai and Pinkaew (1998), Isaacson and Ryu (1998A and 1998B), Isaacson and Premasiri (2001), Pal et al. (1999), Hernandez-Barrios et al. (2007), Chen et al. (2007) and Maleki and Ziyaeifar (2007) studied the effect of sloshing on dynamic response of liquid storage tanks.

For the uplifting and anchoring of steel tanks, Clough (1977 and 1978), Niwa (1978), Niwa and Clough (1982), Manos and Clough (1982) and Shibata and Akiyama (1985) conducted experimental work for partially anchored tanks. Wozniak (1978) proposed an approximate model for the seismic analysis of anchored and unanchored fluid storage tanks, which form the basis of the provisions in the American Petroleum Institute design standard API 650 (1979) Appendix E, and the standard of the American Water Works Association (1984) Appendix A. Many other researchers continuously worked in this field such as Leo and Kausel (1986), Manos (1986), Peek (1986), Peek and Jennings (1988) and Peek et al. (1988) aiming at developing more comprehensive methods for analysis of unanchored tanks, and validating their results with experimental data. Malhotra and Veletsos (1994A, 1994B, 1994C, 1997A, 1997B and 1997C) conducted a series of studies on the effects of base uplifting on seismic response of laterally excited, unanchored, cylindrical liquid-storage tanks. Similar studies were carried out by El-Bkaily and Peek (1998), Taniguchi (2004) and Ahari et al. (2009).

Younan and Veletsos (1998A and 1998B) and Tang (1994A, 1994B, 1994C and 1996) studied the effect of materials filled in tanks.

2.4 Codes and Standards

In North America, there are few codes and standards available for seismic design of liquid containing structures. Currently, the International Building Code (IBC), IBC 2006

is the most widely adopted code in the United States. The latest IBC refers to American Society of Civil Engineers' standard ASCE 7-05 for seismic design of tanks and vessels. The ASCE 7 procedure for tank design applies to most common tank types while some specialty tanks are referenced to their appropriate guidelines and standards.

For concrete LCS, the American Concrete Institute (ACI) published the ACI 350.3 (2006) in the form of a mandatory document for seismic design of ground-supported reinforced concrete tanks. The guidelines for design of concrete-pedestal water towers are given in ACI 371 (1998).

The American Water Work Association (AWWA) introduced two sets of standards for prestressed concrete liquid containing structures, AWWA D110 (1995) for Wire- and Strand-Wound, Circular, Prestressed Concrete Water Tanks and AWWA D115 (1995) for Circular Prestressed Concrete Water Tanks. The design guides of steel tanks are provided by AWWA D100 (2005) for Welded Steel Tanks for Water Storage.

The design of tanks in the petroleum industry has been referred to the standards published by American Petroleum Institute (API). API 650 Welded Steel Tanks for Oil Storage, Appendix E covers the seismic design part. It is worth noting that API 650 pertains to contents stored at atmospheric pressure, while API 620 covers tanks for low pressure (pressures in gas or vapor spaces not to exceed 15 psi).

In the nuclear industry, liquid containing structures are widely used for variety of purposes. The code requirements and procedures of these types of structures are more stringent than those used for other industries. ASCE 4-98 Seismic Analysis of Safety-Related Nuclear Structures and Commentary (ASCE, 1998) and ASCE 58 Structural Analysis and Design of Nuclear Plant Facilities (ASCE, 1980) provide

guidelines for dynamic analysis procedures for seismic design of liquid containing structures in the nuclear industry.

At the international level, New Zealand Society for Earthquake Engineering (NZSEE) first developed the recommendations for seismic design of concrete liquid storage tanks as documented in the New Zealand Standard NZS 3106 (NZSEE, 1986). The latest version of NZS 3106 was published in 2010 incorporating the modification done by Whittake and Jury (2000). Also, the European Eurocode 8, (2006), provides guidelines for seismic design of liquid containing structures.

In the remaining part of this chapter, the approach and procedure for seismic design of liquid containing structures are discussed and compared. The comparison is mainly focused on the codes and standards used in North America such as ASEC7/IBC 2006, ACI 350.3, ACI 371, AWWA D-100, AWWA D-110, AWWA D115 and API 650 because these codes and standards are based on similar design philosophies.

2.4.1 Analytical Approach

Most of the design codes and standards such as ACI 350.3, AWWA D-100, AWWA D-110 and API 650 use the mechanical model proposed by Housner (1963) with some modifications. AWWA D-100 and API 650 deal with circular steel tanks in which the effect of flexibility of tank is considered. Housner's model (Housner, 1963) is also use for dynamic analysis of concrete circular and rectangular liquid storage tanks in ACI 350.3. However, the parameters of impulsive and convective modes are based on the rigid tank models assuming that there is no significant difference between the two models of rigid and flexible tanks.

The New Zealand Standard NZS 3106 (2010) uses mechanical model of Veletsos and Yang (1977) for rigid circular tanks and that of Haroun and Housner (1981) for flexible tanks.

Eurocode 8 refers to the analytical model proposed by Veletsos and Yang (1977) as an acceptable procedure for rigid circular tanks. For flexible circular tanks, models of Veletsos (1984) and Haroun and Housner (1981) are described along with the procedure proposed by Malhotra et al. (2000). For rigid rectangular tanks, Housner's model (1963) is used. However, no practical procedure is adopted for flexible rectangular tanks. The procedure given in NZSEE guidelines is also described in Eurocode 8 for evaluating impulsive and convective mass of liquid for circular tank.

2.4.2 Ground Motion

In ASCE 7-05, the ground motion is based on the Maximum Considered Earthquake (MCE) which is defined as an event with a 2 percent probability of exceedance over 50 years (mean return period of 2475 years). The ground motion is normally represented by response spectra which can be determined using either the general procedure or the site-specific procedure.

The ground motion in ACI 350.3, AWWA D100 and API 650 are now derived from ASCE 7-05. The guidelines of general and site-specific procedures are provided in these codes and standards. It is noted that the site-specific procedure is required if the tank is located on Site Class F type soil in AWWA D100. However, API 650 recommends this approach under a few other conditions as well. ACI 350.3 only applies the site-specific procedure when the more rigorous approach is required. Both AWWA and API also recommend the provisions for such jurisdictions where ASCE 7 has not yet been enforced.

AWWA D-110 still uses 1994 revision of the UBC in determination of the seismic zone classification. The zone coefficients Z represent the peak ground accelerations that have a 10 percent chance of exceedance in 50 years. When multiplied by an importance factor I of 1.25, the probability of exceedance drops to 5 percent. Similar probabilities should be used for site-specific response spectra.

2.4.3 Seismic Design Force

In codes and standards for seismic design of liquid containing structures, the design seismic forces are separated into two components, i.e. the impulsive and convective components. The basic formula to calculate the seismic force F is as follows:

[2.1] $F = CW$

where W is the seismic weight of components and C is the seismic force coefficient. It is worth noting that different terminology is used to define C in different design codes and standards. Fundamentally, the seismic force coefficients are related to the input ground motion. The design response spectral acceleration, damping and response modification factors are discussed later in this section.

It is worth noting that ASCE 7-05 used the direct sum method to combine the impulsive and convective components, though the Square Root of Sum of Square (SRSS) method can also be used in lieu of the direct sum method. However, only the SRSS method is used in ACI 350.3, AWWA D-100, D-110, and API 650.

ACI 350.3 provides the distribution of impulsive and convective hydrodynamic pressures along the height of wall based on Housner's model. ASCE 7-05 does not specify hydrodynamic pressure distribution on wall and base. However, ASCE 7-05 refers to the codes and standards for different types of tanks. AWWA D-100, D-110 and API 650

directly give the stresses rather than providing the hydrodynamic pressure distribution. In all codes and standards, the effect of hydrodynamic pressure on a tank base for overturning moments is included.

2.4.4 Damping for Impulsive and Convective Components

Damping for the impulsive and convective components is specified separately in all codes and standards. A 0.5% damping ratio is used consistently for convective component in all codes and standards.

The damping ratio specified for the impulsive component is different for different codes and standards. This ratio is based on the type of tank, construction material, etc. The damping ratio in ASCE 7, ACI 350.3, AWWA D-100, D-110, and D115 and API 650 for impulsive component is 5% for all types of tanks and the corresponding response spectral acceleration is 1.5 times lower than that for the 0.5% damping ratio used for convective component. However, Eurocode 8 specifies 5% damping for the impulsive component of reinforced concrete and prestressed concrete tanks and 2% damping for steel tanks. The response spectrum for impulsive component is 1.7 times lower than that of convective component.

Variable damping ratios are used for impulsive component of ground-supported tanks in the latest NZS 3106 (2010). It also suggests that the effect of tank material, aspect ratio of tank geometry, and foundation soil shear wave velocity should be considered in determination of damping for impulsive component.

2.4.5 Design Response Spectra for Impulsive and Convective Components

In the equivalent static force procedure, the response spectrum method is used to determine the seismic forces for liquid containing structures. Beside the ground response

spectrum specified in the codes and standards, the design response spectra for impulsive and convective components are provided. This is mainly due to the different response of impulsive and convective components based on the damping ratios used for design.

Based on Eq.2.1, C_i and C_c are defined as the period-dependent seismic response coefficients for impulsive and convective hydrodynamic pressures in ACI 350.3, respectively. Figure 2.4 shows the response spectrum in determining the impulsive seismic response coefficient C_i based on the general procedure.
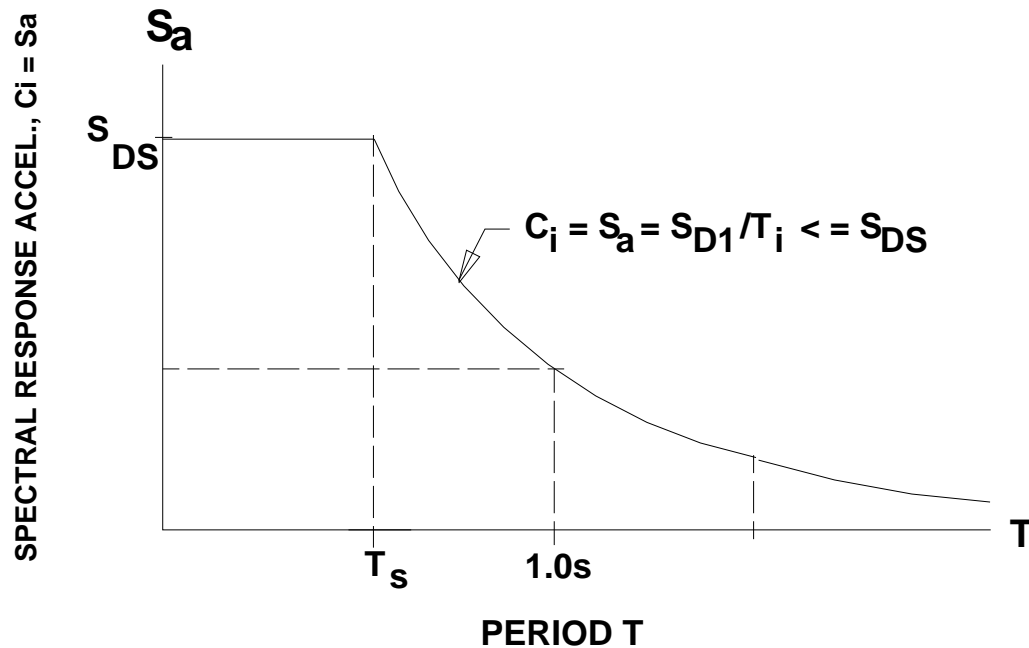
Figure 2.4 ACI 350.3 Design Response Spectrum for Impulsive Component

The parameters shown in Figure 2.4 are defined as follows:

S_{D1} = design spectral response acceleration, 5% damped, at a period of 1 second

S_{DS} = design spectral response acceleration, 5% damped, at short periods

T_i = fundamental period of oscillation of the tank (plus the impulsive component of the contents)

$T_S = S_{D1}/S_{DS}$

The convective seismic response coefficient C_c can be calculated as follows:

For $T_c \leq 1.6/T_s$ sec

$$[2.2] \qquad C_c = \frac{1.5\, S_{D1}}{T_c} \leq 1.5\, S_{DS}$$

For $T_c > 1.6/T_s$ sec

$$[2.3] \qquad C_c = 6\left(\frac{0.4 S_{DS}}{T_c^2}\right) = \frac{2.4\, S_{DS}}{T_c^2}$$

where T_c is natural period of the first (convective) mode of sloshing

It is noted that the factor 1.5 in Eq.2.2 is to adjust the response spectra based on 5% damping to 0.5% damping. In Eq.2.3, $0.4 S_{DS}$ is used as an approximation of the effective peak ground acceleration, S_0 (at T =0) reduced by a factor of 2/3.

For the elevated tank, only the seismic response coefficient for the impulsive component is provided in ACI 371. No provisions for convective components are specified. The response spectrum for the impulsive components is the same as ACI 350.3.

In AWWA D100, the design response spectra for impulsive and convective components based on the general procedure are provided as shown in Figure 2.5. It is noted that similar to the factor shown in Eq.2.2, K is the damping scaling factor equal to 1.5 to convert spectrum from 5% damping to 0.5% damping.

Figure 2.6 shows the design response spectra for impulsive and convective components based on the general procedure as indicated in API 650.
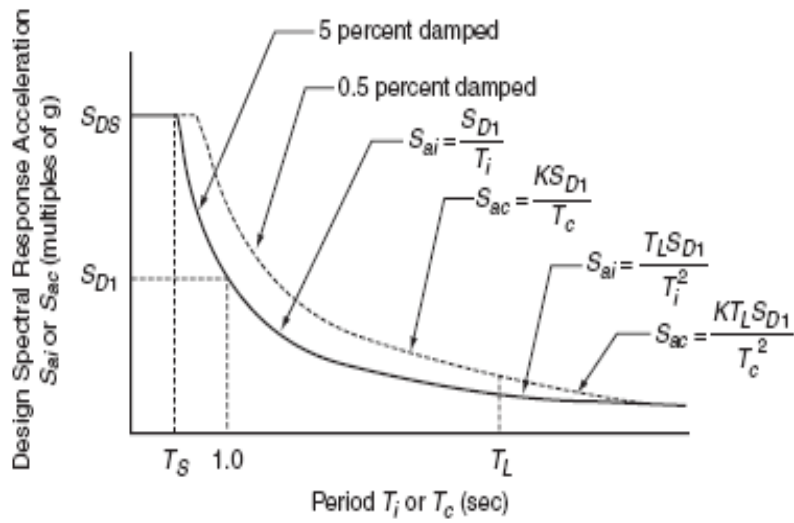
Figure 2.5 AWWA D100 Design Response Spectra for Impulsive and Convective Components
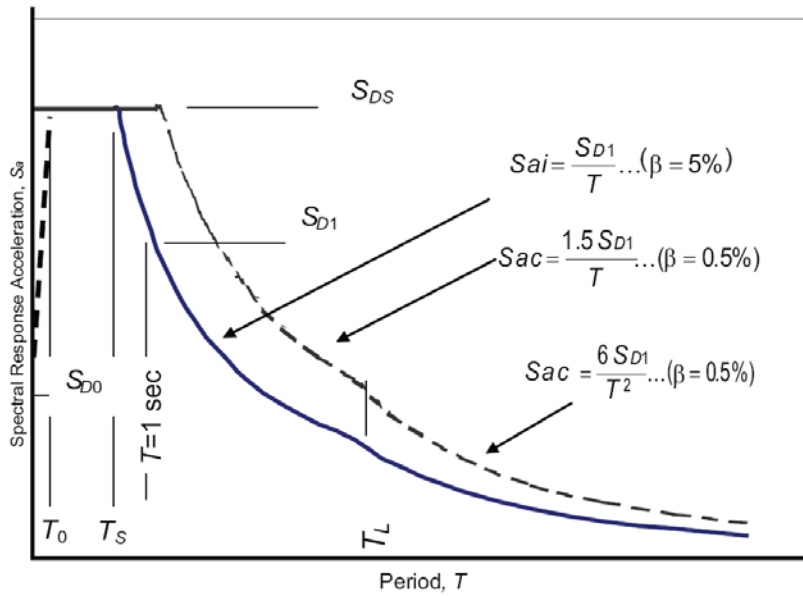
Figure 2.6 API 650 Design Response Spectra for Impulsive and Convective Components

The parameters shown in Figure 2.6 are defined as follows:

S_{ai} = Spectral response acceleration for impulsive component

S_{ac} = Spectral response acceleration for convective component

T = Natural period can be either T_i or T_c

36

T_c = Natural period of the convective (sloshing) mode of behavior of the liquid

T_i = Natural period of vibration for impulsive mode of behavior

T_L = Regional-dependent transition period for longer period ground motion, seconds

$T_0 = 0.2\, F_v S_1 / F_a S_S$

$T_S = F_v S_1 / F_a S_S$

F_a = Acceleration-based site coefficient (at 0.2 sec period)

F_v = Velocity-based site coefficient (at 1.0 sec period)

β = Damping ratio

A comparison shows that response spectra for impulsive and convective components are consistent between ACI 350.3, ACI 371, AWWA D100 and API 650.

2.4.6 Response Modification Factors

The response modification factor R is a numerical coefficient representing the combined effect of the structure's ductility, energy-dissipating capacity, and structural redundancy. Table 2.1 shows the values of response modification factor for different liquid containing structures. The difference in the values for the codes and standards are discussed as follows:

(1) The values for AWWA D-100 are at working stress level. The values for AWWA D-110 and API 650 are based on allowable stress design. Basically, the design philosophies for working stress and allowable stress design are similar. However, the values for ASCE 7, ACI 350.3 and ACI 371 are based on the strength design level. The load factors and material reduction factors are included in the strength design.

(2) Only one response modification factor is indicated for liquid containing structures in ASCE 7-05. ACI 371 refers to ASCE 7-05 for response modification factor. Therefore,

the reduction factor in ACI 371 is the same as ASCE 7-05. ACI 350.3, AWWA D-100, AWWA D-110 and API 650 use two separate factors for the impulsive and convective components. It is noted that Eurocode 8 explicitly mentioned that the response modification factor should not be applied to the convective mode. In fact, ASCE 7 adopt the same approach as specified in Eurocode 8, while API 650 and AWWA D-100 for ground supported tanks still allow some reduction in the convective component. It is worth noting that R_c values in ACI 350.3 are assumed equal to one which means no reduction for the convective design force.

(3) The classification of tanks is different based on the energy dissipating capacity. In ASCE 7-05, liquid containing structures are first categorized into two groups, i.e. ground supported and elevated the tanks. For the elevated tank, the definitions of concrete tank in ACI 350.3 and steel tank in AWWA D-100 are consistent with ASCE 7-05. The category of the ground-supported tanks is then divided into sub-categories of steel and concrete tanks based on their construction material. The anchoring system is used to group the steel tanks which are consistent with the definition of AWWA D100. For concrete tanks, the category of tanks used in AWWA D110 is consistent with ASCE 7-05. However, ACI 350.3 uses fixed or hinged-base tanks as compared to the group of tanks with reinforced nonsliding base defined in ASCE 7 and AWWA D-110. In addition, ACI 350.3 considers buried tanks which are not mentioned in other codes and standards.

(4) For concrete tanks, the values of response modification factor for the impulsive component in ACI 350.3 are the same as that of ASCE 7-05 except that for pedestal-mounted tanks the R_i value in ACI 350.3 is 2 as compared to 3 as indicated in ASCE 7 for elevated concrete tanks. In ACI 371, the response modification factor directly refers to ASCE 7–05. It is worth noting that the values provided in AWWA D-110 are about 1.4 higher than those of ASCE 7-05. This is due to the fact that AWWA

D-110 is still based on the working stress level, while ASCE 7, ACI 350.3 and ACI 371 calculate seismic design forces at the strength design level. However, the overall safety margin is still the same for concrete tanks.

Similarly, both API and AWWA D-100 use allowable stress design for steel tanks. In calculation of design forces, AWWA D-100 uses a factor of 1.4 to convert seismic design forces from strength design level to allowable stress design level. However, API includes 1.4 factor in the response modification factors. As a result, the values of response modification factors are the same for AWWA D-100, ASCE 7 and 1/1.4 of API 650. It can be concluded that the overall safety margin is the same for steel tanks. It is also noted that the pedestal tower referred in D-100 is of steel plates, whereas ASCE 7, ACI 350.3 and ACI 371 refer to the concrete pedestal tower.

Table 2.1 Comparison of Response Modification Factors for Ground-Supported Tanks

| | | ASCE 7 | ACI 350.3 | | AWWA D-110* | |
		R	R_i	R_c	R_i	R_c
Concrete	Tanks with reinforced nonsliding base***	2	2.0	1.0	2.75	1
	Tanks with anchored flexible base	3.25	3.25	1.0	4.5	1
	Tanks with unanchored and unconstrained flexible base	1.5	1.5	1.0	2.0	1
Steel		ASCE 7	API 650**		AWWA D-100**	
		R	R_i	R_c	R_i	R_c
	Mechanically anchored	3	4	2	3.0	1.5
	Self-anchored	2.5	3.5	2	2.5	1.5

* AWWA D-110 is based on working stress design

** AWWA D-100 and API 650 are based on allowable stress design

*** ASCE 7 and AWWA D-110 define tanks with reinforced nonsliding base. ACI 350.3 defines fixed or hinged-base tanks

CHAPTER 3 DYNAMIC RESPONSE DUE TO FLUID STRUCTURE INTERACTION EFFECTS

3.1 Introduction

In this chapter, analytical - finite element models are used for dynamic analysis of liquid containing structures (LCS). The tank wall is modeled using the finite element method, while the analytical method is used to calculate the hydrodynamic pressure in liquid domain.

A dynamic analysis procedure including the sequential coupling analysis procedure is used for fluid-structure interaction (FSI). The sequential coupling analysis procedure is a coupling technique in which the two fields of fluid and structure are coupled by applying the results from the first analysis as loads or boundary conditions for the second analysis. As a result, the effect of flexibility of tank wall in determining the hydrodynamic pressures can be considered using the time history analysis.

The theories for calculation of hydrodynamic pressure in a rectangular container and sequential coupling analysis procedure used for dynamic analysis are presented in Section 3.2. Section 3.3 presents the dynamic analysis using the sequential coupling analysis procedure. The results of analysis are then compared with those obtained using the direct coupling analysis procedure based on the added mass and the current engineering practice. Both the modal superposition and time history methods (Bathe, 1996) are used for dynamic analysis. Based on a two-dimensional model of the tank wall, a tall tank and a shallow tank are used for verification. The results of analysis are compared with those obtained based on other studies and the current design code. It is shown that the base shear determined using the current design code is conservative. In summary, this chapter provides the basis for the simplified design method proposed in the following chapters.

3.2 Theories
3.2.1 Hydrodynamic Pressure
In this section, the theories for calculation of hydrodynamic pressure in a rectangular

container are presented. Two analytical methods based on the lamina fluid theory and velocity potential theory (Currie, 2002) are presented. The next section presents the lamina fluid theory which is used as the basis for Housner's model (Housner, 1957 and 1963). The velocity potential theory is presented subsequently in this chapter. Chen (2003) studied the hydrodynamic pressure based on the velocity potential theory in which the flexibility of tank wall was considered.

3.2.1.1 Lamina Fluid Method

Housner (1957 and 1963) used the lamina fluid theory to calculate the impulsive and convective hydrodynamic pressures in both rectangular and cylindrical tanks. The liquid was assumed to be incompressible and undergo small displacements.

Figure 3.1 shows a container with vertical sidewalls and a horizontal bottom that is symmetrical with respect to the vertical x-y and z-y planes, which are perpendicular to each other. The ground motion is in the x direction which generate fluid acceleration $\ddot{u}$ and $\ddot{v}$ in the x,y directions. It is assumed that the acceleration $\ddot{w}$ in z direction is so small that the ratio $\ddot{w}/\ddot{u}$ can be neglected. Physically this is equivalent to having the fluid restrained by thin vertical membranes, spaced dz apart, which force the fluid motion to take place in the x-y plane only. It is then sufficient to consider the impulsive pressures generated in a lamina of fluid.

Figure 3.1 shows a lamina of fluid of unit thickness in the x-y plane subjected to the horizontal ground acceleration $\ddot{u}_g$ in the x direction. The initial effect of this acceleration is to impart a horizontal acceleration to the fluid and also a vertical component of acceleration. This action of the fluid is similar to that which would result if the horizontal component of fluid velocity $\dot{u}$ were independent of the y coordinate. Or simply to imagine that the fluid is constrained by thin, massless, vertical membranes free to move in the x direction spaced a distance dx apart. When the walls of the container are given an acceleration, the membranes will be accelerated with the fluid, and the fluid will also be squeezed vertically with respect to the membranes.
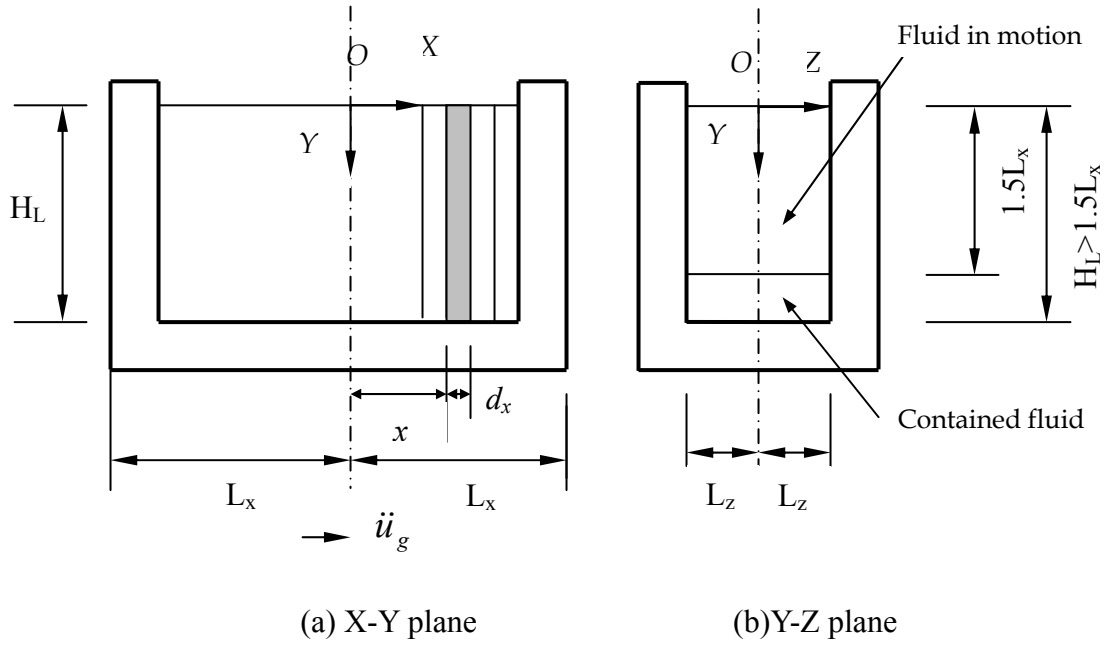
Figure 3.1 Lamina Fluid Model for Hydrodynamic Pressure (Housner, 1957)

It is worth noting that the equations discussed in the flowing part of this section are based on a unit thickness in the x-y plane.

Figure 3.2 shows the element taken from the analysis model as shown in Figure 3.1. It is noted that p is the dynamic impulsive pressure generated by the acceleration $\ddot{u}_g$ as shown in Figure 3.2.

The relation between the vertical velocity, $\dot{v}$, and the horizontal velocity, $\dot{u}$, can be determined from a mass balance on the lamina as follows:

[3.1] $\dot{v}dx + \dot{u}(H_L - y) = (\dot{u} + \frac{\partial \dot{u}}{\partial x}dx)(H_L - y)$ or

[3.2] $\dot{v} = (H_L - y)\frac{\partial \dot{u}}{\partial x}$

(a) Horizontal   (b) Vertical
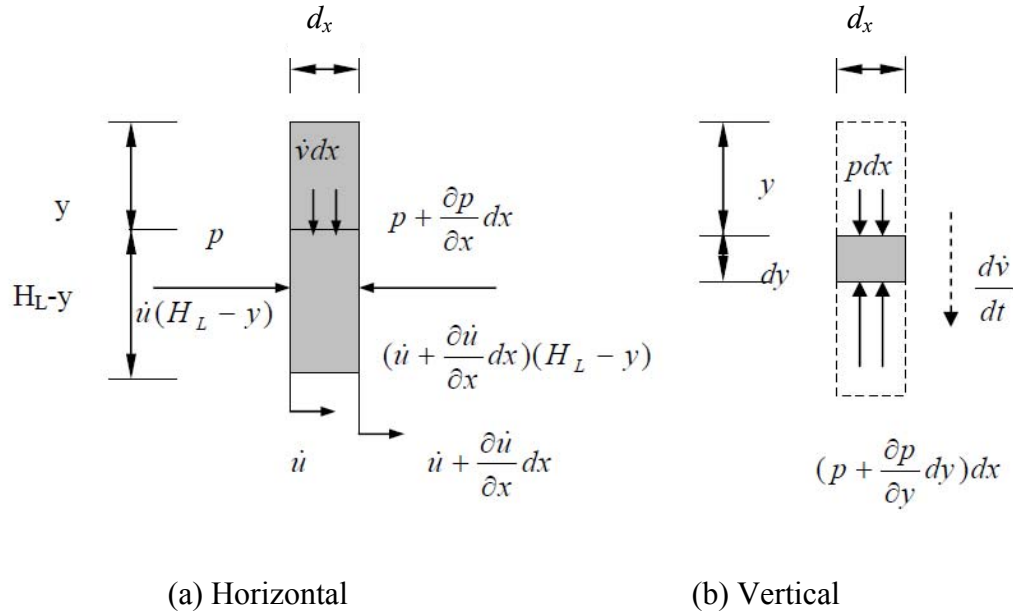
Figure 3.2 Element Used for Analysis of Hydrodynamic Pressure (Housner, 1957)

Differentiating Eq.3.2 with respect to time yields,

[3.3] $\qquad \ddot{v} = (H_L - y)\dfrac{\partial \ddot{u}}{\partial x}$

The equation of motion in the vertical direction, considering only forcers arising from accelerations of the fluid, can be derived by applying Newton's law to a differential element of fluid, as shown in Figure 3.2(b). The net force on the element in the y direction is as follows:

[3.4] $\qquad -\dfrac{\partial p}{\partial y}dxdy = \rho_l dxdy \dfrac{d\dot{v}}{dt}$ or

[3.5] $\qquad \dfrac{\partial p}{\partial y} = -\rho_l \dfrac{d\dot{v}}{dt} = -\rho_l(\dfrac{\partial \dot{v}}{\partial t} + \dfrac{\partial \dot{v}}{\partial x}\dfrac{dx}{dt} + \dfrac{\partial \dot{v}}{\partial y}\dfrac{dy}{dt})$

where ρ_l is liquid density, $\rho_l dxdy$ is the mass of the elements is and $d\dot{v}/dt$ is the acceleration.

It is noted that the velocities in x and y directions can be expressed as:

[3.6] $\dot{u} = dx / dt$

[3.7] $\quad \dot{v} = dy / dt$

Furthermore, since the fluid displacements are assumed to be small, the velocities, and hence the x and y derivatives of the velocities, are also small. Thus, the second and third terms on the right-hand side of Eq.3.5 are of higher order than the first term and can be assumed to be negligible, so that Eq.3.5 becomes

[3.8] $\qquad \dfrac{\partial p}{\partial y} = -\rho_l \dfrac{\partial \dot{v}}{\partial t}$

The total horizontal force on one membrane is

[3.9] $\qquad P = \displaystyle\int_0^{H_L} p\,dy$

Using Eq.3.3 in Eq.3.4 and integrating from zero to y, with the conditions that $p\,|_{y=0} = 0$,

[3.10] $\qquad p = -\rho_l \dfrac{\partial \ddot{u}}{\partial x} \displaystyle\int_0^y (H_L - \bar{y})d\bar{y} = -\rho_l H_L^2 [\dfrac{y}{H_L} - \dfrac{1}{2}(\dfrac{y}{H_L})^2]\dfrac{\partial \ddot{u}}{\partial x}$

The bars under the integral are simply to denote a dummy variable of integration. Substituting Eq.3.10 into Eq.3.9.

[3.11] $\qquad P = -\rho_l H_L^2 \dfrac{\partial \ddot{u}}{\partial x} \displaystyle\int_0^{H_L} [\dfrac{y}{H_L} - \dfrac{1}{2}(\dfrac{y}{H_L})^2]dy = -\dfrac{1}{3}\rho_l H_L^3 \dfrac{\partial \ddot{u}}{\partial x}$

The equation of motion in the x direction can be determined by applying Newton's law to the element of fluid shown in Figure 3.2(a). Neglecting the higher order terms, as before, which arise from the total time derivative of $\dot{u}$, the result can be written

[3.12] $\qquad \dfrac{\partial P}{\partial x} = -\rho_l H_L \ddot{u}$

Substituting P from Eq.3.11 into Eq.3.12,

[3.13] $\qquad \dfrac{\partial^2 \ddot{u}}{\partial x^2} - \dfrac{3}{H_L^2}\ddot{u} = 0$

Considering $\ddot{u}$ to be a dependent variable which is a function only of x, Eq.3.13 can be written as a total differential equation whose solution is

[3.14] $\qquad \ddot{u} = C_1 \cosh \sqrt{3}\,\dfrac{x}{H_L} + C_2 \sinh \sqrt{3}\,\dfrac{x}{H_L}$

Equations 3.10 and 3.14 determine the fluid pressures, and they are strictly applicable only when the surface is horizontal, as was assumed in the derivation of Eq.3.2. However, if consideration is restricted to small displacements of fluid, the equations can be used even when the surface of the fluid has been excited into motion; that is, Eq.3.10 gives the impulsive pressures, *p(t)*, corresponding to arbitrary acceleration, $\ddot{u}_g(t)$.

If the container is slender, having $H_L > 1.5L_x$ or $1.5L_z$, relatively better results are obtained by applying Eqs.3.10 and 3.11 to the upper portion, $h' = 1.5L_x$ or $1.5L_z$, of the fluid only and considering the fluid below this point to move as though it were completely constrained as shown in Figure 3.1(b). It can be imagined that a fixed rigid membrane separates the upper and lower portions of fluid at the plane y = h', so that the preceding equations apply to the upper portion of fluid if H_L is replaced by h'. The equation of motion in the horizontal direction for the constrained fluid below the vertical depth h' can be derived by the method used to obtain Eq.3.8. Assuming a known acceleration $\ddot{u}_g(t)$, Newton's law applied to a differential element gives

[3.15] $\dfrac{\partial p}{\partial x} = -\rho_l \ddot{u}(t)$

Integrating Eq.3.15 with the condition that from symmetry $p\,|_{x=0} = 0$

[3.16] $p = -\rho_l \ddot{u}(t)x$

The moment exerted on the horizontal membrane by the constrained fluid using Eq.3.16 is:

[3.17] $M = \int_{-1} pxdx = -\dfrac{2}{3}\rho_l \ddot{u}(t)L_x^3$

The moment exerted on the imaginary horizontal membrane by the fluid above, if Eqs.3.10 and 3.14 are solved using the appropriate boundary conditions, can be shown to be approximately equal to the value from Eq.3.16 for $h'=1.5L_x$. This implies that the generation of fluid velocity is restricted essentially to the fluid in the upper part of the slender container.

For a rectangular container, the boundary conditions for the impulsive pressures are

[3.18] $\ddot{u} = \ddot{u}_g(t)$ at $X = \pm L_x$

Then, Eq.3.14 becomes:

[3.19] $\ddot{u}(t) = \ddot{u}_g(t) \dfrac{\cosh \sqrt{3}(x/H_L)}{\cosh \sqrt{3}(L_x/H_L)}$

Substitute Eq.3.19 into Eqs.3.10 and 3.11

[3.20] $p = -\rho_l \ddot{u}_g(t) H_L [\dfrac{y}{H_L} - \dfrac{1}{2}(\dfrac{y}{H_L})^2] \dfrac{\sinh \sqrt{3}(x/H_L)}{\cosh \sqrt{3}(L_x/H_L)}$

[3.21] $P = -\rho_l \ddot{u}_g(t) \dfrac{H_L^2}{\sqrt{3}} \dfrac{\sinh \sqrt{3}(x/H_L)}{\cosh \sqrt{3}(L_x/H_L)}$

It can be seen that the effect of impulsive hydrodynamic pressure can be treated as the additional equivalent mass attached to the wall. The equivalent added mass m_i is:

[3.22] $\dfrac{m_i}{M_L} = \dfrac{\tanh \sqrt{3}(L_x/H_L)}{\sqrt{3}(L_x/H_L)}$

where M_L is the total mass of liquid.

The effective height at which the equivalent added mass m_i is applied is equal to 0.375H_L located above the tank bottom.

3.2.1.2 Velocity Potential Method

In velocity potential method, the fluid motion in a vessel can be treated as surface waves and the principle of such free-surface phenomena can be assumed as potential in nature. When fluid is excited, the gravity waves are generated on its free surface. The motion induced by the surface waves may be considered to be irrotational in most instances. Then the velocity vector may be expressed as the gradient of velocity potential $\phi(x, y, z, t)$ which must satisfy Laplace's equation:

[3.23] $\nabla^2 \phi = 0$

By linearizing the boundary condition, some analytical solution can be obtained, while the basic features of the flow are not destroyed. For the linearized boundary conditions, it is assumed that the waves in tanks are of small amplitude waves. It means that the surface wave function η is small compared with the wavelength λ and the liquid depth H_L. Thus, the high order term can be neglected.

Figure 3.3 shows the tank geometry of length $L = 2L_x$ and depth of fluid H_L for liquid in a two-dimensional rectangular tank. The mass density of fluid is ρ_l.
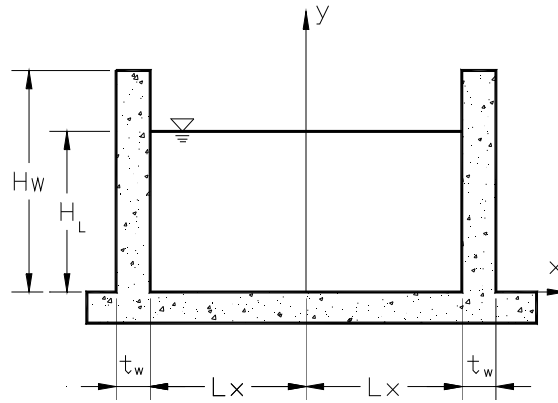
Figure 3.3 Geometry for Liquid in a Rectangular Tank

The satisfied partial different equation is that:

[3.24] $$\frac{\partial^2 \phi}{\partial x^2} + \frac{\partial^2 \phi}{\partial y^2} = 0$$

in which ϕ is the velocity potential function. The velocity components $v_x,\ v_y$ in the directions of x , y are that:

[3.25] $$v_x = \frac{\partial \phi}{\partial x}$$

[3.26] $$v_y = \frac{\partial \phi}{\partial y}$$

The hydrodynamic pressure is expressed by:

[3.27] $$p(x,y,t) = -\rho_l \frac{\partial \phi(x,y,t)}{\partial t}$$

The boundary conditions are:

[3.28] $$\frac{\partial^2 \phi}{\partial t^2}(x, H_L, t) + g \frac{\partial \phi}{\partial y}(x, H_L, t) = 0$$

[3.29] $$\frac{\partial \phi}{\partial y}(x, 0, t) = 0$$

[3.30] $$\frac{\partial \phi}{\partial x}(\pm L_x, y, t) = \dot{u}(t)$$

The velocity potential can be separated into two partial solutions in order to make it easier to solve the problem. ϕ_1 represents the impulsive pressure and ϕ_2 represents the convective pressure. The velocity potential equation and the corresponding boundary conditions are given:

[3.31] $$\phi_1 + \phi_2 = \phi$$

For ϕ_1, the boundary conditions are that:

[3.32] $$\frac{\partial \phi_1}{\partial t}(x, H_L, t) = 0$$

[3.33] $$\frac{\partial \phi_1}{\partial y}(x, 0, t) = 0$$

[3.34] $$\frac{\partial \phi_1}{\partial x}(\pm L_x, y, t) = \dot{u}(t)$$

For ϕ_2, the boundary conditions are that:

[3.35] $$\frac{\partial^2 \phi_2}{\partial t^2}(x, H_L, t) + g \frac{\partial \phi_2}{\partial y}(x, H_L, t) = -g \frac{\partial \phi_1}{\partial y}(x, H_L, t)$$

[3.36] $$\frac{\partial \phi_2}{\partial y}(x, 0, t) = 0$$

[3.37] $$\frac{\partial \phi_2}{\partial x}(\pm L_x, y, t) = 0$$

The main difference in boundary conditions between ϕ_1 and ϕ_2 is that the surface pressure is equal to zero in impulsive condition ϕ_1, while in convective condition ϕ_2 it is combined with the free surface and the effect due to the impulsive pressure.

Another difference is that the velocity of fluid at the surface of sidewall is equal to the velocity of flexible wall in impulsive condition ϕ_1, while in convective condition ϕ_2 it is equal to zero. Therefore, the effect of flexibility of tank wall is not significant to the calculation of convective hydrodynamic pressure and the assumption of rigid wall boundary condition used in the current design practice is still applicable for the convective pressure. As a result, the study is focused on the impulsive pressure.

The solution for the impulsive pressure in terms of ϕ_1 is as follows (Chen, 2003 Appendix A):

$$[3.38] \quad \phi_1 = -\sum_{n=1}^{\infty} \frac{2 \cdot \sinh(\lambda_{i,n} x)}{\lambda_{i,n} \cdot H_L \cdot \cosh(\lambda_{i,n} L_x)} \cos(\lambda_{i,n} y) \int_0^{H_L} \cos(\lambda_{i,n} y) \cdot \dot{u}(t) dy$$

Then the impulsive pressure can be obtained by the application of Eq.3.27, therefore:

$$[3.39] \quad p = -\rho_l \frac{\partial \phi_1}{\partial t} = \sum_{n=1}^{\infty} \frac{2 \cdot \rho_l}{\lambda_{i,n} \cdot H_L} \tanh(\lambda_{i,n} L_x) \cos(\lambda_{i,n} y) \int_0^{H_L} \cos(\lambda_{i,n} y) \, \ddot{u}(t) dy$$

where $\lambda_{i,n} = (2n-1)\pi/2H_L$. As the series in the above equation convergence very fast, only the first term of the series may be used for practical applications.

For the rigid tank $\ddot{u}(y,t) = \ddot{u}_g(t)$ which means that the acceleration along the height of the wall is the same as the ground acceleration, then Eq.3.39 can be simplified further as that:

$$[3.40] \quad p_{rigid} = \sum_{n=1}^{\infty} \frac{2 \cdot (-1)^i \cdot \rho_l}{\lambda_{i,n}^2 \cdot H_L} \tanh(\lambda_{i,n} \cdot L_x) \cdot \cos(\lambda_{i,n} \cdot y) \cdot \ddot{u}_g(t)$$

It is worth noting that this equation is the same as the hydrodynamic pressure equation for the rigid wall derived by Haroun (1984).

3.2.2 Analytical Model and Equation of Motion

Figure 3.4(a) shows a 3-D rectangular tank. The fluid filled in the tank is of height, H_L above the base. It is assumed that the liquid storage tank is fixed to the rigid foundation. A Cartesian coordinate system (x, y, z) is used with the origin located at the center of the tank base. Furthermore, it is assumed that the width of tank $2L_z$ is sufficiently large so

that the unit width of tank can represent the tank wall and the corresponding 2-D model is shown in Figure 3.4(b). It is worth noting that the parameters are defined per unit width of the tank wall in this section.

The governing equation of motion using the finite element method can be expressed by:

[3.41] $[M]\{\ddot{u}_r\} + [C]\{\dot{u}_r\} + [K]\{u_r\} = -[M]\{\ddot{u}_g\} + \{P\}$

where $\{u_r\}, \{\dot{u}_r\}, \{\ddot{u}_r\}$: Displacement, velocity and acceleration of rectangular wall relative to the ground.

$\{\ddot{u}_g\}$: Horizontal ground acceleration in x direction.

$\{P\}$: Hydrodynamic pressure on the wall surface.

$[K]$: Stiffness matrix of rectangular tank wall.

$[M]$: Mass matrix of rectangular tank wall.

$[C]$: Damping matrix of rectangular tank wall
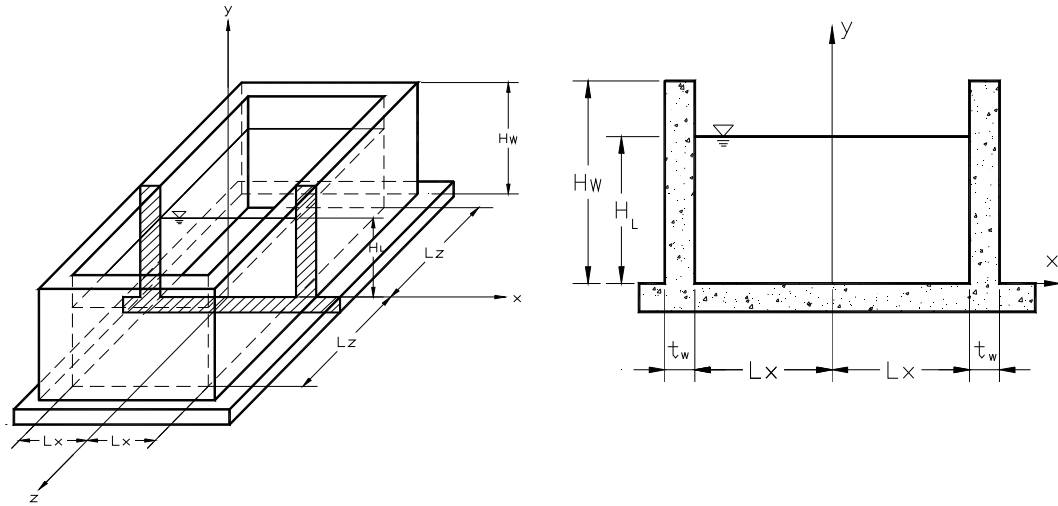
(a) 3 –D model of rectangular tank   (b) 2 –D model of rectangular tank

Figure 3.4 Schematic of Rectangular Tank

For dynamic analysis of fluid structure interaction, the hydrodynamic pressure can be coupled with the response of structure using either the direct or sequential coupling analysis procedure. In the direct coupling analysis procedure, the data are transferred or

shared between at each step of the solution. Due to the complexity of coupling the governing equations of fluid and structure into one equation, normally the added mass approach is used in which the hydrodynamic pressure is simplified as added mass of liquid attached to the structure for the direct coupling analysis procedure. It is worth noting that the added mass of liquid is not the real mass of liquid inside the tank. Rather, the added mass of liquid is a virtual mass which is similar to the inertial mass of tank wall representing the hydrodynamic pressure applied on the structure.

Compared to the direct coupling analysis procedure, the sequential coupling analysis procedure can solve the fluid structure interaction problem using the governing equation of fluid and structure separately and coupling the response in a sequential procedure. Figure 3.5 shows the finite element model used for the sequential method. The tank wall is considered as 2-D plane elements fixed at the base and free at the top. The hydrodynamic pressure is treated as the external force applied on the wall. The application of sequential coupling procedure will be discussed further in this chapter.
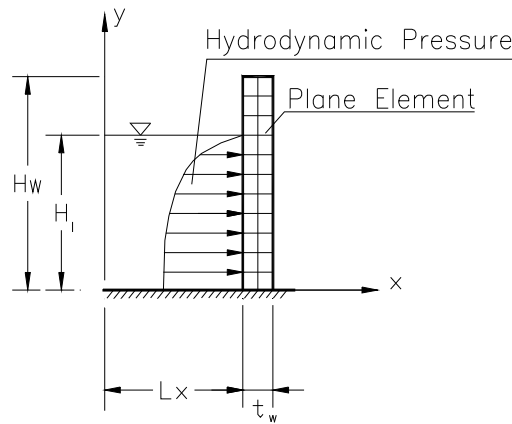
Figure 3.5 Finite Element Model of Rectangular Tank

3.2.3 Added Mass of Liquid due to Impulsive Hydrodynamic Pressure

In the direct coupling analysis procedure, the impulsive hydrodynamic pressure is usually applied on the wall using the added mass approach. This can be calculated using Housner's method. Using this approach, the added mass can be either lumped at the one node or distributed over the height of the wall. In terms of distributed mass this is

expressed as:

$$[3.42] \qquad m_i(y) = -\frac{\sqrt{3} \cdot \rho_l \cdot H_L}{2} \cdot [1 - \frac{y^2}{H_L^2}] \cdot \tanh(\frac{\sqrt{3} \cdot L_x}{H_L})$$

or using the lumped mass:

$$[3.43] \qquad M_{i,total} = \frac{\tanh[0.866(2L_x/H_L)]}{0.866(2L_x/H_L)} M_L$$

In Section 3.2.1.2, the velocity potential method was used to calculate the impulsive hydrodynamic pressure. As a result, the distribution of added mass of liquid can be derived from Eq.3.40 assuming that the walls are rigid. In this case, the distributed mass can be expressed as:

$$[3.44] \qquad m_i(y) = \sum_{n=1}^{\infty} \frac{2 \cdot (-1)^i \cdot \rho_l}{\lambda_{i,n}^2 \cdot H_L} \tanh(\lambda_{i,n} \cdot L_x) \cdot \cos(\lambda_{i,n} \cdot y)$$

and the lumped mass is expressed as:

$$[3.45] \qquad M_{i,total} = \sum_{n=1}^{\infty} \frac{2}{\lambda_{i,n}^3 \cdot H_L^2 \cdot L_x} \tanh(\lambda_{i,n} \cdot L_x) \cdot M_L$$

For the general condition, the hydrodynamic pressure in terms of added mass method can be expressed by:

$$[3.46] \qquad \{P\} = -[M_i]\{\ddot{u}\} = -[M_i]\{\ddot{u}_g + \ddot{u}_r\}$$

Therefore, the equation of motion with respect to the added mass method can be expressed by:

$$[3.47] \qquad [M_w + M_i]\{\ddot{u}_r\} + [C]\{\dot{u}_r\} + [K]\{u_r\} = -[M_w + M_i]\{\ddot{u}_g\}$$

3.2.4 Sequential Coupling Analysis Procedure

The sequential coupling analysis procedure is a coupling technique in which the two fields of fluid and structure are coupled by applying results from the first analysis as loads or boundary conditions for the second analysis.

In the sequential coupling analysis procedure, the hydrodynamic pressure can be treated as the external forces applied on the rectangular tank wall and the boundary conditions of rectangular tank wall determines the hydrodynamic pressure as shown in Eq.3.39.

Actually, the Eqs.3.39 and 3.41 must be solved simultaneously because the interaction between the rectangular tank wall and the hydrodynamic pressure occurs at the same time. Since it is difficult to solve the dynamic response of wall and hydrodynamic pressure directly from Eq.3.41, the sequential method can be applied to approximate it.

The sequential method is carried out by the following procedure. First the dynamic response of the flexible tank wall subjected to an earthquake is analyzed at time t. Then the hydrodynamic pressure is determined, which also includes the effect of flexibility of the tank wall. Finally, the hydrodynamic pressure is applied on the tank wall at the next time step $t+\Delta t$. The procedure is then repeated at each time step until the analysis is complete. Figure 3.6 shows in a flowchart format the procedure for analysis and Figure 3.7 shows how the data is transferred between rectangular tank wall and fluid.

The equation of motion in terms of sequential method at time t can be expressed as:

[3.48] $[M_w]\{\ddot{u}_{r,t}\}+[C]\{\dot{u}_{r,t}\}+[K]\{u_{r,t}\}=-[M_w]\{\ddot{u}_{g,t}\}-\{R_i(t-\Delta t)\}\{\ddot{u}_{g,t-\Delta t}+\ddot{u}_{r,t-\Delta t}\}$

where $R_i(t-\Delta t)$ is time dependent functional for impulsive hydrodynamic pressure.

If $R_i(t-\Delta t)$ is treated as $M_i(t-\Delta t)$, the time dependent function of added mass matrix related to hydrodynamic pressure at time t-Δt. Eq.3.48 becomes:

[3.49] $[M_w]\{\ddot{u}_{r,t}\}+[C]\{\dot{u}_{r,t}\}+[K]\{u_{r,t}\}=-[M_w]\{\ddot{u}_{g,t}\}-\{M_i(t-\Delta t)\}\{\ddot{u}_{g,t-\Delta t}+\ddot{u}_{r,t-\Delta t}\}$

It can be seen that if the impulsive hydrodynamic pressure due to the acceleration of the flexible wall is moved to right hand side, Eq.3.49 is similar to Eq.3.47 except that the effect of wall flexibility in calculating the hydrodynamic pressure is ignored. After the hydrodynamic pressure at time t-Δt is established, it is easily applied as external force on the tank wall to obtain the dynamic response of tank wall at time t. Furthermore, if the

time interval Δt is decreased in the calculations, the accuracy of final results may be improved. For this investigation, the time interval Δt used is 0.01 sec which is considered as sufficiently accurate for practical purposes.

```
┌─────────────────────────────────┐
│ Specify the Initial Condition of │
│ Rectangular Tank (solid wall)    │
└─────────────────────────────────┘
              ↓
┌─────────────────────────────────┐
│ Specify the Initial Condition of │
│ Fluid inside ({P}=0 at first     │
│ time step)                       │
└─────────────────────────────────┘
              ↓
┌─────────────────────────────────┐
│ Apply the Seismic Ground Motion  │
│ and Hydrodynamic Pressure on the │
│ Rectangular Tank Wall            │
└─────────────────────────────────┘
              ↓
┌─────────────────────────────────┐
│ Calculate the Structural Dynamic │
│ Response of Rectangular Tank Wall│
└─────────────────────────────────┘
              ↓
┌─────────────────────────────────┐
│ Transfer Dynamic Response of     │
│ Flexible Wall to Fluid Domain    │
└─────────────────────────────────┘
              ↓
┌─────────────────────────────────┐
│ Calculate the Hydrodynamic       │
│ Pressure (Boundary Condition Is  │
│ Defined by Dynamic Response of   │
│ Wall.)                           │
└─────────────────────────────────┘
              ↓
┌─────────────────────────────────┐
│ Input Ground Accerleration Record│
│ for the Next Time Step           │
└─────────────────────────────────┘
              ↓  No.
     yes   ┌─────────┐
           │   End   │
           └─────────┘
```

Figure 3.6 Procedure of Sequential Analysis

Vibration mode of flexible wall

| Rectangular Tank Wall | ────→ | Fluid |
| | ←──── | |

Hydrodynamic pressure
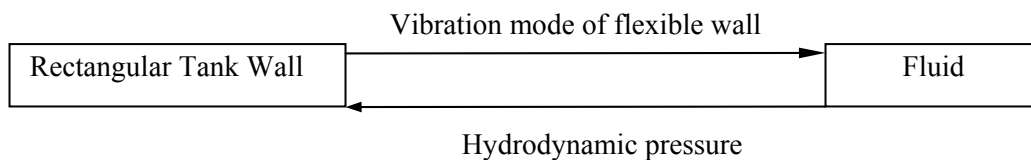
Figure 3.7 Transfer Data between Two Fields

The sequential coupling analysis procedure is incorporated into a computer software

package SAP IV (Bathe et al. 1974) using the subroutine called HYDRO (Chen, 2003) developed for this purpose. The direct step-by-step integration method is used because this method can calculate the displacement, velocity and acceleration of the flexible wall subjected to an earthquake at each time step. The impulsive hydrodynamic pressure is calculated by the subroutine HYDRO that considers the effect of flexibility of tank wall in the boundary condition.

3.3 Dynamic Analysis

3.3.1 Parameters for Analysis

In order to demonstrate the efficiency of the sequential method as described above, and to study the effect of different modeling approaches on dynamic response of storage tanks, two different rectangular tanks, a tall tank and a shallower tank are analyzed under a horizontal ground motion. The dimensions and properties of the tanks are as follows:

(1) Tall Tank:

$L_x = 9.8$ m $L_z = 28$ m $H_w = 12.3$ m $H_L = 11.2$ m $t_w = 1.2$ m $E_c = 20.776 \times 10^3$ MPa

(2) Shallow Tank:

$L_x = 15$ m $L_z = 30$ m $H_w = 6.0$ m $H_L = 5.5$ m $t_w = 0.6$ m $E_c = 26.44 \times 10^3$ MPa

Other properties for both tanks are:

$\rho_w = 2300$ kg/m^3 $\rho_l = 1000$ kg/m^3 $\nu = 0.17$

The first eight seconds of the North-South component of El-Centro accelerogram of 1940 Imperial Valley record (EERI, 1976) with a maximum peak ground acceleration of 0.33 g is used (Figure 3.8). This is the same rectangular tank that has been analyzed by Kim et al. (1996) in their investigations.

For two-dimensional analysis, a one-meter strip of tank wall is considered. The tank wall is discretized into two and 22 elements in the horizontal and vertical directions respectively using a 2-D plane rectangular element (see Figure 3.2).
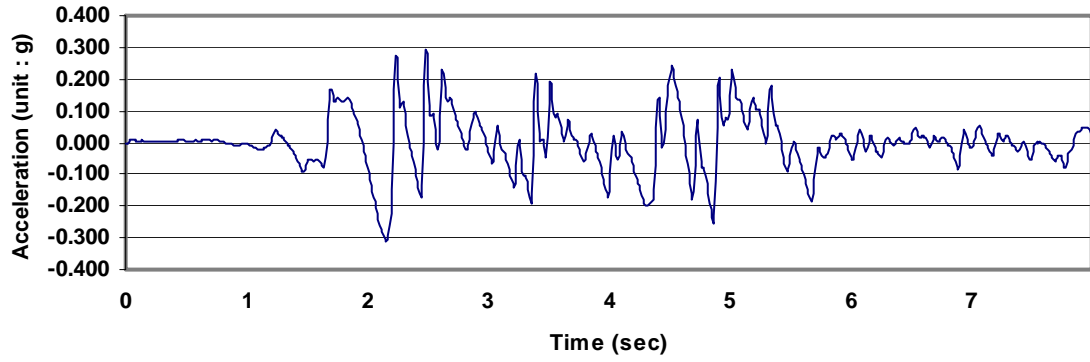
Figure 3.8 N-S Component of El Centro Accelerogram: 1940 Imperial Valley Earthquake

3.3.2 Analytical Models for Comparisons

For the full tank, six conditions referred to as models are considered. In both models 1 and 2, the impulsive mass of liquid is determined using the procedure described by Housner (1963). In model 1, both the impulsive mass and the inertial mass of wall is lumped at an equivalent height h, determined by:

$$[3.50] \quad h = \frac{M_i \cdot h_i + M_w \cdot h_w}{h_i + h_w}$$

where:

h_i = height from the base of the wall to the centre of gravity of the impulsive lateral force

h_w = height from the base of the wall to the centre of gravity of the tank wall

M_i = equivalent mass of impulsive component of stored liquid

M_w = equivalent mass of wall

In model 1, the period of vibration of the tank wall is determined using the classical approach for a cantilever wall. This represents a typical model for tank wall used in most of the current codes and standards for design of concrete liquid containing structures.

In model 2, the mass of wall is distributed over the height of the wall while the impulsive mass of the liquid is lumped at height h_i as given by Housner (1963). Model 3 is the same as model 2, but the impulsive mass is determined using the proposed method assuming rigid wall condition. In this case, the impulsive mass is lumped at height h_i. Models 4, 5

and 6 are also based on the proposed method. Model 4 is the same as model 3 except that the impulsive mass is distributed over the height of the wall. In model 5, the hydrodynamic impulsive pressure is determined considering the wall flexibility. This model is expected to provide the most accurate results among the six different models. Model 6 is the same as model 5 except that the wall is assumed to be infinitely rigid. In this case, the hydrodynamic pressure is determined assuming a rigid wall condition. In models 1 to 4, the mode superposition method is used for dynamic analysis while the last two models are analyzed using the direct step-by-step integration method including the sequential coupling analysis procedure.

In this study, two types of dynamic analysis procedures are used to investigate the dynamic response of liquid storage tanks, the mode superposition method with the added mass approach and direct step-by-step integration method, which includes the sequential method. The unconditional stable Wilson θ method is used for direct integration.

Damping ratio for all cases is assumed to be 5% of critical. The Rayleigh damping $[C] = \alpha[M] + \beta[K]$ is used in the direct step-by-step integration method. The values α and β are determined using the procedure as described by Bathe et al. (1974) which are as follows:

[3.51] $\quad \alpha = \dfrac{4\pi(T_j \cdot \lambda_j - T_i \cdot \lambda_i)}{T_j^2 - T_i^2}$

[3.52] $\quad \beta = \dfrac{T_i \cdot T_j \cdot (T_j \cdot \lambda_j - T_i \cdot \lambda_i)}{T_j^2 - T_i^2}$

where λ_n is proportion of critical damping in the n-th mode, and T_n is period of vibration in the nth mode. Only the first two modes of vibration are considered in this study.

3.3.3 Results of Analysis
3.3.3.1 Tall Tank
A summary of the analytical results for all models is listed in Table 3.1. This is in terms of the maximum base shear and top displacement during the time history analysis. Peak

values corresponding to two different times at which maximum values occur are shown. These results indicate that the response is considerably less for model 5 as compared to the other models. The results also show that the values obtained from the proposed model assuming rigid boundary conditions (model 3) are similar to that of Housner's model (model 2).

From calculation results, it is observed that for model 1, the results in particular base shear is much higher than those observed in other models. This gives an indication that the procedure adopted in the codes and standards are too conservative.

It is observed that the results of model 2 and 3 are very similar. The difference in results between these two models does not exceed 10%.

For model 4, although the period of first two modes are not much different from models 2 and 3, there is a major difference in the values of the base shear which is less for model 4. This effect is due to the mass distribution. In these three models (model 2, 3 and 4), the rigid wall boundary condition is used to calculate the impulsive pressure, which is approximated by added masses placed on the wall.

The time history analysis together with the sequential coupling analysis procedure is applied to model 5. In this case, the effect of flexibility of wall on hydrodynamic pressure and tank wall is considered. The base shear is increased due to the flexibility of tank wall as compared to model 4 but the maximum displacement is relatively smaller. From calculation results, it is observed that the results obtained in terms of base shear using the lumped mass models (model 1, 2 and 3) are higher than those obtained for distributed mass models for the liquid. However, the peak values of displacement and base shear occur almost at the same time during the time history analysis.

Figure 3.9 shows acceleration and hydrodynamic pressure distribution along the height of wall at the time the maximum base shear is reached. The hydrodynamic pressure calculated using the flexible wall boundary condition is significantly larger than that of

rigid wall as shown in Figure 3.9(b).

Model 6, which is considered for a special case, represents an infinitely rigid wall. In this case, the wall moves with the ground motion. The maximum base shear is less than that in the flexible wall (model 5) as expected.

3.3.3.2 Shallow Tank

The same analytical procedures as discussed above for the tall tank (full) are carried out for the shallow tank. The results of analysis are summarized in Table 3.2. Results of analysis show that the general trend in the behavior of the shallow tank is very similar to the tall tank. In particular, a comparison in the results in terms of base shear between models 1 and 5 indicates that this value is significantly higher for model 1. In this case, the difference is 195% as compared to 230% observed in the tall tank.

(a) Acceleration of Wall   (b) Hydrodynamic Pressure
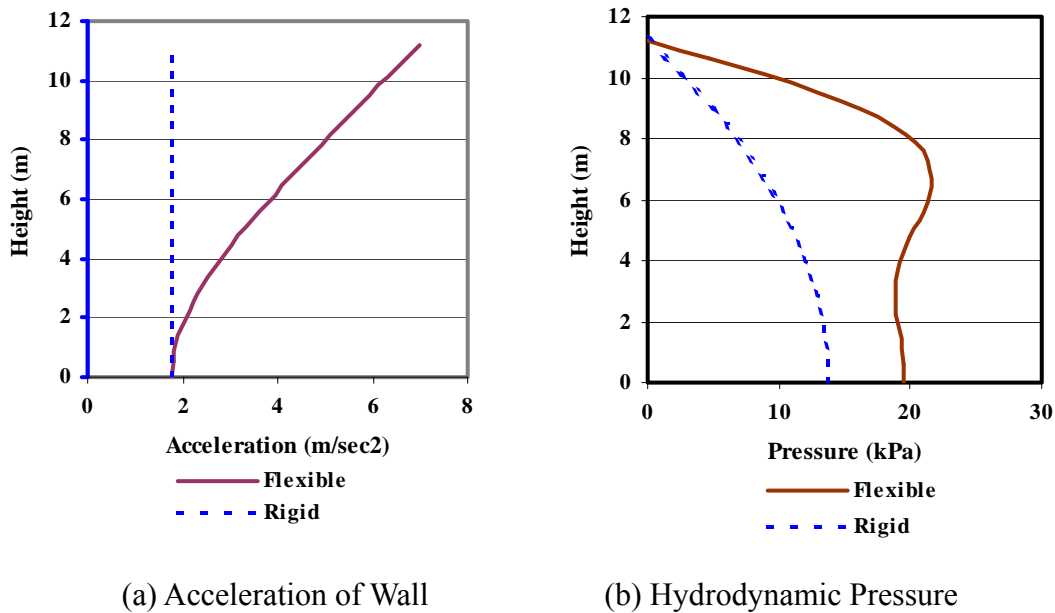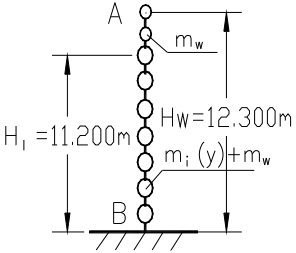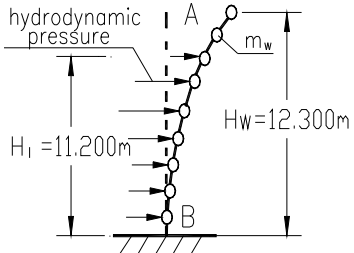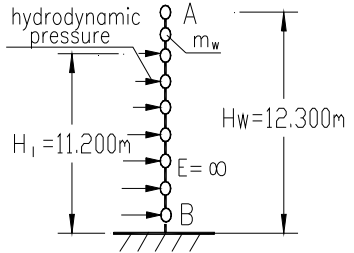
Figure 3.9 Dynamic Response of Wall and Impulsive Pressure Distribution at the Time of Maximum Response (Tall Tank and Model 5)

Table 3.1 Summary of Dynamic Response of Tall Tank

Model		Model 1 (Housner)		Model 2 (Housner)		Model 3 (Proposed)	
Fluid	Impulsive Component	Lumped		Lumped		Lumped	
	Boundary Condition	Rigid		Rigid		Rigid	
Wall	Inertial Mass	Lumped		Distributed		Distributed	
	Wall Type	Flexible		Flexible		Flexible	
Analysis Method		Mode Superposition Method		Mode Superposition Method		Mode Superposition Method	
Schematic of Model							
Period (sec)		$T_1 = 0.2353$ $T_2 = 0$		$T_1 = 0.2956$ $T_2 = 0.08088$		$T_1 = 0.2923$ $T_2 = 0.07880$	
Damping Ratio		5%		5%		5%	
t_{max} (sec)		2.56	4.30	2.63	4.52	2.63	4.51
Base Shear F_B (kN)		790.0	423.8	433.8	312.8	406.0	262.3
Displacement d_A (mm)		34.73	18.63	34.54	24.97	33.24	21.54
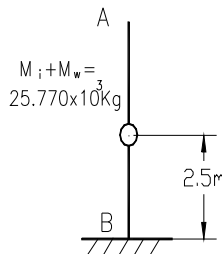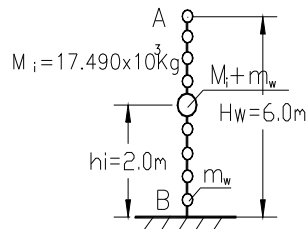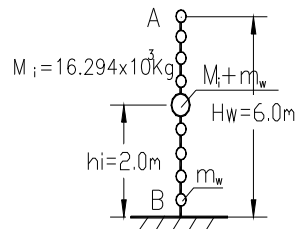
* t_{max} : time at which the first two maximum values of dynamic response are reached.

60

Table 3.1 Summary of Dynamic Response of Tall Tank – (continued)

Model		Model 4 (Proposed)		Model 5 (Proposed)		Model 6 (Proposed)	
Fluid	Impulsive Component	Distributed		Distributed		Distributed	
	Boundary Condition	Rigid		Flexible		Rigid	
Wall	Inertial Mass	Distributed		Distributed		Distributed	
	Wall Type	Flexible		Flexible		Rigid	
Analysis Method		Mode Superposition Method		Direct Step-by-Step Integration Method and Sequential Method		Direct Step-by-Step Integration Method and Sequential Method	
Schematic of Model							
Period (sec)		$T_1 = 0.3413$ $T_2 = 0.06365$		-- --		-- --	
Damping Ratio		5%		$\alpha=1.552, \beta=0.0027$		$\alpha=0, \beta=0$	
t_{max} (sec)		2.69	4.76	2.65	4.56	2.16	5.030
Base Shear F_B (kN)		314.8	290.0	319.0	338.1	284.0	202.9
Displacement d_A (mm)		32.68	30.11	23.04	26.90 (t=4.57sec)	0	0
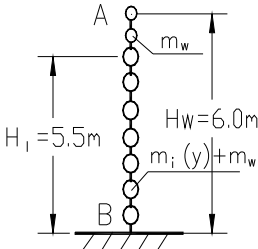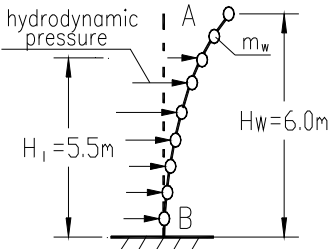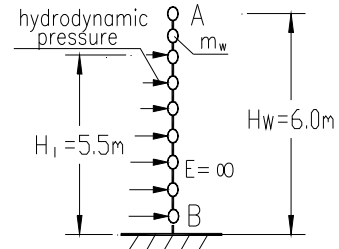
* t_{max} : time at which the first two maximum values of dynamic response are reached.

Table 3.2 Summary of Dynamic Response of Shallow Tank

Model	Model 1 (Housner)			Model 2 (Housner)			Model 3 (Proposed same as Haroun)		
Fluid — Impulsive Component	Lumped			Lumped			Lumped		
Fluid — Boundary Condition	Rigid			Rigid			Rigid		
Wall — Inertial Mass	Lumped			Distributed			Distributed		
Wall — Wall Type	Flexible			Flexible			Flexible		
Analysis Method	Mode Superposition Method			Mode Superposition Method			Mode Superposition Method		
Schematic of Model	$M_i + M_w = 25.770 \times 10^3 Kg$, 2.5m			$M_i = 17.490 \times 10^3 Kg$, $M_i + m_w$, $H_W = 6.0m$, $h_i = 2.0m$, m_w			$M_i = 16.294 \times 10^3 Kg$, $M_i + m_w$, $H_W = 6.0m$, $h_i = 2.0m$, m_w		
Period (sec)	$T_1 = 0.1055$ $T_2 = 0$			$T_1 = 0.1217$ $T_2 = 0.03503$			$T_1 = 0.1208$ $T_2 = 0.03430$		
Damping Ratio	5%			5%			5%		
t_{max} (sec)	2.51	3.54	4.54	2.65	3.55	5.06	2.65	3.55	5.06
Base Shear F_B (kN)	153.2	151.7	142.9	121.5	106.8	97.1	113.9	99.5	92.4
Moment M_B (kNm)	372.9	369.3	347.8	381.5	335.4	305.0	362.9	317.3	294.4
Displacement d_A (mm)	5.09	5.04	4.74	6.93	6.09	5.54	6.65	5.81	5.39

* t_{max} : the time at which the first three maximum values of dynamic response are reached

Table 3.2 Summary of Dynamic Response of Shallow Tank (continue)

Model		Model 4 (Proposed)			Model 5 (Proposed)			Model 6 (Proposed)		
Fluid	Impulsive Component	Distributed			Distributed			Distributed		
	Boundary Condition	Rigid			Flexible			Rigid		
Wall	Inertial Mass	Distributed			Distributed			Distributed		
	Wall Type	Flexible			Flexible			Rigid		
Analysis Method		Mode Superposition Method			Direct Step-by-Step Integration Method and Sequential Method			Direct Step-by-Step Integration Method and Sequential Method		
Schematic of Model										
Period (sec)		$T_1 = 0.1476$ $T_2 = 0.02798$			-- --			-- --		
Damping Ratio		5%			$\alpha=3.579, \beta=0.0012$			$\alpha=0, \beta=0$		
t_{max} (sec)		2.69	3.59	4.95	2.28	3.57	4.56	2.16	3.40	4.87
Base Shear F_B (kN)		73.2	78.9	74.3	78.7	54.6	64.6	74.5	49.2	59.4
Moment M_B (kNm)		278.2	300.0	282.4	241.8	167.8	179.2	179.5	119.2	143.0
Displacement d_A (mm)		5.48	5.91	5.56	4.54	3.15	3.25	0	0	0

* t_{max} : the time at which the first three maximum values of dynamic response are reached

3.3.4 Comparison with other Results

Kianoush et al. (2006) and Ghaemian et al. (2005) applied the staggered method to solve the coupled liquid storage tank problems in three-dimensional space. The staggered method is a partitioned solution procedure that can be organized in terms of sequential execution of a single-field analyser. The scheme of staggered method is to find the displacement and hydrodynamic pressure at the end of the time increment $i + 1$, given the displacement and hydrodynamic pressure at time i.

One tank that is similar to the shallow tank used in this study was analyzed using the staggered method as shown in the study of Kianoush et al. (2006). The dimensions and properties of the considered concrete rectangular LCS and the liquid are as follows:

$L_x = 20$ m $H_w = 6.5$ m $H_L = 6.0$ m $t_w = 0.5$ m $E_c = 26.64 \times 10^3$ MPa $v = 0.17$
$\rho_w = 23.537$ kN/m^3 $\rho_l = 9.807$ kN/m^3

Figures 3.10 and 3.11 show the dynamic response of tanks due to the horizontal excitation considering the walls flexibility (Kianoush et al. 2006). The absolute maximum values of the resulting base shear and base moment are 107 kN/m and 385 kNm/m, respectively.
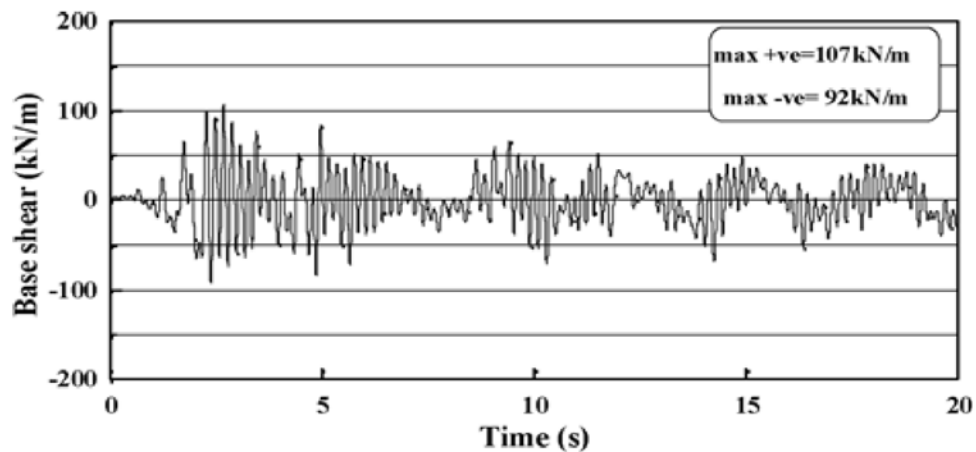
Figure 3.10 Time History of Base Shear Resulting from the Proposed Method due to Horizontal Excitation (Kianoush et al. 2006)
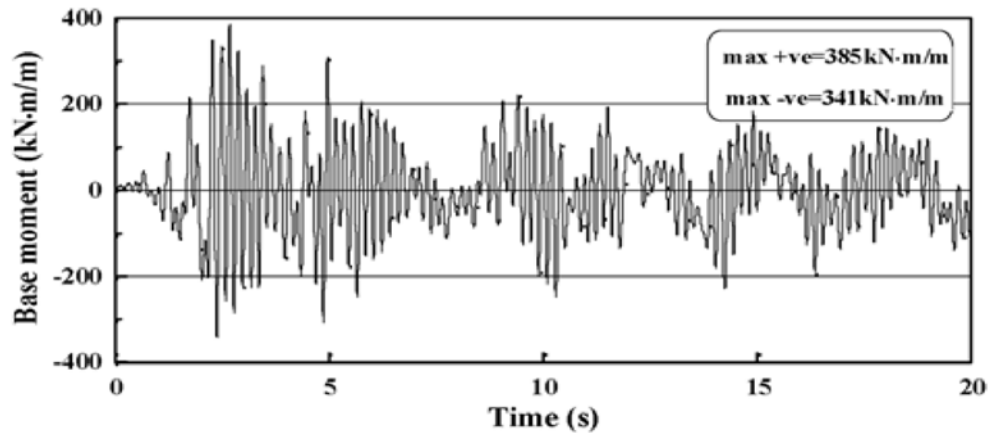
Figure 3.11 Time History of Base Moment Resulting from the Proposed Method due to Horizontal Excitation (Kianoush et al. 2006)

As indicated in Table 3.2, the maximum values of base shear and base moment for the shallow tank using the sequential method (Model 5) are 78.7 kN/m and 241.8 kNm/m, respectively. The results are similar to those obtained using the staggered method in the study of Kianoush et al. (2006) for the similar containers.

It is worth noting that in the study of Kianoush et al. (2006) the ground motions are scaled in such a way that the peak ground acceleration in the horizontal component is 0.400g based on the recorded for the 1940 El-Centro earthquake in their studies. However, the PGA of ground motions used for the time history analysis and sequential coupling method in this study is 0.33g. In addition, Kianoush et al. (2006) and Ghaemian et al. (2005) concluded that the current practice overestimates the response of container which is consistent with the conclusions in this study.

3.4 Conclusions

The dynamic response of liquid storage tanks is studied in this chapter. The sequential coupling analysis procedure is applied for fluid structure interaction. The hydrodynamic pressures are treated as external forces rather than the added mass. The advantage of the model using the sequential coupling analysis procedure is that it can consider the effect of the flexibility of the wall in the calculation of hydrodynamic pressures during the time history analysis.

To demonstrate the efficiency of the proposed finite element – analytical model using the sequential method, the response of rectangular tanks is studied based on a time-history analysis. The study shows that the dynamic response of liquid storage tanks calculated using the current design codes and standards is too conservative. It is concluded that the effect of the flexibility of the tank wall should be considered in the calculation of hydrodynamic pressures in concrete rectangular tanks.

CHAPTER 4 FINITE ELEMENT ANALYSIS

4.1 Introduction

This chapter presents the theories of finite element analysis used for dynamic analysis of concrete rectangular LCS. The results of analysis based on a full finite element model are used to verify the proposed simplified method as will be discussed later in Chapter 5.

The general purpose finite element analysis software ANSYS$^{®}$ is used for dynamic analysis for its analysis capabilities in structural mechanics, fluid dynamic and multiphysics simulation. The dynamic response of concrete liquid storage tanks can be defined as a multiple physics problem including structural transient analysis of tank wall and fluid dynamic analysis of liquid inside tank. In this chapter, structural modeling of tank wall using transient structural analysis system is described first.

Advanced computational fluid dynamics (CFD) analysis techniques are used to model the dynamic response of fluid and analyze the fluid structure interaction effect. The fluid flow theory is used to simulate the impulsive pressure based on ANSYS$^{®}$ CFX analysis system. The fluid flow theory and the boundary conditions in simulation of impulsive hydrodynamic pressure are discussed. The coupling analysis method for fluid structure interaction is also described. Finally, the dynamic response of a tall tank is presented. It is worth noting that since the purpose of this study is mainly to compare the impulsive pressure using different models, the convective pressure is not included in the finite element model for fluid domain. The effect of convective pressures using finite element method is described by Ghaemmaghami (2010).

It is also noted that since finite element method is applied in both structural and liquid domains using ANSYS$^{®}$, such analytical model is defined as full finite element model.

However, only the tank wall was analyzed based on finite element method in Chapter 3. The impulsive hydrodynamic pressure was calculated based on the analytical method and input into the structural model as loads in dynamic analysis. Therefore, the analytical models discussed in Chapter 3 such as Models 4 and 5 are defined as analytical - finite element models.

4.2 Theories

4.2.1 Structural Modeling of Tank

In this section, the structural modeling of tank wall in ANSYS$^{®}$ is presented. The transient structural analysis system is used to model the structural part of tank.

In Chapter 3, the concrete tank was modeled using two dimensional plane strain elements. Because a certain volume of liquid is required in fluid domain for ANSYS$^{®}$ CFX analysis system, the entire tank and liquid system is modeled using three-dimensional elements. Therefore, a 3-D solid element SOLID185 which has 8 nodes with three degrees of freedom at each node is used for modeling tank wall. It is noted that only a one-meter strip of tank wall is considered in the dynamic analysis. Therefore, the analysis is still based on 2-D model which is consistent with the study discussed in Chapter 3.

Figure 4.1 shows a 3-D model of tank with unit strip. It is assumed that the liquid storage tank is fixed to the rigid foundation. It is worth noting that only one sidewall that is fixed at the bottom is used to obtain the dynamic response of tank. This is because the dynamic response of tank wall is determined based on the ground acceleration which is applied as load to the tank wall. Therefore, the tank wall needs to be restrained at its boundaries to obtain reaction forces. The other sidewall is modeled as a massless rigid wall which is used to simulate the boundary conditions for fluid domain. The boundary condition of liquid domain correspondent to wall and base slab will be discussed later.
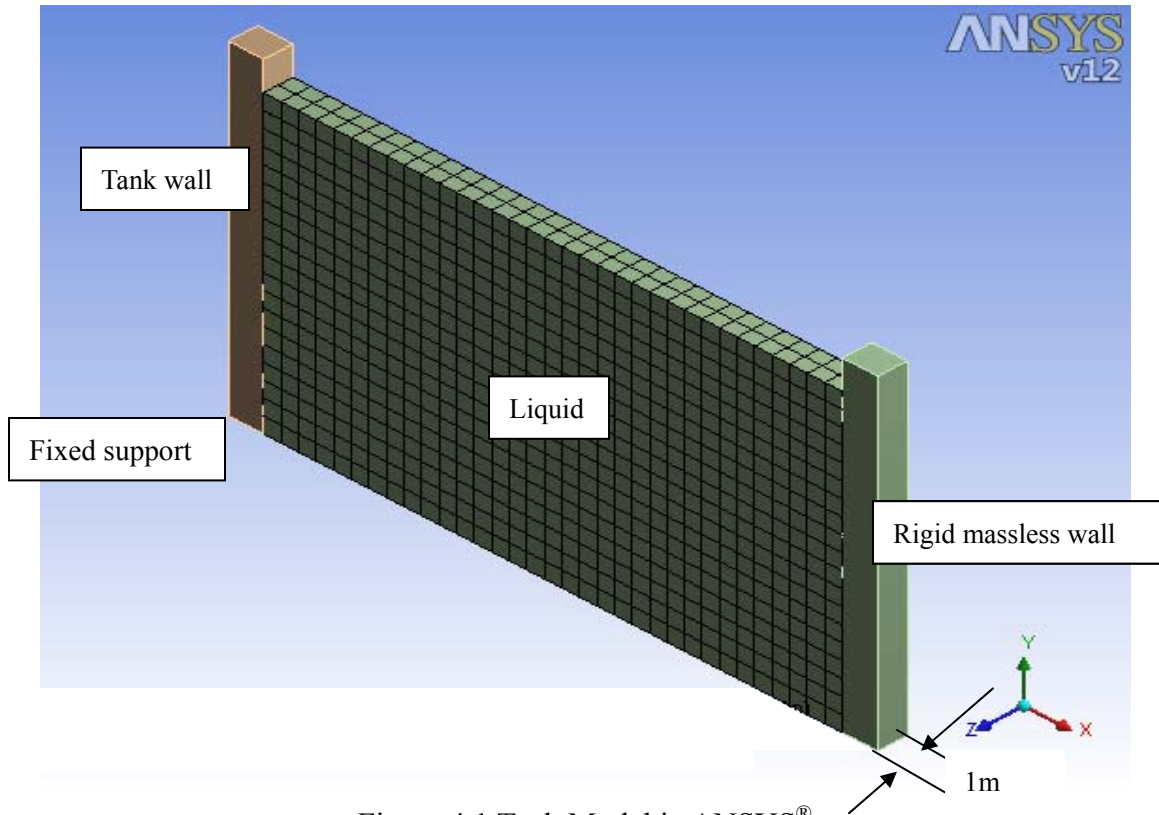
Figure 4.1 Tank Model in ANSYS®

4.2.2 Fluid Dynamic Analysis

ANSYS® CFX analysis system is used for fluid dynamic analysis of liquid inside tank. The fluid flow theory is applied in dynamic analysis. The fluid flow theory is based on the laws of conservation of mass, momentum, and energy.

In this study, the liquid is incompressible and the fluid flow is laminar flow without turbulence. The governing equations of continuity, mesh displacement and momentum are considered in the analysis. The 3-D fluid element FLUID142 is used in the fluid domain. It is noted that only the theories that are applied for dynamic analysis of concrete rectangular LCS are summarized in this section. More details regarding ANSYS® CFX analysis system can be found in the ANSYS® User Manual (ANSYS®, 2009).

4.2.2.1 Fluid Flow Theory

Currently, the techniques of computational fluid dynamics (CFD) are widely used in study of fluid dynamics problems. In this study, the fluid flow theory is used to calculate the impulsive hydrodynamic pressure in fluid domain. The fluid flow theory is incorporated into the ANSYS$^®$ FLOTRAN CFD analysis tools which can analyze 2-D and 3-D fluid flow field. It is worth noting that as compared to the acoustic theory used in ANSYS$^®$, the fluid flow theory is more suitable for modeling the impulsive pressure based on the boundary conditions of fluid domain discussed in Chapter 3 using the velocity potential theory. The acoustic theory can be used for dynamic analysis of wave problems in liquid domain and is suitable for modeling the convective pressure.

The fluid flow theory is based on the laws of conservation of mass, momentum, and energy and discussed as follows.

Continuity Equation

Based on the law of conservation of mass, the continuity equation is that:

[4.1] $$\frac{\partial \rho}{\partial t} + \frac{\partial (\rho v_x)}{\partial x} + \frac{\partial (\rho v_y)}{\partial y} + \frac{\partial (\rho v_z)}{\partial z} = 0$$

where v_x, v_y and v_z are the components of the velocity vector in the x, y and z directions, respectively; ρ is fluid density; x, y, z are the global Cartesian coordinates and t is time.

The rate of change of density can be replaced by the rate of change of pressure and the rate at which density changes with pressure P:

[4.2] $$\frac{\partial \rho}{\partial t} = \frac{\partial \rho}{\partial P} \frac{\partial P}{\partial t}$$

The evaluation of the derivative of the density with respect to pressure can be obtained from the equation of state for an ideal gas as follows:

[4.3]
$$\rho = \frac{P}{RT} \Rightarrow \frac{\partial \rho}{\partial P} = \frac{1}{RT}$$

where R is the gas constant and T is temperature.

For incompressible fluid, an infinite value can be specified for the bulk modulus β_{bulk} which is defined as follows:

[4.4]
$$\frac{\partial \rho}{\partial P} = \frac{1}{\beta_{bulk}}$$

The infinite value for β_{bulk} implies that for a perfectly incompressible fluid, pressure waves will travel infinitely fast throughout the entire problem domain, e.g. a change in mass flow will be seen downstream immediately.

Momentum Equation

In a Newtonian fluid, the relationship between the stress and rate of deformation of the fluid (in index notation) is:

[4.5]
$$\tau_{ij} = -P\delta_{ij} + \mu(\frac{\partial u_i}{\partial x_j} + \frac{\partial u_j}{\partial x_i}) + \delta_{ij}\lambda \frac{\partial u_i}{\partial x_i}$$

where: τ_{ij} = stress tensor

u_i = orthogonal velocities ($u_1 = v_x$, $u_2 = v_y$, $u_3 = v_z$)

μ = dynamic viscosity

λ = second coefficient of viscosity

The final term, the product of the second coefficient of viscosity and the divergence of the velocity, is zero for a constant density fluid and is considered small enough to be neglected in a compressible fluid.

Equation 4.5 can transform the momentum equations to the Navier-Stokes equations as follows:

$$[4.6] \quad \frac{\partial \rho v_x}{\partial t} + \frac{\partial (\rho v_x v_x)}{\partial x} + \frac{\partial (\rho v_y v_x)}{\partial y} + \frac{\partial (\rho v_z v_x)}{\partial z} = \rho g_x - \frac{\partial P}{\partial x}$$
$$+ R_x + \frac{\partial}{\partial x}(\mu_e \frac{\partial v_x}{\partial x}) + \frac{\partial}{\partial y}(\mu_e \frac{\partial v_x}{\partial y}) + \frac{\partial}{\partial z}(\mu_e \frac{\partial v_x}{\partial z}) + T_x$$

$$[4.7] \quad \frac{\partial \rho v_y}{\partial t} + \frac{\partial (\rho v_x v_y)}{\partial x} + \frac{\partial (\rho v_y v_y)}{\partial y} + \frac{\partial (\rho v_z v_y)}{\partial z} = \rho g_y - \frac{\partial P}{\partial y}$$
$$+ R_y + \frac{\partial}{\partial x}(\mu_e \frac{\partial v_y}{\partial x}) + \frac{\partial}{\partial y}(\mu_e \frac{\partial v_y}{\partial y}) + \frac{\partial}{\partial z}(\mu_e \frac{\partial v_y}{\partial z}) + T_y$$

$$[4.8] \quad \frac{\partial \rho v_z}{\partial t} + \frac{\partial (\rho v_x v_z)}{\partial x} + \frac{\partial (\rho v_y v_z)}{\partial y} + \frac{\partial (\rho v_z v_z)}{\partial z} = \rho g_z - \frac{\partial P}{\partial z}$$
$$+ R_z + \frac{\partial}{\partial x}(\mu_e \frac{\partial v_z}{\partial x}) + \frac{\partial}{\partial y}(\mu_e \frac{\partial v_z}{\partial y}) + \frac{\partial}{\partial z}(\mu_e \frac{\partial v_z}{\partial z}) + T_z$$

where g_x, g_y, g_z = components of acceleration due to gravity

μ_e = effective viscosity

R_x, R_y, R_z = distributed resistances

T_x, T_y, T_z = viscous loss terms

For a laminar case, the effective viscosity is merely the dynamic viscosity which is a fluid property. The terms R_x, R_y, R_z represent any source terms.

The terms T_x, T_y, T_z are viscous loss terms which are eliminated in the incompressible, constant property case. The order of the differentiation is reversed in each term, reducing the term to a derivative of the continuity equation, which is zero.

Incompressible Energy Equation

The conservation of energy can be expressed in terms of the static temperature for low speed incompressible analysis of liquid in tanks. As a result, there is no energy dissipated from the system due to the static temperature.

Fluid Element

The laws of conservation of mass, momentum, and energy as mentioned above are expressed in terms of partial differential equations which can be discretized with a finite element. From the element library of ANSYS®, the fluid element FLUID142 is the one that can be used for 3D modeling of the fluid medium based on the fluid flow theory. The geometry, node locations, and the coordinate system for this element are shown in Figure 4.2.
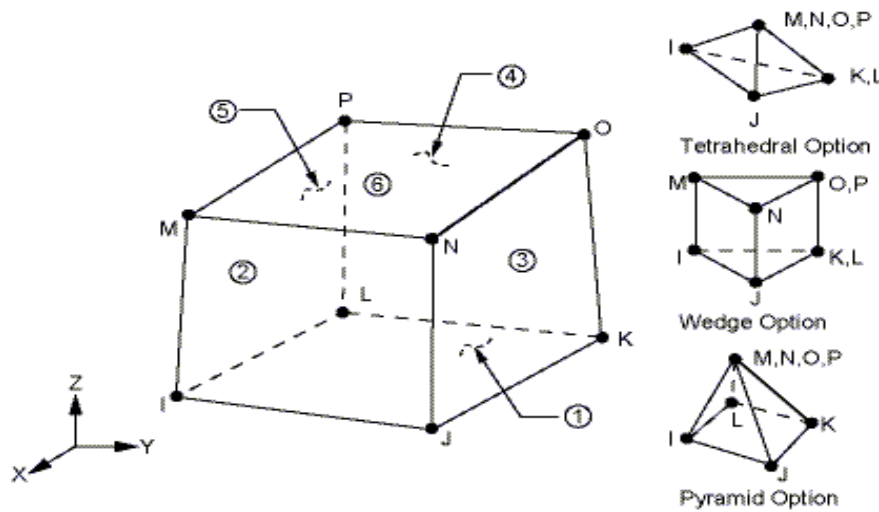
Figure 4.2 FLUID142 Geometry

The element FLUID142 can be used for the calculation of 3-D velocity and pressure distributions in a single phase, namely Newtonian fluid. It is assumed that the fluid is laminar and incompressible in the analysis which means the velocity field is very ordered and smooth, as it is in highly viscous, slow-moving flows.

FLUID142 can model transient or steady state fluid/thermal systems that involve fluid and/or non-fluid regions. The conservation equations for viscous fluid flow and energy are solved in the fluid region, while only the energy equation is solved in the non-fluid region. It is worth noting that FLUID142 can be used in a fluid solid interaction analysis using the fluid-solid interaction flag.

For the ANSYS$^{\circledR}$ FLOTRAN CFD elements, the velocities are obtained from the conservation of momentum principle, and the pressure is obtained from the conservation of mass principle. A segregated sequential solver algorithm is used; that is, the matrix system derived from the finite element discretization of the governing equation for each degree of freedom is solved separately. The flow problem is nonlinear and the governing equations are coupled together. The sequential solution of all the governing equations, combined with the update of any temperature- or pressure-dependent properties, constitutes a global iteration. The number of global iterations required to achieve a converged solution may vary considerably, depending on the size and stability of the problem.

Pressure

For fluid flow analysis in ANSYS$^{\circledR}$, the algorithm solves for a relative pressure rather than an absolute pressure for better numerical accuracy (ANSYS$^{\circledR}$, 2009).

4.2.2.2 Boundary Conditions

The input of boundary conditions for the impulsive pressure in liquid domain are based on the velocity potential method as described in Chapter 3. The boundary condition for the surface pressure is equal to zero and the velocity of fluid at the surface of sidewall is equal to the absolute velocity of flexible wall for impulsive hydrodynamic pressure.

The boundary condition for the surfaces of liquid domain parallel to ground motion is a symmetry plane boundary condition. In ANSYS$^{\circledR}$ CFX, the symmetry plane boundary condition imposes constraints that 'mirror' the flow on either side of it (ANSYS$^{\circledR}$, 2009). Since the 3-D fluid element FLUID142 is used in analysis, by specifying the symmetry plane boundary condition on the two side surfaces parallel to ground motion, the liquid domain can be treated as a 2-D model.

In the fluid domain, the boundary conditions at the bottom and top surfaces are specified as free slip wall. Therefore, there can be free flow without loss of energy. It is noted that since the fluid is assumed to flow in the tank and the sloshing or convective component is not considered in this study, the vertical displacement at the top surface is zero which is consistent with boundary condition of impulsive hydrodynamic pressure.

The boundary condition of liquid surfaces in contact with tank walls are specified as solid fluid interface in which fluid structure interaction is considered. As a result, the loads and boundary conditions can be transferred between fluid and structural domains.

It is worth noting that the tank wall with fixed support is used to obtain the dynamic response of tank wall. The velocity along the height of wall is the relative velocity to the ground and used as boundary condition for the fluid structure interface. In the liquid domain, however, the absolute velocity along the height of tank wall is used to determine impulsive hydrodynamic pressure. The boundary condition of impulsive hydrodynamic pressure is the sum of ground velocity and the velocity relative to the ground along the height of tank wall. Therefore, ground velocity shall be included in the dynamic analysis in the liquid domain. This is achieved through another sidewall which is modeled as massless and rigid wall.

The time history of ground motions is input to the rigid massless wall. Therefore, the wall can move relative to the fixed support and can be treated as an excitation instrument for hydrodynamic pressure. Since the relative velocity to the ground can be obtained through the dynamic analysis of tank wall with fixed support, both velocities due to the ground motion and flexible wall are considered in the liquid domain. As a result, the combination of velocity due to fixed wall and rigid massless wall can simulate the boundary condition of impulsive hydrodynamic pressure.

4.2.3 Dynamic Analysis of Fluid Structure Interaction

4.2.3.1 Solid-Fluid Interaction

The setup for creation of the fluid and solid domain/physical models in ANSYS® CFX and Mechanical application were discussed in the previous sections. The data transfer between CFX and the Mechanical application is automated by the MFX branch of the ANSYS® Multi-field solver. The specification of coupling data transfers and controls is in the CFX. Execution and run-time monitoring of the coupled simulation is performed from the CFX-Solver Manager.

The coupled simulation follows a timestep/iteration structure that is similar to the one within the CFX-Solver. During coupled simulations, the ANSYS® CFX and the Mechanical application solver execute the simulation through a sequence of multi-field timesteps, each of which consists of one or more "stagger" (or coupling) iterations.

Figure 4.3 illustrates a sequence of synchronization points (SPs) in ANSYS® for fluid solid interaction. Coupled simulations begin with the execution of the Mechanical application and CFX field solvers. The Mechanical application solver acts as a coupling master process to which the CFX-Solver connects. Once that connection is established, the solvers advance through a sequence of six pre-defined synchronization points (SPs). At each of these SPs, each field solver gathers the data it requires from the other solver in order to advance to the next point.

The first three SPs are used to prepare the solvers for the calculation intensive solution process, which takes place during the final three SPs. These final SPs define a sequence of coupling steps, each of which consists of one or more stagger/coupling iterations.
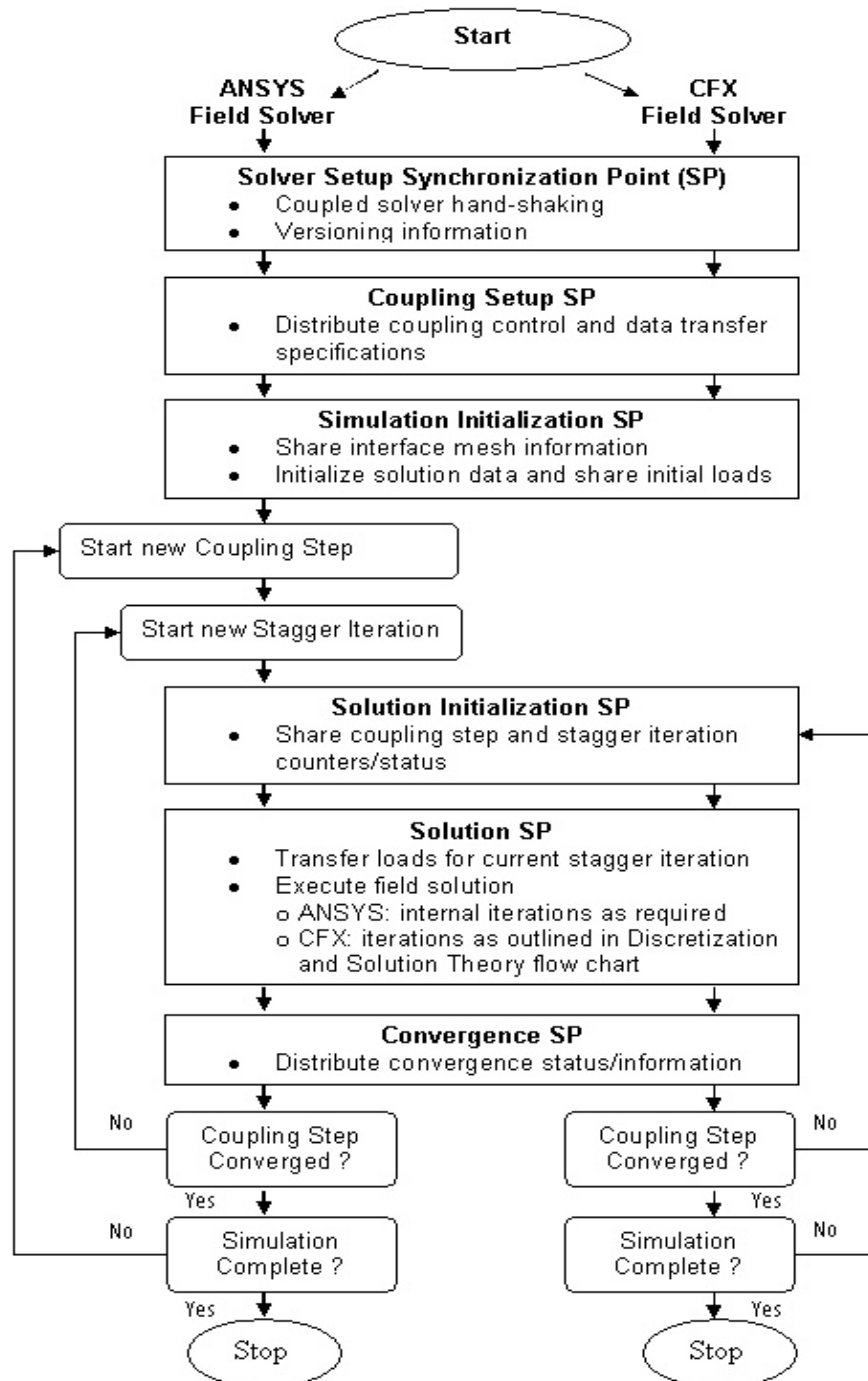
Figure 4.3 Sequence of Synchronization Points

During every stagger iteration, each field solver gathers the data it requires from the other

solver, and solves its field equations for the current coupling step. Stagger iterations are

repeated until a maximum number of stagger iterations is reached or until the data

transferred between solvers and all field equations have converged. The latter guarantees an implicit solution of all fields for each coupling step.

4.2.3.2 Time History Analysis

The transient analysis system is used for time history analysis. The ground acceleration is applied to the tank wall with fixed support and the ground velocity is applied to the moving plate as discussed before.

It is worth noting that the time step set up for time history analysis of tank and liquid domain shall be the same due to the transferring data between structure and liquid domain at each coupling time step.

4.3 Results of Analysis

The tall tank studied in Chapter 3 is used for verification. The dimensions and properties of the tank are as follows:

$L_x = 9.8$ m $\qquad L_z = 28$ m $\qquad H_w = 12.3$ m $\qquad H_L = 11.2$ m $\qquad t_w = 1.2$ m

$E_c = 2.0776 \times 10^4$ MP $\qquad \rho_w = 2300$ kg/m^3 $\qquad \rho_l = 1000$ kg/m^3 $\qquad \nu = 0.17$

The tank wall is modeled using the 8 node structural solid element SOLID185 with 3-translation degree of freedom at each node. The mesh size for elements is 21x2x2 (H_w x t_w x 1m) as shown in Figure 4.1. Fluid element FLUID142 is used for 3D modeling of the fluid medium. The size of element is 594mm x 589mm x 500mm and the mesh size for elements is 33x19x2 (2L_x x H_L x 1m).

Figure 4.4 shows the ground motion of first twenty seconds of 1940 El Centro earthquake (Imperial Valley, California). The maximum peak ground acceleration (PGA) is 0.34g and

the maximum velocity is 0.32 m/sec. The time steps for the recorded acceleration and velocity are 0.02 sec and 0.04 sec, respectively. It is noted that the ground velocity is also needed in the dynamic analysis using finite element method.
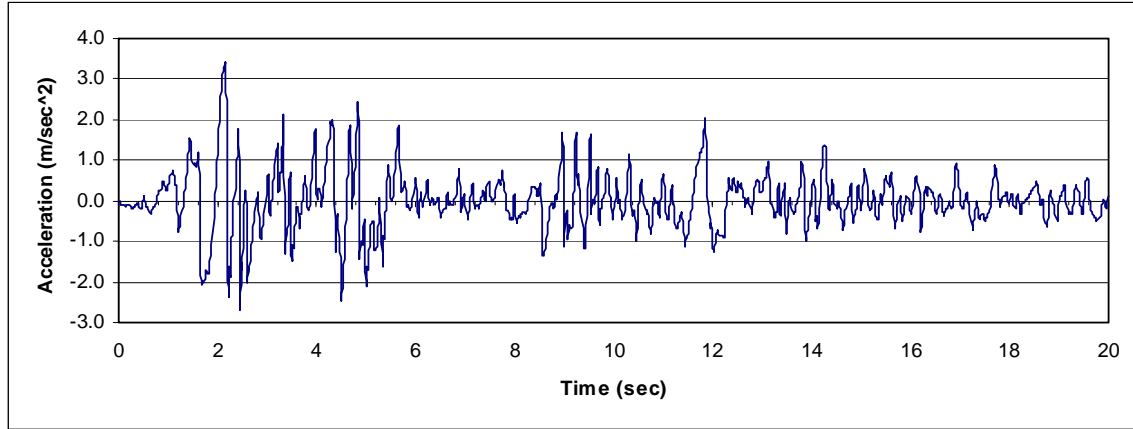
(a) Acceleration
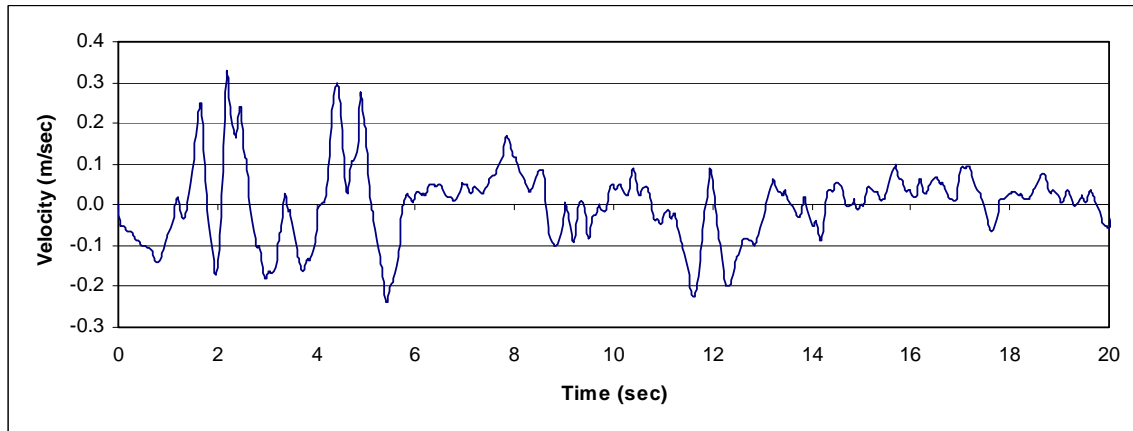
(b) Velocity

Figure 4.4 Ground Motion of 1940 El Centro Earthquake, (Imperial Valley, California)

For time history analysis, the initial parameters of ground motion are set to be zero in transient analysis system which means the system is in the static condition. The time step for dynamic analysis in structural domain is 0.01 sec which is the same as that used in fluid domain using ANSYS® CFX. It is worth noting that the time step 0.01 sec for dynamic analysis is less than those of recorded ground acceleration and velocity. In addition, the test using the smaller time step in dynamic analysis shows that using 0.01

sec time step is adequate to provide accurate results.

4.3.1 Response of Empty Tank

The dynamic response of empty tank is calculated using the modal analysis system. The first two natural frequencies of tank wall are 3.83Hz and 23.1Hz, respectively. The results are consistent with 3.87 Hz and 23.6 Hz for the first two modes as shown in Chapter 3.

4.3.2 Response of Full Tank

Figure 4.5 shows the contours of response of tank wall for one time step. Figures 4.5(a) and 4.5(b) demonstrate the relative magnitude of velocity and acceleration along the height of tank walls, respectively. It can be seen that for the tank wall with fixed support at the bottom, the response is equal to zero at the support and increase with the increase of height of tank wall. However, the response of rigid wall is the absolute values of ground motion. The plot of contours confirms that the values of acceleration and velocity are relative with respect to the ground for the wall with the fixed support.
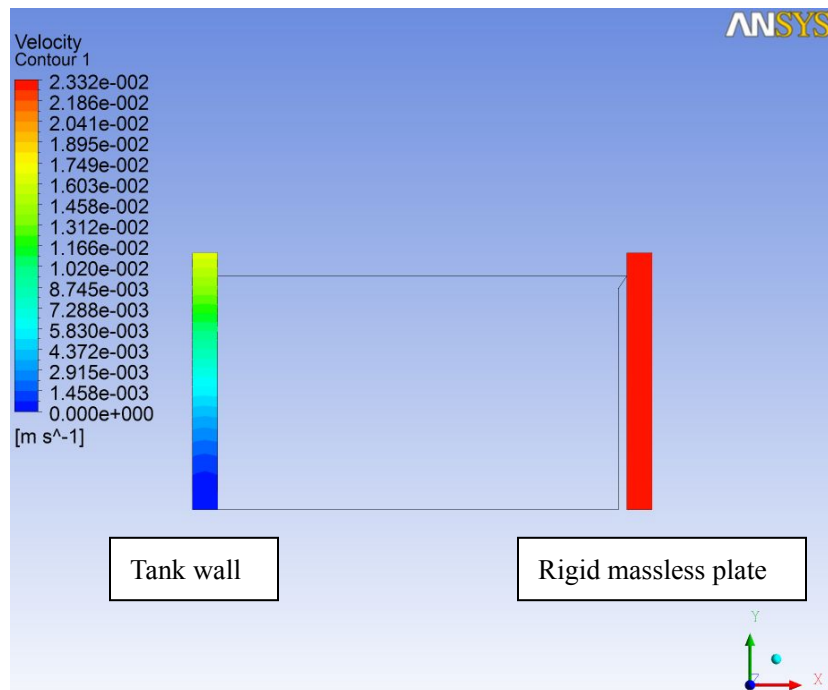
(a) Velocity
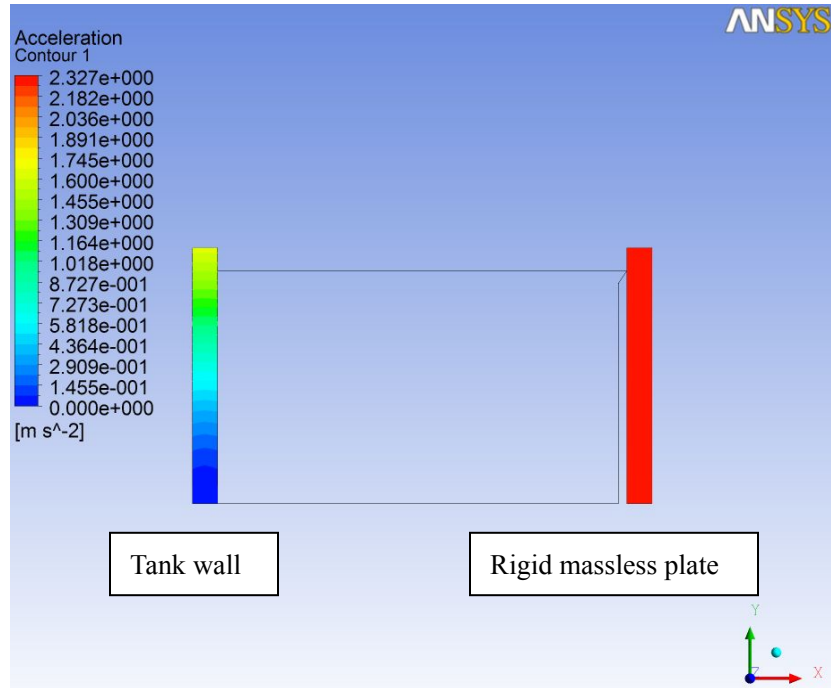
(b) Acceleration

Figure 4.5 Response of Tank Walls at Typical Time Step

The time history response of tank wall with the fixed support is shown in Figure 4.6. The maximum displacement at the top, base shear and base moment are 28mm, 294 kN and 2659 kNm, respectively. The comparison of results using different analytical models will be further discussed in Chapter 5.
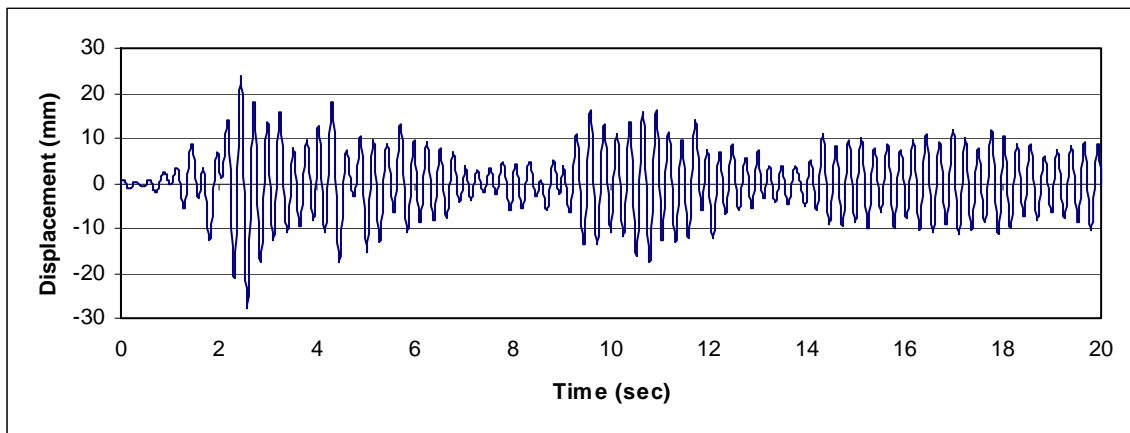
(a) Top displacement
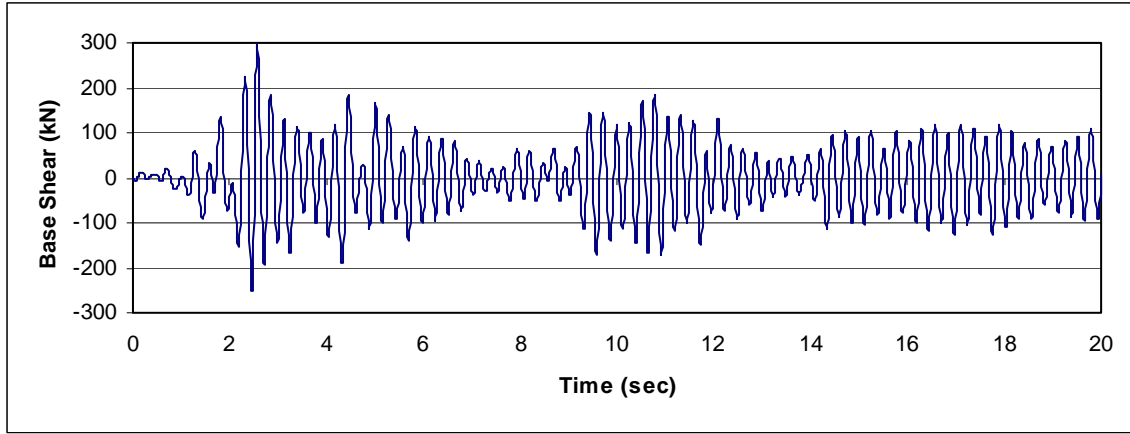
(b) Base shear
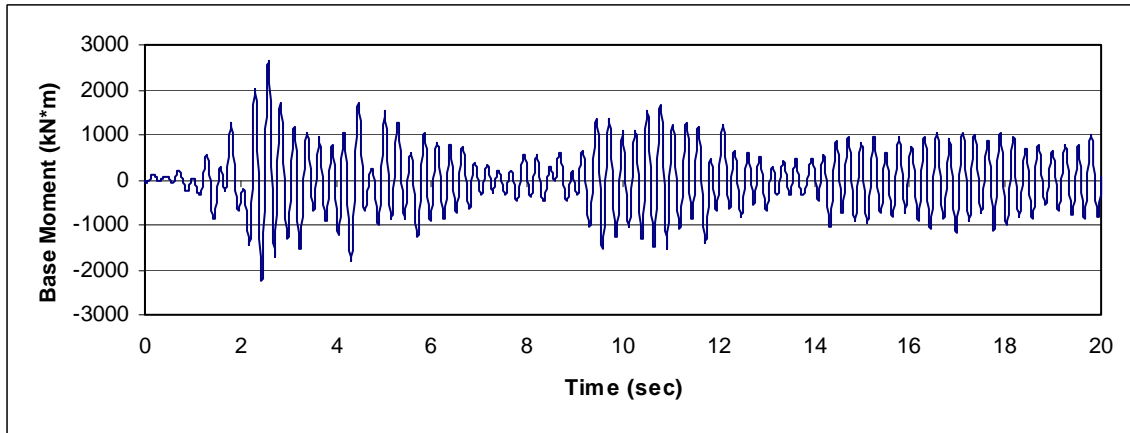
(c) Base moment

Figure 4.6 Time Histories of Tank Wall

4.4 Conclusions

In this chapter, dynamic response of concrete rectangular liquid storage tanks is studied using the general purpose finite element analysis software ANSYS[®]. The tank and liquid are modeled using the Mechanical transient and CFX analysis systems, respectively. The boundary condition for impulsive hydrodynamic is also discussed. The fluid structure interaction based on the staggered iteration coupling procedure is used for the time history analysis. Both response of empty and full tank is presented for the tall tank. The results are further compared with those obtained using the other analytical models for verification of the proposed generalized SDOF system as will be discussed in Chapter 5.

CHAPTER 5 GENERALIZED SDOF SYSTEM

5.1 Introduction

This chapter presents a simplified method using the generalized single degree of freedom (SDOF) system for seismic analysis and design of concrete rectangular liquid storage tanks. In most of the current design codes and standards for concrete liquid storage tanks, the response of liquid and tank structure is determined using rigid tank wall and the lumped mass approach. However, the results of analysis show that the flexibility of tank wall increases the hydrodynamic pressures as compared to the rigid wall assumption as discussed in Chapter 3. On the other hand, the consistent mass approach reduces the response of liquid containing structure as compared to the lumped mass approach. In the proposed method, the consistent mass approach and the effect of flexibility of tank wall on hydrodynamic pressures are considered. Five prescribed vibration shape functions representing the first mode shape of fluid structure interaction system are studied. The application of the proposed shape functions and their validity are examined using two different case studies including a tall and a shallow tank. The results are then compared with those using the analytical - finite element models and the full finite element model from previous investigation. The results indicate that the proposed method is fairly accurate which can be used in the structural design of liquid containing structures.

5.2 Theories

Figure 5.1 shows a 2-D model of tank wall. It is assumed that the liquid storage tank is fixed to the rigid foundation. A Cartesian coordinate system (x, y) is used with the origin located at the center of the tank base. It is assumed that the direction of ground motion is in the "x" direction and the width of tank $2L_z$ is sufficiently large so that a unit width of tank can represent the tank wall.

5.2.1 Hydrodynamic Pressure

The hydrodynamic pressure is obtained using the velocity potential method as described in Chapter 3. Only the impulsive component is considered in this study.
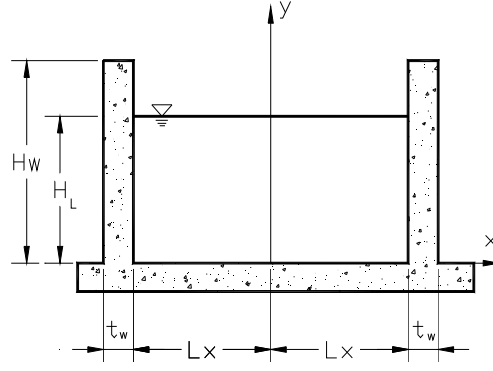
Figure 5.1 Schematic of Rectangular Tank for Generalized SDOF System

The hydrodynamic pressure distribution on the flexible wall related to the velocity potential can be expressed as:

[5.1] $\quad p = \sum_{n=1}^{\infty} \frac{2 \cdot \rho_l \cdot \tanh(\lambda_{i,n} \cdot L_x)}{\lambda_{i,n} \cdot H_L} \cdot \cos(\lambda_{i,n} \cdot y) \cdot \int_0^{H_L} \cos(\lambda_{i,n} \cdot y) \cdot \ddot{u}(y,t)dy$

where $\lambda_{i,n} = (2n-1)\pi/2H_L$. As the series in the above equation converge very fast, only the first term of the series may be used for practical applications.

For the rigid tank $\ddot{u}(y,t) = \ddot{u}_g(t)$ which means that the acceleration along the height of the wall is the same as the ground acceleration at specific time, then Eq.5.1 can be simplified further as that:

[5.2] $\quad p_{rigid} = \sum_{n=1}^{\infty} \frac{2 \cdot (-1)^n \cdot \rho_l}{\lambda_{i,n}^2 \cdot H_L} \tanh(\lambda_{i,n} \cdot L_x) \cdot \cos(\lambda_{i,n} \cdot y) \cdot \ddot{u}_g(t)$

The total lateral force P due to hydrodynamic pressure is calculated by integrating the pressure distribution p along the height of liquid as follows:

[5.3] $\quad P = \int_0^{H_L} \sum_{n=1}^{\infty} \frac{2 \cdot \rho_l}{\lambda_{i,n} \cdot H_L} \tanh(\lambda_{i,n} L_x) \cos(\lambda_{i,n} y) \int_0^{H_L} \cos(\lambda_{i,n} y) \ddot{u}(y,t)dy \cdot dy$

The height at which the lateral force P is applied above the base is:

[5.4] $$h_i = (\int_0^{H_L} \sum_{n=1}^{\infty} \frac{2 \cdot \rho_l}{\lambda_{i,n} \cdot H_L} \tanh(\lambda_{i,n} L_x) \cos(\lambda_{i,n} y) \int_0^{H_L} \cos(\lambda_{i,n} y) \, \ddot{u}(y,t) dy \cdot y dy) / P$$

5.2.2 Generalized SDOF System

For a system with distributed mass and stiffness characteristics, the structure can exhibit an infinite number of degrees of freedom for flexural mode of deformations. If there are some predetermined shapes to approximate the vibration of system, and only the amplitude of vibration varies with time, then the motion of the system can be described by a single variable, or generalized coordinate in which only one DOF exists. The system idealized in this manner is referred to as generalized SDOF systems (Chopra, 2001). In this chapter, the generalized SDOF system is applied to solve the dynamic response of liquid containing structures subjected to earthquakes.

5.2.2.1 Equation of Motion

Figure 5.2 shows a tank wall with the distributed mass m(y) and stiffness EI(y) per unit height subjected to the earthquake ground motion $u_g(t)$. The distributed mass m(y) and stiffness EI(y) can be either uniform or non-uniform. It is determined by the configuration of the tank, such as the wall dimensions and the material properties. As the tank wall possesses an infinite number of natural frequencies and corresponding natural modes in vibration, for exact analysis, the wall must be treated as an infinite degree freedom system.
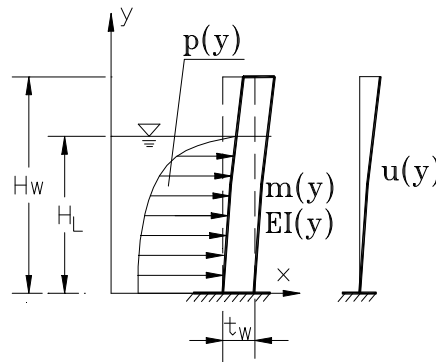
Figure 5.2 Concrete Rectangular Tank in Generalized SDOF System

For simplicity, the distributed mass and stiffness system can be treated as a generalized SDOF system. The equation of motion for a generalized SDOF system is that:

[5.5] $\tilde{m} \cdot \ddot{u} + \tilde{c} \cdot \dot{u} + \tilde{k} \cdot u = \tilde{p}(t)$

where $\tilde{m}$, $\tilde{c}$, $\tilde{k}$, $\tilde{p}$ are defined as the generalized system of mass, damping, stiffness and force, respectively. These generalized properties are associated with the selected generalized displacement $u(t)$ as discussed below.

In order to obtain the approximate response of the generalized SDOF system with distributed mass and stiffness, the deflections of the wall for liquid containing structures relative to the ground can be assumed a single shape function $\psi(y)$ that approximates the fundamental vibration mode in the form of:

[5.6] $u_r(y,t) = \psi(y) \cdot u(t)$

where $u(t)$ is the defined time function related to a single generalized displacement, and $\psi(y)$ is the assumed shape function.

Therefore, the total displacement can be expressed by:

[5.7] $u(y,t) = u_r(y,t) + u_g(t) = \psi(y) \cdot u(t) + u_g(t)$

The work or energy principle is applied to obtain the equation of dynamic equilibrium of liquid-structure system. In this study, the principle of virtual displacement is used to deduce the equation of motion of a generalized SDOF system.

The internal virtual work is due to the bending moments acting through the curvature of wall using an assumed shape function. In terms of the generalized coordinate u and shape function $\psi(y)$, it can be expressed as that:

[5.8] $$\delta W_I = \delta u \cdot [u \cdot \int_0^{H_W} EI(y) \cdot [\frac{\partial^2 \psi(y)}{\partial y^2}]^2 \cdot dy]$$

The external virtual work is the result of the ground acceleration and the consequence of hydrodynamic pressures. The external virtual work due to the inertial mass of wall subjected to ground acceleration can be formulated in terms of the generalized coordinate and assumed shape function as follows:

[5.9] $$\delta W_{E1} = -\delta u \cdot [\ddot{u} \cdot \int_0^{H_W} m(y) \cdot [\psi(y)]^2 \cdot dy + \ddot{u}_g(t) \cdot \int_0^{H_W} m(y) \cdot \psi(y) \cdot dy]$$

The external virtual work due to hydrodynamic pressure can be expressed in terms of the generalized coordinate and assumed shape function as that:

[5.10] $$\delta W_{E2} = -\delta u \cdot [\int_0^{H_L} p(y) \cdot \psi(y) \cdot dy]$$

where $p(y)$ is a function of hydrodynamic pressure distribution along the height of wall as discussed before. Since it is also a function of the acceleration of ground motion in an earthquake, after substituting Eq.5.1 into Eq.5.10, it results in that:

[5.11] $$\delta W_{E2} = -\delta u \cdot [\ddot{u} \cdot f_1(y, \psi(y)) + \ddot{u}_g(t) \cdot f_2(y, \psi(y))]$$

where $f_1(y, \psi(y))$ and $f_2(y, \psi(y))$ are the two functions related to the shape function and vertical coordinate as follows:

[5.12] $$f_1(y, \psi(y)) = \sum_{n=1}^{\infty} \frac{2 \cdot \rho_l}{\lambda_{i,n} \cdot H_L} \tanh(\lambda_{i,n} L_x)[\int_0^{H_L} \cos(\lambda_{i,n} y) \cdot \psi(y) dy]^2$$

[5.13] $$f_2(y, \psi(y)) = \sum_{n=1}^{\infty} \frac{2 \cdot (-1)^{n+1} \rho_l}{\lambda_{i,n}^2 \cdot H_L} \tanh(\lambda_{i,n} L_x) \int_0^{H_L} \cos(\lambda_{i,n} y) \cdot \psi(y) dy$$

5.2.2.2 Coupling Analysis

For the coupling analysis between the structure and the contained liquid, the direct coupling method is used in the analysis. It means that the responses of liquid and

structure can be directly solved through the equation of motion.

Comparing Eq.5.9 with Eq.5.11, it can be found that the external virtual work due to hydrodynamic pressure is similar to the external force due to inertial mass of the wall. Both these equations have one part related to the ground acceleration and another part related to the magnitude of acceleration along the height of wall.

After mathematical manipulation of the equation of motion, the generalized system of mass, stiffness and force in terms of the generalized coordinate and assumed shape function can be obtained as follows:

[5.14] $$\widetilde{m} = \int_{0}^{H_W} m(y) \cdot [\psi(y)]^2 \cdot dy + f_1(y, \psi(y))$$

[5.15] $$\widetilde{k} = \int_{0}^{H_W} EI(y) \cdot [\frac{\partial^2 \psi(y)}{\partial y^2}]^2 \cdot dy$$

[5.16] $$\widetilde{p} = \ddot{u}_g(t) \cdot [\int_{0}^{H_W} m(y) \cdot \psi(y) \cdot dy + f_2(y, \psi(y))]$$

The generalized mass in Eq.5.14 can be written as two separate parts, the generalized inertial mass of wall $\widetilde{m}_w$ and the generalized added mass of liquid due to the impulsive hydrodynamic pressure $\widetilde{m}_L$ as shown below:

[5.17] $$\widetilde{m}_W = \int_{0}^{H_W} m(y) \cdot [\psi(y)]^2 \cdot dy$$

[5.18] $$\widetilde{m}_L = f_1(y, \psi(y))$$

Also, from Eq.5.16, the effective inertial mass of wall m_w and the effective added mass of liquid due to impulsive hydrodynamic pressure m_L can be defined based on the shape function as that:

[5.19] $$m_W = \int_{0}^{H_W} m(y) \cdot \psi(y) \cdot dy$$

[5.20] $m_L = f_2(y, \psi(y))$

Therefore, the equation of motion for coupling the structure and the contained liquid subjected to earthquake is obtained by substituting the Eqs.5.14 to 5.16 into Eq.5.5. Then, by dividing both sides of the equation by $\tilde{m}$, the following relationship is obtained:

[5.21] $\ddot{u} + 2 \cdot \zeta \cdot \omega_n \cdot \dot{u} + \omega_n^2 \cdot u = -\hat{q} \cdot \ddot{u}_g(t)$

where $\omega_n^2 = \tilde{k}/\tilde{m}$ represent the circular frequencies associated with liquid containing system and $\hat{q}$ is the factor of external load applied, that is:

[5.22] $\hat{q} = \hat{p}/\tilde{m} = \dfrac{m_W + m_L}{\tilde{m}_W + \tilde{m}_L}$

where $\hat{p}$ is the total effective mass of liquid-tank system as follows:

[5.23] $\hat{p} = m_W + m_L$

If an estimated damping ratio ζ is assumed, then all the unknown parameters, i.e. $u, \dot{u}, \ddot{u}$ can be determined by an assumed shape function. Therefore, the infinite degrees of freedom of liquid containing system can be simplified to a generalized SDOF system.

It is worth noting that the generalized SDOF system used in this study is not as the same as the lumped SDOF system in Housner's model (Housner, 1963). In Housner's model, the entire inertial mass associated with the impulsive component of the liquid and the tank wall is lumped at an effective height above the base of the tank wall. In this study, a generalized coordinate system which is based on the consistent mass approach is used to approximate the vibration mode. As a result, the predefined shape function can reduce the infinite degrees of freedom system into a SDOF system. The efficiency of the generalized SDOF system used for dynamic response of liquid containing structures will be presented using the two different case studies.

5.2.2.3 Shape Functions

To choose a proper shape function is critical to accurately estimate the natural frequencies of liquid containing structures when using the generalized SDOF system. In principle, any shape function may be selected if it satisfies the displacement boundary conditions at the supports. However, a shape function that satisfies only the geometric boundary conditions does not always ensure an accurate result for the fundamental natural frequency. For initial estimation, an upper bound or a lower bound shape function may be introduced for analysis.

It is worth noting that the configuration of concrete rectangular tanks may vary. In this study, only the top open rectangular tank is considered in the analysis for simplicity. The prescribed shape functions are based on the cantilever wall boundary condition. However, the generalized SDOF system can be applied to any configuration of concrete rectangular tanks provided that the proper mode shape function is used for approximation of vibration mode of rectangular tanks.

In this study, five different shape functions are selected for analysis. They are listed below and referenced as SF1 to SF5.

[5.24] $\text{SF1}(y)= \psi(y)=\dfrac{1}{2}\dfrac{y^2}{H_W^2}+\dfrac{1}{2}\dfrac{y}{H_W}$

[5.25] $\text{SF2}(y)=\psi(y)=\dfrac{y^2}{H_W^2}$

[5.26] $\text{SF3}(y)=\psi(y)=\dfrac{3}{2}\dfrac{y^2}{H_W^2}-\dfrac{1}{2}\dfrac{y^3}{H_W^3}$

[5.27] $\text{SF4}(y)=\psi(y)=1-\cos(\dfrac{\pi \cdot y}{2H_W})$

[5.28] $\text{SF5}(y)=\psi(y)=\sin(\dfrac{\pi \cdot y}{2H_W})$

Figure 5.3 shows the normalized height versus normalized deformation based on the above shape functions. The purpose of using these selected shape functions is to find the

most appropriate shape that can approximate the dynamic response of liquid containing structures while maintaining the efficiency of analysis in terms of application to engineering design.
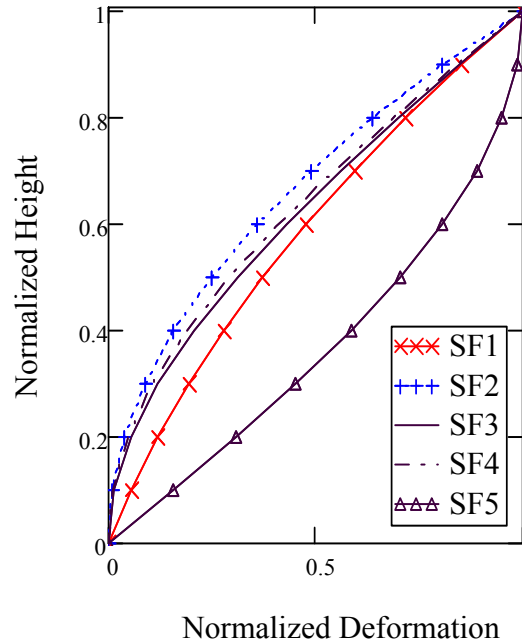
Figure 5.3 Normalized Shape Functions for First Mode

It is worth noting that since the hydrodynamic pressure can affect the vibration mode of tank wall, the mode shape based on a cantilever beam may not reflect the response of liquid containing system. Therefore, the shape functions SF1 and SF2 are used as upper bounds and lower bounds for the initial estimate of mode shapes for fluid structure interaction. In addition, the shape functions SF1 and SF2 can also represent the more flexible and more rigid tank wall conditions, respectively. Therefore, these two shape functions can be used to study the effect of flexibility of tank wall on dynamic response of liquid containing structures.

The shape functions SF3 and SF4 are to approximate the cantilever wall boundary condition that it is fixed at bottom and free at top which is very common in concrete liquid containing structures. It is noted that the shape functions SF1 to SF4 represent the flexural dominated deformation function. The one that gives the best approximation to

exact response of liquid containing structure can be used for dynamic analysis.

In certain conditions, the concrete tank wall may be pin connected at both ends at top and bottom. Therefore, the shape function SF5 is introduced to represent the shear dominated deformation function. This can demonstrate that the generalized SDOF system may also be used with the different boundary conditions provided that the mode shape can be assumed by a generalized coordinate.

5.2.2.4 Natural Frequencies
In this study, the Rayleigh-Ritz method is used to calculate the natural frequencies of liquid containing system. This method has proved to give good accuracy even if the selected shape function is not so close to the exact mode shape function (Chopra, 2001). In addition, the natural frequency obtained from an assumed shape function cannot be smaller than the exact value of the lowest or the fundamental natural frequency of the system in Rayleigh-Ritz method. As a result, this principle can be used as a criteria to determine the best approximated shape function among the group of selected shape functions.

For the generalized SDOF system with distributed mass and stiffness, the circular frequencies of the system can be obtained using the Rayleigh-Ritz method from the following equation.

[5.29] $$\omega_n^2 = \frac{\widetilde{k}}{\widetilde{m}_W + \widetilde{m}_L}$$

Since the generalized system of mass and stiffness are known, the natural frequencies of liquid containing structures can be easily obtained.

5.2.2.5 Peak Earthquake Response
Once the fundamental natural frequency of the generalized SDOF system is known, the response of liquid containing structure can be easily calculated using the response spectrum method for the specific earthquake record or the design response spectrum which is specified in the design standards and codes.

It is worth noting that the response spectrum is developed based on the lumped SDOF system. However, the same methodology can still be applied in the generalized SDOF as compare the equation of motion for the lumped SDOF system with that of the generalized SDOF system.

The maximum displacement at top of tank wall can be calculated using the formula:

[5.30] $u_{max} = \dfrac{\hat{q}}{\omega_n^2} \cdot A_a$

where A_a is the pseudo-acceleration which can be obtained from the response spectrum at period $T_n = 2 \cdot \pi / \omega_n$ for the damping ratio ζ.

The base shear and base moment can be calculated using the following relationship:

[5.31] $V_B = \hat{p} \cdot \hat{q} \cdot A_a$

[5.32] $M_B = \bar{p} \cdot \hat{q} \cdot A_a$

where $\hat{q}$ and $\hat{p}$ are defined in Eqs.5.24 and 5.25 respectively, and $\bar{p}$ is defined as that:

[5.33] $\bar{p} = \displaystyle\int_0^{H_W} m(y) \cdot \psi(y) \cdot y \, dy + \int_0^{H_L} f_2(y, \psi(y)) \cdot y \, dy = m_W \cdot h_W + m_L \cdot h_i$

where h_w and h_i are the effective heights of inertial mass of tank wall and added mass of liquid due to impulsive hydrodynamic pressure with respect to the tank base, respectively.

The hydrodynamic force P and the effective height at which the hydrodynamic pressure is applied h_i at peak earthquake response can be obtained by substituting the acceleration function Eq.5.34 into Eq.5.3 and Eq.5.4, respectively.

[5.34] $\ddot{u}(t) = \psi(y) \cdot \hat{q} \cdot A_a$

As a result, the dynamic response of liquid containing structure can be evaluated by the generalized SDOF system.

5.3 Case Studies

5.3.1 Tall Tank

To demonstrate the efficiency of the generalized SDOF system for dynamic analysis of liquid containing structures, a tall tank that was studied previously is used in this chapter. Both empty as well as full tank is considered. The dimensions and the properties of the tank are as follows:

$\rho_w = 2300 \text{ Kg/m}^3$ $\quad \rho_l = 1000 \text{ Kg/m}^3$ $\quad E_c = 2.0776 \text{x} 10^4 \text{MPa}$ $\quad \nu = 0.17$

$L_x = 9.8 \text{ m}$ $\qquad L_z = 28 \text{ m}$ $\qquad H_w = 12.3 \text{ m}$ $\qquad H_L = 11.2 \text{ m}$ $\qquad t_w = 1.2 \text{ m}$

In Chapter 3, six models were presented for dynamic analysis of concrete rectangular LCS. The dynamic response of tank wall was analyzed using finite element method. However, the impulsive hydrodynamic pressure was calculated based on the analytical method and input into the structural model using the added mass or external force. The mode superposition method was used in Model 4 in which the distributed added mass of liquid due to hydrodynamic pressure was considered. In Model 5, the time history analysis including the sequential coupling analysis procedure was used. The effect of flexibility of tank wall on dynamic response for both the tank wall and hydrodynamic pressure was considered. As the distributed mass was considered in Models 4 and 5, they represented the more accurate analysis in that study. The results obtained using Models 4 and 5 are shown in Figure 5.4 for comparison with those obtained from the generalized SDOF system which is described subsequently.

A summary of mass ratios for the generalized SDOF system is presented in Figure 5.5. The generalized mass of tank wall $\tilde{m}_W$ for the first mode based on the selected shape functions is presented and compared to the total generalized mass of tank wall $\widetilde{M}_W$ based on the rigid wall condition. It can be seen that except for shape function SF5, the mass percentages obtained from the shape functions SF1 to SF4 are in the range of 20% to 26%.
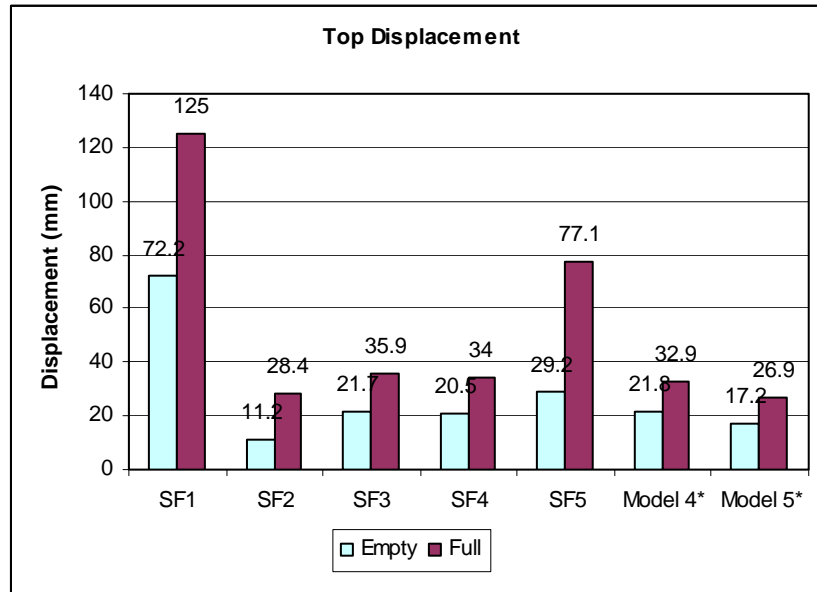
(a) Top displacement
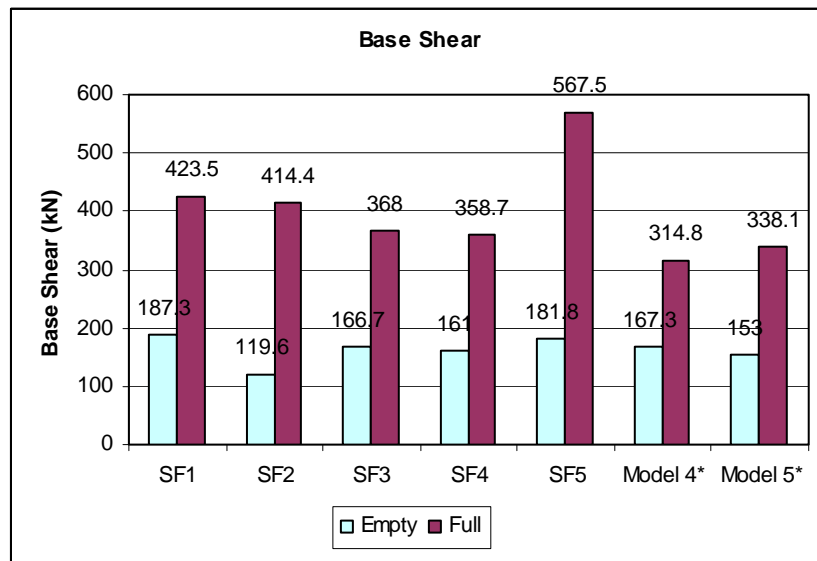
(b) Base shear
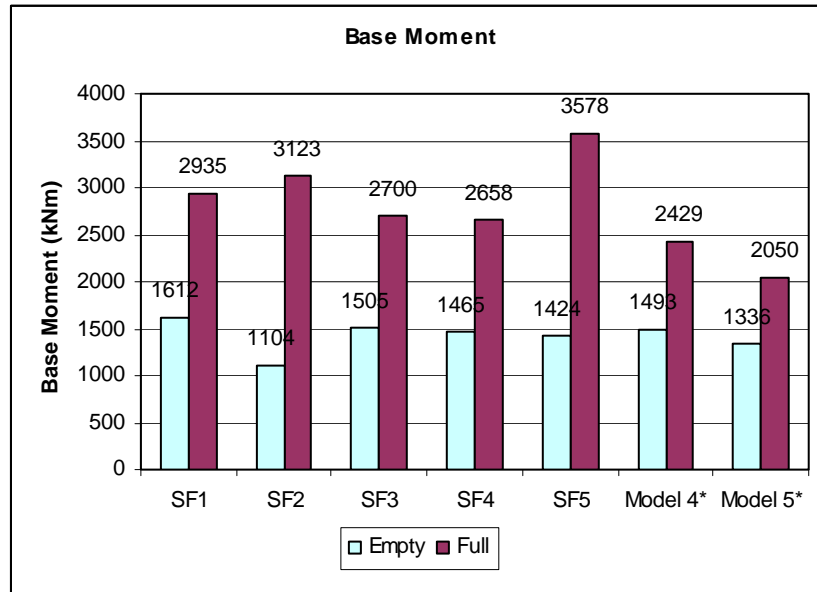
(c) Base moment

Figure 5.4 Comparison of Dynamic Reponses of Tall Tank
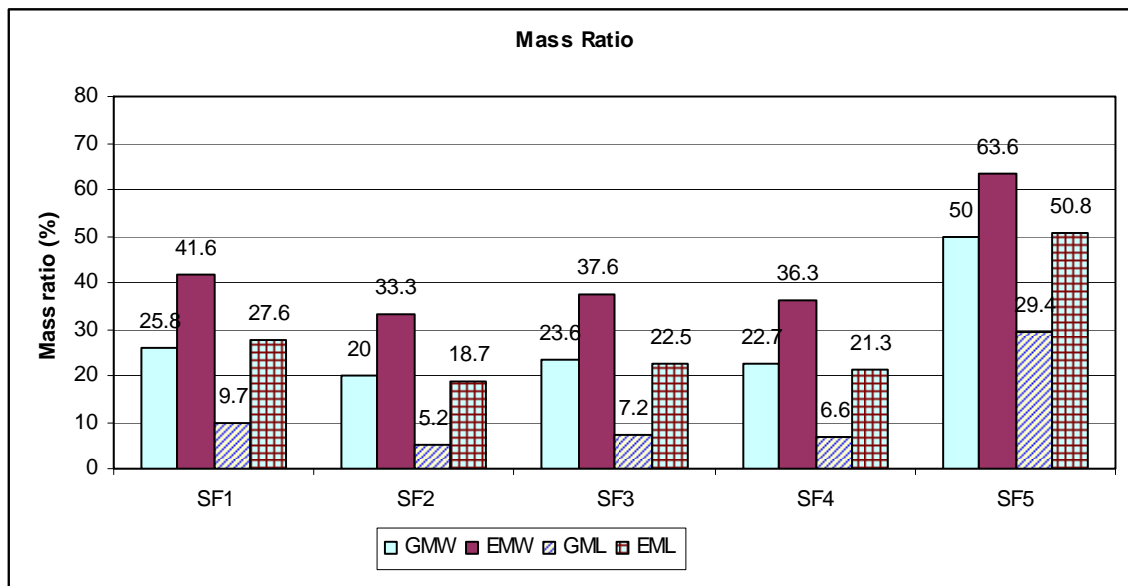
GMW: Generalized Inertial Mass of Wall

EMW: Effective Inertial Mass of Wall

GML: Generalized Added Mass of Liquid

EMW: Effective Added Mass of Liquid

Figure 5.5 Comparisons of Mass Ratios for Generalized SDOF System - Tall Tank

For the effective mass of tank wall m_W, the mass percentages obtained from the shape functions SF1 to SF4 in terms of M_W are in the range of 33% to 42%. M_W is the total effective mass of tank wall based on the rigid wall condition and is equal to $\widetilde{M}_W$ for the shape function $\psi(y)=1$.

As expected, because there are infinite degrees of freedom for the tank wall, the participation of generalized and effective mass of tank wall for the first mode using the consistent mass is less than that using the lumped mass based on the rigid wall boundary condition. It is worth noting that only the first mode is considered in this section. The effect of higher modes on dynamic response of liquid containing structures is discussed in Chapter 6.

For the full tank, the value of $\widetilde{m}_L$ and m_L, which are the generalized and effective added masses of liquid due to impulsive hydrodynamic pressure respectively based on the first mode shape function are calculated as shown in Figure 5.5. In addition, it is assumed that the generalized and effective added masses based on the rigid wall boundary condition, $\widetilde{M}_L$ and M_L, represent the total generalized and effective added masses of liquid due to hydrodynamic pressure for the liquid containing system. Since the shape function $\psi(y)=1$ is applied to evaluate the rigid wall boundary condition, the total generalized and effective added mass of liquid due to impulsive hydrodynamic pressure, $\widetilde{M}_L$ and M_L are both equal.

It can be found that only part of generalized and effective added mass of liquid for the first mode, $\widetilde{m}_L$ and m_L, participate in the dynamic analysis as compared to the total generalized and effective added mass $\widetilde{M}_L$ and M_L. The same trends can be found in the generalized and effective inertial mass of tank wall for the first mode shape function, $\widetilde{m}_W$ and m_W, as discussed above. The mass participation factors are on average about 23% of the total generalized inertial mass of tank wall and 7% of total generalized added mass of liquid due to impulsive hydrodynamic pressure. For the shape functions SF3 and SF4,

these values are 36% of the total effective inertial mass and 22% of the total effective added mass for impulsive hydrodynamic pressure. As SF1 and SF2 represent the more flexible and the more rigid walls respectively, it can be concluded that a larger portion of inertial mass of tank wall and added mass of liquid due to hydrodynamic pressure participate the first mode when the wall is more flexible.

The generalized stiffness of structure is calculated using Eq.5.15. Based on a unit load applied at the top of the wall, the wall stiffness can also be determined using the following simple relationship:

[5.35] $$\tilde{k} = \frac{E_c}{4} \cdot (\frac{t_W}{H_W})^3$$

Based on the above equation, the stiffness of tank wall is 4823 kN/m. This agrees well with the results obtained from the shape functions SF3 and SF4.

The fundamental natural periods of empty tank based on the shape functions SF3 and SF4 are 0.256 sec and 0.249 sec respectively as shown in Table 5.1. This shows that the shape functions SF3 and SF4 provide the most accurate results in this respect. For shape functions SF1 and SF2 which represent the more flexible and the more rigid tank wall conditions respectively, the true fundamental natural frequencies are expected to be between the values of these two limits.

The fundamental natural periods of the first mode for the full tank are 0.318 sec and 0.307 sec for shape functions SF3 and SF4, respectively. These values are also similar to those obtained using Model 4 as discussed in Chapter 3.

The maximum response of structure can be obtained using the pseudo-ground acceleration of the response spectrum. The El Centro 1940 Earthquake used in the previous investigation is also used in this study. The response spectrum for such a record is based on a 5% damping ratio as shown in Figure 5.6. The pseudo-ground accelerations A_a corresponding to the periods for different shape functions are listed in Table 5.1. It should be noted that the actual response spectrum rather than the design response

spectrum is used in this study. This is because the previous study was based on time history analysis using the El Cento record which is used as the basis for comparison.

It is worth noting that the pseudo-ground acceleration varies in the range of periods between 0.1 and 0.7 sec for this specific site response spectrum. However, if a standard design spectrum is used, this kind of deviation can be eliminated because the design spectrum is not intended to match the response spectrum for any particular ground motion but is constructed to represent the average characteristics of many ground accelerations.
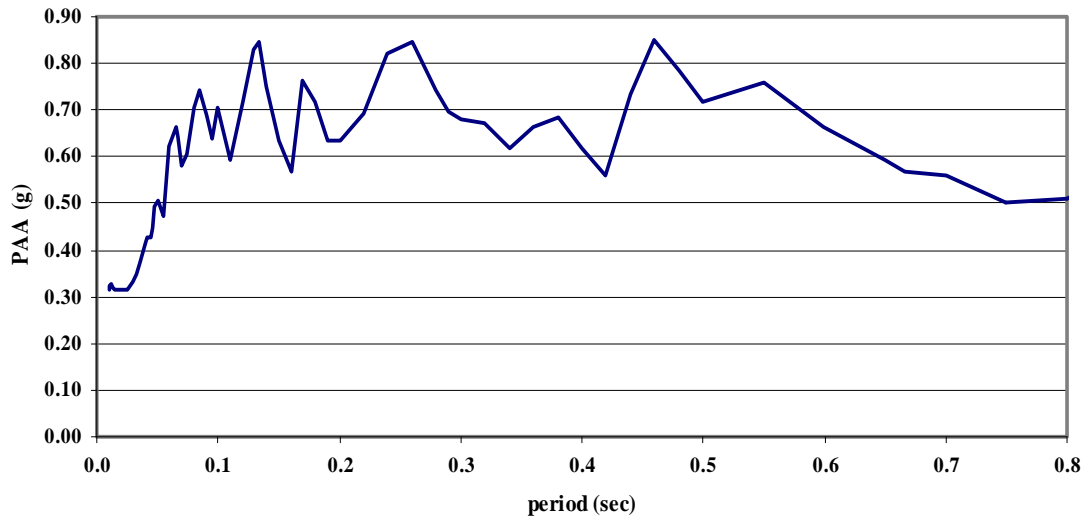
Figure 5.6 Response Spectrum - 1940 El Centro Earthquake

Figure 5.4 shows the maximum top displacement, base shear and base moment calculated using Eqs.5.25 to 5.27, respectively. Based on the results obtained using Model 4, for the empty tank, the maximum displacement at the top of the concrete wall was 21.79 mm with a maximum base shear of 167.3 kN. It can be observed that the results using the shape functions SF3 and SF4 match those obtained using Model 4 very well. A similar conclusion can be drawn concerning the maximum base moment.

For the full tank, the maximum displacement at the top of the concrete wall is about 35 mm for both SF3 and SF4. This is similar to the result obtained for Model 4 in the

previous study. The maximum displacements based on the previous study are 32.7 mm for Model 4 but it is 26.7 mm for Model 5. This difference in results may be attributed to the response within the small range of period in the response spectrum curve. However, it can be concluded that the shape functions SF3 and SF4 provide the most accurate results based on the maximum displacements.

The maximum base shears are 368.0 kN and 358.7 kN for SF3 and SF4, respectively. The maximum base shears from the previous study are 314.8 kN and 338.1 kN for Models 4 and 5, respectively. Again, the generalized SDOF system can provide accurate results in this respect. The values obtained for maximum base moments are also very similar to those of Models 4 and 5.

The hydrodynamic pressure is calculated by using Eq.5.1. The total hydrodynamic pressures P_i are calculated by integration of the hydrodynamic pressure along the depth of liquid as shown in Table 5.1. The distribution of hydrodynamic pressure along the height of wall is demonstrated in Figure 5.7. The overall response from this study compares very well with that obtained using Model 5 in which the effect of wall flexibility was considered in the analysis. However, hydrodynamic pressure distribution in the lower portion of tank wall obtained from this study is less than that of Model 5. This is due to the difference in magnitude of acceleration along the height of tank wall. The accelerations for the lower part of tank calculated using generalized SDOF is less than those from the Model 5 in previous study.

The effective height at which hydrodynamic pressure is applied, h_i, and the ratio of the height at which hydrodynamic pressure is applied to the depth of stored liquid h_i/H_L are shown in the Table 5.1. The value of h_i is about 5.7m and the h_i / H_L ratio is 0.51 for the shape functions SF3 and SF4. As stated earlier, in current design standards and codes, Housner's model (Housner 1963) is commonly used. The effective height at which the hydrodynamic pressure is applied is calculated using the following equations:

Table 5.1 Summary of Dynamic Response of Tall Tank for Different Shape Functions

Items		SF1	SF2	SF3	SF4	SF5
Empty Tank	$m_W / \widetilde{m}_W$	1.613	1.667	1.591	1.602	1.273
	$K_W (10^3 kN/m)$	1.608	6.431	4.823	4.894	4.894
	T1 (sec)	0.464	0.204	0.256	0.249	0.370
	A_a (m/sec^2)	0.837g	0.647g	0.840g	0.831g	0.674g
Full Tank	$\dfrac{m_W + m_L}{\widetilde{m}_W + \widetilde{m}_L}$	2.107	2.273	2.126	2.154	1.504
	T1 (sec)	0.598	0.246	0.318	0.307	0.528
	A_a (m/sec^2)	0.668g	0.827g	0.674g	0.677g	0.740g
	P_i (kN)	228.2	205.9	189.1	182.3	331.5
	M_i (kNm)	1253.5	1198.3	1086.2	1053.5	1730.4
	h_i (m)	5.493	5.821	5.744	5.779	5.220
	h_i / H_L	0.490	0.520	0.513	0.516	0.466
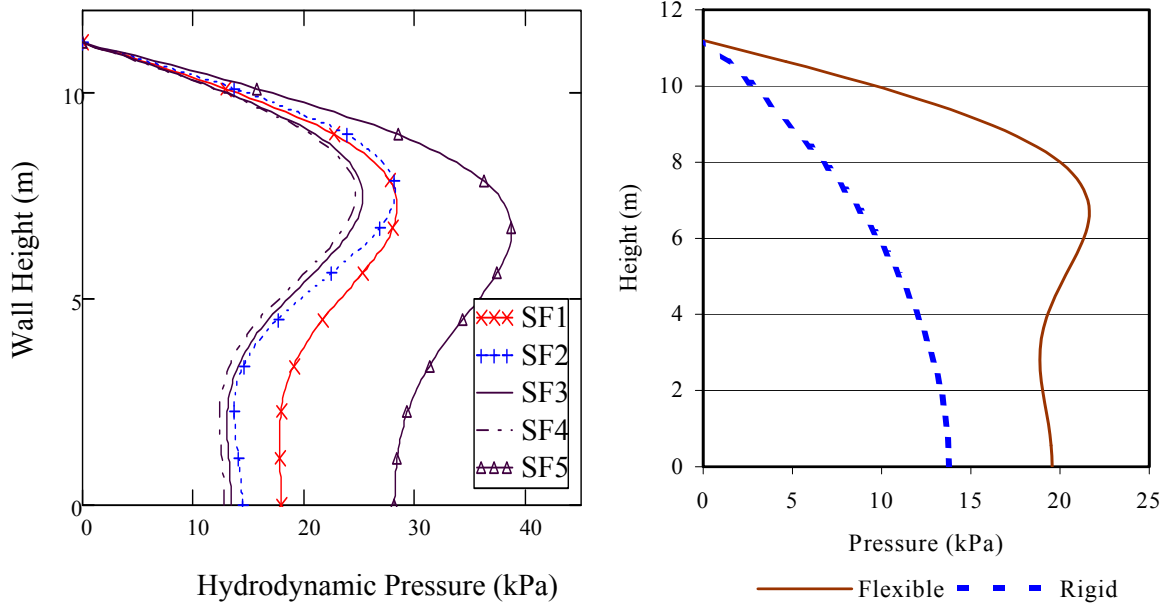
(a) Generalized SDOF System   (b) Model 5 (Sequential Coupling)

Figure 5.7 Hydrodynamic Pressure Distributions along Height of Wall - Tall Tank

For tanks with $\dfrac{2L_x}{H_L} < 1.333$,

[5.36] $\dfrac{h_i}{H_L} = 0.5 - 0.09375 \,(\dfrac{2L_x}{H_L})$

For tanks with $\dfrac{2L_x}{H_L} \geq 1.333$,

[5.37] $\dfrac{h_i}{H_L} = 0.375$

Based on the above equations, the value of h_i is 4.2m and the h_i / H_L ratio is 0.375 in this case. It can be seen that the height at which the hydrodynamic pressure is applied is higher than the one obtained using Housner's formula. This difference is due to the effect of the flexibility of tank wall which is not considered in Housner's model.

Figure 5.8 shows the comparison of results obtained using Models 4 and 5, finite element method using ANSYS® and the generalized SDOF system based on shape function SF3. Overall, the results are very similar between the different analysis models. It is noted that the results obtained using the generalized SDOF systems are more conservative than those obtained using the other models. For the sequential method using Models 5, the top displacement and base moment are less than those of the other models. For finite element method using ANSYS®, the base shear is less than those of the other models. This is due to the different sequential coupling analysis procedure used in the dynamic analysis.
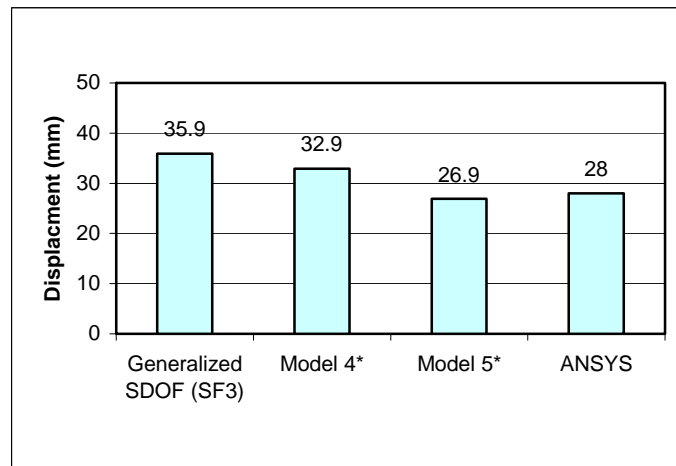
(a) Top displacement
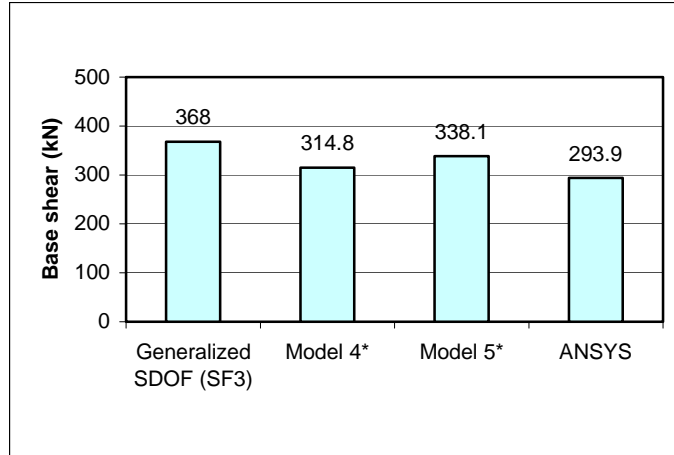
(b) Base shear
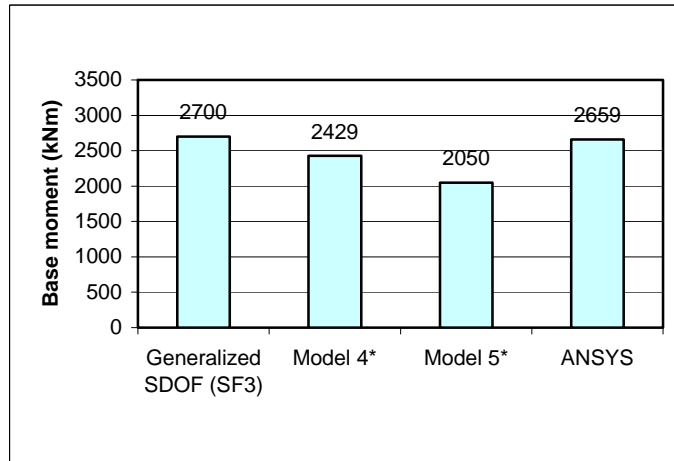
(c) Base moment

Figure 5.8 Comparison of Response of Tall Tank Using Different Analytical Models

5.3.2 Shallow Tank

Another example for a shallow tank studied previously is analyzed herein to further verify the efficiency of generalized SDOF system on dynamic analysis of liquid containing structures. The dimensions and properties of the shallow tank are as follows:

$\rho_w = 2300$ Kg/m^3 $\rho_l = 1000$ Kg/m^3 $E_c = 2.644 \times 10^4$ MPa $v = 0.17$

$L_x = 15$ m $L_z = 30$ m $H_w = 6.0$ m $H_l = 5.5$ m $t_w = 0.6$ m

The results of analysis are summarized in Table 5.2 and Figures 5.9 and 5.10 in the same forms that were presented for the case of tall tank. The hydrodynamic pressure distribution along the height of wall is shown in Figure 5.11.

Table 5.2 Summary of Dynamic Response of Shallow Tank

for Different Shape Functions

Items		SF1	SF2	SF3	SF4	SF5
Empty Tank	$m_W / \widetilde{m}_W$	1.613	1.667	1.591	1.602	1.273
	$K_W(10^3 kN/m)$	2.203	8.813	6.610	6.707	6.707
	T1 (sec)	0.196	0.086	0.108	0.105	0.156
	A_a (m/sec^2)	0.635g	0.731g	0.616g	0.650g	0.594g
Full Tank	$\dfrac{m_W + m_L}{\widetilde{m}_W + \widetilde{m}_L}$	2.159	2.341	2.187	2.217	1.530
	T1 (sec)	0.257	0.105	0.136	0.131	0.228
	A_a(m/sec^2)	0.841g	0.650g	0.806g	0.834g	0.744g
	P_i (kN)	79.87	45.18	63.05	62.64	91.93
	M_i (kNm)	210.06	125.15	172.8	172.9	229.8
	h_i (m)	2.63	2.77	2.74	2.76	2.50
	h_i / H_L	0.478	0.504	0.498	0.502	0.455
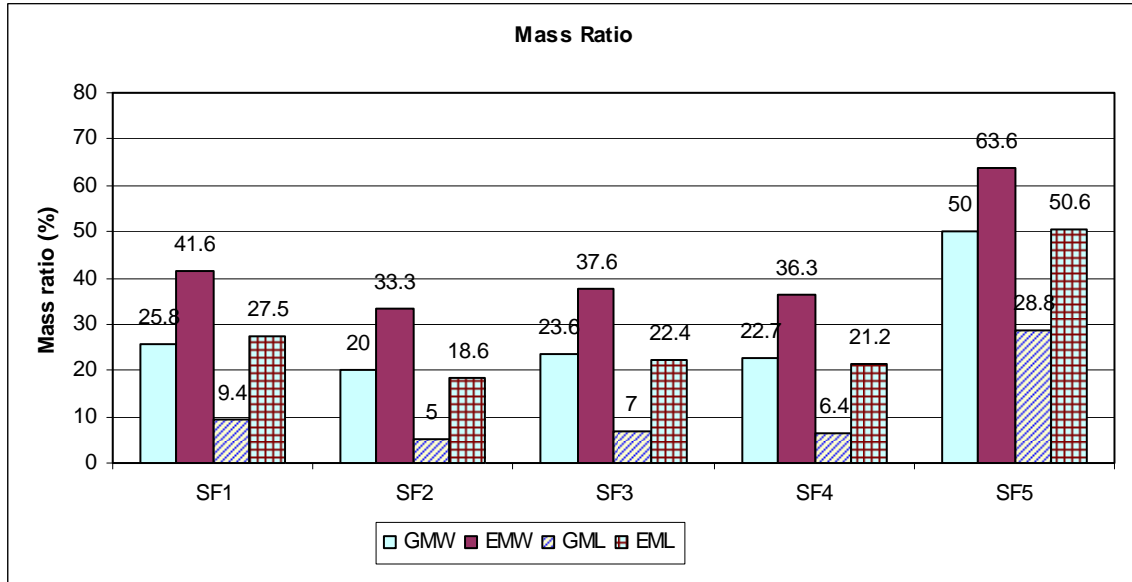
Figure 5.9 Comparison of Mass Ratios for Generalized SDOF Systems - Shallow Tank
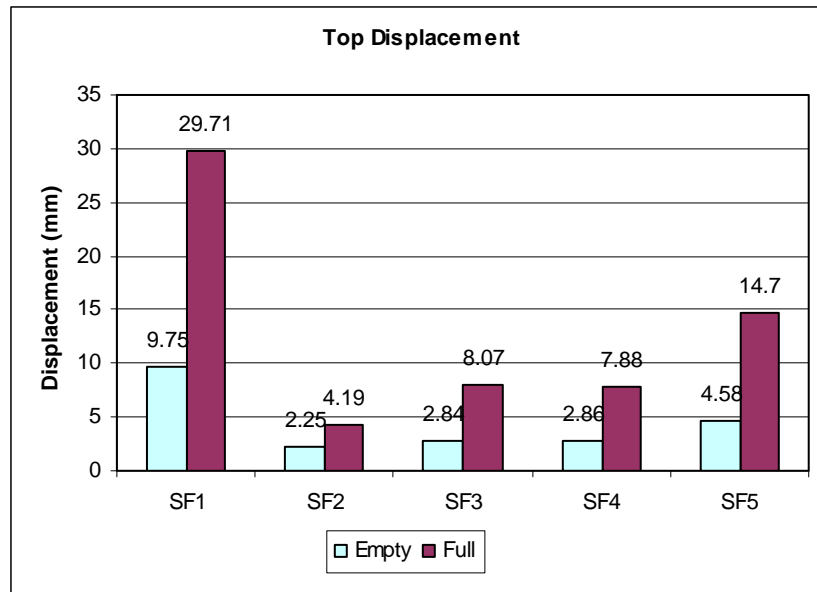
(a) Top displacement
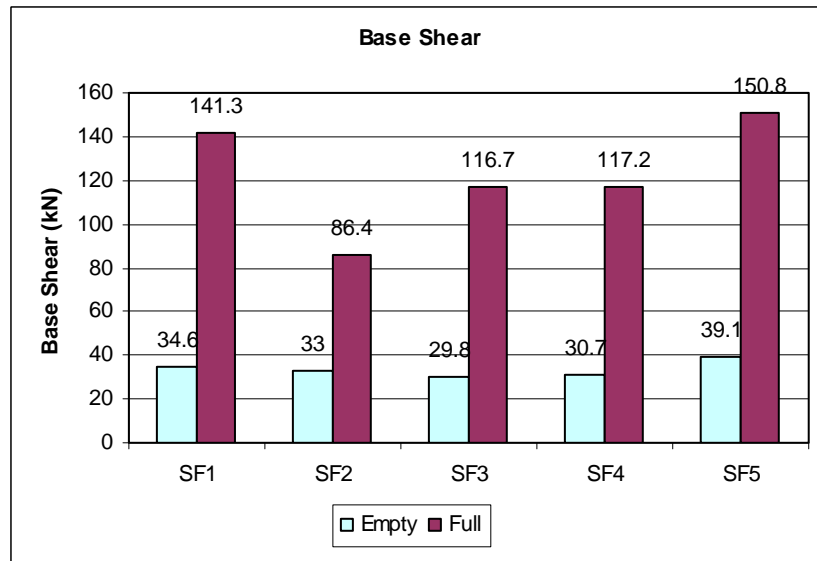
(b) Base shear
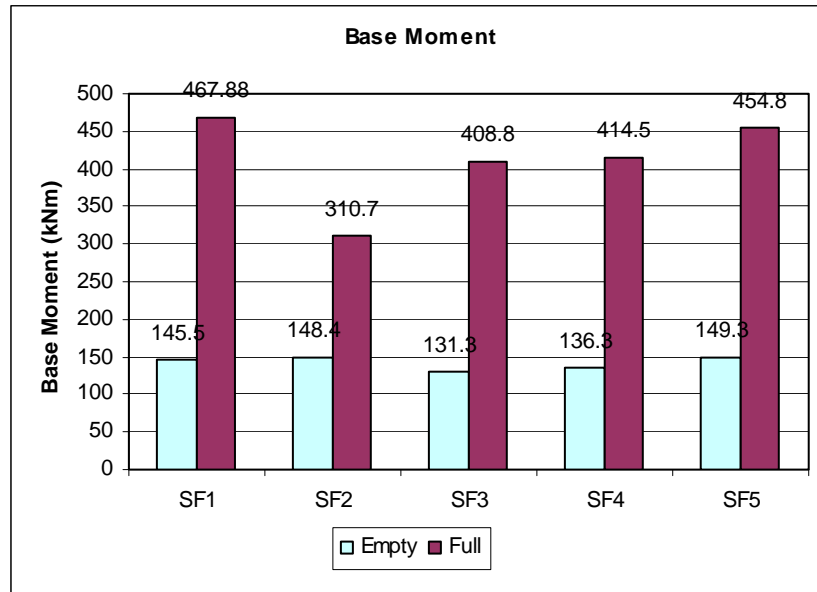
(c) Base moment

Figure 5.10 Comparison of Dynamic Reponses of Shallow Tank

(a) Generalized SDOF System

(b) Model 5 (Sequential Coupling)
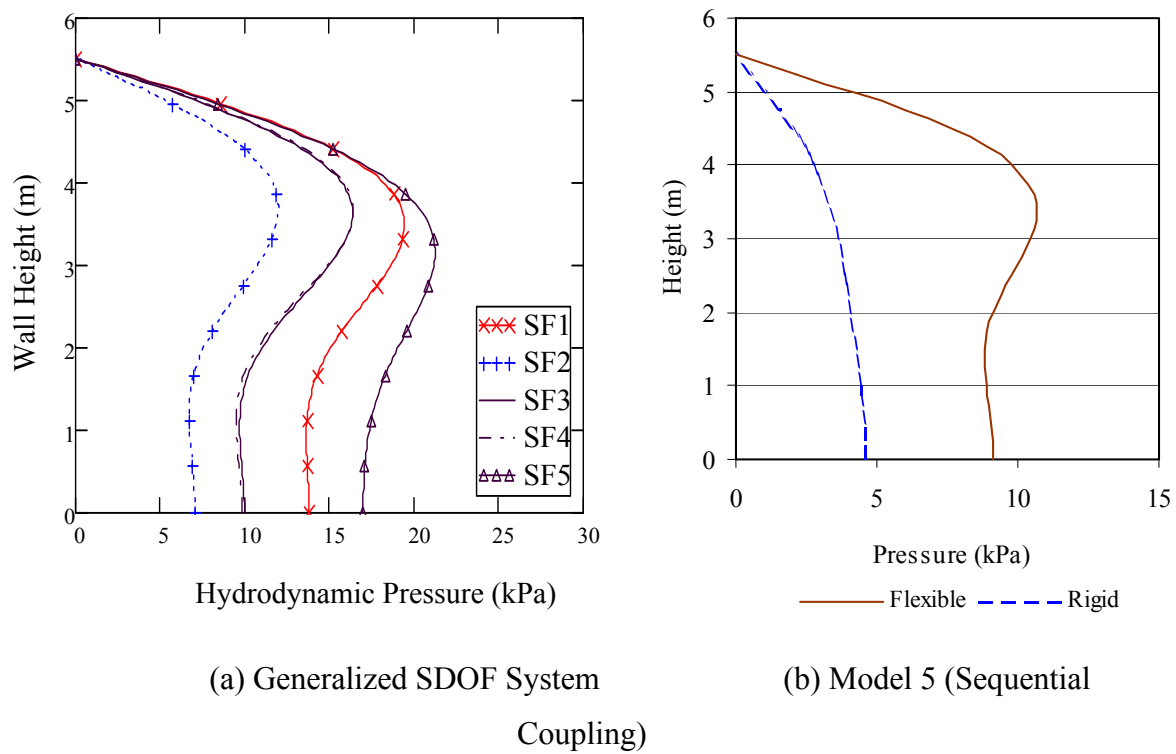
Figure 5.11 Hydrodynamic Pressure Distributions along Height of Wall – Shallow Tank

A similar trend in the behavior as that of the tall tank is observed for the shallow tank. However, there are small differences between the results of prescribed shape functions as compared to the results of previous study using Models 4 and 5. This can be attributed to difference in the periods of vibration for the response spectrum analysis. If similar periods were used for the two cases, the difference of results would be very small as shown in Table 5.3.

Table 5.3 Comparisons of Results of Analysis - Shallow Tank

Cases		SF3	SF4	Model 4*	Model 5*
Empty Tank	T1 (sec)	0.109	0.109	0.109	-
	A_a (m/sec^2)	0.604	0.604	-	-
	d_{max} (mm)	2.84	2.86	3.03	2.87
	V_B (kN)	29.3	28.6	33.0	33.4
	M_B (kNm)	128.7	126.7	143.5	138.5
Full Tank	T1 (sec)	0.148	0.148	0.148	-
	A_a(m/sec^2)	0.657	0.657	-	-
	d_{max} (mm)	7.82	7.92	5.91	4.50
	V_B (kN)	95.1	92.3	78.9	78.7
	M_B (kNm)	333.2	325.6	300.0	240.2
	P_i (kN)	51.4	49.3	-	-
	M_i (kNm)	140.8	136.0	-	-

5.4 Conclusions

A simplified method using the generalized SDOF system is presented in this chapter to determine the dynamic response of concrete rectangular liquid storage tanks. The theories are based on the well-known dynamic analysis principle in engineering practice. Compared to Housner's model in the current practice, the consistent mass and the effect of flexibility of tank wall on hydrodynamic pressures are considered. The advantage of the proposed method to the finite element method is to provide fairly accurate results while maintaining the simplicity in analysis.

Five prescribed shape functions representing the first mode shape of the fluid structure interaction system are used for analysis. It represents the typical open top rectangular tanks commonly used in water and wastewater treatment plants. For rectangular tanks with any other configurations, the generalized SDOF can also be applied provided that the proper mode shape functions are used in the analysis.

A tall and a shallow liquid storage tank studied previously are analyzed to demonstrate the efficiency of the generalized SDOF system applied for the dynamic analysis of liquid storage tanks. Comparing the results obtained using the generalized SDOF system as proposed in this chapter with those obtained using the other models and finite element method presented in Chapters 3 and 4, the proposed method can provide sufficiently accurate results. The study recommends that the effect of the flexibility of tank wall should be considered in the calculation of hydrodynamic pressures for concrete rectangular tanks. It is also recommended to use the design response spectrum method when using the generalized SDOF system for dynamic analysis of liquid storage tanks.

The other conclusions based on the results of analysis are as follows:

1. The shape functions SF3 and SF4 provide the most accurate results among the selected shape functions for the cantilever wall condition.
2. The results obtained from the generalized SDOF system based on the first mode shape functions agree well with those obtained using Models 4 and 5 as discussed in

Chapter 3.

3. With the increase in wall flexibility, more inertial mass of tank wall and added mass of liquid due to hydrodynamic pressure participate in the first mode of response.

4. The effective height at which the hydrodynamic pressure is applied considering the effect of flexibility of tank wall is higher than that in the rigid wall condition.

CHAPTER 6 PARAMETRIC STUDIES I
- EFFECTS OF ADDED MASS, EFFECTIVE HEIGHT AND HIGHER MODES

6.1 Introduction

In Chapter 5, a simplified method using the generalized single degree of freedom (SDOF) system was proposed for dynamic analysis of concrete rectangular liquid containing structures (LCS). In this chapter, parametric studies based on the generalized SDOF system are carried out. The five selected shape functions SF1 to SF5 corresponding to the first mode described in Chapter 5 are used in the study. The tall and the shallow tanks studied previously are used for parametric studies. The model used for analysis is based on 2D model which is represented by a unit width of liquid containing structure.

6.2 Amplification Factors for Hydrodynamic Pressure Considering Flexibility of Tank Wall

The factors affecting the flexibility of tank wall include the geometry of the structure such as height and thickness of wall, the modulus of elasticity of concrete and steel, reinforcement ratio, the state of cracking and boundary condition. Previous studies have indicated that the flexibility of tank wall can increase the hydrodynamic pressures significantly. In this section, the amplification factors for hydrodynamic pressure considering the flexibility of tank wall are studied.

In Chapter 5, the velocity potential method was used to calculate the hydrodynamic pressure applied on tank wall. The hydrodynamic pressure distribution for flexible and rigid wall conditions can be expressed based on Eqs.6.1 and 6.2 respectively as follows:

[6.1] $\quad p_{flex}(y) = \sum_{n=1}^{\infty} \frac{2\rho_l \tanh(\lambda_{i,n} L_x)}{\lambda_{i,n} H_L} \cos(\lambda_{i,n} y) \int_{0}^{H_L} \cos(\lambda_{i,n} y) \cdot \ddot{u}(y,t) dy$

[6.2] $\quad p_{rigid}(y) = \sum_{n=1}^{\infty} \frac{2(-1)^n \rho_l}{\lambda_{i,n}^2 H_L} \tanh(\lambda_{i,n} L_x) \cos(\lambda_{i,n} y) \cdot \ddot{u}_g(t)$

where $\lambda_{i,n}$ equals to $(2n-1)\pi/2H_L$ for the n-th mode, $\ddot{u}(y,t)$ and $\ddot{u}_g(t)$ are the acceleration along the height of wall and the ground acceleration, respectively.

The total hydrodynamic force P can be calculated by integrating the pressure distribution p along the height of liquid. The total hydrodynamic force considering the flexible wall P_{flex} and total hydrodynamic force based on the rigid wall condition P_{rigid} can be expressed as:

[6.3] $\qquad P_{flex} = \int_0^{H_L} p_{flex}(y) \cdot dy$

[6.4] $\qquad P_{rigid} = \int_0^{H_L} p_{rigid}(y) \cdot dy$

As presented in Chapter 5, the total acceleration along the height of wall can be calculated by the sum of acceleration relative to the ground and that due to the ground acceleration as follows (Chopra, 2001):

[6.5] $\qquad \ddot{u}(y,t) = \ddot{u}_r(y,t) + \ddot{u}_g(t)$

where $\ddot{u}_r(y,t)$ is the acceleration relative to the ground along the height of wall. For the generalized SDOF system, the generalized acceleration $\ddot{u}(t)$ at the specific time t along with the shape function $\psi(y)$ can be used to simplify the calculation. Then, the acceleration relative to the ground along the height of wall can be expressed as follows:

[6.6] $\qquad \ddot{u}_r(y,t) = \psi(y) \cdot \ddot{u}(t)$

The amplification factor $A_{acc}(t)$ is defined as the ratio of the generalized acceleration relative to the ground motion to that due to the ground acceleration under the maximum response. This is defined as:

[6.7] $\qquad A_{acc}(t) = \dfrac{\ddot{u}(t)}{\ddot{u}_g(t)}$

The amplification factor due to acceleration $A_{acc}(t)$ reflects the intensity on the wall when the tank wall is subjected to horizontal ground motion. With the increase in the ground acceleration, the acceleration relative to the ground $\ddot{u}(t)$ increases which results in increase of $A_{acc}(t)$.

The prescribed mode shapes as discussed in Chapter 5 reflect the flexibility of tank wall in the dynamic analysis. Therefore, amplification factors are introduced to consider the effect of flexibility of tank wall on hydrodynamic pressures. In this chapter, the five prescribed shape functions are used to investigate this effect.

The factor $a_{flex}(y)$ is defined as the amplification factor for hydrodynamic pressure distributions for a defined mode shape as expressed as follows:

$$[6.8] \quad a_{flex}(y) = \frac{\displaystyle\sum_{n=1}^{\infty} \frac{2 \cdot \rho_l}{\lambda_{i,n} \cdot H_L} \tanh(\lambda_{i,n} L_x) \cos(\lambda_{i,n} y) \int_0^{H_L} \cos(\lambda_{i,n} y) \cdot \psi(y) \cdot dy}{\displaystyle\sum_{n=1}^{\infty} \frac{2 \cdot \rho_l}{\lambda_{i,n} \cdot H_L} \tanh(\lambda_{i,n} L_x) \cos(\lambda_{i,n} y) \int_0^{H_L} \cos(\lambda_{i,n} y) \cdot dy}$$

Also, the factor A_{flex} is defined as the amplification factor for hydrodynamic force based on specified mode shape and can be obtained by integrating $a_{flex}(y)$ along the height of liquid as follows:

$$[6.9] \quad A_{flex} = \int_0^{H_L} a_{flex}(y) \cdot dy$$

It is worth noting that the factor $a_{flex}(y)$ represents the amplification due to the hydrodynamic pressure distribution and the factor A_{flex} represents the amplification factor due to the hydrodynamic force.

Substituting Eqs.6.2, 6.7 and 6.8 into Eq.6.1, the hydrodynamic pressure distribution considering the flexibility of tank wall p_{flex} can be written in a simplified form as follows:

[6.10] $p_{flex}(y) = (1 + a_{flex}(y) \cdot A_{Acc}(t)) p_{rigid}(y)$

Similar to the hydrodynamic pressure distribution, by substituting Eqs.6.4, 6.7 and 6.9 into Eq.6.3 the total hydrodynamic force considering the flexibility of tank wall can be simplified as that:

[6.11] $P_{flex} = (1 + A_{flex} A_{Acc}(t)) P_{rigid}$

Therefore, the total increase of hydrodynamic force due to the flexibility of tank wall can be expressed as that:

[6.12] $\Delta P = A_{flex} A_{Acc}(t) P_{rigid}$

It is worth noting that the amplification factor due to mode shape $A_{flex,}$ in combination with the amplification factor due to acceleration $A_{acc,}$ affect the hydrodynamic force when considering the flexibility of tank wall.

Figure 6.1 (a) and (b) show the hydrodynamic pressure distributions along the height of a tank wall for two different values of $A_{acc}(t)$. The ratio of L_x/H_L is assumed as 6.0 and $f(H_L)$ is a function of depth of liquid. The figures show that the increase in the amplification factor due to acceleration $A_{acc}(t)$ results in an increase in the hydrodynamic pressure distribution along the tank wall.

Figure 6.2 shows the relationship between the amplification factor due to mode shape A_{flex} and the ratio of L_x/H_L for the five selected shape functions. As mentioned previously, the shape functions SF1 and SF2 represent more flexible and a more rigid wall conditions, respectively. The increase of flexibility of tank wall results in higher amplification factors due to mode shape. In addition, it can be observed that for values of $L_x/H_L>1$, the amplification factor is constant for a prescribed shape function. This means that the increase in the ratio of hydrodynamic pressure due to the mode shape is constant when $L_x/H_L>1$.
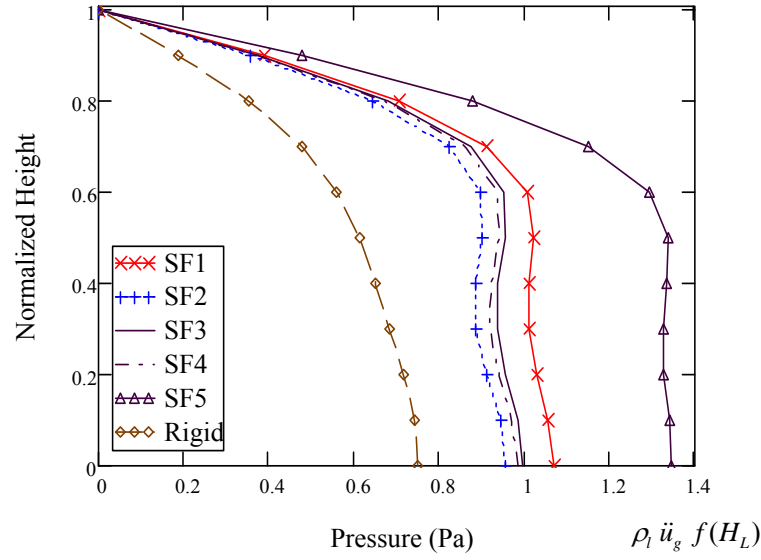
(a) $A_{acc} = 2.0$
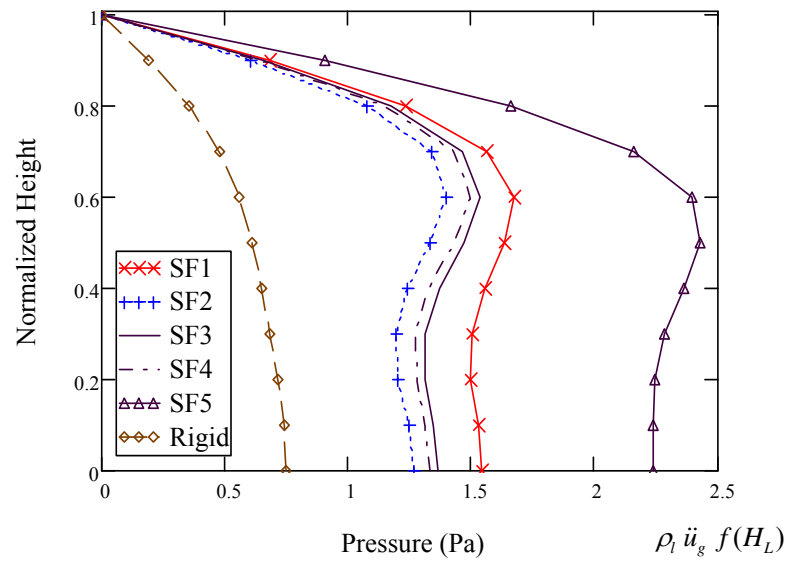
(b) $A_{acc} = 5.0$

Figure 6.1 Typical Hydrodynamic Pressure Distribution Based on Selected Shape Functions

Figure 6.3 shows the relationship between $\Delta P / P_{rigid}$ and A_{acc} for the tall tank that was used in the case studies in the previous chapters. The slope for each shape function is

equal to A_{flex} which can be also obtained from Figure 6.2 based on the L_x/H_L ratio. This indicates that the amplitude of hydrodynamic pressure due to the flexibility of tank wall increases by a constant value determined by the selected mode shape and the ratio of L_x/H_L. The increase in horizontal ground motion result in proportional increase in hydrodynamic force applied on the tank wall.
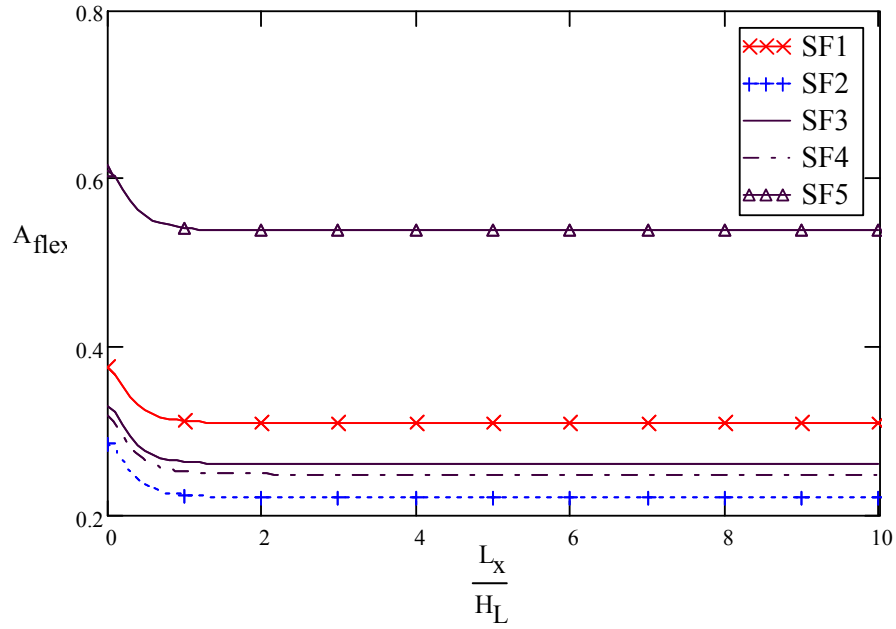
Figure 6.2 Amplification Factor due to Mode Shape A_{flex} vs. L_x / H_L
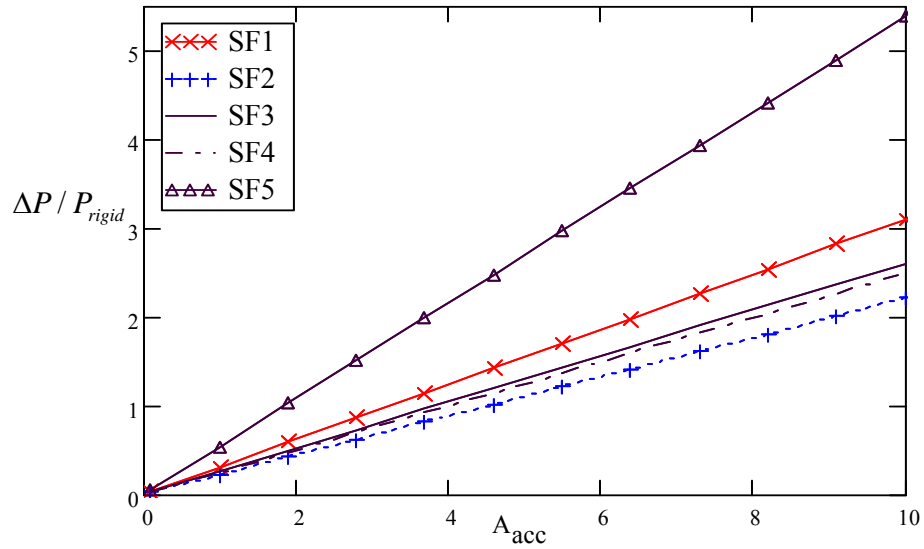
Figure 6.3 Amplification of Hydrodynamic Pressure vs. Amplification Factor due to Acceleration A_{acc}

6.3 Ratio of Added Mass of Liquid due to Impulsive Hydrodynamic Pressure to Half Mass of Liquid in Containment

When using the generalized SDOF system in the dynamic analysis of LCS, the hydrodynamic pressure is incorporated into the coupling analysis through the added mass of liquid in the system. The generalized and effective added mass of liquid due to impulsive hydrodynamic pressure can be calculated using Eqs.6.13 and 6.14 respectively as follows:

$$[6.13] \qquad \tilde{m}_L = \sum_{n=1}^{\infty} \frac{2 \cdot \rho_l}{\lambda_{i,n} \cdot H_L} \tanh(\lambda_{i,n} L_x)[\int_0^{H_L} \cos(\lambda_{i,n} y) \cdot \psi(y) dy]^2$$

$$[6.14] \qquad m_L = \sum_{n=1}^{\infty} \frac{2 \cdot (-1)^{n+1} \rho_l}{\lambda_{i,n}^2 \cdot H_L} \tanh(\lambda_{i,n} L_x) \int_0^{H_L} \cos(\lambda_{i,n} y) \cdot \psi(y) dy$$

Figure 6.4(a) shows the ratio of generalized added mass of liquid due to impulsive hydrodynamic pressure to the half mass of liquid in the containment $\tilde{m}_L / M_{L1}$ as a function of the ratio of half-length of tank to depth of liquid, L_x/H_L. Figure 6.4(b) shows the effect of similar ratio but the effective added mass of liquid due to impulsive hydrodynamic pressure m_L is used. The vertical coordinates in both cases represent the percentage of the added mass of liquid due to the impulsive component in participation of dynamic analysis in terms of the half mass of liquid in containment. The horizontal coordinate represents the relationship between water level and the length of tank wall parallel to the direction of earthquake. It is worth noting that M_{L1} is the half mass of liquid in the containment. As a result, $\tilde{m}_L / M_{L1}$ and m_L / M_{L1} can be calculated using Eqs.6.15 and 6.16 respectively as follows:

$$[6.15] \qquad \frac{\tilde{m}_L}{M_{L1}} = \sum_{n=1}^{\infty} \frac{2}{\lambda_{i,n} \cdot H_L^2 \cdot L_x} \tanh(\lambda_{i,n} L_x)[\int_0^{H_L} \cos(\lambda_{i,n} y) \cdot \psi(y) dy]^2$$

$$[6.16] \qquad \frac{m_L}{M_{L1}} = \sum_{n=1}^{\infty} \frac{2 \cdot (-1)^{n+1}}{\lambda_{i,n}^2 \cdot H_L^2 \cdot L_x} \tanh(\lambda_{i,n} L_x) \int_0^{H_L} \cos(\lambda_{i,n} y) \cdot \psi(y) dy$$
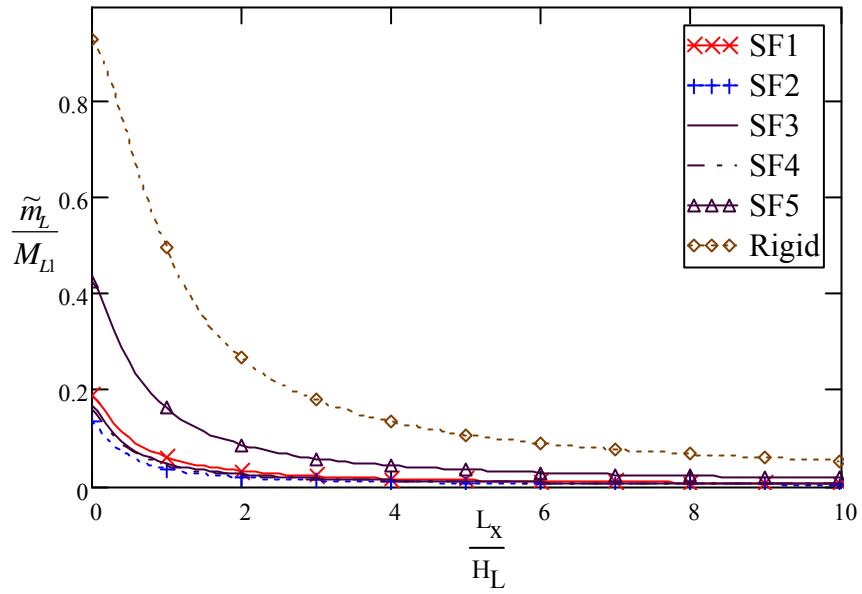
(a) Generalized Added Mass
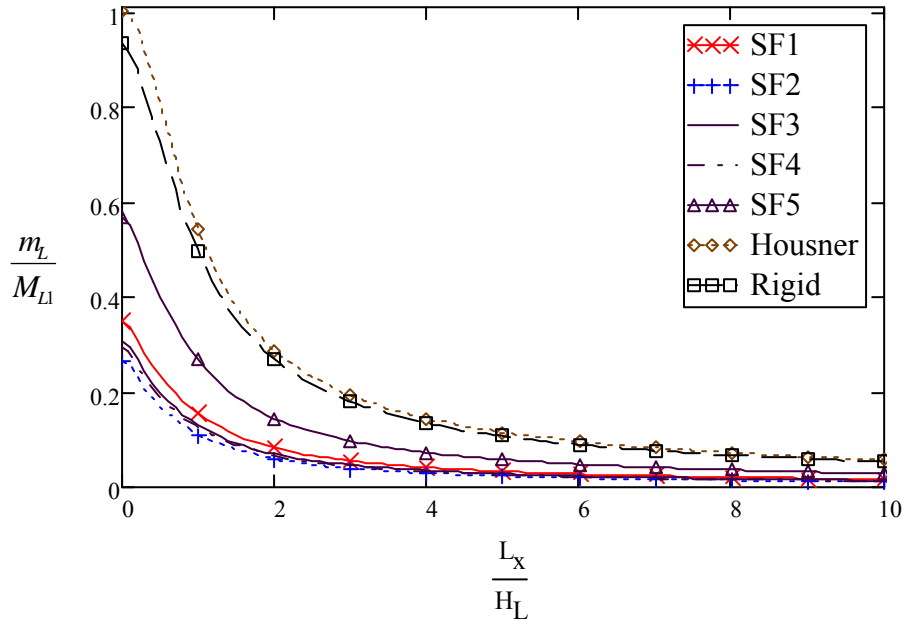
(b) Effective Added Mass

Figure 6.4 Ratio of Added Mass of Liquid due to Impulsive Hydrodynamic Pressure to Half Mass of Liquid in Tank vs. L_x / H_L Ratio

The graphs shown in Figure 6.4(b) also include Housner's model and the shape function corresponding to $\psi(y)=1$ in Eqs.6.15 and 6.16 for the rigid wall boundary condition. For Housner's model (Housner, 1963), the relationship between the effective added mass of liquid due to impulsive hydrodynamic pressure and the total mass of liquid in the containment is given as:

[6.17] $$\frac{M_i}{M_L} = \frac{\tanh[0.866\,(2L_x\,/\,H_L)]}{0.866\,(2L_x\,/\,H_L)}$$

Figure 6.4 shows similar trends for the curves based on the five selected shape functions, Housner's Model and $\psi(y)=1$ for the rigid wall boundary condition. It is worth noting that Housner's model is adopted in most of the current codes and standards for seismic analysis of LCS in which the effect of flexibility of tank wall is neglected.

The trends of added mass of liquid due to impulsive hydrodynamic pressure for rigid wall and flexible wall boundary condition are similar. It can be found that the added mass of liquid due to impulsive hydrodynamic pressure from the selected five shape functions are less than that obtained from the rigid wall boundary condition. This is due to the flexible wall condition in which only a fraction of the added mass of liquid due to impulsive hydrodynamic pressure participates in the first mode in the dynamic analysis of LCS as compared to the added mass of liquid due to impulsive hydrodynamic pressure based on the rigid wall boundary condition.

Based on the shape functions SF1 and SF2 which represent a more flexible and a more rigid wall conditions respectively, it can be found that when the wall become more flexible, more added mass of liquid due to impulsive hydrodynamic pressure participates in the first mode, but the difference is not very significant. For the realistic situation, the shape functions SF3 and SF4 can be used for the cantilever wall boundary condition.

In terms of the effect of ratio of L_x/H_L on $\tilde{m}_L/M_{L1}$ and m_L/M_{L1}, when L_x/H_L is less than

2.0, the values of $\widetilde{m}_L / M_{L1}$ and m_L / M_{L1} decrease at a faster rate than that for the case when L_x/H_L is larger than 2.0. When L_x/H_L is relatively large, $\widetilde{m}_L / M_{L1}$ and m_L / M_{L1} are constant. In other words, when the length of tank is significantly larger than the depth of liquid, a condition similar to an infinite reservoir can be assumed. In this situation, increasing the tank length in the direction parallel to the earthquake has no significant effect on the dynamic response of LCS.

6.4 Ratio of Added Mass of Liquid due to Impulsive Hydrodynamic Pressure to that in Rigid Wall Condition

In the previous section, the ratio of added mass of liquid due to impulsive hydrodynamic component to the half liquid mass in the containment was discussed. It was shown that when the values of L_x/H_L are relatively large, the percentage of added mass of liquid in participation of dynamic response for the prescribed shape functions become minimal.

For more insight on the effect of added mass of liquid due to impulsive hydrodynamic pressure in participation of dynamic response of LCS, the ratio of added mass of liquid due to impulsive hydrodynamic pressure to that of rigid wall condition is introduced. The factors $\widetilde{f}_{mass}$ and f_{mass} are for the generalized and the effective added masses of liquid, respectively, and defined as:

$$[6.18] \qquad \widetilde{f}_{mass} = \frac{\widetilde{m}_L}{\widetilde{M}_{rigid}} = \frac{\displaystyle\sum_{n=1}^{\infty} \frac{2 \cdot \rho_l \tanh(\lambda_{i,n} L_x)}{\lambda_{i,n} H_L} [\int_0^{H_L} \cos(\lambda_{i,n} y) \cdot \psi(y) dy]^2}{\displaystyle\sum_{n=1}^{\infty} \frac{2 \cdot \rho_l \tanh(\lambda_{i,n} L_x)}{\lambda_{i,n} H_L} [\int_0^{H_L} \cos(\lambda_{i,n} y) dy]^2}$$

$$[6.19] \qquad f_{mass} = \frac{m_L}{M_{rigid}} = \frac{\displaystyle\sum_{n=1}^{\infty} \frac{2 \cdot (-1)^{n+1} \rho_l \tanh(\lambda_{i,n} L_x)}{\lambda_{i,n}^2 H_L} \int_0^{H_L} \cos(\lambda_{i,n} y) \cdot \psi(y) dy}{\displaystyle\sum_{n=1}^{\infty} \frac{2 \cdot (-1)^{n+1} \rho_l \tanh(\lambda_{i,n} L_x)}{\lambda_{i,n}^2 H_L} \int_0^{H_L} \cos(\lambda_{i,n} y) dy}$$

where $\widetilde{m}_L$ and m_L are the generalized and effective added masses of liquid due to impulsive hydrodynamic pressure, respectively. $\widetilde{M}_{rigid}$ and M_{rigid} are the total generalized

and effective added masses of liquid due to impulsive hydrodynamic pressure using $\psi(y)=1$ for the rigid wall boundary condition, respectively. It can be found that the values of $\widetilde{M}_{rigid}$ and M_{rigid} are generally the same.

The advantages of introducing $\widetilde{f}_{mass}$ and f_{mass} in the dynamic analysis of LCS are as follows:

(1) The factors $\widetilde{f}_{mass}$ and f_{mass} consider the effect of flexibility of tank wall on hydrodynamic pressures. Eqs.6.18 and 6.19 show that selecting an appropriate mode shape function is critical to determine the factors $\widetilde{f}_{mass}$ and f_{mass}. Since the mode shape function reflects the flexibility of tank wall in dynamic analysis, the effect of flexibility of tank wall on hydrodynamic pressure can be incorporated in the dynamic analysis of LCS through the factors $\widetilde{f}_{mass}$ and f_{mass} which is currently ignored in the design practice.

(2) The factors $\widetilde{f}_{mass}$ and f_{mass} can reflect the participation of generalized and effective added mass of liquid due to impulsive hydrodynamic pressure in dynamic analysis. This study shows that only part of added mass of liquid participates in the dynamic analysis of LCS in the flexible tank wall condition. Therefore, it is important to determine the total added mass of liquid due to impulsive component and its percentage in participation of the dynamic response for different selected mode shapes. This is especially useful when considering the higher mode effect which is discussed later in this chapter.

Figures 6.5(a) and 6.5(b) show the participation factors of generalized and effective added mass of liquid due to impulsive hydrodynamic pressure including the flexibility of tank wall $\widetilde{f}_{mass}$ and f_{mass} as function of L_x/H_L, respectively. Though the horizontal coordinate is the same as that in Figure 6.4, the vertical coordinate represents the ratio of the added mass of liquid due to impulsive hydrodynamic pressure for the first mode shape to that in the rigid wall boundary condition.
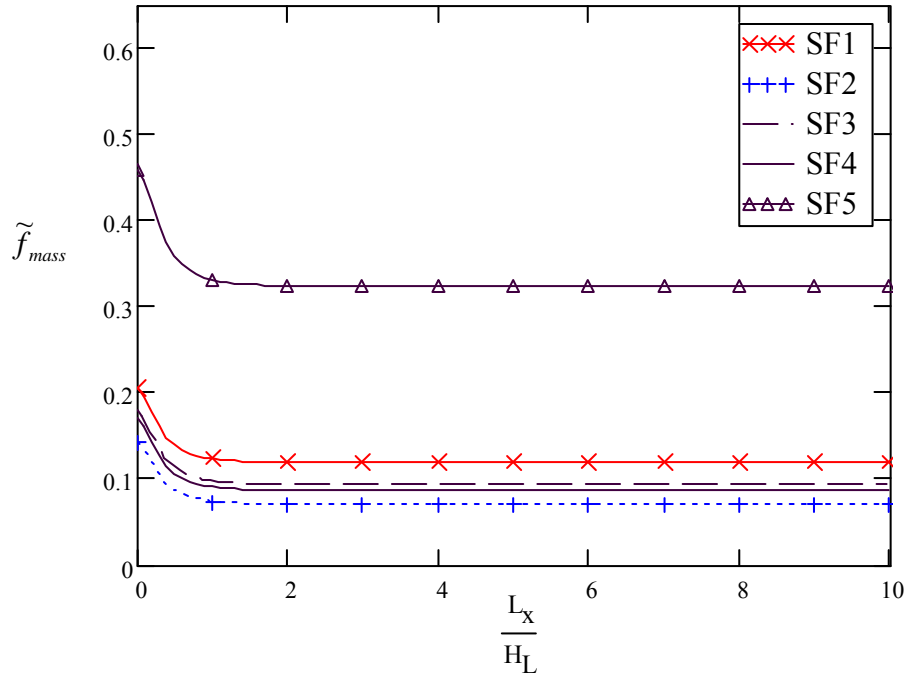
(a) Generalized Added Mass
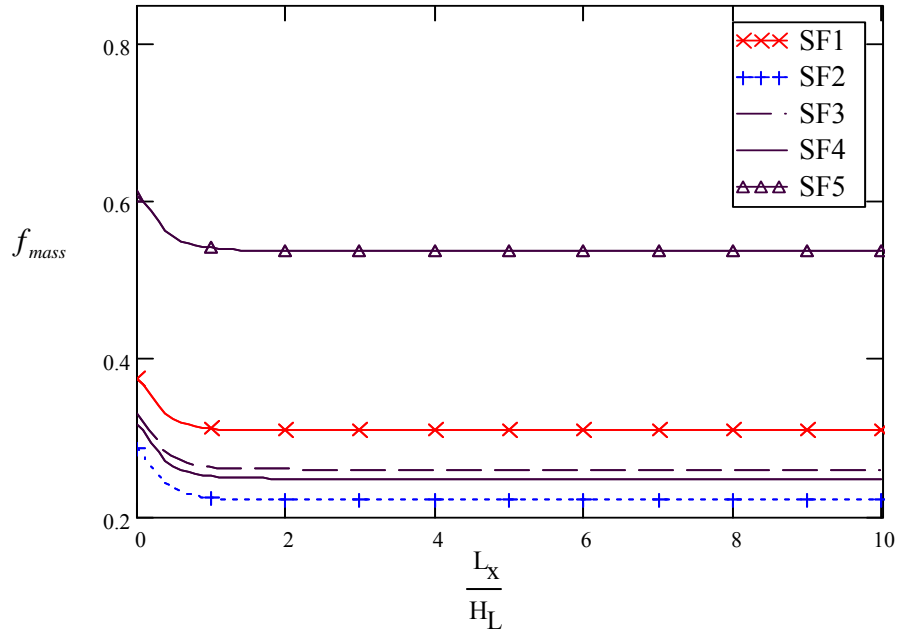
(b) Effective Added Mass

Figure 6.5 Ratio of Added Mass of Liquid due to Impulsive Hydrodynamic Pressure to that in Rigid Wall Condition vs. L_x / H_L Ratio

Figure 6.5 shows that for the values of $L_x/H_L>1$, the factors $\tilde{f}_{mass}$ and f_{mass} remain constant. This means that the ratio of the added mass of liquid due to impulsive hydrodynamic pressure to that in the rigid wall condition in participation of dynamic response is the same when $L_x/H_L>1$. This Figure is similar to that of the amplification factors for hydrodynamic pressure due to mode shape A_{flex} as shown in Figure 6.2. Therefore, the amplification factor considering the flexibility of tank wall is appropriately included in the generalized SDOF system in the dynamic analysis of LCS.

6.5 Effective Height

In the lumped mass SDOF system, the mass of the structure and the corresponding equivalent static force is applied at an effective height above the base. Based on the lumped mass SDOF system, Housner (Housner (1963)) developed a model for the dynamic analysis of LCS in which the inertial mass of concrete wall and the added mass of liquid due to hydrodynamic pressure are both lumped at the defined effective heights. The inertial mass of concrete tank wall is lumped at the center of gravity of the tank wall. If the tank wall is uniform, the inertial mass of tank wall is lumped at the middle height of tank wall. The added mass of liquid due to impulsive hydrodynamic pressure is lumped at a height above the base of the wall which represents the center of gravity of the impulsive lateral force. Accordingly, the effective heights can be calculated using Eqs.6.20 and 6.21 as follows:

For tanks with $\dfrac{2L_x}{H_L} < 1.333$,

[6.20] $\qquad \dfrac{h_i}{H_L} = 0.5 - 0.09375 \left(\dfrac{2L_x}{H_L}\right)$

For tanks with $\dfrac{2L_x}{H_L} \geq 1.333$,

[6.21] $\qquad \dfrac{h_i}{H_L} = 0.375$

The above effective heights are specified in current codes and standards for design

purpose. In the generalized SDOF system, the inertial mass of tank wall and the added mass of liquid due to hydrodynamic pressure can still be treated as lumped masses. However, the effective height defined in the generalized SDOF system is different compared to the lumped mass SDOF system used in Housner's model.

The effective height at which the effective inertial mass of tank wall is applied can be calculated as that:

$$[6.22] \qquad h_w = \frac{\displaystyle\int_0^{H_W} m(y) \cdot \psi(y) \cdot y \cdot dy}{\displaystyle\int_0^{H_W} m(y) \cdot \psi(y) \cdot dy}$$

Similarly, the effective height at which the effective added mass of liquid due to impulsive hydrodynamic pressure is applied can be calculated as that:

$$[6.23] \qquad h_i = \frac{\displaystyle\int_0^{H_L} \sum_{n=1}^{\infty} \frac{2\rho_l \tanh(\lambda_{i,n} L_x)}{\lambda_{i,n} H_L} \cos(\lambda_{i,n} y) \int_0^{H_L} \cos(\lambda_{i,n} y) \cdot \psi(y) dy \cdot y dy}{\displaystyle\sum_{n=1}^{\infty} \frac{2 \cdot (-1)^{n+1} \rho_l \tanh(\lambda_{i,n} L_x)}{\lambda_{i,n}^{2} H_L} \int_0^{H_L} \cos(\lambda_{i,n} y) \psi(y) dy}$$

Tables 6.1 and 6.2 show the effective heights for the shallow and tall tanks discussed in Chapter 5 using the generalized SDOF system.

The effective height h_w for the effective inertial mass of tank wall in the rigid wall boundary condition using $\psi(y)=1$ is $0.5H_w$ which is the same as that in Housner's model. However, in the flexible tank wall condition using the selected shape functions, the results are different as shown in Tables 6.1 and 6.2. The effective heights for the selected shape functions are higher than those calculated based on the rigid wall condition. The effective height for the effective inertial mass is about $0.75H_w$ for the cantilever wall based on the shape functions SF3 and SF4 for both tall and shallow tanks.

Table 6.1 Effective Heights –Tall Tank

Cases	Parameters	SF1	SF2	SF3	SF4	SF5	Rigid	Housner
Wall	h_W (m)	8.607	9.231	9.028	9.099	7.833	6.150	6.150
	h_W /H_W	0.70	0.75	0.73	0.74	0.64	0.5	0.5
Hydrodynamic Pressure	h_i (m)	5.493	5.821	5.744	5.779	5.220	4.500	4.681
	h_i / H_L	0.490	0.520	0.513	0.516	0.466	0.402	0.418
Combined Response	h (m)	6.930	7.541	7.343	7.414	6.309	5.097	5.075
	h/H_W	0.56	0.61	0.60	0.60	0.51	0.414	0.413

Table 6.2 Effective Heights –Shallow Tank

Cases	Parameters	SF1	SF2	SF3	SF4	SF5	Rigid	Housner
Wall	h_W (m)	4.205	4.497	4.406	4.440	3.818	3.00	3.00
	h_W /H_W	0.70	0.75	0.73	0.74	0.64	0.5	0.5
Hydrodynamic Pressure	h_i (m)	2.630	2.771	2.740	2.760	2.500	2.186	2.063
	h_i / H_L	0.48	0.50	0.50	0.50	0.45	0.397	0.375
Combined Response	h (m)	3.310	3.599	3.503	3.539	3.016	2.460	2.383
	h/H_W	0.55	0.60	0.58	0.59	0.50	0.410	0.397

The effective height h_i for the effective added mass of liquid due to impulsive hydrodynamic pressure obtained from the flexible wall condition based on the shape functions SF1 to SF5 are higher than those obtained using Housner's Model and the rigid wall condition using $\psi(y)=1$. For the cantilever wall condition in the tall tank, the effective heights h_i based on the shape functions SF3 and SF4 are about $0.51H_L$ which is about 28% and 23% higher than those obtained using Housner's Model and the rigid wall condition using $\psi(y)=1$, respectively. In the shallow tank, the effective heights h_i based on the shape functions SF3 and SF4 are about $0.5H_L$ which is about 26% and 33% higher than those obtained using Housner's Model and the rigid wall condition using $\psi(y)=1$, respectively.

Figure 6.6 shows the normalized effective height at which the effective hydrodynamic force is applied as function of the ratio of length of tank to liquid height L_x/H_L. The five selected shape functions, the rigid wall condition $\psi(y)=1$ and Housner's model are considered. It can be seen that for the rigid wall condition, the effective heights h_i obtained from Housner's model are close to those of rigid wall condition $\psi(y)=1$. It is worth noting that compared to the results obtained using $\psi(y)=1$ for the rigid wall

condition, the effective height h_i based on Housner's Model is higher than that of the tall tank and less than that of the shallow tank as indicated in Tables 6.1 and 6.2.
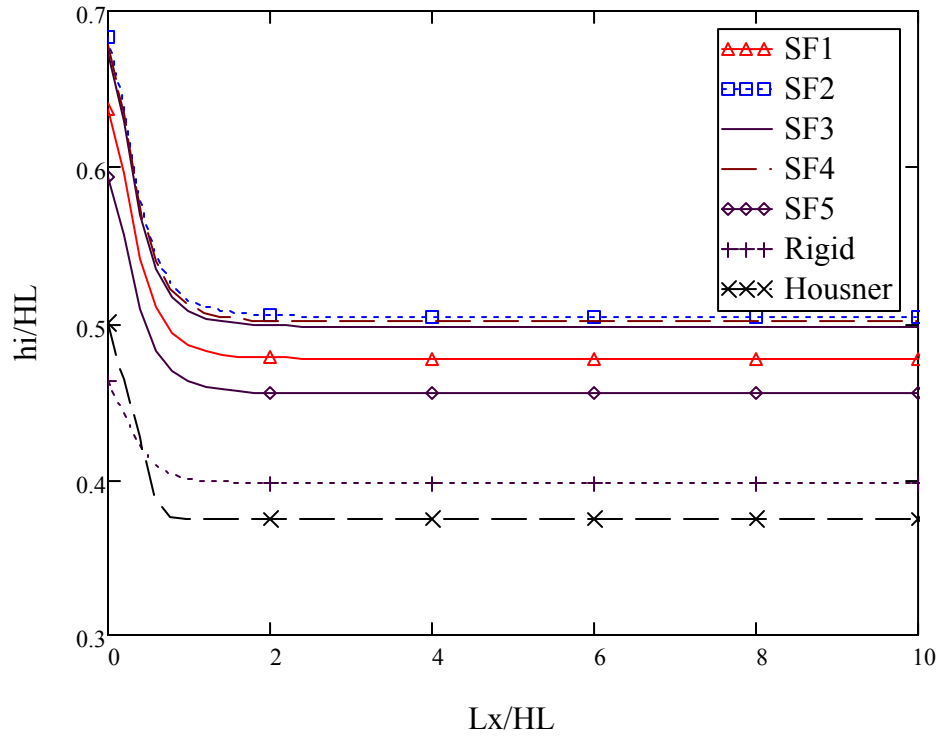
Figure 6.6 Ratio of Effective Height of Liquid for Impulsive Hydrodynamic Force to Height of Liquid vs. L_x/H_L Ratio

For the flexible wall condition, the effective height h_i is determined by the shape function along the height of wall. Figure 6.6 shows the effective height h_i is smaller for the shape function SF5 which is a shear dominated shape function in comparison with shape functions SF1 to SF4 which are flexural dominated shape functions. The reason is that for shape function SF5, the lower portion of the tank wall is expected to deflect more in comparison to the other shape functions.

For a tank containing liquid, the effective height at which the dynamic force is applied can be expressed using Eq.6.24. This is obtained by combining the inertial mass of tank wall and the added mass of liquid due to impulsive hydrodynamic pressure.

$$[6.24] \quad h = \frac{\left[\displaystyle\int_0^{H_W} m(y) \cdot \psi(y) \cdot y \cdot dy + \int_0^{H_L} \sum_{n=1}^{\infty} \frac{2\rho_l \tanh(\lambda_{i,n} L_x)}{\lambda_{i,n} H_L} \cos(\lambda_{i,n} y) \int_0^{H_L} \cos(\lambda_{i,n} y) \, \psi(y) dy \cdot y dy\right]}{\displaystyle\int_0^{H_W} m(y) \cdot \psi(y) \cdot dy + \sum_{n=1}^{\infty} \frac{2(-1)^{n+1} \rho_l}{\lambda_{i,n}^2 H_L} \tanh(\lambda_{i,n} L_x) \int_0^{H_L} \cos(\lambda_{i,n} y) \, \psi(y) dy}$$

Tables 6.1 and 6.2 also include the effective height h at which the dynamic force is applied on the liquid containing system. It shows that the effective height of liquid containing system considering the flexibility of tank wall is higher than that in the rigid wall condition. The increase is about 45% for the tall tank as compared to those using Housner's Model and the rigid wall condition $\psi(y)=1$. For the shallow tank, the increase is about 47% as compared to that using Housner's Model and 43% as compared to the rigid wall condition $\psi(y)=1$.

6.6 Contribution of Higher Modes

The effect of higher vibration modes on dynamic response of LCS has generally been ignored in the past because only the rigid wall condition is considered. However, when considering the flexibility of tank wall, the effect of higher vibration modes must be included in dynamic analysis. In this section, the contribution of higher modes on dynamic response of LCS is studied.

In a general condition, the beam vibrating function can be used as an admissible function to approximate the vibration mode (Paz, 1997). The general form can be expressed as that:

$$[6.25] \quad \psi_n(y) = a_n \sin(k_n y) + b_n \cos(k_n y) + c_n \sinh(k_n y) + d_n \cosh(k_n y)$$

Where a_n, b_n, c_n, d_n are constants and k_n is the eigenvalue for the n-th mode. All these parameters are determined based on the boundary conditions.

For the cantilever wall condition, the vibration function for the n-th mode is that:

$$[6.26] \quad \psi_n(y) = (\cosh(k_n y) - \cos(k_n y)) - \sigma_n(\sinh(k_n y) - \sin(k_n y))$$

126

where

[6.27]
$$\sigma_n = \frac{\cos(k_n H_W) + \cosh(k_n H_W)}{\sin(k_n H_W) + \sinh(k_n H_W)}$$

For the first mode, n=1, $k_n = 1.875/H_W$ and $\sigma_n = 0.734$. This shape function is defined as a new shape function SF6 expressed as:

[6.28]
$$SF6 = \psi_n(y) = (\cosh(1.875 \frac{y}{H_W}) - \cos(1.875 \frac{y}{H_W})) - 0.734((\sinh(1.875 \frac{y}{H_W}) + \sin(1.875 \frac{y}{H_W}))$$

The natural frequencies and normalized modes for cantilever wall for the first five modes of SF6 are summarized in Table 6.3.

Table 6.3 Natural Frequencies and Normal Modes for Cantilever Wall

Mode	$\psi_n(y) = (\cosh(k_n y) - \cos(k_n y)) - \sigma_n(\sinh(k_n y) - \sin(k_n y))$ $\sigma_n = \frac{\cos(k_n H_W) + \cosh(k_n H_W)}{\sin(k_n H_W) + \sinh(k_n H_W)}$, $\omega_n = C_n \sqrt{\frac{EI}{m(y)L^4}}$		
	k_n	σ_n	C_n
n=1	1.875/H_W	0.734	3.516
n=2	4.694/H_W	1.018	22.035
n=3	7.855/H_W	0.999	61.697
n=4	10.959/H_W	1.000	120.090
n=5	14.137/H_W	1.000	199.860

Figure 6.7 shows the normalized shape functions for the first five vibration modes of SF6 as well as the first mode of SF3. It can be seen that the shape function SF3 is similar to that of SF6 for the first mode using the general vibration equation for cantilever wall condition. However, the shape function SF6 is more complex in terms of mathematical expression as compared to the shape functions SF3 and SF4.

(a) 1st Mode   (b) 2nd Mode   (c) 3rd Mode

(d) 4th Mode   (e) 5th Mode
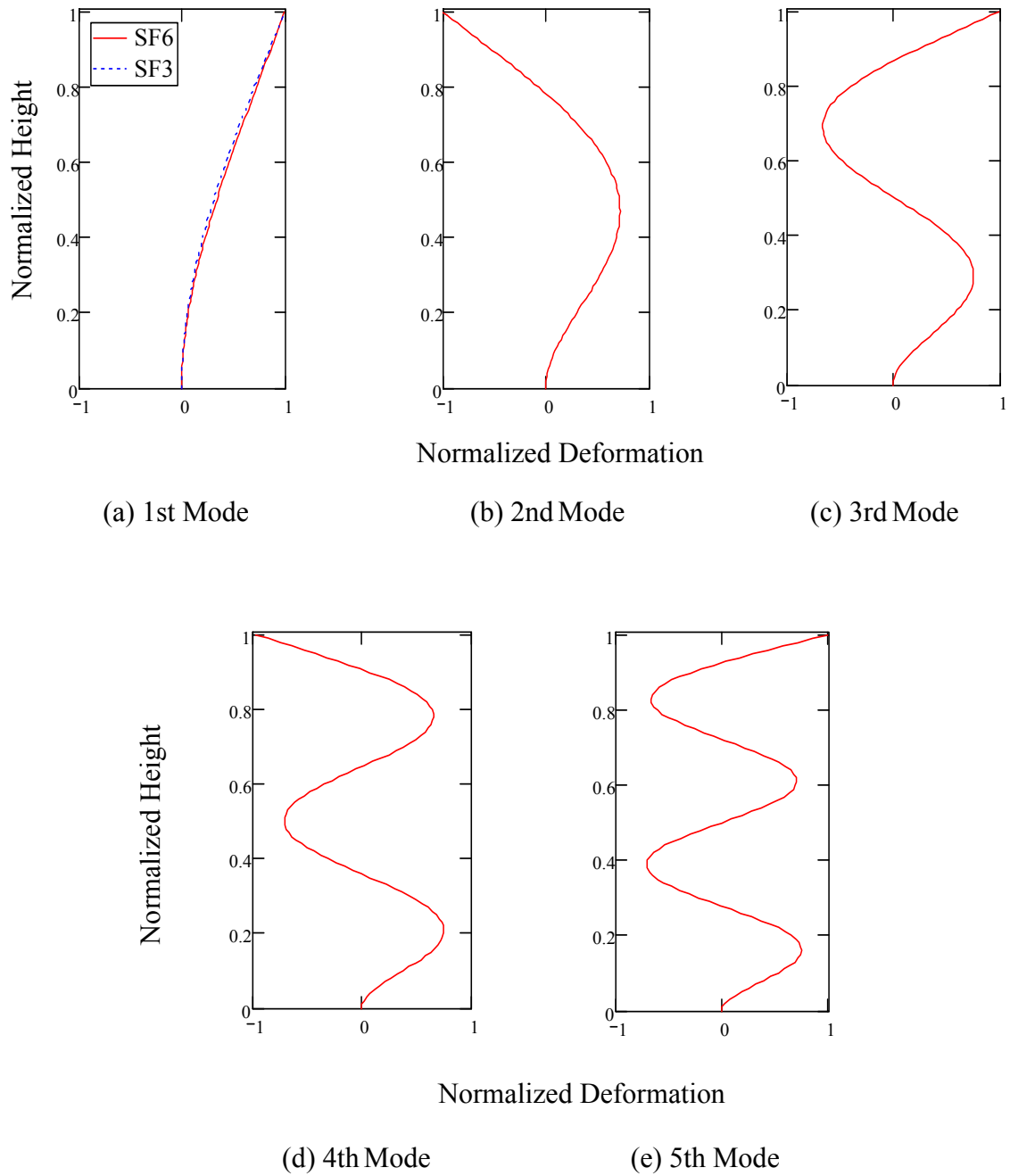
Figure 6.7 Normalized Shape Functions for Higher Modes

To study the effect of higher modes, both the tall and the shallow tanks studied previously are analyzed in this section. Figure 6.8 shows the design response spectrum based on ASCE 7-05 (ASCE, 2006) which is used to obtain the dynamic response of LCS. The site is assumed in the west coast of U.S. in Washington State and the parameters for the

design response spectrum are that:

(1) Short period maximum spectral response acceleration: S_s=1.25

(2) At a period of 1-second, the maximum spectral response acceleration: S_1=0.60

(3) Site class B
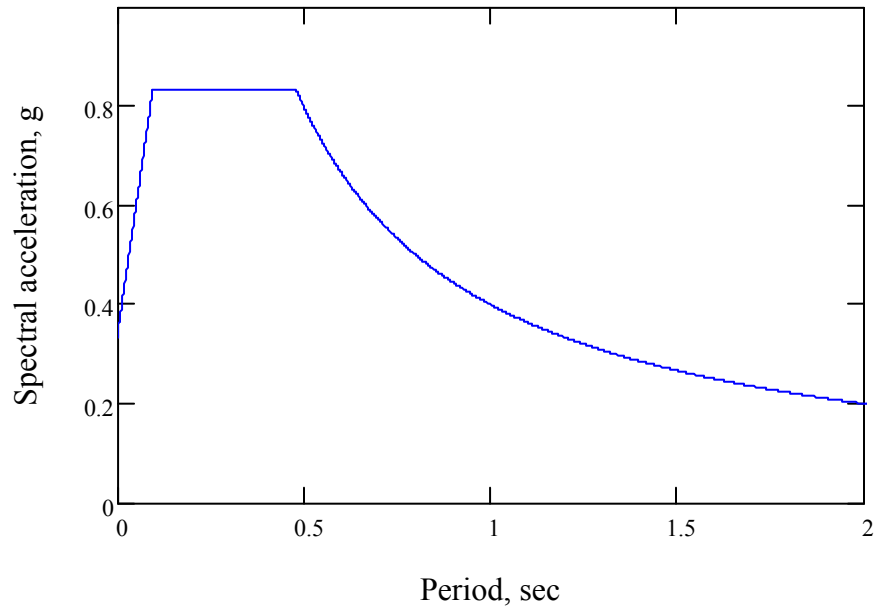
Figure 6.8 Design Response Spectrum

The results of analysis are summarized in Tables 6.4 and 6.5. For the first mode, the results obtained from shape function SF6 are similar to those obtained from the shape function SF3. For the empty tank, the fundamental periods obtained from SF6 are 0.260 sec and 0.110 sec for the tall and shallow tanks, respectively. This is consistent with the values of 0.256 sec for the tall tank and 0.108 sec for the shallow tank based on the shape function SF3.

For the full tank, the fundamental periods obtained from SF6 are 0.344 sec and 0.148 sec for the tall and shallow tanks, respectively. This is also consistent with the values of 0.335 sec for the tall tank and 0.145 sec for the shallow tank based on the shape function SF3. The dynamic response of LCS is also calculated based on the design response

spectrum as shown in Tables 6.4 and 6.5. The results obtained from shape function SF3 agree well with those obtained from shape function SF6 for the first mode.

Table 6.4 Summary of Dynamic Response of Tall Tank for Higher Modes

Mode		n=1(SF3)	n=1	n=2	n=3	n=4	n=5
Empty Tank	$\widetilde{m}_W\ (10^3\mathrm{kg})$	8.00	8.49	8.49	8.49	8.49	8.49
	% of $\widetilde{M}_W$	23.6	25.0	25.0	25.0	25.0	25.0
	$m_W\ (10^3\mathrm{kg})$	12.73	13.29	7.366	4.319	3.212	2.401
	% of M_W	37.6	39.1	21.7	12.7	9.5	7.1
	$m_W\ /\,\widetilde{m}_W$	1.591	1.566	0.868	0.509	0.382	0.283
	$K_W (10^3\mathrm{kN/m})$	4.823	4.969	195.144	1530	5815	16050
	T_n (sec)	0.256	0.260	0.041	0.015	$7.553\ \mathrm{x}10^{-3}$	$4.568\mathrm{x}10^{-3}$
	$A_a\ (\mathrm{m/sec}^2)$	0.833g	0.833g	0.547g	0.411g	0.373g	0.357g
	d_{max} (mm)	21.56	21.85	0.202	0.011	$2.021\ \mathrm{x}10^{-3}$	$5.237\ \mathrm{x}10^{-4}$
	V_B (kN)	165.45	170.02	34.29	8.857	4.492	2.379
	M_B (kNm)	1492	1519	88.22	13.88	6.83	2.07
Full Tank	$\widetilde{m}_L\ (10^3\mathrm{kg})$	4.32	4.876	10.02	6.375	2.523	1.629
	% of $\widetilde{M}_L$	7.2	8.1	16.7	10.6	4.2	2.7
	$m_L\ (10^3\mathrm{kg})$	13.46	14.43	23.16	10.13	7.594	7.103
	% of M_L	22.5	24.1	38.7	16.9	12.7	11.9
	$\dfrac{m_W + m_L}{\widetilde{m}_W + \widetilde{m}_L}$	2.126	2.074	1.649	0.972	0.989	0.939
	T_n (sec)	0.318	0.326	0.061	0.020	$8.613\ \mathrm{x}10^{-3}$	$4.988\ \mathrm{x}10^{-3}$
	$A_a(\mathrm{m/sec}^2)$	0.833g	0.833g	0.651g	0.438g	0.378g	0.359g
	d_{max} (mm)	44.362	45.574	0.999	0.041	$6.888\ \mathrm{x}10^{-3}$	$2.084\mathrm{x}10^{-3}$
	V_B (kN)	454.832	469.739	321.389	60.34	39.614	31.434
	M_B (kNm)	3337	3409	1352	102.23	93.283	88.67
	P_i (kN)	233.767	244.523	243.842	42.306	27.838	23.491
	M_i (kNm)	1343	1396	1152	73.967	75.373	81.759
	h_i (m)	5.744	5.710	4.726	1.748	2.708	3.480
	$h_i /\ H_L$	0.513	0.510	0.422	0.156	0.242	0.311

Table 6.5 Summary of Dynamic Response of Shallow Tank for Higher Modes

Mode	n=1(SF3)	n=1	n=2	n=3	n=4	n=5
$\widetilde{m}_W$ (10^3kg)	1.952	2.07	2.07	2.07	2.07	2.07
% of $\widetilde{M}_W$	23.6	25.0	25.0	25.0	25.0	25.0
m_W (10^3kg)	3.105	3.242	1.796	1.053	0.784	0.586
% of M_W	37.6	39.1	21.7	12.7	9.5	7.1
$m_W / \widetilde{m}_W$	1.591	1.566	0.868	0.509	0.382	0.283
K_W(10^3kN/m)	6.610	6.810	267.44	2097	7970	22000
T_n (sec)	0.108	0.110	0.017	6.234×10^{-3}	3.187×10^{-3}	1.927×10^{-3}
A_a (m/sec^2)	0.833g	0.833g	0.422g	0.366g	0.350g	0.343g
d_{max} (mm)	3.84	3.89	0.028	1.803×10^{-3}	3.374×10^{-4}	8.954×10^{-5}
V_B (kN)	40.35	41.47	6.45	1.92	1.03	0.56
M_B (kNm)	177.55	180.75	8.10	1.47	0.76	0.24
$\widetilde{m}_L$ (10^3kg)	1.137	1.284	2.667	1.609	0.650	0.410
% of $\widetilde{M}_L$	7.0	7.9	16.4	9.9	4.0	2.5
m_L (10^3kg)	3.648	3.91	6.266	2.826	2.124	1.922
% of M_L	22.4	24.0	38.4	17.3	13.0	11.8
$\dfrac{m_W + m_L}{\widetilde{m}_W + \widetilde{m}_L}$	2.187	2.132	1.702	1.055	1.077	1.011
T_n (sec)	0.136	0.139	0.026	8.323×10^{-3}	3.658×10^{-3}	2.110×10^{-3}
A_a(m/sec^2)	0.833g	0.833g	0.469g	0.377g	0.352g	0.344g
d_{max} (mm)	8.35	8.58	0.139	6.840×10^{-3}	1.259×10^{-3}	3.845×10^{-4}
V_B (kN)	120.6	124.6	63.1	15.125	10.806	8.533
M_B (kNm)	422.5	431.6	129.2	14.232	13.605	12.160
P_i (kN)	65.2	68.1	49.0	11.02	7.894	6.555
M_i (kNm)	178.5	185.5	111.6	11.09	11.445	11.312
h_i (m)	2.74	2.723	2.275	1.007	1.450	1.726
h_i / H_L	0.498	0.495	0.414	0.183	0.264	0.314

(The "Empty Tank" label spans the first eleven data rows; the "Full Tank" label spans the remaining rows.)

The results obtained from the second to the fifth mode shape are also presented in Tables 6.4 and 6.5. For the higher modes, a parameter referred to as the mode participation factor is calculated in a general equation as follows:

[6.29]
$$f_{part} = \frac{m_W + m_L}{\widetilde{m}_W + \widetilde{m}_L}$$

The above factor is used to evaluate the degree to which the n-th mode participates in the response. Compared to other building structures, the participation factor in the dynamic analysis of LCS includes not only the structure but also the added mass of liquid due to hydrodynamic pressure. Table 6.4 shows that the mode participation factor decreases significantly for the empty tank from 1.566 to 0.868 compared to the full tank from 1.882 to 1.424 corresponding to the first mode and second mode, respectively. This indicates that the added mass of liquid due to impulsive hydrodynamic pressure affects the mode participation factor significantly and the second mode shape must be considered in the dynamic response of LCS.

Tables 6.6 and 6.7 show the combination of dynamic response of LCS for the first two modes for the tall and shallow tanks, respectively. The Square Root of Sum of Square (SRSS) method is used for the combination. It can be seen that for the empty tank the contribution from the second mode is not significant. The base shear by including the second mode only increases by 2% and 1.2% compared to those obtained from the first mode shape for the tall and shallow tanks, respectively. However, it increases 21.2% and 12.1% for the tall and shallow tanks respectively in the full tank condition. Also, the contribution of second mode shape for the tall tank is more than that for the shallow tank. To investigate the effects of higher modes, the results of analysis including the combination of first three modes using SRSS method are presented in Tables 6.6 and 6.7. It can be observed that there is no significant increase in response of the tall and shallow tanks as compared to those including the combination of the first two modes. Therefore, it can be concluded that the second mode should be considered in the dynamic analysis of LCS, especially for tall tanks and the effect of third and higher modes can be ignored.

Table 6.6 Combination of Response of Higher Modes - Tall Tank

Items	Response	n=1	n=2	n=3	2 modes		3 modes	
					Combination	Increase %	Combination	Increase %
Empty Tank	d_{max} (mm)	21.850	0.202	0.011	21.851	0.00%	21.851	0.00%
	V_B (kN)	170.02	34.29	8.86	173.44	2.01%	173.67	2.15%
	M_B (kNm)	1519	88.22	13.88	1521.56	0.17%	1521.62	0.17%
Full Tank	d_{max} (mm)	45.574	0.999	0.041	45.585	0.02%	45.585	0.02%
	V_B (kN)	469.74	321.39	60.34	569.16	21.17%	572.35	21.84%
	M_B (kNm)	3409	1352	102.2	3667.3	7.58%	3668.7	7.62%

Table 6.7 Combination of Response of Higher Modes - Shallow Tank

Items	Response	n=1	n=2	n=3	2 modes		3 modes	
					Combin-ation	Increase %	Combin-ation	Increase %
Empty Tank	d_{max} (mm)	3.89	0.028	0.002	3.89	0.00%	3.89	0.00%
	V_B (kN)	41.47	6.45	1.92	41.97	1.20%	42.01	1.31%
	M_B (kNm)	180.75	8.10	1.47	180.93	0.10%	180.94	0.10%
Full Tank	d_{max} (mm)	8.58	0.139	6.840×10^{-3}	8.58	0.01%	8.58	0.01%
	V_B (kN)	124.6	63.1	15.1	139.7	12.09%	140.5	12.75%
	M_B (kNm)	431.6	129.2	14.2	450.5	4.38%	450.7	4.44%

6.7 Conclusions

The effect of different parameters on dynamic response of LCS using the generalized SDOF system is investigated in this chapter. The effect of flexibility of tank wall on dynamic response of LCS, which is generally ignored in design, is studied. The amplification factors due to acceleration and mode shape are introduced in which the effect of flexibility of tank wall can be incorporated in dynamic analysis of LCS. The amplitude of hydrodynamic pressure distribution considering the flexibility of tank wall is discussed.

The generalized and effective added masses of liquid due to impulsive hydrodynamic pressure in participation of dynamic response of LCS are studied. The participation ratios of added mass based on the half mass of liquid in LCS and the added mass in rigid wall condition are compared. The effects of flexibility of tank wall and length to height (L_x/H_L) ratio on the participation ratio of added masses of liquid in dynamic response of LCS are studied.

The effective heights at which the effective inertial mass of tank wall, the effective added mass of liquid and the total lateral force for the entire liquid containing system that are applied are studied in this study. The results obtained using the generalized SDOF system and the lumped mass SDOF system based on the rigid wall condition are compared.

A general beam vibrating function is used as an admissible function to study the effect of

higher vibration modes on the dynamic response of LCS. The natural frequencies and dynamic response of the tall and the shallow tanks for the first five modes in the cantilever wall condition are investigated.

Based on the results of the parametric studies, the conclusions that can be drawn in this chapter are summarized as follows:

(1) The hydrodynamic pressures increase significantly under stronger earthquakes having more flexible wall conditions.

(2) The ratio of the added mass of liquid for the n-th mode to the half mass of liquid in the container does not reflect the added mass of liquid in participation of dynamic response of LCS. However, the participation of added mass of liquid based on the rigid wall condition reflects the dynamic response of LCS more accurately.

(3) With the increase in the flexibility of tank wall, there is increase in the participation of the added mass of the liquid due to impulsive hydrodynamic pressure in dynamic analysis of LCS.

(4) When $L_x/H_L>1$, the ratio of the added mass of liquid due to impulsive hydrodynamic pressure to that in the rigid wall condition in participation of dynamic analysis is constant. A similar trend is observed in the amplification factor due to mode shape A_{flex}.

(5) The effective heights considering the flexibility of tank wall is higher than those of the rigid wall condition.

(6) For the empty tank condition, the use of only the first mode of response is appropriate. However, the second mode should be considered in the full tank condition, especially for tall tanks.

CHAPTER 7 PARAMETRIC STUDIES II
- EFFECTS OF TANK SIZE AND LIQUID HEIGHT

7.1 Introduction

In this chapter, the effects of tank size and liquid height on dynamic response of liquid containing structures (LCS) are studied. Compared to the previous chapters in which only two different tank sizes are considered for dynamic analysis, this chapter presents the trends of dynamic response of concrete rectangular LCS for different tank sizes. In addition, the current design codes and standards assume that the normalized distribution of hydrodynamic pressure along the height of tank wall is the same for different heights of liquid, i.e. $H_L=0\sim H_W$ in dynamic analysis. This assumption is correct for the rigid boundary condition in the calculation of hydrodynamic pressure. However, if the flexibility of tank wall is considered, the added mass of liquid varies with the height of liquid which is relative to the height of tank wall. Therefore, the effect of liquid height on the added mass of liquid should be considered. In this chapter, the trends of the added mass of liquid for different liquid heights are presented and can be used for design applications. Finally, the effects of tanks size and wall flexibility on the effective height of tank and the natural frequencies of LCS are investigated. It is worth noting that the shape function SF3 which provides the most accurate results for the first mode in the cantilever condition is used in this chapter.

7.2 Added Mass of Liquid Due to Impulsive Hydrodynamic Pressure

When using the generalized SDOF system in the dynamic analysis of LCS, the hydrodynamic pressure is incorporated into the coupling analysis through the added mass of liquid in the system. The generalized and effective added mass of liquid due to impulsive hydrodynamic pressure can be calculated using Eqs.7.1 and 7.2 respectively as follows:

[7.1] $$\widetilde{m}_L = \sum_{n=1}^{\infty} \frac{2 \cdot \rho_l}{\lambda_{i,n} \cdot H_L} \tanh(\lambda_{i,n} L_x)[\int_0^{H_L} \cos(\lambda_{i,n} y) \cdot \psi(y) dy]^2$$

[7.2] $$m_L = \sum_{n=1}^{\infty} \frac{2 \cdot (-1)^{n+1} \rho_l}{\lambda_{i,n}^2 \cdot H_L} \tanh(\lambda_{i,n} L_x) \int_0^{H_L} \cos(\lambda_{i,n} y) \cdot \psi(y) dy$$

The ratio of generalized and effective added mass of liquid due to impulsive hydrodynamic pressure to the half mass of liquid in the containment $\tilde{m}_L / M_{L1}$ and m_L / M_{L1} can be calculated using Eqs.7.3 and 7.4 respectively as follows:

[7.3] $\dfrac{\tilde{m}_L}{M_{L1}} = \sum\limits_{n=1}^{\infty} \dfrac{2}{\lambda_{i,n} \cdot H_L^2 \cdot L_x} \tanh(\lambda_{i,n} L_x)[\int\limits_0^{H_L} \cos(\lambda_{i,n} y) \cdot \psi(y) dy]^2$

[7.4] $\dfrac{m_L}{M_{L1}} = \sum\limits_{n=1}^{\infty} \dfrac{2 \cdot (-1)^{n+1}}{\lambda_{i,n}^2 \cdot H_L^2 \cdot L_x} \tanh(\lambda_{i,n} L_x) \int\limits_0^{H_L} \cos(\lambda_{i,n} y) \cdot \psi(y) dy$

It is worth noting that compared to the total mass of liquid in Housner's model, only half the mass of liquid is considered in the generalized SDOF system based on the two-fold symmetric fluid structural model. In addition, when the values of L_x/H_L are relatively large, the ratios of $\tilde{m}_L / M_{L1}$ and m_L / M_{L1} become minimal. Therefore, it is recommended to use the ratios of the added mass of liquid to that of rigid wall condition in the dynamic analysis of LCS. Therefore, the ratios of $\tilde{f}_{mass}$ and f_{mass} can be defined as follows:

[7.5] $\tilde{f}_{mass} = \dfrac{\tilde{m}_L}{\tilde{M}_{rigid}} = \dfrac{\sum\limits_{n=1}^{\infty} \dfrac{2 \cdot \rho_l \tanh(\lambda_{i,n} L_x)}{\lambda_{i,n} H_L}[\int\limits_0^{H_L} \cos(\lambda_{i,n} y) \cdot \psi(y) dy]^2}{\sum\limits_{n=1}^{\infty} \dfrac{2 \cdot \rho_l \tanh(\lambda_{i,n} L_x)}{\lambda_{i,n} H_L}[\int\limits_0^{H_L} \cos(\lambda_{i,n} y) dy]^2}$

[7.6] $f_{mass} = \dfrac{m_L}{M_{rigid}} = \dfrac{\sum\limits_{n=1}^{\infty} \dfrac{2 \cdot (-1)^{n+1} \rho_l \tanh(\lambda_{i,n} L_x)}{\lambda_{i,n}^2 H_L} \int\limits_0^{H_L} \cos(\lambda_{i,n} y) \cdot \psi(y) dy}{\sum\limits_{n=1}^{\infty} \dfrac{2 \cdot (-1)^{n+1} \rho_l \tanh(\lambda_{i,n} L_x)}{\lambda_{i,n}^2 H_L} \int\limits_0^{H_L} \cos(\lambda_{i,n} y) dy}$

where $\tilde{M}_{rigid}$ and M_{rigid} are the generalized and effective added masses of liquid due to impulsive hydrodynamic pressure using the shape function $\psi(y)=1$ for the rigid wall boundary condition, respectively. It can be found that the values of $\tilde{M}_{rigid}$ and M_{rigid} are generally the same.

7.2.1 Liquid Height H_L

When engineers design liquid containing systems, generally the process engineers determine the design liquid level based on the hydraulic requirements. However, when the liquid containing structures are in operation, it is possible that the actual liquid level may be less than the design maximum liquid level. Also, the liquid level H_L is normally less than the height of wall H_W for free sloshing of open top tanks and may vary for the process and maintenance reasons.

It is worth noting that the maximum design liquid height may not result in the maximum dynamic response in seismic design of LCS. It is possible that the fundamental natural frequency of LCS resulting from the lower liquid level condition causes higher dynamic response based on the response spectral acceleration and the participation of added mass of liquid. As a result, the effect of variable liquid level H_L on the dynamic response of liquid containing structures should be investigated. In this study, the liquid level inside tank can vary from the empty condition $H_L=0$ to the full level of tank height, i.e. $H_L=H_W$.

Another reason to consider the variable liquid level H_L in dynamic analysis is due to the distribution of added mass of liquid. As was shown in Chapter 5, the distribution of added mass of liquid along the height of tank wall is based on the prescribed shape functions. When the flexibility of tank wall is considered, the total added mass of liquid varies with the increase of liquid height in tank. Therefore, the effect of variable liquid level inside the tank should be considered in the calculation of the added mass of liquid based on the flexible wall condition. However, the current design codes and standards assume that the normalized hydrodynamic pressure distribution along the height of tank wall is the same for different height of liquid, i.e. $H_L=0\sim H_W$ in dynamic analysis which is only correct for the rigid wall boundary condition.

Figures 7.1(a) to 7.1(e) show the ratios of added mass of liquid as function of L_x/H_W. The horizontal coordinates L_x/H_W represents the different size of tanks as will be discussed later in this chapter. The vertical coordinates show the ratios of added mass of liquid based on the half mass of liquid in tanks, i.e. Figures 7.1(a) to 7.1(c) and for the rigid

boundary condition $\psi(y)=1$, i.e. Figures 7.1(d) and 7.1(e). Also, the Figures present the effect of variable liquid height on the added mass of liquid for which the liquid heights are $0.4H_W$, $0.6H_W$, $0.8H_W$ and $1.0H_W$.

(a) M_{rigid}/M_{L1} vs. L_x / H_W

(b) $\tilde{m}_L / M_{L1}$ vs. L_x / H_W
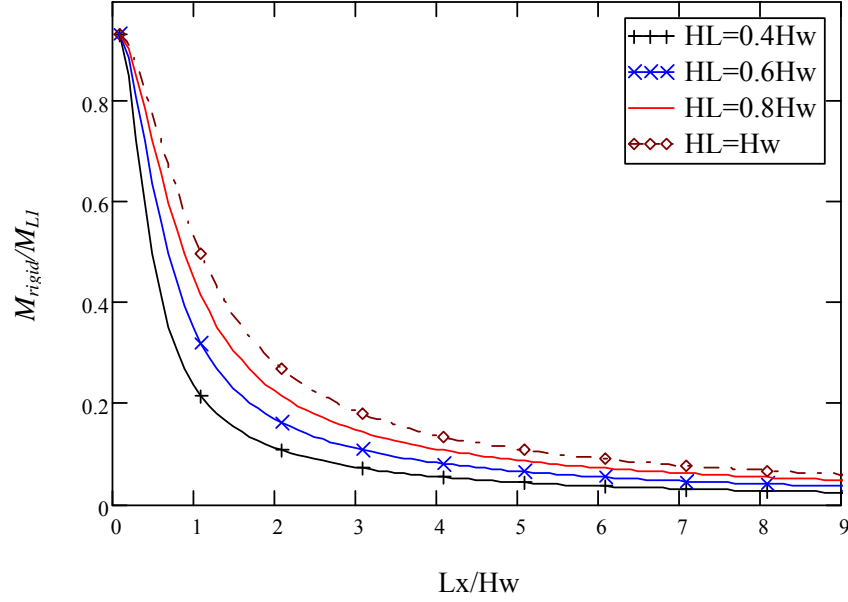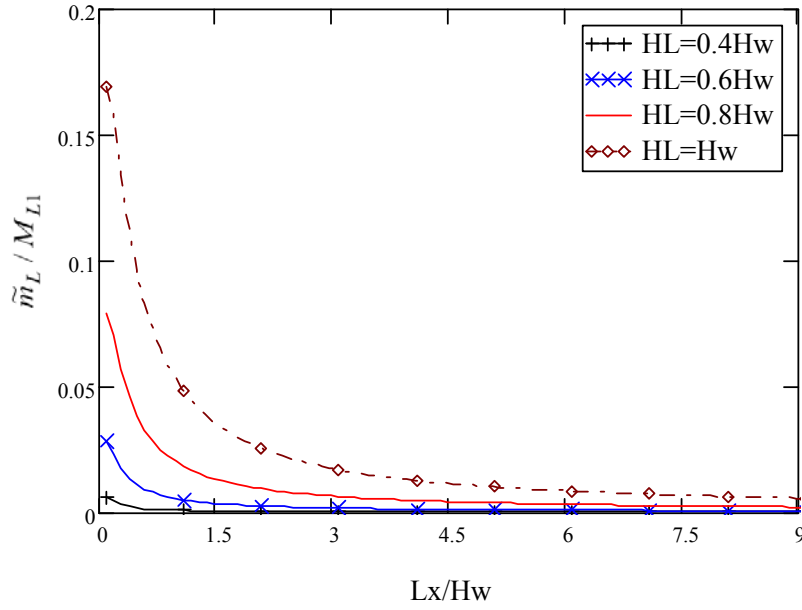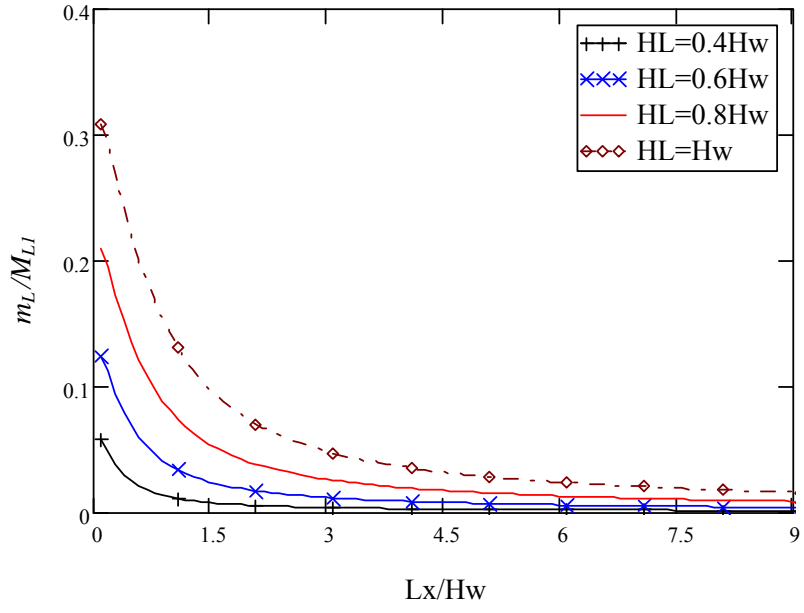
(c) m_L / M_{L1} vs. L_x / H_W
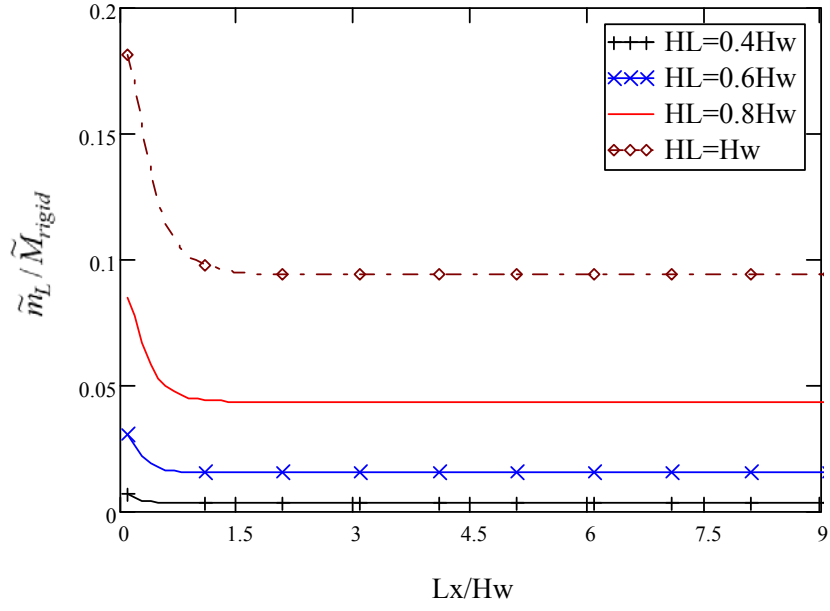
(d) $\widetilde{m}_L / \widetilde{M}_{rigid}$ vs. L_x / H_W
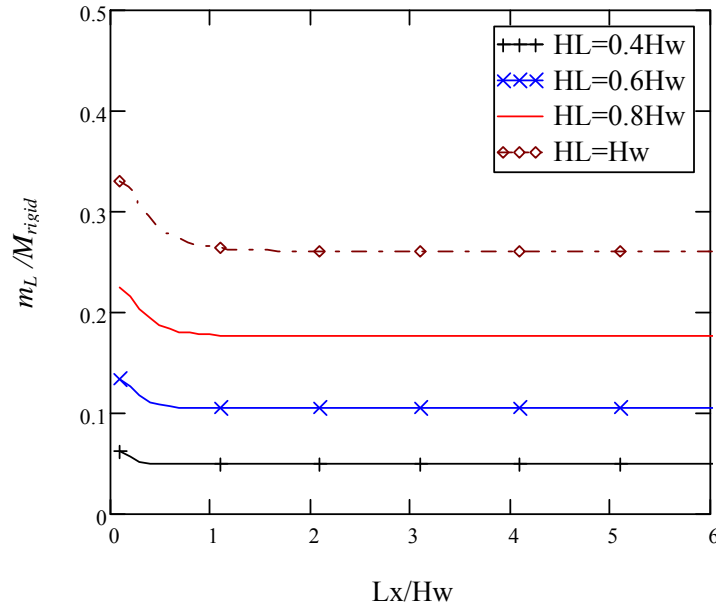
(e) m_L / M_{rigid} vs. L_x / H_W

Figure 7.1 Effect of Liquid Level on Added Mass of Liquid

It is worth noting that the ratios of added mass of liquid in the current design codes and standards are based on the total mass of liquid in tank. The design diagrams are similar to Figures 7.1(a) to 7.1(c). However, if the length of tank in the direction parallel to earthquake is significantly larger than the depth of liquid, increasing the tank length has no significant effect on the dynamic response of LCS. As a result, it is recommended to use the factors $\widetilde{f}_{mass}$ and f_{mass} for design purpose as shown in Figures 7.1(d) and 7.1(e).

Figure 7.1 shows that with the increase of liquid level in the tank, the added mass of liquid due to impulsive hydrodynamic pressure increases as expected.

Figure 7.1(a) shows that with the increase in the values of L_x/H_W up to about 3.0, the ratios of added mass of liquid based on the rigid boundary condition $\psi(y)=1$ to the mass of liquid in tank M_{rigid}/M_{L1} drop significantly for all levels of liquid height. With the increase in the value of L_x/H_W beyond 3.0, the ratio of M_{rigid}/M_{L1} approaches a constant

value. In addition, the value of L_x/H_W for the ratio of M_{rigid}/M_{L1} within the constant range is smaller for the lower liquid level as compared to the higher liquid level.

A similar trend to that shown in Figure 7.1(a) appears in the ratio of generalized and effective added mass of liquid to the half mass of liquid in tank as shown in Figures 7.1(b) and 7.1(c). When the value of L_x/H_W exceeds 1.5, the ratio of $\tilde{m}_L / M_{L1}$ approaches a constant value.

It is worth noting that the hydrodynamic pressure is a function of the effective added mass of liquid as discussed in Chapter 5. Provided that the acceleration is known, the hydrodynamic pressure can be calculated. Therefore, Figure 7.1(c) also reflects the trend of the force due to hydrodynamic pressure for different heights of liquid in a tank.

Figures 7.1(d) and 7.1(e) show that for values of $L_x/H_W > 1$, the factors $\tilde{f}_{mass}$ and f_{mass} remain constant. This means that there is no significant change on the ratio of the added mass in participation of dynamic response based on the rigid wall boundary condition, when $L_x/H_W > 1$.

7.2.2 Effect of Length of Tank L_x

The ratio of length of tank to the liquid height, L_x/H_L is normally used as a parameter to study the effect of tank size and liquid height on the dynamic response of LCS. It is presumed that the tank is full with liquid height equal to height of tank wall. However, as the liquid level may vary as discussed in the previous section, the ratio of L_x/H_L may not remain constant. In this study, the height of tank wall H_w rather than the height of liquid H_L is used to consider the size effect of tank. The advantages of using such an approach are as follows:

(1) Both L_x and H_w are fundamental parameters representing the configuration of a tank, and

(2) The height of a tank wall is a pre-determined parameter in dynamic analysis while the height of liquid may be considered as a variable.

In this study, four cases are considered to study the effect of length of tank, L_x. They are $0.1H_w$, $0.5H_w$, $1.0H_w$ and $5H_w$. The case when L_x is equal to $0.1H_w$ may not be considered as practical but it will give an indication of trend of results in terms of convergence of the hydrodynamic pressure and the corresponding added mass. The cases of $0.5H_w$, $1.0H_w$ and $5H_w$ represent the narrow, median and broad tanks, respectively.

The curves in Figure 7.2 demonstrate the effect of tank length L_x on the generalized and effective added mass of liquid due to impulsive hydrodynamic pressure. The horizontal coordinate is the ratio of the height of liquid to the height of tank wall H_L/H_W, which represents the different height of liquid inside tank. The vertical coordinates are the parameters in relation with the generalized and effective added mass of liquid due to hydrodynamic pressure. As mentioned before, two approaches, i.e. using the half mass of liquid in tanks similar to that in the current design codes and standards, and the added mass of liquid based on the rigid boundary condition proposed in this study are presented.

(a) M_{rigid}/M_{L1} vs. H_L / H_W (b) $\widetilde{m}_L / M_{L1}$ vs. H_L / H_W
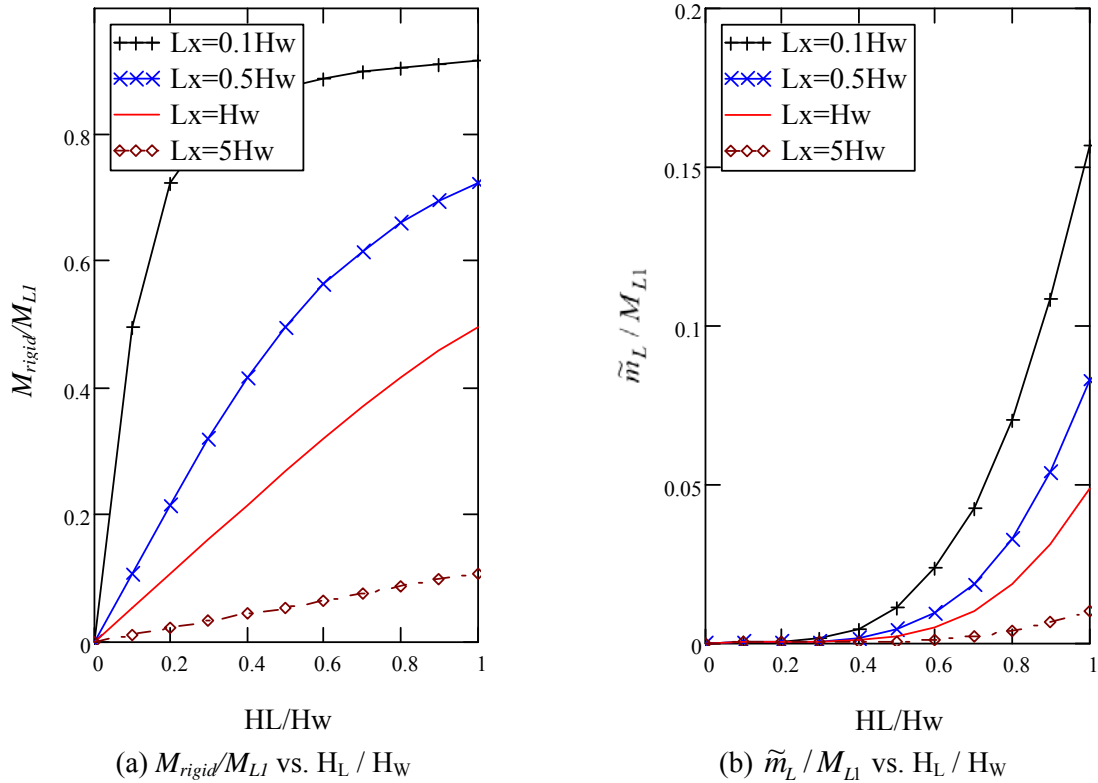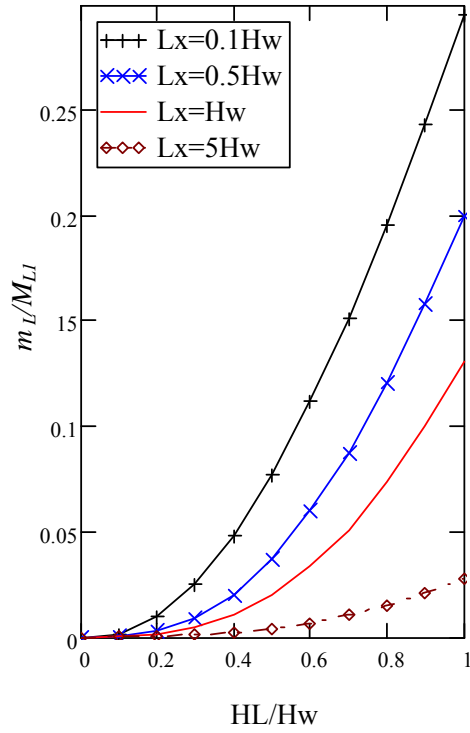
(c) m_L / M_{L1} vs. H_L / H_W
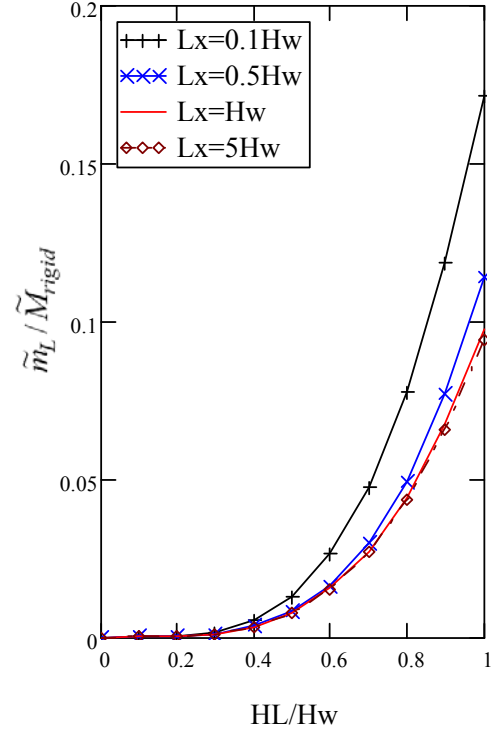
(d) $\widetilde{m}_L / \widetilde{M}_{rigid}$ vs. H_L / H_W
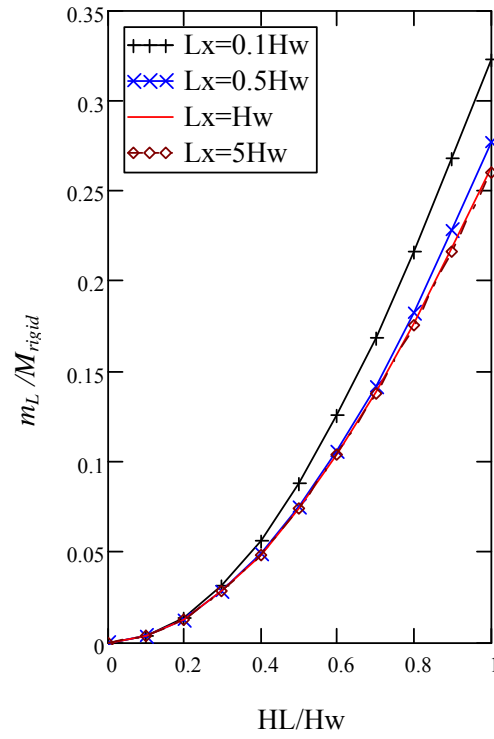
(e) m_L / M_{rigid} vs. H_L / H_W

Figure 7.2 Effect of Length of Tank and Height of Liquid on Added Mass of Liquid

Figure 7.2(a) shows that the ratio of added mass of liquid due to hydrodynamic pressure based on the rigid boundary condition to the half mass of liquid inside tank M_{rigid}/M_{L1} increases with the increase in H_L/H_w. This rate of increase is more significant for smaller L_x/H_w values. For values of L_x equal or larger than the height of tank wall, this relationship is almost linear.

Figures 7.2(b) and 7.2(c) show that the ratio of generalized and effective added mass of liquid due to hydrodynamic pressure to the half mass of liquid inside tank $\tilde{m}_L/M_{L1}$ and m_L/M_{L1}. It can be seen that for the broad tank, the rates of increase in the mass ratios are less with the increase in the height of liquid. Also it can be concluded that tanks with liquid level closer to top of the tank wall contributes more added mass in the dynamic analysis.

Figures 7.2(d) and 7.2(e) show the ratios of generalized and effective added mass of liquid due to impulsive hydrodynamic pressure to the added mass based on the rigid boundary condition, i.e. $\tilde{m}_L/\tilde{M}_{rigid}$ and m_L/M_{rigid}, with respect to the different lengths of tank. It can be concluded that with the exception of the case when $L_x/H_W=0.1$, the curves converge almost to the same values. This is consistent with the conclusion drawn in Figure 7.1(d) and 7.1(e). In addition, when the liquid level is below $0.3H_W$, the ratio of $\tilde{m}_L/\tilde{M}_{rigid}$ is very small, and when the liquid levels exceed this limit, the mass ratios increase rapidly as shown in Figure 7.2(d).

7.2.3 Combined Effect of Length of Tank And Liquid Height

Tables 7.1 to 7.5 present the data considering the effect of both length of tank L_X and liquid height H_L on the dynamic response of LCS. The vertical column represents the variable liquid height H_L from the empty condition to the full tank level using the ratio of liquid height H_L to the height of wall H_W. The ratio of length of tank L_X to the height of wall H_W is used to consider the size effect of tank along the horizontal row in theses tables. Both different liquid level inside tank and the flexibility of tank wall are considered.

Table 7.1 Ratio of M_{rigid}/M_{L1} in relationship with L_x/H_W and H_L/H_W

		Lx/Hw
		0.0	0.1	0.2	0.3	0.4	0.5	0.8	1.0	1.5	2.0	3.0	4.0	5.0	6.0	7.0	8.0	9.0
	0.0	0.0000	0.0000	0.0000	0.0000	0.0000	0.0000	0.0000	0.0000	0.0000	0.0000	0.0000	0.0000	0.0000	0.0000	0.0000	0.0000	0.0000
	0.1	0.9331	0.4965	0.2687	0.1797	0.1348	0.1079	0.0674	0.0539	0.0360	0.0270	0.0180	0.0135	0.0108	0.0090	0.0077	0.0067	0.0060
	0.2	0.9331	0.7226	0.4965	0.3534	0.2687	0.2155	0.1348	0.1079	0.0719	0.0539	0.0360	0.0270	0.0216	0.0180	0.0154	0.0135	0.0120
	0.3	0.9331	0.8086	0.6391	0.4965	0.3929	0.3203	0.2021	0.1618	0.1079	0.0809	0.0539	0.0404	0.0324	0.0270	0.0231	0.0202	0.0180
	0.4	0.9331	0.8504	0.7226	0.5998	0.4965	0.4155	0.2687	0.2155	0.1438	0.1079	0.0719	0.0539	0.0431	0.0360	0.0308	0.0270	0.0240
HL/Hw	0.5	0.9331	0.8742	0.7743	0.6718	0.5774	0.4965	0.3328	0.2687	0.1797	0.1348	0.0899	0.0674	0.0539	0.0449	0.0385	0.0337	0.0300
	0.6	0.9331	0.8891	0.8086	0.7226	0.6391	0.5629	0.3929	0.3203	0.2155	0.1618	0.1079	0.0809	0.0647	0.0539	0.0462	0.0404	0.0360
	0.7	0.9331	0.8991	0.8327	0.7595	0.6862	0.6164	0.4476	0.3695	0.2511	0.1887	0.1258	0.0944	0.0755	0.0629	0.0539	0.0472	0.0419
	0.8	0.9331	0.9061	0.8504	0.7873	0.7226	0.6594	0.4965	0.4155	0.2861	0.2155	0.1438	0.1079	0.0863	0.0719	0.0616	0.0539	0.0479
	0.9	0.9331	0.9112	0.8638	0.8086	0.7513	0.6942	0.5396	0.4579	0.3203	0.2422	0.1618	0.1213	0.0971	0.0809	0.0693	0.0607	0.0539
	1.0	0.9331	0.9150	0.8742	0.8256	0.7743	0.7226	0.5774	0.4965	0.3534	0.2687	0.1797	0.1348	0.1079	0.0899	0.0770	0.0674	0.0599

Table 7.2 Ratio of $\widetilde{m}_L / M_{L1}$ in relationship with L_x/H_W and H_L/H_W

		Lx/Hw
		0.0	0.1	0.2	0.3	0.4	0.5	0.8	1.0	1.5	2.0	3.0	4.0	5.0	6.0	7.0	8.0	9.0
	0.0	0.0000	0.0000	0.0000	0.0000	0.0000	0.0000	0.0000	0.0000	0.0000	0.0000	0.0000	0.0000	0.0000	0.0000	0.0000	0.0000	0.0000
	0.1	0.0000	0.0000	0.0000	0.0000	0.0000	0.0000	0.0000	0.0000	0.0000	0.0000	0.0000	0.0000	0.0000	0.0000	0.0000	0.0000	0.0000
	0.2	0.0004	0.0002	0.0001	0.0001	0.0001	0.0000	0.0000	0.0000	0.0000	0.0000	0.0000	0.0000	0.0000	0.0000	0.0000	0.0000	0.0000
	0.3	0.0021	0.0013	0.0008	0.0006	0.0004	0.0004	0.0002	0.0002	0.0001	0.0001	0.0001	0.0000	0.0000	0.0000	0.0000	0.0000	0.0000
	0.4	0.0062	0.0044	0.0030	0.0022	0.0017	0.0014	0.0009	0.0007	0.0005	0.0004	0.0002	0.0002	0.0001	0.0001	0.0001	0.0001	0.0001
HL/Hw	0.5	0.0144	0.0113	0.0080	0.0060	0.0048	0.0040	0.0026	0.0021	0.0014	0.0010	0.0007	0.0005	0.0004	0.0003	0.0003	0.0003	0.0002
	0.6	0.0281	0.0234	0.0174	0.0135	0.0110	0.0092	0.0061	0.0049	0.0033	0.0025	0.0016	0.0012	0.0010	0.0008	0.0007	0.0006	0.0005
	0.7	0.0491	0.0426	0.0330	0.0262	0.0216	0.0183	0.0123	0.0100	0.0067	0.0051	0.0034	0.0025	0.0020	0.0017	0.0014	0.0013	0.0011
	0.8	0.0787	0.0703	0.0566	0.0458	0.0381	0.0325	0.0223	0.0183	0.0124	0.0093	0.0062	0.0047	0.0037	0.0031	0.0027	0.0023	0.0021
	0.9	0.1182	0.1080	0.0896	0.0738	0.0621	0.0535	0.0373	0.0308	0.0210	0.0159	0.0106	0.0079	0.0063	0.0053	0.0045	0.0040	0.0035
	1.0	0.1687	0.1566	0.1332	0.1118	0.0951	0.0824	0.0583	0.0485	0.0335	0.0253	0.0169	0.0127	0.0101	0.0084	0.0072	0.0063	0.0056

Table 7.3 Ratio of m_L / M_{L1} in relationship with L_x/H_W and H_L/H_W

		Lx/Hw																
		0.0	0.1	0.2	0.3	0.4	0.5	0.8	1.0	1.5	2.0	3.0	4.0	5.0	6.0	7.0	8.0	9.0
	0.0	0.0000	0.0000	0.0000	0.0000	0.0000	0.0000	0.0000	0.0000	0.0000	0.0000	0.0000	0.0000	0.0000	0.0000	0.0000	0.0000	0.0000
	0.1	0.0039	0.0016	0.0009	0.0006	0.0004	0.0003	0.0002	0.0002	0.0001	0.0001	0.0001	0.0000	0.0000	0.0000	0.0000	0.0000	0.0000
	0.2	0.0153	0.0098	0.0064	0.0045	0.0034	0.0027	0.0017	0.0014	0.0009	0.0007	0.0005	0.0003	0.0003	0.0002	0.0002	0.0002	0.0002
	0.3	0.0335	0.0253	0.0185	0.0140	0.0110	0.0090	0.0056	0.0045	0.0030	0.0023	0.0015	0.0011	0.0009	0.0008	0.0006	0.0006	0.0005
	0.4	0.0581	0.0479	0.0373	0.0299	0.0244	0.0202	0.0130	0.0104	0.0070	0.0052	0.0035	0.0026	0.0021	0.0017	0.0015	0.0013	0.0012
HL/Hw	0.5	0.0885	0.0769	0.0626	0.0519	0.0437	0.0372	0.0247	0.0199	0.0133	0.0100	0.0066	0.0050	0.0040	0.0033	0.0028	0.0025	0.0022
	0.6	0.1242	0.1117	0.0939	0.0799	0.0688	0.0597	0.0410	0.0333	0.0224	0.0168	0.0112	0.0084	0.0067	0.0056	0.0048	0.0042	0.0037
	0.7	0.1645	0.1515	0.1308	0.1135	0.0994	0.0876	0.0622	0.0511	0.0347	0.0260	0.0174	0.0130	0.0104	0.0087	0.0074	0.0065	0.0058
	0.8	0.2089	0.1957	0.1727	0.1521	0.1350	0.1206	0.0882	0.0734	0.0503	0.0379	0.0253	0.0189	0.0152	0.0126	0.0108	0.0095	0.0084
	0.9	0.2570	0.2437	0.2188	0.1952	0.1752	0.1581	0.1188	0.1000	0.0695	0.0525	0.0350	0.0263	0.0210	0.0175	0.0150	0.0131	0.0117
	1.0	0.3080	0.2949	0.2686	0.2423	0.2195	0.1998	0.1536	0.1307	0.0922	0.0700	0.0468	0.0351	0.0281	0.0234	0.0201	0.0175	0.0156

Table 7.4 Ratio of $\tilde{m}_L / \tilde{M}_{rigid}$ in relationship with L_x/H_W and H_L/H_W

		Lx/Hw												
		0.0	0.1	0.2	0.3	0.4	0.5	0.8	1.0	1.5	2.0	3.0	4.0	5.0
	0.0	0.0000	0.0000	0.0000	0.0000	0.0000	0.0000	0.0000	0.0000	0.0000	0.0000	0.0000	0.0000	0.0000
	0.1	0.0000	0.0000	0.0000	0.0000	0.0000	0.0000	0.0000	0.0000	0.0000	0.0000	0.0000	0.0000	0.0000
	0.2	0.0005	0.0003	0.0002	0.0002	0.0002	0.0002	0.0002	0.0002	0.0002	0.0002	0.0002	0.0002	0.0002
	0.3	0.0022	0.0016	0.0013	0.0012	0.0011	0.0011	0.0011	0.0011	0.0011	0.0011	0.0011	0.0011	0.0011
	0.4	0.0067	0.0052	0.0041	0.0037	0.0035	0.0034	0.0034	0.0034	0.0034	0.0034	0.0034	0.0034	0.0034
HL/Hw	0.5	0.0154	0.0129	0.0103	0.0090	0.0084	0.0081	0.0078	0.0078	0.0078	0.0078	0.0078	0.0078	0.0078
	0.6	0.0302	0.0263	0.0215	0.0187	0.0172	0.0164	0.0155	0.0154	0.0153	0.0153	0.0153	0.0153	0.0153
	0.7	0.0526	0.0474	0.0397	0.0345	0.0314	0.0296	0.0275	0.0271	0.0269	0.0268	0.0268	0.0268	0.0268
	0.8	0.0843	0.0776	0.0665	0.0581	0.0527	0.0493	0.0450	0.0440	0.0434	0.0433	0.0433	0.0433	0.0433
	0.9	0.1267	0.1185	0.1037	0.0913	0.0827	0.0770	0.0691	0.0672	0.0657	0.0654	0.0654	0.0654	0.0654
	1.0	0.1808	0.1712	0.1524	0.1354	0.1228	0.1141	0.1011	0.0976	0.0947	0.0941	0.0939	0.0939	0.0939

Table 7.5 Ratio of m_L/M_{rigid} in relationship with L_x/H_W and H_L/H_W

		Lx/Hw												
		0.0	0.1	0.2	0.3	0.4	0.5	0.8	1.0	1.5	2.0	3.0	4.0	5.0
HL/Hw	0.0	0.0000	0.0000	0.0000	0.0000	0.0000	0.0000	0.0000	0.0000	0.0000	0.0000	0.0000	0.0000	0.0000
	0.1	0.0042	0.0033	0.0032	0.0032	0.0032	0.0032	0.0032	0.0032	0.0032	0.0032	0.0032	0.0032	0.0032
	0.2	0.0164	0.0135	0.0128	0.0127	0.0127	0.0127	0.0127	0.0127	0.0127	0.0127	0.0127	0.0127	0.0127
	0.3	0.0359	0.0313	0.0289	0.0282	0.0280	0.0279	0.0279	0.0279	0.0279	0.0279	0.0279	0.0279	0.0279
	0.4	0.0623	0.0563	0.0516	0.0498	0.0491	0.0487	0.0485	0.0485	0.0485	0.0485	0.0485	0.0485	0.0485
	0.5	0.0949	0.0880	0.0808	0.0773	0.0757	0.0748	0.0741	0.0740	0.0740	0.0740	0.0740	0.0740	0.0740
	0.6	0.1331	0.1256	0.1162	0.1106	0.1077	0.1061	0.1044	0.1041	0.1040	0.1039	0.1039	0.1039	0.1039
	0.7	0.1763	0.1685	0.1571	0.1494	0.1448	0.1422	0.1390	0.1384	0.1380	0.1380	0.1380	0.1380	0.1380
	0.8	0.2239	0.2160	0.2030	0.1932	0.1868	0.1828	0.1777	0.1766	0.1758	0.1757	0.1757	0.1757	0.1757
	0.9	0.2754	0.2675	0.2533	0.2414	0.2332	0.2277	0.2202	0.2183	0.2169	0.2166	0.2166	0.2166	0.2166
	1.0	0.3301	0.3223	0.3072	0.2936	0.2835	0.2764	0.2660	0.2632	0.2609	0.2604	0.2603	0.2603	0.2603

Table 7.1 shows the ratio of added mass of liquid due to hydrodynamic pressure based on the rigid boundary condition to the half mass of liquid inside tank M_{rigid}/M_{L1}. Tables 7.2 and 7.3 show the ratio of generalized and effective added mass of liquid due to hydrodynamic pressure to the half mass of liquid inside tank $\widetilde{m}_L/M_{L1}$ and m_L/M_{L1}. Tables 7.4 and 7.5 show the ratios of generalized and effective added mass of liquid due to impulsive hydrodynamic pressure to the added mass based on the rigid boundary condition $\widetilde{m}_L/\widetilde{M}_{rigid}$ and m_L/M_{rigid}. The effects of liquid level and length of tank wall were discussed previously. The curves representing the effect of the added mass of liquid due to impulsive hydrodynamic pressure in relation with H_L/H_W and L_X/H_W are shown in Figure 7.3.

7.3 Effective Height

In the generalized SDOF system, the added mass of liquid due to hydrodynamic pressure can still be treated similar to that of Housner's model as lumped mass as discussed in Section 5.5. The effective height at which the effective added mass of liquid due to impulsive hydrodynamic pressure is applied can be calculated as that:

$$[7.7] \qquad h_i = \frac{\int_0^{H_L} \sum_{n=1}^{\infty} \frac{2\rho_l \tanh(\lambda_{i,n} L_x)}{\lambda_{i,n} H_L} \cos(\lambda_{i,n} y) \int_0^{H_L} \cos(\lambda_{i,n} y) \cdot \psi(y) dy \cdot y dy}{\sum_{n=1}^{\infty} \frac{2 \cdot (-1)^{n+1} \rho_l \tanh(\lambda_{i,n} L_x)}{\lambda_{i,n}^2 H_L} \int_0^{H_L} \cos(\lambda_{i,n} y) \psi(y) dy}$$

For a tank containing liquid, the overall effective height at which the dynamic force is applied can be expressed using Eq.7.8. This is obtained by combining the inertial mass of tank wall and the added mass of liquid due to impulsive hydrodynamic pressure as follows:

$$[7.8] \qquad h = \frac{[\int_0^{H_W} m(y) \cdot \psi(y) \cdot y \cdot dy + \int_0^{H_L} \sum_{n=1}^{\infty} \frac{2\rho_l \tanh(\lambda_{i,n} L_x)}{\lambda_{i,n} H_L} \cos(\lambda_{i,n} y) \int_0^{H_L} \cos(\lambda_{i,n} y) \psi(y) dy \cdot y dy]}{\int_0^{H_W} m(y) \cdot \psi(y) \cdot dy + \sum_{n=1}^{\infty} \frac{2(-1)^{n+1} \rho_l}{\lambda_{i,n}^2 H_L} \tanh(\lambda_{i,n} L_x) \int_0^{H_L} \cos(\lambda_{i,n} y) \psi(y) dy}$$
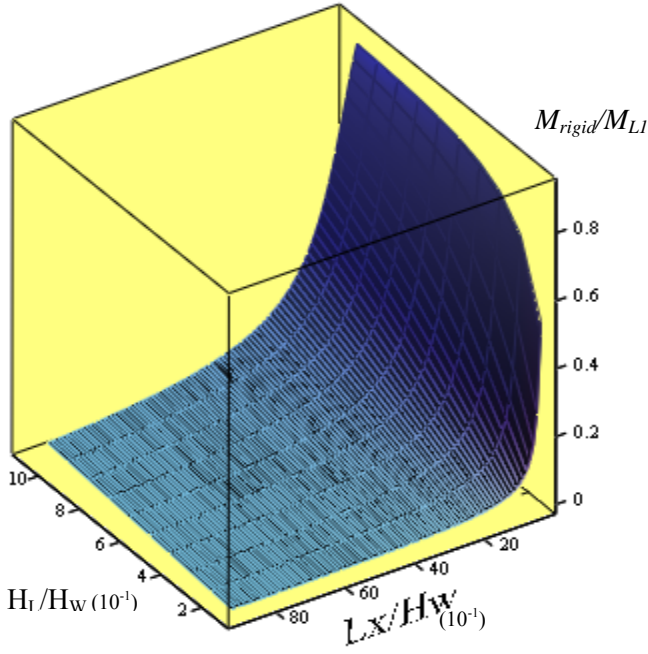
(a) M_{rigid}/M_{L1} vs. L_x / H_W and H_L/H_W

(b) $\tilde{m}_L / M_{L1}$ vs. L_x/H_W and H_L/H_W
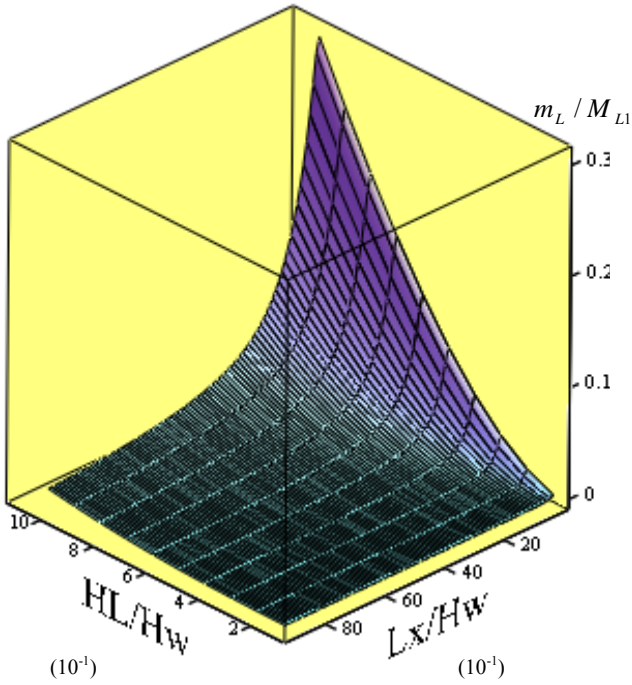
(c) m_L / M_{L1} vs. L_x / H_W and H_L/H_W
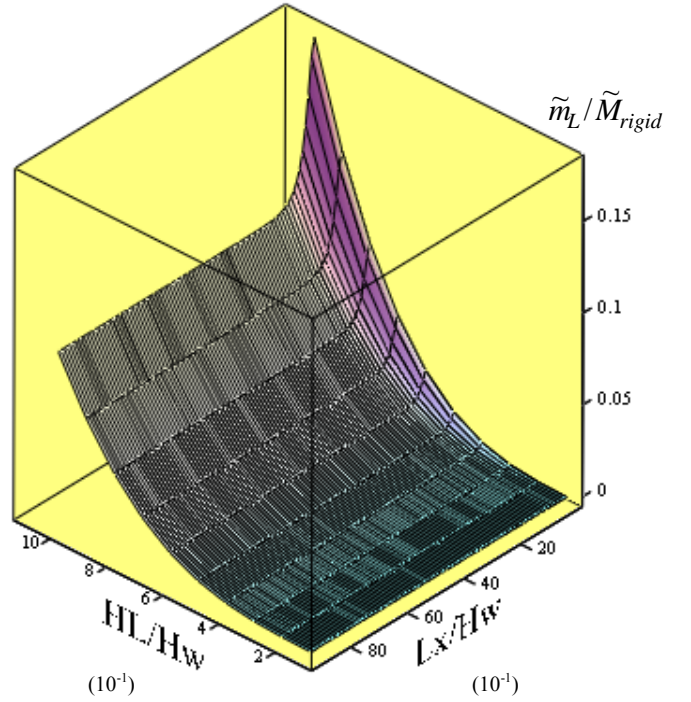
(d) $\tilde{m}_L / \tilde{M}_{rigid}$ vs. L_x / H_W and H_L/H_W

149
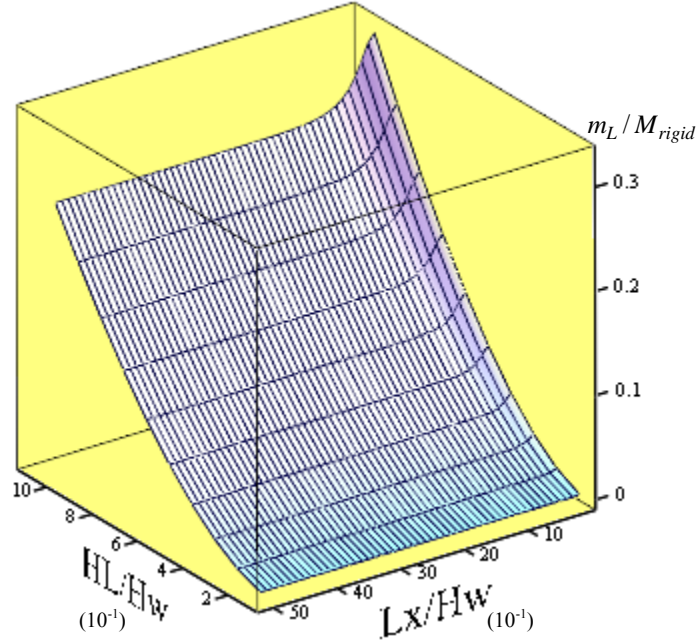
(e) m_L / M_{rigid} vs. L_x / H_W and H_L / H_W

Figure 7.3 Added Mass of Liquid as Function of H_L/H_W and L_X/H_W

In addition, the effective height of added mass of liquid due to impulsive pressure and overall effective height of LCS can also be determined using Hounser's model as follows:

For tanks with $\dfrac{2L_x}{H_L} < 1.333$,

$$[7.9] \qquad \frac{h_i}{H_L} = 0.5 - 0.09375 \left(\frac{2L_x}{H_L}\right)$$

For tanks with $\dfrac{2L_x}{H_L} \geq 1.333$,

$$[7.10] \qquad \frac{h_i}{H_L} = 0.375$$

For the liquid containing structures, the effective height at which the total dynamic lateral force is applied can be calculated using Eq.7.11 as follows:

$$[7.11] \qquad h = \frac{m_w \cdot h_w + m_L \cdot h_i}{m_w + m_L}$$

It is worth noting that the boundary condition is assumed to be rigid in Housner's model.

7.3.1 Effects of Liquid Height H_L and Length of Tank L_x

Figure 7.4(a) shows the normalized effective height at which the effective added mass of liquid due to hydrodynamic pressure is applied as function of the ratio of length of tank to the height of wall L_x/H_W. The liquid heights considered are $0.4H_W$, $0.6H_W$, $0.8H_W$ and $1.0H_W$.

Similar to the added mass of liquid due to impulsive hydrodynamic pressure as discussed previously, the ratio of length of tank to the liquid height L_X/H_W is used to consider the size effect of tank on the effective height of added mass of liquid. Figure 7.4(a) shows that when the value of L_x/H_W is less than 1.0, the values of h_i/H_L decrease at a fast rate. However, for values of L_x/H_W greater than 1.0, the values of h_i/H_L remain constant which means increasing the tank length in the direction parallel to the direction of earthquake has no significant effect on the effective height of added mass of liquid.

Figure 7.4(b) shows the variable liquid level in relation with the ratio of the effective height at which the effective added mass of li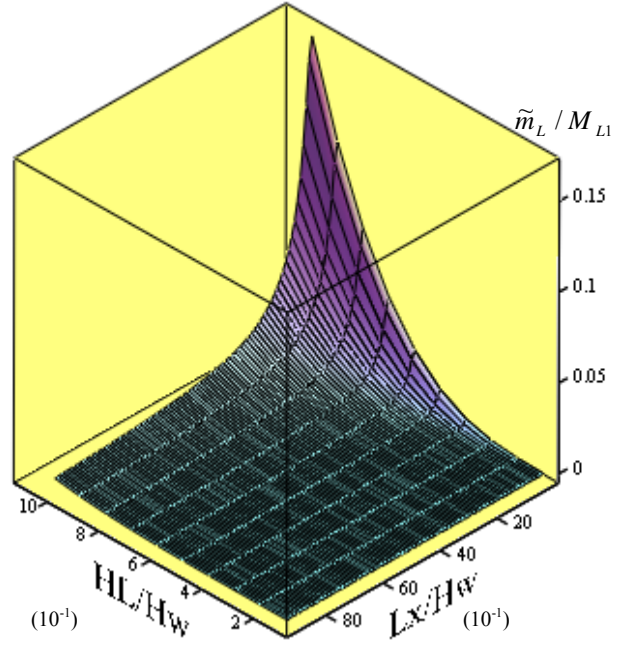quid due to impulsive hydrodynamic pressure is applied to the height of liquid h_i/H_L. When the liquid level H_L increases, the ratio of h_i/H_L also increases based on the distribution of added mass of liquid along the height of wall. It is worth noting that the effective height has a linear relationship with the increase of liquid level inside tank.

Figure 7.4(b) also compares the effect of length of tank raging from $0.1H_w$ to $5H_w$. The ratio of h_i/H_L increases with decrease of length of tank. This means that the effective height is higher for the effective added mass of liquid closer to tank as a result of distribution of acceleration along the tank wall.

Table 7.6 shows both effects of size of tank and height of liquid on the ratio of h_i/H_L. Figure 7.4(c) show the curves for the ratio of h_i/H_L in relation with H_L/H_W and L_X/H_W.
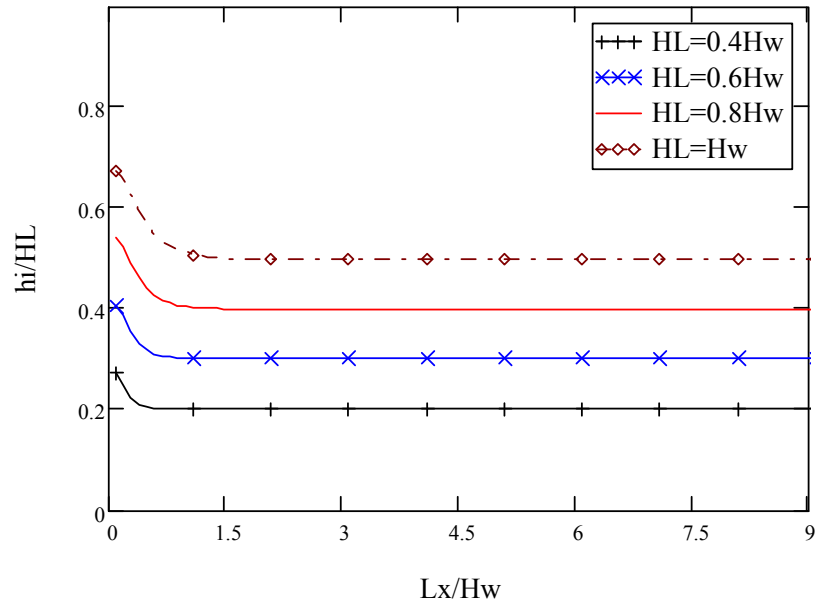
(a) Effect of Liquid Level
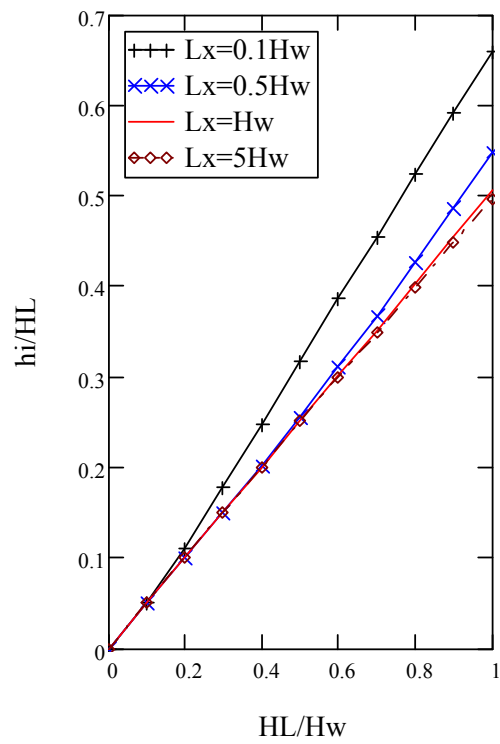
(b) Effect of Length of Tank

152
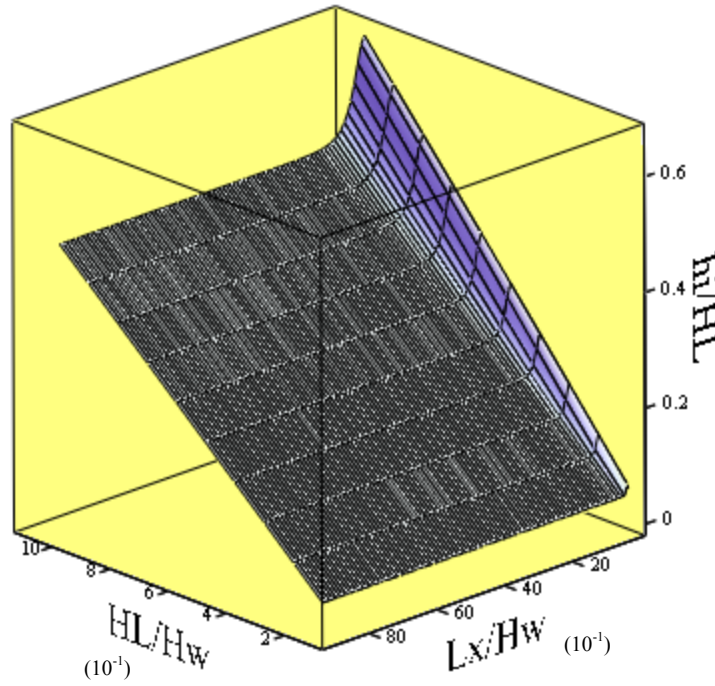
(c) h_i/H_L vs. L_x / H_W and H_L/H_W

Figure 7.4 Effective Height

7.3.2 Overall Effective Height

In this study, a tall and a shallow tank, which were used in previous chapters, are used to investigate of the effects of liquid level and length of tank on the overall effective height of liquid containing structures. The dimensions and properties of the tanks are as follows:

(1) Tall Tank:

$L_x = 9.8$ m $L_z = 28$ m $H_w = 12.3$ m $H_L = 11.2$ m $t_w = 1.2$ m $E_c = 20.776 \times 10^3$ Mpa

(2) Shallow Tank:

$L_x = 15$ m $L_z = 30$ m $H_w = 6.0$ m $H_L = 5.5$ m $t_w = 0.6$ m $E_c = 26.44 \times 10^3$ MPa

Other properties of both tanks are:

$\rho_w = 2300$ kg/m^3 $\rho_l = 1000$ kg/m^3 $v = 0.17$

Table 7.6 Ratio of h_i/H_L in relationship with L_x/H_W and H_L/H_W

		Lx/Hw												
		0.0	0.1	0.2	0.3	0.4	0.5	0.8	1.0	1.5	2.0	3.0	4.0	5.0
HL/Hw	0.0	0.0000	0.0000	0.0000	0.0000	0.0000	0.0000	0.0000	0.0000	0.0000	0.0000	0.0000	0.0000	0.0000
	0.1	0.0683	0.0514	0.0504	0.0504	0.0504	0.0504	0.0504	0.0504	0.0504	0.0504	0.0504	0.0504	0.0504
	0.2	0.1364	0.1112	0.1027	0.1011	0.1007	0.1007	0.1006	0.1006	0.1006	0.1006	0.1006	0.1006	0.1006
	0.3	0.2043	0.1780	0.1598	0.1538	0.1518	0.1511	0.1508	0.1508	0.1508	0.1508	0.1508	0.1508	0.1508
	0.4	0.2719	0.2473	0.2217	0.2099	0.2048	0.2026	0.2009	0.2008	0.2008	0.2008	0.2008	0.2008	0.2008
	0.5	0.3394	0.3171	0.2870	0.2693	0.2603	0.2556	0.2513	0.2508	0.2506	0.2506	0.2506	0.2506	0.2506
	0.6	0.4065	0.3865	0.3543	0.3315	0.3182	0.3106	0.3024	0.3010	0.3003	0.3003	0.3003	0.3003	0.3003
	0.7	0.4734	0.4553	0.4225	0.3959	0.3784	0.3676	0.3542	0.3516	0.3500	0.3498	0.3498	0.3498	0.3498
	0.8	0.5399	0.5236	0.4911	0.4617	0.4405	0.4263	0.4071	0.4027	0.3996	0.3992	0.3991	0.3991	0.3991
	0.9	0.6061	0.5913	0.5596	0.5283	0.5040	0.4867	0.4610	0.4545	0.4493	0.4484	0.4482	0.4482	0.4482
	1.0	0.6720	0.6584	0.6278	0.5955	0.5686	0.5484	0.5161	0.5070	0.4992	0.4976	0.4972	0.4972	0.4972

It is worth noting that since this study is based on the 2-D model, the definition of tall and shallow tanks are relative terms. Also, this study is based on the assumption of sufficiently large width of tank perpendicular to the direction of earthquake as discussed previously. It is also noted that the parameters H_L and L_x are considered as variables in this study in order to study the effects of liquid level and length of tank on the dynamic response of LCS.

In addition to the shape function SF3, shape functions SF1 and SF2 which represent a more flexible and a more rigid wall conditions, respectively for the first mode in the cantilever condition are used to study the effect of flexibility of tank wall on the dynamic response of LCS. The shape functions are defined as follows:

[7.12] $SF1(y) = \psi(y) = \dfrac{1}{2}\dfrac{y^2}{H_W^2} + \dfrac{1}{2}\dfrac{y}{H_W}$

[7.13] $SF2(y) = \psi(y) = \dfrac{y^2}{H_W^2}$

Figures 7.5 and 7.6 show the variable liquid level in relation with the overall effective height of LCS for the tall and the shallow tanks respectively. When the tank is empty, the effective height of containment structure is the same as the effective height of tank wall which is $0.75H_W$ for the cantilever wall condition. These figures show that the overall effective height of liquid containing tank reduces with increase of liquid level for both the tall and the shallow tanks. It is worth noting that the overall effective height shows a rapid decrease when the liquid level is between $0.4H_L$ and $0.8H_L$. When the liquid level is lager than $0.8H_L$, the overall effective height tends to remain constant.

The overall effective heights for the rigid boundary condition using the shape function $\psi(y)=1$ and Hounser's model are also presented in Figures 7.5 and 7.6. The effective height of the effective inertial mass of tank wall h_w in the rigid wall boundary condition using $\psi(y)=1$ is $0.5H_W$ which is as the same as that of Housner's Model.
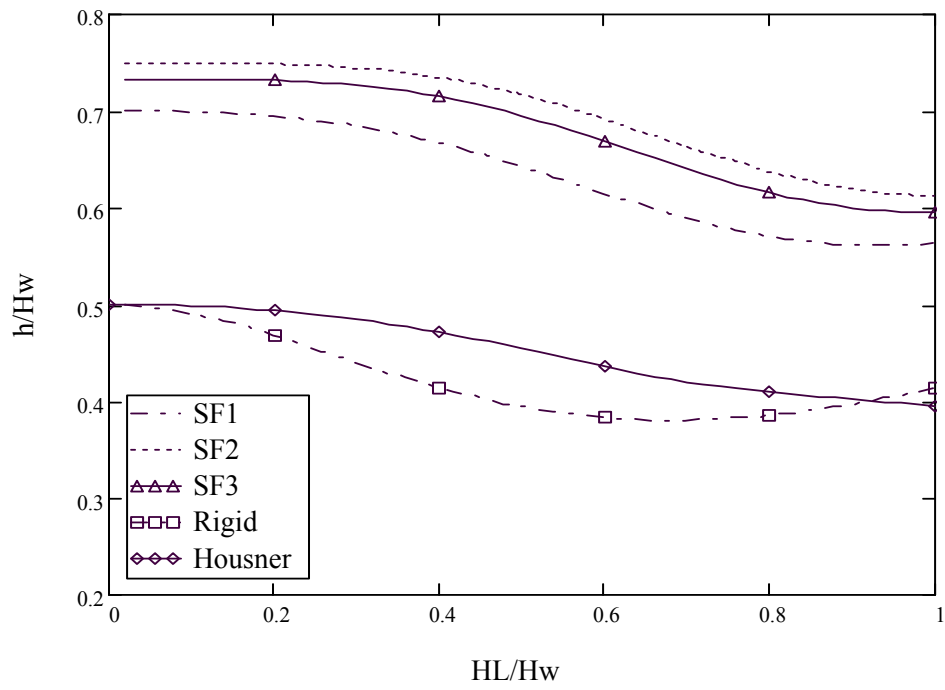
Figure 7.5 Effective Height of Overall Liquid Containing Structure vs. Liquid Depth
(Tall Tank)
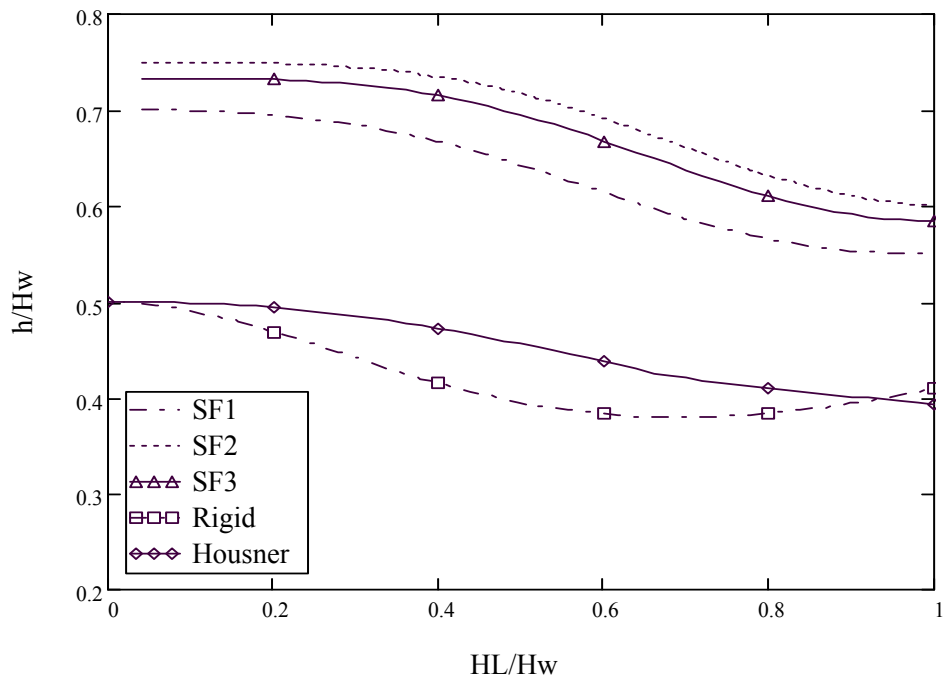
Figure 7.6 Effective Height of Overall Liquid Containing Structure vs. Liquid Depth
(Shallow Tank)

Figures 7.5 and 7.6 demonstrate that the overall effective heights for the empty condition, i.e. $H_L/H_W=0$, and at full liquid level, i.e. $H_L/H_W=1$, are the same in the rigid boundary condition. When the liquid level varies between these two levels, the overall effective height for the Housner's model is higher than that of rigid wall boundary condition using $\psi(y)=1$. A comparison of the results for more flexible and rigid wall conditions using the shape functions SF=1 and SF=2 shows that the overall effective height increases with increase in the flexibility of the wall.

7.4 Natural Frequencies

The Rayleigh-Ritz method is used to study the dynamic response of LCS using the generalized SDOF system. The natural frequencies f of the system can be obtained using the following equation:

[7.14] $$\omega_n^2 = \frac{\tilde{k}}{\tilde{m}_W + \tilde{m}_L}$$

[7.15] $$f = \frac{\omega}{2\pi}$$

Where $\tilde{k}$ and $\tilde{m}_w$ are the generalized stiffness and inertial mass of wall. The inertial mass of wall can be calculated as follows:

[7.16] $$\tilde{m}_W = \int_0^{H_W} m(y) \cdot [\psi(y)]^2 \cdot dy$$

The tall and the shallow tanks are used to study the effects of length of tank L_x and liquid level H_L on natural frequencies of LCS as will be discussed in this section. It is worth noting that the liquid level H_L is considered as the design level in the parametric study. The actual liquid level h_L varies between the liquid level H_L and empty condition.

7.4.1 Effect of Length of Tank L_x

Figures 7.7(a) and 7.8(a) show the effect of length of tank L_x on the natural frequencies of the tall and the shallow tank respectively, when the actual liquid level h_L varies. Four cases when L_x equals to $0.1H_w$, $0.5H_w$, $1.0H_w$, $10H_w$ are considered.
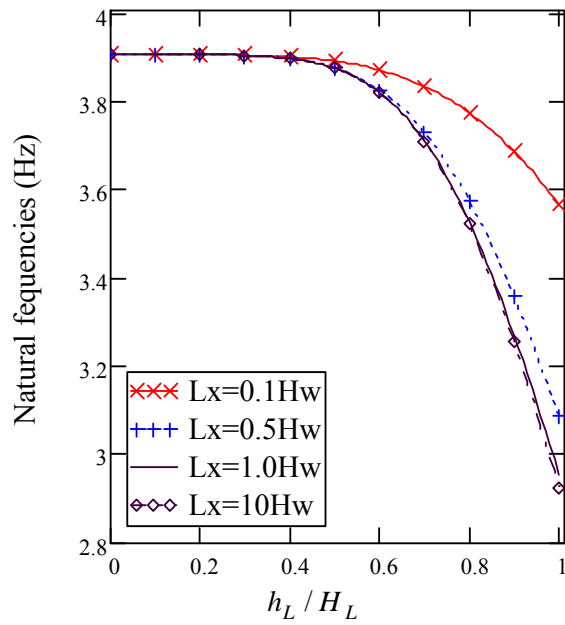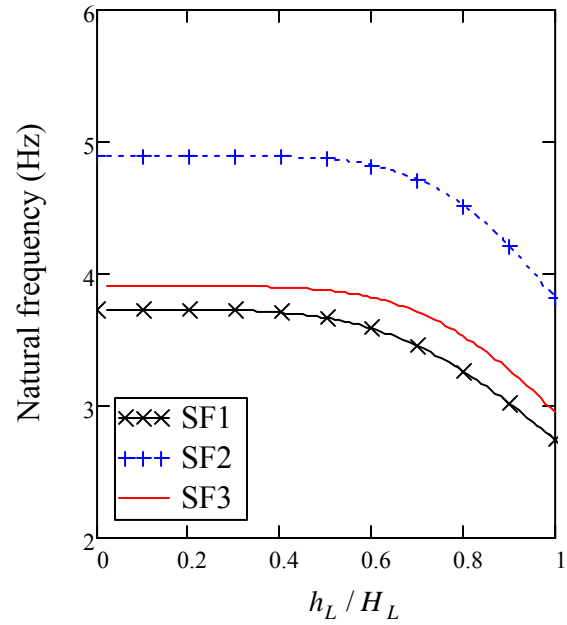
(a) Length Effect　　　　　　　　(b) Effect of Shape Functions

Figure 7.7 Effect of Liquid Level on Natural Frequencies of Tank – Tall Tank
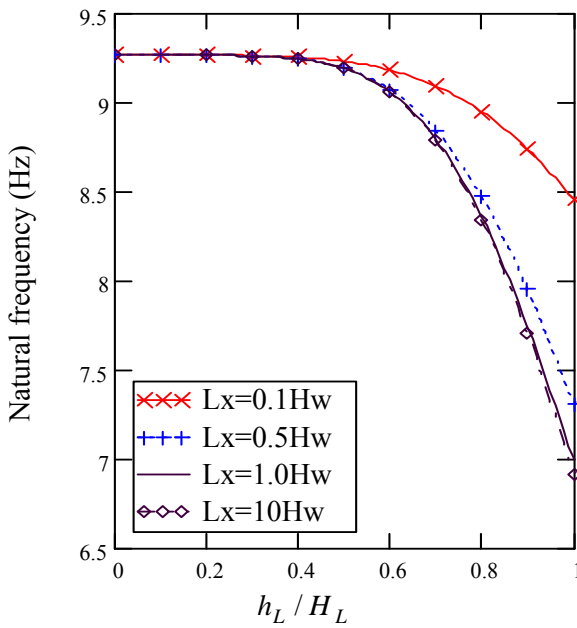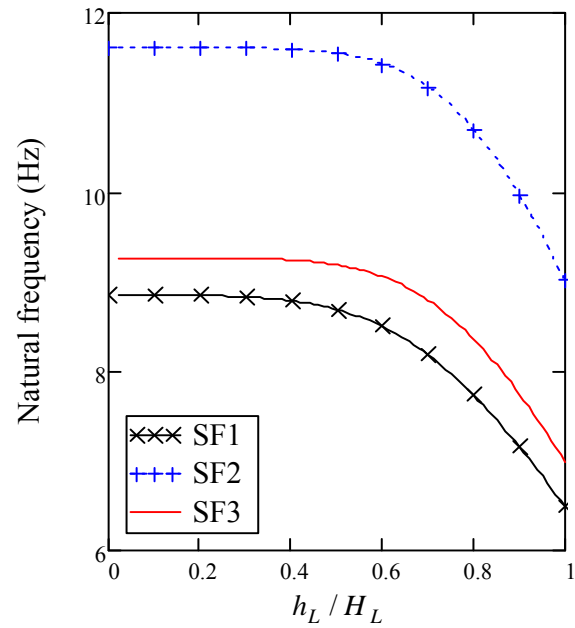
(a) Length Effect　　　　　　　　(b) Effect of Shape Functions

Figure 7.8 Effect of Liquid Level on Natural Frequencies of Tank – Shallow Tank

Figures 7.7(a) and 7.8(a) show that when the liquid level is less than $0.4H_L$, the length of tanks L_x has no significant effect on the natural frequencies. When the liquid level exceeds $0.4H_L$, the natural frequencies decrease at a faster ratio with the increase of length of tank L_x. When the length of tank is large enough, the natural frequencies of LCS converge to the limit. This is consistent with the effect of length of tank L_x on hydrodynamic pressure presented previously.

7.4.2 Effect of Liquid Height H_L

Figures 7.7(b) and 7.8(b) show the natural frequencies of the tall and the shallow tank respectively as function of the actual height of liquid level h_L in tank and the length of tank L_x. It can be seen that with the increase of liquid level in the tank the natural frequencies of liquid containing structures decrease, or in other words that the natural vibration period increase.

Figures 7.7(b) and 7.8(b) also shows the effect of the actual liquid level h_L on the natural frequencies of LCS based on the three selected shape functions. It is found that with the increase of flexibility of tank wall, the natural frequencies of liquid containing structures reduce.

It is worth noting that when the actual liquid level h_L is zero, it represents an empty tank and when the actual liquid level h_L equals to H_L, it represents a full tank based on the design liquid height. It is possible that the actual liquid level h_L can be at any level between the empty and the design operation level. Therefore, the actual natural frequencies of liquid containing structures are within a band of natural frequencies between these two limits.

7.5 Conclusions

In this chapter, the effects of size of tank and liquid level on dynamic response of liquid containing structures (LCS) are investigated. It is recommended to use the ratio of length of tank to the height of tank wall L_x/H_w rather than the ratio of length of tank to liquid height, L_x/H_L to study the size effect of tanks. This is because the liquid level may be a

variable in the design and operation. In addition, when the flexibility of tank wall is considered in the dynamic analysis of LCS, the liquid level affects the added mass of liquid due to impulsive pressure. This is due to variation of added mass distribution along the height of the tank wall. Therefore, the ratio of height of liquid to the height of wall H_L/H_w is introduced to study the variable depth of liquid inside the tank.

The generalized and effective added masses of liquid due to impulsive hydrodynamic pressure are calculated based on the parameters L_x/H_w and H_L/H_w. The values of the added mass of liquid due to impulsive hydrodynamic pressure presented in this study can be used in the seismic design of LCS.

The effects of size of tank and liquid level on the effective height of added mass of liquid, the overall effective height and the natural frequencies of LCS are also investigated. Since the natural frequencies of LCS are within a band of natural frequencies between the full level of liquid H_L and empty tank, it is recommended to use the frequency which may cause the maximum dynamic response of LCS.

Other conclusions drawn for this study considering the first mode of dynamic response of LCS and the flexibility of tank wall are:

(1) When the length of tank is relatively large, the increase in the length of tank has no significant effect on dynamic response of LCS.

(2) With the increase of liquid height, the effective height of added mass of liquid and the natural frequencies reduce.

(3) With no change of other parameters, the natural frequencies reduce with the increase in the length of tank.

(4) With the increase of flexibility of tank wall, the overall effective height of LCS increases and the natural frequency reduces.

CHAPTER 8 DESIGN APPLICATION

8.1. Introduction

In this chapter, a design procedure based on the structural model using the generalized SDOF system is proposed. The proposed structural model can overcome the deficiencies in the current design codes and standards. The theories and procedures for dynamic analysis of liquid containing structure (LCS) are summarized. The design charts and tables for the added mass of liquid due to impulsive hydrodynamic pressure and the corresponding effective height are presented and compared with those adopted in the current design codes and standards. The contribution of higher modes to the dynamic response of LCS is included in the proposed model. The SRSS method is used for the combination of the first two modes. Two sets of calculations for a tall and a shallow tank are presented. The results are compared with those obtained using Housner's model as well as Model 4 discussed in Chapter 3. The proposed structural model using the generalized SDOF system can be considered as simple model to overcome the current deficiencies in seismic design of LCS.

It is noted that the theories to use the generalized SDOF system for dynamic analysis of concrete rectangular LCS are discussed in the previous chapters. However, the application of proposed model is summarized systematically in this chapter. Although, some formula may be repetitive, the detailed derivation is still referred to the previous chapters.

8.2. Generalized SDOF System for Dynamic Analysis of LCS

8.2.1 Analysis Model

The analytical model is presented in Chapter 5. Figure 5.1 shows a 2-D model of tank wall. It is assumed that the liquid storage tank is fixed to the rigid foundation. A Cartesian coordinate system (x, y) is used with the origin located at the center of the tank base. It is assumed that the direction of ground motion is in the "x" direction and the width of tank $2L_z$ is sufficiently large so that a unit width of tank can represent the tank wall.

The walls for the concrete rectangular LCS are considered as fixed at bottom and free at top. Figure 5.2 shows a cantilever wall with the distributed mass m(y) and stiffness EI(y) per unit height subjected to earthquake ground motion $u_g(t)$.

8.2.2 Equation of Motion

The equation of motion for the generalized SDOF system in the dynamic analysis of LCS is that:

[8.1] $\qquad \widetilde{m} \cdot \ddot{u} + \widetilde{c} \cdot \dot{u} + \widetilde{k} \cdot u = \widetilde{p}$

where $\widetilde{m}$, $\widetilde{c}$, $\widetilde{k}$, $\widetilde{p}$ are defined as the generalized system of mass, damping, stiffness and force, respectively, as shown below:

[8.2] $\qquad \widetilde{m} = \int_0^{H_W} m(y) \cdot [\psi(y)]^2 \cdot dy + \widetilde{m}_L$

[8.3] $\qquad \widetilde{k} = \int_0^{H_W} EI(y) \cdot [\ddot{\psi}(y)]^2 \cdot dy$

[8.4] $\qquad \widetilde{p} = \ddot{u}_g(t) \cdot [\int_0^{H_W} m(y) \cdot \psi(y) \cdot dy + m_L]$

where $\psi(y)$ is the assumed shape function, and $\widetilde{m}_L$ and m_L are the generalized and effective added mass of liquid due to impulsive hydrodynamic pressure.

The direct coupling method is used in the dynamic analysis. The interaction between liquid and tank wall is solved directly in the equation of motion using the added mass method. The application of generalized and effective added masses of liquid due to impulsive hydrodynamic pressure in the coupling system of liquid containing structures is discussed later in this chapter.

The equation of motion for coupling the structure and the contained liquid subjected to earthquakes is obtained by substituting the Eqs.8.2 to 8.4 into Eq.8.1. Then, by dividing both sides of equation by $\widetilde{m}$, the following relationship is obtained:

[8.5] $\qquad \ddot{u}+2\cdot\zeta\cdot\omega_n\cdot\dot{u}+\omega_n^2\cdot u=-\hat{q}\cdot u_g(t)$

where $\omega_n=\sqrt{\tilde{k}/\tilde{m}}$ are the circular frequencies of liquid containing structure system and $\hat{q}$ is the factor of external applied load that is:

[8.6] $\qquad \hat{q}=\hat{p}/\tilde{m}=\dfrac{m_W+m_L}{\tilde{m}_W+\tilde{m}_L}$

If an estimated damping ratio ζ is assumed, all the unknown parameters, i.e. u, $\dot{u}$ and $\ddot{u}$ can be determined by an assumed shape function. Therefore, the infinite degrees of freedom of liquid containing structure can be simplified to a generalized SDOF system.

8.2.3 Hydrodynamic Pressure

The fluid in the tank is considered to be ideal, which is incompressible, inviscid, and with a mass density ρ_l. The response of the body of fluid to an earthquake can be obtained using the velocity potential method as discussed in Chapter 3. Only the impulsive component is considered in this study.

The hydrodynamic pressure was solved using the separation of variables method which satisfies the boundary conditions. The hydrodynamic pressure distribution on the flexible wall condition can be expressed as follows:

[8.7] $\qquad p=\displaystyle\sum_{n=1}^{\infty}\dfrac{2\cdot\rho_l\cdot\tanh(\lambda_{i,n}\cdot L_x)}{\lambda_{i,n}\cdot H_L}\cdot\cos(\lambda_{i,n}\cdot y)\cdot\int_0^{H_L}\cos(\lambda_{i,n}\cdot y)\cdot\ddot{u}(t)dy$

where $\lambda_{i,n}=(2n-1)\pi/2H_L$. As the series in the above equation convergence very fast, only the first terms of the series are used for practical applications.

For the rigid tank when $\ddot{u}(t)=\ddot{u}_g(t)$, Eq.8.7 can be simplified as that:

[8.8] $\qquad p_{rigid}=\displaystyle\sum_{n=1}^{\infty}\dfrac{2\cdot(-1)^n\cdot\rho_l}{\lambda_{i,n}^2\cdot H_l}\tanh(\lambda_{i,n}\cdot L_x)\cdot\cos(\lambda_{i,n}\cdot y)\cdot\ddot{u}_g(t)$

8.2.4 Shape Functions

The general beam vibrating function can be used as an admissible shape function to approximate the vibration mode. The general form can be expressed in that (Paz, 1997):

[8.9] $\psi_n(y) = a_n \sin(k_n\, y) + b_n \cos(k_n\, y) + c_n \sinh(k_n\, y) + d_n \cosh(k_n\, y)$

where a_n, b_n, c_n, d_n are the constants and k_n is the eigenvalue for the n-th mode. All these parameters are determined based on the boundary conditions.

For simplicity, the prescribed vibration shape function SF3 representing the first mode shape for the cantilever wall boundary condition can be used for the dynamic analysis of LCS. The shape function SF3 can be expressed as follows:

[8.10] $\mathrm{SF3}(y) = \dfrac{3}{2} \dfrac{y^2}{H_W^2} - \dfrac{1}{2} \dfrac{y^3}{H_W^3}$

The validity of the shape function SF3 was verified and discussed in Chapter 5.

For the cantilever wall boundary condition, the vibration function for the n-th mode is that:

[8.11] $\psi_n(y) = (\cosh(k_n\, y) - \cos(k_n\, y)) - \sigma_n(\sinh(k_n\, y) - \sin(k_n\, y))$

where

[8.12] $\sigma_n = \dfrac{\cos(k_n\, H_W) + \cosh(k_n\, H_W)}{\sin(k_n\, H_W) + \sinh(k_n\, H_W)}$

For the second mode, n=2, $k_n = 4.694/H_W$ and $\sigma_n = 1.018$. Then, the shape function corresponding to this mode is defined as SF7 in this study as follows:

[8.13] $\mathrm{SF7} = (\cosh(4.694\, \tfrac{y}{H_W}) - \cos(4.694\, \tfrac{y}{H_W})) - 1.018((\sinh(4.694\, \tfrac{y}{H_W}) + \sin(4.694\, \tfrac{y}{H_W}))$

The normalized shape functions SF3 and SF7 are shown in Figure 8.1.

It is worth noting that the configuration of concrete rectangular tanks in terms of boundary condition could be different for a simple open top rectangular tank used in the study. The prescribed shape functions used in this study are based on the cantilever wall boundary condition. However, the generalized SDOF system can be applied to any

configuration of concrete rectangular tanks provided that the proper mode shape functions are used for approximation of vibration modes.
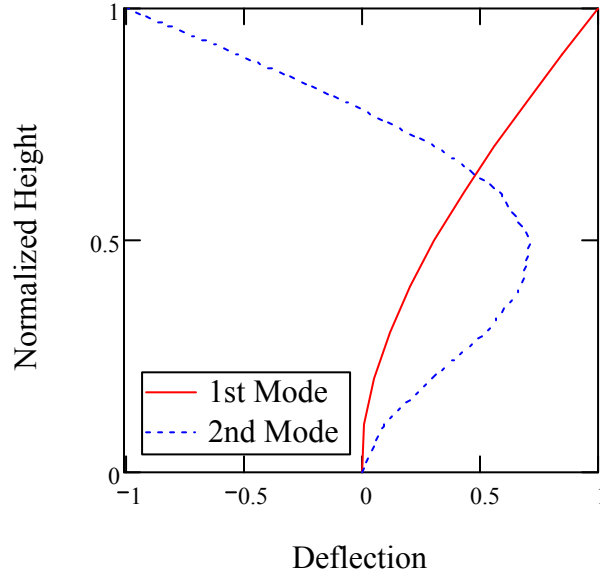
Figure 8.1 Normalized Shape Functions for First Two Modes

8.2.5 Masses of Tank Wall and Liquid

The generalized inertial mass of tank wall $\tilde{m}_w$ and the effective inertial mass of tank wall m_w can be defined as that:

[8.14] $$\tilde{m}_W = \int_0^{H_W} m(y) \cdot [\psi(y)]^2 \cdot dy$$

[8.15] $$m_W = \int_0^{H_W} m(y) \cdot \psi(y) \cdot dy$$

The results in Chapters 5 to 7 show that the generalized inertial mass of tank wall $\tilde{m}_w$ is approximately 25% of total mass of tank wall and the effective inertial mass of tank wall m_w corresponding to the first and second mode shapes are about 39% and 22% of total mass of tank wall, respectively. These ratios are used for the cantilever wall in this study. For more complex conditions such as tapered wall, the mass distribution along the height of wall m(y) should be considered.

When using the generalized SDOF system in the dynamic analysis of LCS, the hydrodynamic pressure is incorporated into the coupling analysis through the added mass. The generalized and effective added mass of liquid due to impulsive hydrodynamic pressure, $\widetilde{m}_L$ and m_L, can be calculated using Eqs.8.16 and 8.17, respectively. The details of these equations were discussed in Chapter 5.

[8.16]
$$\widetilde{m}_L = \sum_{n=1}^{\infty} \frac{2 \cdot \rho_l}{\lambda_{i,n} \cdot H_L} \tanh(\lambda_{i,n} L_x) [\int_0^{H_L} \cos(\lambda_{i,n} y) \cdot \psi(y) dy]^2$$

[8.17]
$$m_L = \sum_{n=1}^{\infty} \frac{2 \cdot (-1)^{n+1} \rho_l}{\lambda_{i,n}^2 \cdot H_L} \tanh(\lambda_{i,n} L_x) \int_0^{H_L} \cos(\lambda_{i,n} y) \cdot \psi(y) dy$$

The ratio of generalized and effective added mass of liquid due to hydrodynamic pressure for the prescribed mode shape to the half mass of liquid in LCS can be calculated as follows:

[8.18]
$$\frac{\widetilde{m}_L}{M_L} = \sum_{n=1}^{\infty} \frac{2}{\lambda_{i,n} \cdot H_L^2 \cdot L_x} \tanh(\lambda_{i,n} L_x) [\int_0^{H_L} \cos(\lambda_{i,n} y) \cdot \psi(y) dy]^2$$

[8.19]
$$\frac{m_L}{M_L} = \sum_{n=1}^{\infty} \frac{2 \cdot (-1)^{n+1}}{\lambda_{i,n}^2 \cdot H_L^2 \cdot L_x} \tanh(\lambda_{i,n} L_x) \int_0^{H_L} \cos(\lambda_{i,n} y) \cdot \psi(y) dy$$

It is worth noting that the total mss of liquid in Housner's model shall be divided by 2 to consider the two-fold symmetric fluid structural model which is consistent with the propose method using half the mass of liquid in the generalized SDOF system.

Chapter 6 shows that when the values of L_x/H_L are relatively large, the ratio of added mass of liquid due to impulsive hydrodynamic pressure to the half liquid mass in the containment for the prescribed shape functions, or the percentage of added mass of liquid in participation of dynamic response become minimal. It was recommended to use the ratio of the generalized and effective added mass of liquid due to impulsive hydrodynamic pressure to that of rigid wall condition in the dynamic analysis of liquid containing structures. Therefore, the ratios of $\widetilde{f}_{mass}$ and f_{mass} for the generalized and the effective added masses of liquid due to hydrodynamic pressure are introduced

respectively as follows:

$$[8.20] \quad \tilde{f}_{mass} = \frac{\tilde{m}_L}{\tilde{M}_{L-rigid}} = \frac{\displaystyle\sum_{n=1}^{\infty} \frac{2 \cdot \rho_l \tanh(\lambda_{i,n} L_x)}{\lambda_{i,n} H_L} [\int_0^{H_L} \cos(\lambda_{i,n} y) \cdot \psi(y) dy]^2}{\displaystyle\sum_{n=1}^{\infty} \frac{2 \cdot \rho_l \tanh(\lambda_{i,n} L_x)}{\lambda_{i,n} H_L} [\int_0^{H_L} \cos(\lambda_{i,n} y) dy]^2}$$

$$[8.21] \quad f_{mass} = \frac{m_L}{M_{L-rigid}} = \frac{\displaystyle\sum_{n=1}^{\infty} \frac{2 \cdot (-1)^{n+1} \rho_l \tanh(\lambda_{i,n} L_x)}{\lambda_{i,n}{}^2 H_L} \int_0^{H_L} \cos(\lambda_{i,n} y) \cdot \psi(y) dy}{\displaystyle\sum_{n=1}^{\infty} \frac{2 \cdot (-1)^{n+1} \rho_l \tanh(\lambda_{i,n} L_x)}{\lambda_{i,n}{}^2 H_L} \int_0^{H_L} \cos(\lambda_{i,n} y) dy}$$

where $\tilde{M}_{L-rigid}$ and $M_{L-rigid}$ are the total generalized and effective added mass of liquid due to impulsive hydrodynamic pressure for the rigid boundary condition. It is worth noting that $\tilde{M}_{L-rigid}$ and $M_{L-rigid}$ are calculated using the shape function $\psi(y)=1$ and generally are the same.

In the current design standards and codes the ratio of length of tank to the liquid height, L_x/H_L is the only parameter used to calculate the added mass of liquid due to impulsive hydrodynamic pressure. It is assumed that the wall is in the rigid wall boundary condition. As a result, the accelerations along the height of wall are constant and the effect of liquid height H_L inside the tank on the added mass of liquid due to impulsive pressure is not significant.

In the proposed generalized SDOF system, the flexibility of tank wall is considered. The distribution of added mass of liquid due to impulsive hydrodynamic pressure varies along the height of wall. As a result, the effect of variable liquid level inside the tank shall be considered. In addition, the liquid level can be variable during operation and maintenance, Therefore, it is recommended to use H_L/H_W and L_X/H_W to consider the variable liquid level in tanks and the configuration of tanks, respectively.

Tables 7.1 to 7.5 in Chapter 7 present the values of added mass of liquid due to impulsive pressure for the first mode considering the effect of length of tank L_X and liquid height H_L in dynamic analysis of liquid containing structures.

Table 7.1 shows the ratio of added mass of liquid due to hydrodynamic pressure based on the rigid boundary condition to the half mass of liquid inside the tank $M_{L\text{-}rigid}/M_L$. Tables 7.2 and 7.3 show the ratio of generalized and effective added mass of liquid due to hydrodynamic pressure to the half mass of liquid inside tank $\widetilde{m}_L/M_L$ and m_L/M_L, respectively. Tables 7.4 and 7.5 show the ratios of generalized and effective added mass of liquid due to impulsive hydrodynamic pressure to the added mass based on the rigid boundary condition $\widetilde{m}_L/\widetilde{M}_{L\text{-}rigid}$ and $m_L/M_{L\text{-}rigid}$. The details are discussed in Chapter 7.

Figures 8.2(a) and 8.2(b) show the mass ratios of liquid due to impulsive pressure versus the length of tank to depth of liquid L_x/H_L. The mass ratios are based on Hounser's model and the generalized SDOF system using shape function $\psi(y)=1$ which are both corresponding to a rigid tank wall, and the ratios of $\widetilde{m}_L/M_L$ and m_L/M_L. The shape functions SF3 and SF6 are used for the first two modes considering the flexibility of tank wall in dynamic analysis. The curves for shape functions SF3 and SF6 are corresponding to the values of Tables 7.2 and 7.3 for the first mode shape and Tables 8.1 and 8.2 for the second mode respectively in full tank condition, i.e. $H_L = H_W$. The effect of the mode shapes is presented later in this paper.

Figure 8.2 shows that the trend of curves for Housner's model and the generalized SDOF system is similar. It is worth noting that the sum of the effective added mass of liquid for the first two modes is less than that based on the rigid boundary condition as shown in Figure 8.2(b). However, if the higher modes are considered, the sum of the effective added mass of liquid including higher modes is larger than that based on the rigid boundary condition as shown in Figure 7.2(b). It is consistent with the research conclusions that the wall flexibility increases the added mass of liquid due to impulsive hydrodynamic pressure (Yang, 1976).

Table 8.1 Ratio of $\tilde{m}_L/M_L$ in relationship with L_x/H_W and H_L/H_W (2nd mode)

		Lx/Hw																
		0.0	0.1	0.2	0.3	0.4	0.5	0.8	1.0	1.5	2.0	3.0	4.0	5.0	6.0	7.0	8.0	9.0
	0.0	0.0000	0.0000	0.0000	0.0000	0.0000	0.0000	0.0000	0.0000	0.0000	0.0000	0.0000	0.0000	0.0000	0.0000	0.0000	0.0000	0.0000
	0.1	0.0013	0.0004	0.0002	0.0001	0.0001	0.0001	0.0000	0.0000	0.0000	0.0000	0.0000	0.0000	0.0000	0.0000	0.0000	0.0000	0.0000
	0.2	0.0150	0.0073	0.0043	0.0030	0.0022	0.0018	0.0011	0.0009	0.0006	0.0004	0.0003	0.0002	0.0002	0.0001	0.0001	0.0001	0.0001
	0.3	0.0545	0.0347	0.0223	0.0161	0.0124	0.0101	0.0063	0.0051	0.0034	0.0025	0.0017	0.0013	0.0010	0.0008	0.0007	0.0006	0.0006
	0.4	0.1174	0.0875	0.0606	0.0457	0.0362	0.0298	0.0190	0.0152	0.0101	0.0076	0.0051	0.0038	0.0030	0.0025	0.0022	0.0019	0.0017
HL/Hw	0.5	0.1849	0.1522	0.1132	0.0885	0.0720	0.0602	0.0393	0.0316	0.0211	0.0159	0.0106	0.0079	0.0063	0.0053	0.0045	0.0040	0.0035
	0.6	0.2325	0.2044	0.1625	0.1317	0.1100	0.0937	0.0631	0.0511	0.0343	0.0257	0.0172	0.0129	0.0103	0.0086	0.0074	0.0064	0.0057
	0.7	0.2447	0.2251	0.1898	0.1598	0.1369	0.1189	0.0829	0.0679	0.0459	0.0345	0.0230	0.0172	0.0138	0.0115	0.0099	0.0086	0.0077
	0.8	0.2246	0.2125	0.1879	0.1641	0.1444	0.1281	0.0928	0.0770	0.0527	0.0397	0.0265	0.0198	0.0159	0.0132	0.0113	0.0099	0.0088
	0.9	0.1938	0.1846	0.1667	0.1495	0.1345	0.1216	0.0917	0.0772	0.0537	0.0405	0.0271	0.0203	0.0162	0.0135	0.0116	0.0102	0.0090
	1.0	0.1836	0.1712	0.1504	0.1335	0.1205	0.1097	0.0847	0.0722	0.0510	0.0387	0.0259	0.0194	0.0155	0.0129	0.0111	0.0097	0.0086

Table 8.2 Ratio of m_L/M_L in relationship with L_x/H_W and H_L/H_W (2nd mode)

|		Lx/Hw																
		0.0	0.1	0.2	0.3	0.4	0.5	0.8	1.0	1.5	2.0	3.0	4.0	5.0	6.0	7.0	8.0	9.0
	0.0	0.0000	0.0000	0.0000	0.0000	0.0000	0.0000	0.0000	0.0000	0.0000	0.0000	0.0000	0.0000	0.0000	0.0000	0.0000	0.0000	0.0000
	0.1	0.0262	0.0110	0.0059	0.0039	0.0029	0.0024	0.0015	0.0012	0.0008	0.0006	0.0004	0.0003	0.0002	0.0002	0.0002	0.0001	0.0001
	0.2	0.0918	0.0594	0.0389	0.0274	0.0208	0.0167	0.0104	0.0084	0.0056	0.0042	0.0028	0.0021	0.0017	0.0014	0.0012	0.0010	0.0009
	0.3	0.1779	0.1363	0.1004	0.0764	0.0600	0.0488	0.0308	0.0246	0.0164	0.0123	0.0082	0.0062	0.0049	0.0041	0.0035	0.0031	0.0027
	0.4	0.2670	0.2241	0.1771	0.1426	0.1165	0.0970	0.0625	0.0501	0.0334	0.0251	0.0167	0.0125	0.0100	0.0084	0.0072	0.0063	0.0056
HL/Hw	0.5	0.3439	0.3054	0.2538	0.2128	0.1798	0.1534	0.1020	0.0823	0.0550	0.0413	0.0275	0.0206	0.0165	0.0138	0.0118	0.0103	0.0092
	0.6	0.3971	0.3661	0.3169	0.2741	0.2380	0.2075	0.1433	0.1166	0.0784	0.0588	0.0392	0.0294	0.0235	0.0196	0.0168	0.0147	0.0131
	0.7	0.4189	0.3970	0.3559	0.3162	0.2809	0.2498	0.1792	0.1475	0.1001	0.0752	0.0502	0.0376	0.0301	0.0251	0.0215	0.0188	0.0167
	0.8	0.4062	0.3934	0.3643	0.3321	0.3012	0.2727	0.2032	0.1696	0.1166	0.0878	0.0586	0.0440	0.0352	0.0293	0.0251	0.0220	0.0195
	0.9	0.3598	0.3552	0.3401	0.3185	0.2953	0.2722	0.2107	0.1786	0.1248	0.0944	0.0630	0.0473	0.0378	0.0315	0.0270	0.0236	0.0210
	1.0	0.2836	0.2861	0.2848	0.2758	0.2624	0.2468	0.1993	0.1718	0.1226	0.0932	0.0624	0.0468	0.0374	0.0312	0.0267	0.0234	0.0208
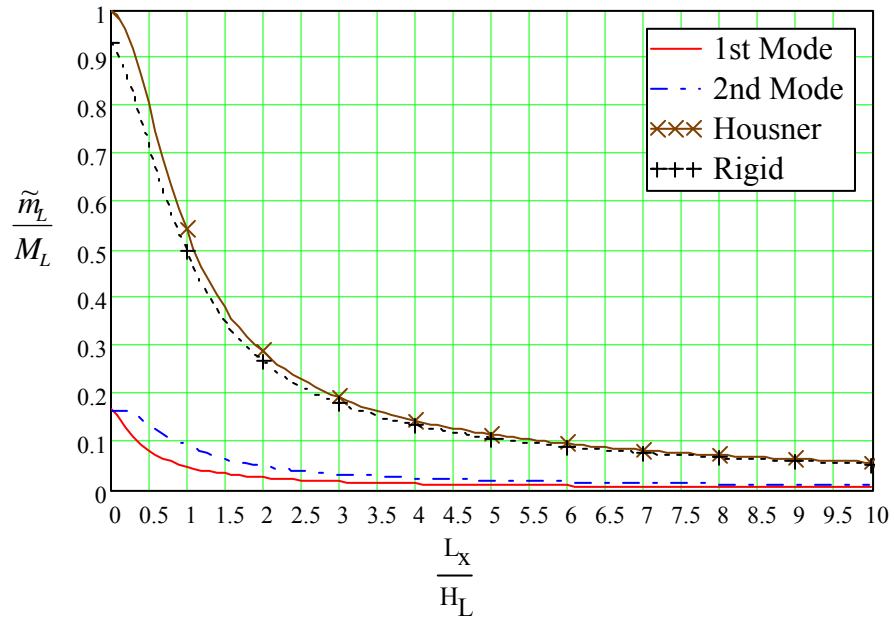
(a) Generalized Added Mass
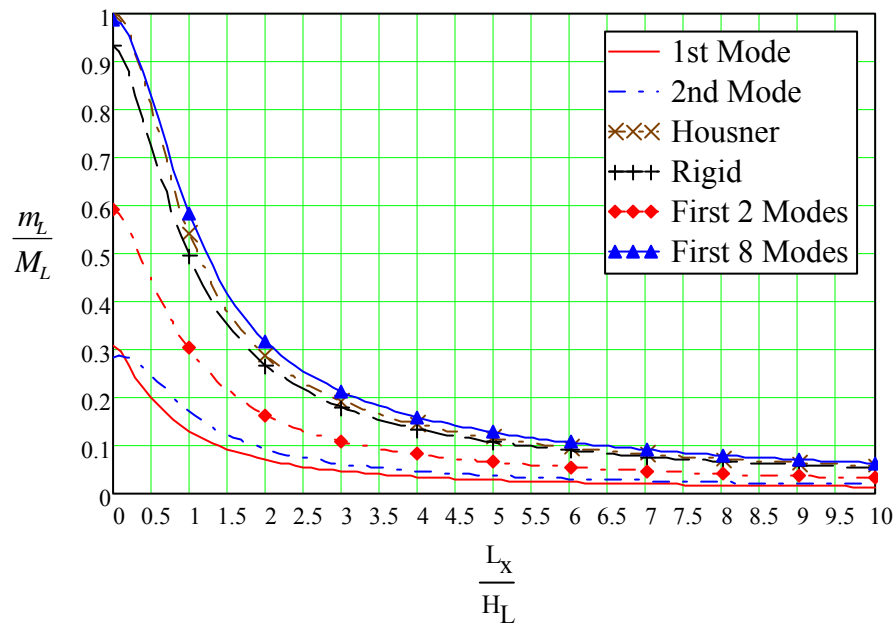
(b) Effective Added Mass

Figure 8.2 Ratio of Added Mass of Liquid due to Impulsive Hydrodynamic Pressure vs.

L_x / H_L Ratio ($H_L = H_W$)

Figures 8.3(a) and 8.3(b) show the amplification factors of added mass of liquid due to impulsive hydrodynamic pressure $\widetilde{f}_{mass}$ and f_{mass} in full tank condition as function of L_x/H_L, respectively. The curves for shape functions SF3 and SF6 are corresponding to the values of Tables 7.4 and 7.5 for the first mode shape and Tables 8.3 and 8.4 for the second mode respectively in full tank condition, i.e. $H_L = H_W$. These figures show that when $L_x/H_L > 1$, the factors $\widetilde{f}_{mass}$ and f_{mass} are constants. This indicates that when the half-length of tank, L_x exceeds the liquid height, the increase of the added mass of liquid due to hydrodynamic pressure considering the flexibility of tank wall is constant.

Tables 7.1 to 7.5 and Figures 8.2 and 8.3 can be used as design tables and charts to calculate the generalized and effective added mass of liquid due to hydrodynamic pressure for the first mode. It is noted that Tables 7.1 to 7.5 consider the variable liquid level in tank while Figures 8.2 and 8.3 is only for the full tank condition, i.e. $H_L = H_W$. The ratio of added mass of liquid for the first mode shape can be directly obtained from Tables 7.2, 7.3 or Figure 8.2, in terms of the half mass of liquid in the tank. Alternatively, the generalized and effective added mass of liquid due to hydrodynamic pressure are firstly calculated based on the rigid boundary condition as shown in Table 7.1 or Figure 8.2 using the shape function $\psi(y)=1$. Then, $\widetilde{M}_{L-rigid}$ and $M_{L-rigid}$ are multiplied by the amplification factors of added mass of liquid due to impulsive hydrodynamic pressure $\widetilde{f}_{mass}$ and f_{mass} for the first mode shape as shown in Tables 7.4, 7.5 or Figure 8.3. It should be noted that the flexibility of tank wall and the consistent mass are considered in the added mass of liquid due to impulsive hydrodynamic pressure.

Table 8.3 Ratio of $\widetilde{m}_L/\widetilde{M}_{rigid}$ in relationship with L_x/H_W and H_L/H_W (2nd mode)

		Lx/Hw												
		0.0	0.1	0.2	0.3	0.4	0.5	0.8	1.0	1.5	2.0	3.0	4.0	5.0
HL/Hw	0.0	0.0000	0.0000	0.0000	0.0000	0.0000	0.0000	0.0000	0.0000	0.0000	0.0000	0.0000	0.0000	0.0000
	0.1	0.0013	0.0007	0.0007	0.0007	0.0007	0.0007	0.0007	0.0007	0.0007	0.0007	0.0007	0.0007	0.0007
	0.2	0.0161	0.0101	0.0087	0.0084	0.0083	0.0083	0.0083	0.0083	0.0083	0.0083	0.0083	0.0083	0.0083
	0.3	0.0584	0.0429	0.0348	0.0325	0.0317	0.0314	0.0313	0.0313	0.0313	0.0313	0.0313	0.0313	0.0313
	0.4	0.1258	0.1029	0.0838	0.0761	0.0730	0.0716	0.0706	0.0705	0.0705	0.0705	0.0705	0.0705	0.0705
	0.5	0.1982	0.1741	0.1462	0.1317	0.1247	0.1213	0.1182	0.1178	0.1176	0.1176	0.1176	0.1176	0.1176
	0.6	0.2492	0.2299	0.2010	0.1823	0.1721	0.1664	0.1605	0.1595	0.1591	0.1590	0.1590	0.1590	0.1590
	0.7	0.2622	0.2504	0.2280	0.2104	0.1995	0.1930	0.1852	0.1837	0.1828	0.1827	0.1827	0.1827	0.1827
	0.8	0.2407	0.2345	0.2209	0.2085	0.1998	0.1942	0.1869	0.1853	0.1842	0.1840	0.1840	0.1840	0.1840
	0.9	0.2077	0.2026	0.1930	0.1848	0.1791	0.1752	0.1699	0.1686	0.1675	0.1674	0.1673	0.1673	0.1673
	1.0	0.1968	0.1871	0.1721	0.1618	0.1556	0.1518	0.1467	0.1454	0.1443	0.1441	0.1440	0.1440	0.1440

Table 8.4 Ratio of m_L/M_{rigid} in relationship with L_x/H_W and H_L/H_W (2nd mode)

		Lx/Hw												
		0.0	0.1	0.2	0.3	0.4	0.5	0.8	1.0	1.5	2.0	3.0	4.0	5.0
HL/Hw	0.0	0.0000	0.0000	0.0000	0.0000	0.0000	0.0000	0.0000	0.0000	0.0000	0.0000	0.0000	0.0000	0.0000
	0.1	0.0280	0.0221	0.0219	0.0218	0.0218	0.0218	0.0218	0.0218	0.0218	0.0218	0.0218	0.0218	0.0218
	0.2	0.0983	0.0823	0.0783	0.0776	0.0775	0.0774	0.0774	0.0774	0.0774	0.0774	0.0774	0.0774	0.0774
	0.3	0.1906	0.1686	0.1572	0.1538	0.1527	0.1524	0.1522	0.1522	0.1522	0.1522	0.1522	0.1522	0.1522
	0.4	0.2861	0.2635	0.2451	0.2377	0.2347	0.2334	0.2325	0.2324	0.2324	0.2324	0.2324	0.2324	0.2324
	0.5	0.3686	0.3493	0.3278	0.3167	0.3115	0.3089	0.3065	0.3062	0.3061	0.3061	0.3061	0.3061	0.3061
	0.6	0.4256	0.4118	0.3919	0.3793	0.3724	0.3687	0.3647	0.3641	0.3637	0.3637	0.3637	0.3637	0.3637
	0.7	0.4489	0.4415	0.4274	0.4163	0.4093	0.4052	0.4003	0.3993	0.3988	0.3987	0.3987	0.3987	0.3987
	0.8	0.4353	0.4341	0.4284	0.4218	0.4169	0.4136	0.4093	0.4083	0.4077	0.4076	0.4075	0.4075	0.4075
	0.9	0.3856	0.3899	0.3937	0.3939	0.3930	0.3921	0.3905	0.3901	0.3898	0.3897	0.3897	0.3897	0.3897
	1.0	0.3039	0.3126	0.3257	0.3341	0.3388	0.3416	0.3452	0.3461	0.3468	0.3470	0.3470	0.3470	0.3470
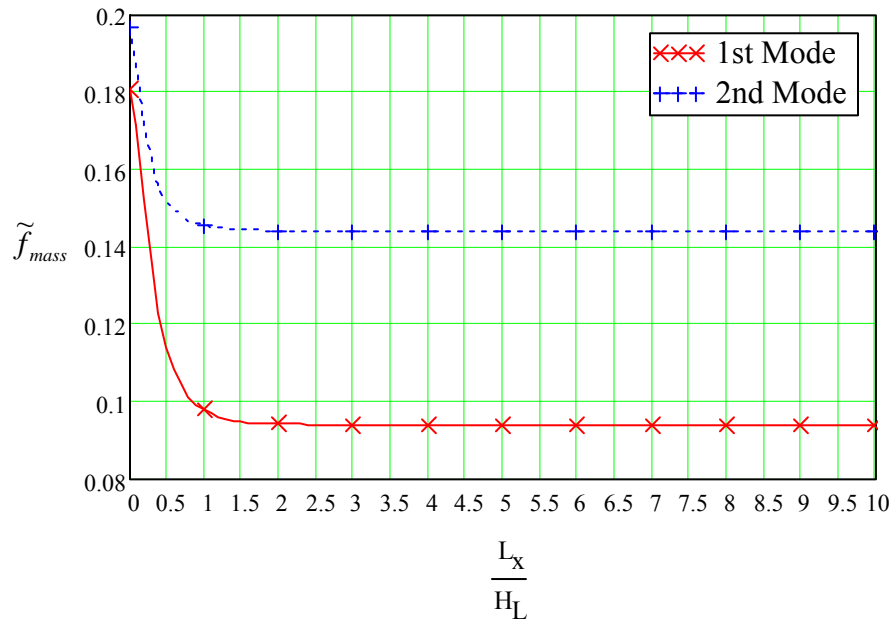
(a) Generalized Added Mass

(b) Effective Added Mass

Figure 8.3 Ratio of Added Mass of Liquid due to Impulsive Hydrodynamic Pressure
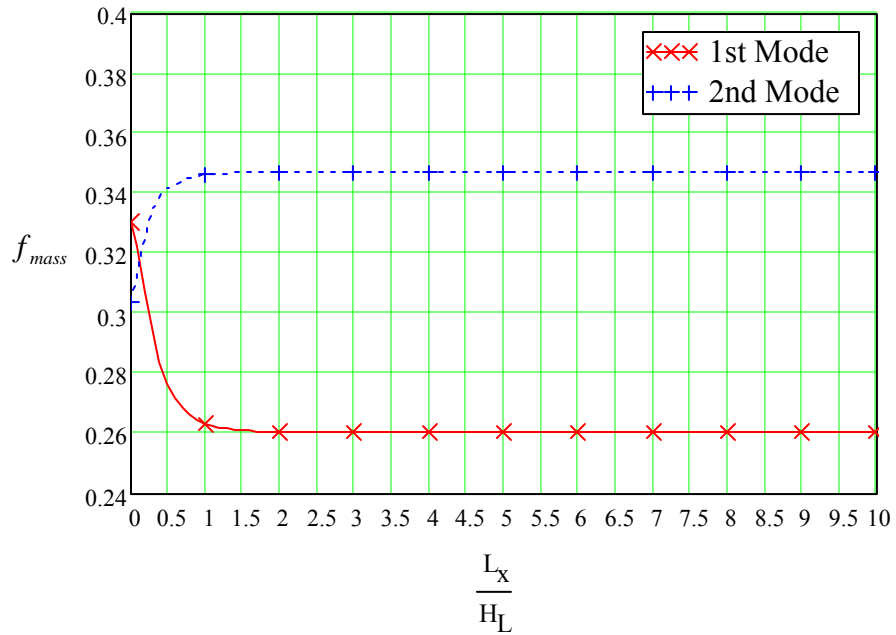Considering Flexibility of Tank Wall vs. L_x / H_L Ratio ($H_L = H_W$)

8.2.6 Stiffness of Tank Wall

The stiffness of tank wall can be calculated using Eq.8.3 defined previously. Also, the stiffness of the tank wall can be calculated using the following simple relationship assuming a unit load applied at the top of the cantilever wall.

$$[8.22] \qquad \tilde{k} = \frac{E_c}{4} \cdot (\frac{t_W}{H_W})^3$$

It is noted that Eq.8.23 can only be used for the first mode. The generalized stiffness of structure for the second mode is about forty times of that for the first mode.

8.2.7 Effective Height

In the generalized SDOF system, the effective heights at which the effective inertial mass of tank wall and the effective added mass of liquid due to hydrodynamic pressure is applied are h_w and h_i, and can be calculated as follows:

$$[8.23] \qquad h_w = \frac{\int_0^{H_W} m(y) \cdot \psi_n(y) \cdot y \cdot dy}{\int_0^{H_W} m(y) \cdot \psi_n(y) \cdot dy}$$

$$[8.24] \qquad h_i = \frac{\int_0^{H_L} \sum_{n=1}^{\infty} \frac{2 \cdot \rho_l}{\lambda_{i,n} \cdot H_L} \tanh(\lambda_{i,n} L_x) \cos(\lambda_{i,n} y) \int_0^{H_L} \cos(\lambda_{i,n} y) \, \psi(y) \cdot dy \cdot y \cdot dy}{\int_0^{H_L} \sum_{n=1}^{\infty} \frac{2 \cdot \rho_l}{\lambda_{i,n} \cdot H_L} \tanh(\lambda_{i,n} L_x) \cos(\lambda_{i,n} y) \int_0^{H_L} \cos(\lambda_{i,n} y) \, \psi(y) \cdot dy \cdot dy}$$

For the liquid containing structures, the effective height at which the total dynamic lateral force is applied can be calculated using Eq.8.28. This expression includes both the effects of inertial mass of tank wall and the added mass of liquid due to hydrodynamic pressure.

$$[8.25] \qquad h = \frac{m_w \cdot h_w + m_L \cdot h_i}{m_w + m_L}$$

For the rigid wall condition, the inertial mass of concrete tank wall is lumped at the center of gravity of the tank wall. However, when the flexibility of tank wall is

174

considered, the effective height of tank wall equals to 75% and 21% of tank height corresponding to the first two modes in the cantilever wall condition, respectively.

Figure 8.4 shows the normalized effective height at which the hydrodynamic pressure is applied as function of the ratio of half length of tank to liquid depth L_x/H_L for the full tank condition, i.e. $H_L = H_W$. The figure shows the first two modes, the rigid wall boundary condition $\psi(y)=1$ and Housner's model. The figure shows that the effective heights h_i obtained from Hounser's model and the rigid wall boundary condition $\psi(y)=1$ are similar. For the flexible wall boundary condition, the effective height h_i is determined using the shape function along the height of wall. The curves for shape functions SF3 and SF6 are corresponding to the values of Tables 7.6 and 8.5 for the first two mode shapes respectively in full tank condition, i.e. $H_L = H_W$. For the variable liquid level condition, the effective height at which the hydrodynamic pressure is applied can be calculated using the Tables 7.6 and 8.5 as function of H_L/H_W and L_X/H_W.
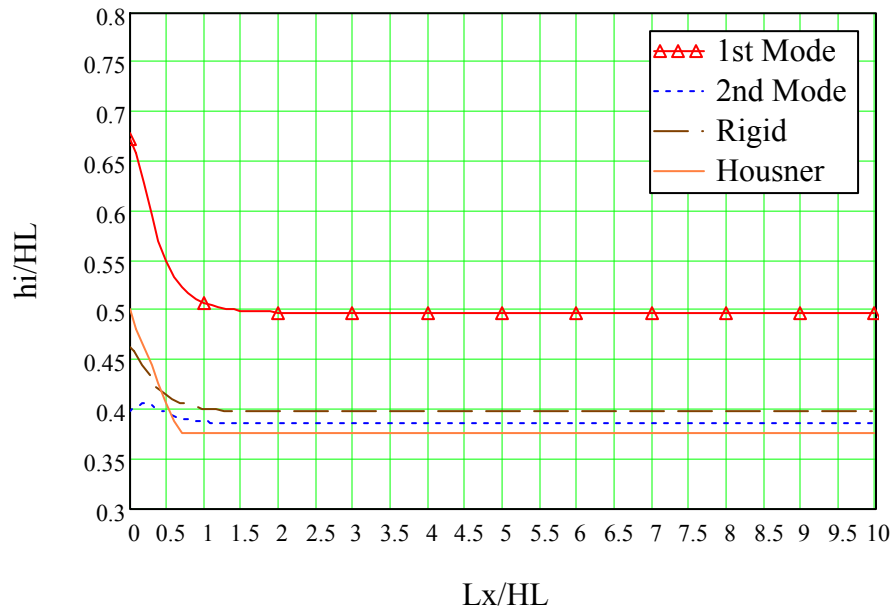

Figure 8.4 Effective Height Factors for Impulsive Hydrodynamic Pressure vs. L_x/H_L Ratio ($H_L = H_W$)

It is worth noting that considering the flexibility of tank wall, the effective height h at

which the overall lateral dynamic force is applied is higher than that obtained from the rigid wall condition.

8.2.8 Effect of Higher Modes

Chapter 6 shows that the response of LCS increases by about 10% to 20% when considering the second mode effect. This is due to the effect of flexibility of tank wall and hydrodynamic pressure for the second mode. For design purposes, it may conservatively be assumed to increase the response due to the first mode by 20% to include the effect of higher modes. However, if more rigorous analysis is required, the effect of higher modes can be calculated using the design parameters as discussed below.

Similar to the calculation for the first mode shape, the generalized mass of tank wall is assumed to be 25% of total mass of tank for the second mode effect. The corresponding effective height of tank wall is assumed as 21% of overall height of tank wall. The generalized stiffness for the second mode is about forty times of that for the first mode.

The generalized and effective added mass of liquid due to impulsive hydrodynamic pressure for the full tank can be calculated using the design curves for the second mode as shown in Figures 8.2 and 8.3 for the full tank condition, or directly from Tables 8.1 and 8.2 for the variable liquid level. Alternatively, similar to the calculation of added mass of liquid due to impulsive hydrodynamic pressure for the first mode, Table 8.1 or Figure 8.2 can be used to obtain the generalized and effective added mass of liquid due to impulsive hydrodynamic pressure based on the rigid boundary condition using the shape function $\psi(y)=1$ and multiply the amplification factors of added mass of liquid due to impulsive hydrodynamic pressure $\tilde{f}_{mass}$ and f_{mass} for the second mode shape as shown in Tables 8.3 and 8.4, or Figure 8.2.

The effective height of effective added mass of liquid due to impulsive hydrodynamic pressure can be obtained from Figure 8.4 for the full tank condition, or Tables 7.6 and 8.5 for the variable liquid level for the first two modes.

Table 8.5 Ratio of h_i / H_W in relationship with L_x/H_W and H_L/ H_W (2nd mode)

HL/Hw		Lx/Hw												
		0.0	0.1	0.2	0.3	0.4	0.5	0.8	1.0	1.5	2.0	3.0	4.0	5.0
	0.0	0.0000	0.0000	0.0000	0.0000	0.0000	0.0000	0.0000	0.0000	0.0000	0.0000	0.0000	0.0000	0.0000
	0.1	0.0679	0.0511	0.0502	0.0501	0.0501	0.0501	0.0501	0.0501	0.0501	0.0501	0.0501	0.0501	0.0501
	0.2	0.1345	0.1098	0.1015	0.0999	0.0996	0.0995	0.0995	0.0995	0.0995	0.0995	0.0995	0.0995	0.0995
	0.3	0.1994	0.1739	0.1565	0.1508	0.1489	0.1482	0.1479	0.1479	0.1479	0.1479	0.1479	0.1479	0.1479
	0.4	0.2617	0.2382	0.2142	0.2032	0.1985	0.1965	0.1949	0.1948	0.1948	0.1948	0.1948	0.1948	0.1948
HL/Hw	0.5	0.3202	0.2996	0.2721	0.2563	0.2482	0.2442	0.2404	0.2399	0.2397	0.2397	0.2397	0.2397	0.2397
	0.6	0.3732	0.3555	0.3274	0.3080	0.2968	0.2905	0.2836	0.2825	0.2820	0.2819	0.2819	0.2819	0.2819
	0.7	0.4175	0.4030	0.3765	0.3554	0.3418	0.3336	0.3235	0.3216	0.3204	0.3202	0.3202	0.3202	0.3202
	0.8	0.4475	0.4367	0.4143	0.3940	0.3797	0.3703	0.3578	0.3550	0.3531	0.3528	0.3528	0.3528	0.3528
	0.9	0.4512	0.4458	0.4314	0.4158	0.4035	0.3949	0.3824	0.3793	0.3769	0.3765	0.3764	0.3764	0.3764
	1.0	0.3982	0.4034	0.4065	0.4035	0.3991	0.3952	0.3887	0.3870	0.3854	0.3851	0.3850	0.3850	0.3850

The SRSS method can be used for the combination of higher modes. Generally, the inclusion of the first two modes should provide sufficiently accurate results for design purpose as shown in Chapter 6.

8.3. Calculation Procedure for the Proposed Model

A design procedure using the generalized SDOF systems for seismic design of concrete rectangular LCS is proposed. The procedure is developed considering the consistent mass and the effect of flexibility of tank wall based on the theories discussed previously. The conceptual procedure for this methodology is similar to that using Housner's model. However, the generalized and effective added mass of liquid due to impulsive hydrodynamic pressure and the corresponding effective heights are introduced in this proposed model. The calculation procedure is summarized as follows:

1. Calculate the generalized and effective inertial mass of tank wall, $\widetilde{m}_w$ and m_w.

    For the cantilever wall condition, the generalized inertial mass of tank wall $\widetilde{m}_w$ is 25% of total mass of tank wall and the effective inertial mass of tank wall m_w is about 39% and 22% of total mass of tank wall for the first and second mode shapes, respectively.

2. Calculate the generalized and effective added mass of liquid due to impulsive hydrodynamic pressure, $\widetilde{m}_L$ and m_L.

    First, the generalized and effective added mass of liquid due to impulsive hydrodynamic pressure in the rigid wall boundary condition $\widetilde{M}_{L-rigid}$ and $M_{L-rigid}$ are obtained from Figure 8.2 for the full tank or Table 7.1 for the variable liquid level in tank. Then, $\widetilde{M}_{L-rigid}$ and $M_{L-rigid}$ are multiplied by the amplification factor of added mass of liquid due to hydrodynamic pressure $\widetilde{f}_{mass}$ and f_{mass} which are shown in Figure 8.3 for the full tank, or Tables 7.4 and 7.5 for the first mode and Tables 8.3 and 8.4 for the second mode respectively for the variable liquid level in tank. As a result, the effect of flexibility of tank wall on dynamic response is considered.

Alternatively, the ratio of added mass of liquid for the first two modes can be directly obtained from the curves in Figure 8.2 for the full tank, or Tables 7.2 and 7.3 for the first mode and Tables 8.1 and 8.2 for the second mode for the variable liquid level based on the half mass of liquid in the tank.

3. Calculate the generalized stiffness of tank wall using Eq.8.23, or Eq.8.3 considering the stiffness distribution along the height of wall. For the second mode, the generalized stiffness of tank wall is forty times of that for the first mode.

4. Calculate the natural period of vibration, T_i, including the effect of the tank wall and the impulsive hydrodynamic pressure component.

$$[8.26] \qquad T_i = 2\pi \sqrt{\frac{\tilde{m}_W + \tilde{m}_L}{\tilde{k}}}$$

5. Use the applicable seismic ground motion maps in the codes to obtain the mapped maximum earthquake response spectral acceleration A_a.

6. Calculate the maximum displacement at top of tank wall.

$$[8.27] \qquad u_{max} = \frac{\hat{q}}{\omega_i^2} \cdot A_a$$

7. Calculate the base shear using the following relationship.

$$[8.28] \qquad V_B = \hat{p} \cdot \hat{q} \cdot A_a$$

where $\hat{q}$ and $\hat{p}$ are defined in the Eq.8.6.

8. Calculate the effective heights of wall and effective added mass of liquid due to impulsive hydrodynamic pressure. For cantilever wall condition, the effective height of wall is $0.75h_w$ and $0.21h_w$ for the first and the second modes, respectively. The effective height of effective added mass of liquid due to impulsive hydrodynamic pressure can be obtained from Figure 8.4 for the full tank, or Table 7.6 for the first mode and Table 8.5 for the second mode for the variable liquid level in tank. The

effective height of liquid containing structure h can be calculated using Eq.8.28.

9. Calculate the base bending moment:

[8.29] $M_B = V_B h$

10. Calculate the vertical distribution of the impulsive hydrodynamic component and the impulsive hydrodynamic force.

[8.30] $P_i = m_L \cdot \hat{q} \cdot A_a$

11. Include the effect of the second mode in dynamic response of LCS. The calculation procedure is the same as that for the first mode. The inertial mass of tank wall, the added mass of liquid due to hydrodynamic pressure and the corresponding effective highs are calculated using the design parameter as discussed in Section 7.2.8. Alternatively, the response of the LCS due to the second mode can be considered by 20% increase of the response due to the first mode. The overall dynamic response of LCS can be calculated using the SRSS method to combine the dynamic response of the first two modes.

ACI 350.3 (2006) outlines the calculation procedure for dynamic analysis of concrete rectangular LCS. Housner's model is adopted and the lumped added mass and the rigid wall boundary condition are considered in the practice. The effect of ductility and damping is considered through the response spectral acceleration A_a and the response modification factor R which is a numerical coefficient representing the combined effect of the structure's ductility, energy-dissipating capacity, and structural redundancy. It is worth noting that and response modification factor R and the importance factor, I are not considered in this study. Therefore, the comparison between the proposed model and Housner's model is on the basis of elastic analysis.

8.4. Design Examples

In this investigation, a tall and a shallow tanks are used as design examples. The dimensions and properties of the tanks are as follows:

(1) Tall Tank:

L_x = 9.8 m L_z = 28 m H_w =12.3 m H_L =11.2 m t_w = 1.2 m E_c = 20.776x10³Mpa

(2) Shallow Tank:

L_x = 15 m L_z = 30 m H_w =6.0 m H_L =5.5 m t_w = 0.6 m E_c = 26.44x10³MPa

Other properties for both tanks are:

ρ_w = 2300 kg/m³ ρ_l = 1000 kg/m³ v = 0.17

The design response spectrum based on ASCE 7-05 is used to obtain the response spectral acceleration as shown in Figure 6.8. The site is assumed to be located in the west coast of US in Washington State and the parameters for the design response spectrum are that:

(1) Short period maximum spectral response acceleration: S_s=1.25
(2) 1-second maximum spectral response acceleration: S_1=0.60
(3) Site class B

8.4.1 Tall Tank

1. The total inertial mass of concrete tank wall is M_w= 2300 kg/m³ x 1.2m x 12.3m x 1.0m=33.9x10³ kg. For the first mode shape, the generalized mass $\tilde{m}_w$= 8.48x10³ kg is 25% of M_w and the effective mass m_w= 13.2x10³ kg is 39% of M_w.

2. The total mass of liquid considered in the dynamic analysis is M_L= 1000 kg/m³ x 9.8m x 11.2m x 1.0m=109.8x10³ kg. For L_x/H_W = 0.797 and H_L/H_W = 0.911, $\tilde{M}_{L-rigid}/M_L$ = $M_{L-rigid}/M_L$ =0.545 obtained from Table 7.1 and $\tilde{f}_{mass}$ =0.072 and f_{mass} =0.225 obtained from Tables 7.4 and 7.5. Therefore, the generalized and effective added mass of liquid due to the impulsive hydrodynamic pressure $\tilde{m}_L$ = 0.545x0.072x M_L =4.32x10³ kg and m_L= 0.545x0.225x M_L =13.46x10³ kg

3. The generalized stiffness per meter is

$$\tilde{k} = \frac{E_c}{4} \cdot (\frac{t_W}{H_W})^3 = \frac{2.0776 \times 10^4 MPa}{4} (\frac{1.2m}{12.3m})^3 = 4823 kN/m/m$$

4. The combined natural frequency of vibration of the containment structure and the impulsive component of the stored liquid for rectangular tanks is:

$$\omega_1 = \sqrt{\frac{\tilde{k}}{\tilde{m}}} = \sqrt{\frac{4823 kN/m}{8.48 \times 10^3 kg + 4.32 \times 10^3 kg}} = 19.4 Hz$$

The corresponding natural period of vibration, T_1 is 0.324sec.

5. From the earthquake response spectrum, the maximum response accelerations A_a=0.833g for T_i=0.324sec.

6. Calculate $\hat{q} = \hat{p}/\tilde{m} = \dfrac{m_W + m_L}{\tilde{m}_W + \tilde{m}_L} = 2.085$

7. Calculate the maximum displacement $d_{max} = (\hat{q}/\omega_i^2) \times A_a = 45.2mm$

8. Calculate the maximum base shear $V_{max} = \hat{q} \times (m_w + m_L) \times A_a = 454.8 kN/m$.

9. The effective height of tank wall is h_w=0.75x12.3m=9.225m. The effective height of the effective added mass due to impulsive hydrodynamic pressure is h_i=0.463x12.3m=5.7m which is obtained from Table 7.6. The equivalent effective height of dynamic force including both the tank wall and the impulsive hydrodynamic pressure is h=8.1m calculated from Eq.8.26.

10. Calculate the base moment M= V_{max}xh=454.8kNx8.1m=3661kNm/m.

11. For the second mode, the effective mass of tank wall m_w is 22% of M_w and the effective height is $0.21H_w$. The generalized stiffness for the second mode is forty times the generalized stiffness of the first mode. For L_x/H_W = 0.797 and H_L/H_W = 0.911, $\tilde{f}_{mass}$ =0.17 and f_{mass} =0.39 obtained from Tables 8.3 and 8.4. Therefore, the generalized and effective added mass of liquid due to the impulsive pressure are $\tilde{m}_L$ = 0.545x0.17x M_L =10.02x10^3 kg and m_L= 0.545x0.39x M_L =23.2x10^3 kg. The effective height of added mass due to impulsive hydrodynamic pressure for the second mode is h_i=0.384x12.3m=4.723m which is obtained from Table 8.5. The equivalent effective height of dynamic force is h=3.74m calculated from Eq.8.26. The calculation results

for the first two modes and the combination using the SRSS method are shown in Table 8.6.

Table 8.6 Summaries of Dynamic Response - Tall Tank

Method	Model 4	Proposed Model			ACI 350.3
		1st Mode	2nd mode	SRSS	
$\widetilde{m}_W$ (10^3kg)	-	8.487	8.487	-	-
% of $\widetilde{M}_W$	-	25	25	-	-
m_W (10^3kg)	-	13.24	7.463	-	33.95
% of M_W	-	39	22	-	100
h_w (m)	-	9.225	2.583	-	6.15
h_w / H_w	-	0.75	0.21	-	0.5
$\widetilde{m}_L$ (10^3kg)	-	4.32	10.02	-	-
% of $\widetilde{M}_L$	-	3.9	9.1	-	-
m_L (10^3kg)	59.8	13.46	23.16	-	65.76
% of M_L	-	12.3	21.1	-	59.9
h_i (m)	-	5.744	4.726	-	4.2
h_i / H_L	-	0.513	0.422	-	0.375
h (m)	-	8.051	3.744	-	4.864
h/ H_w	-	0.655	0.304	-	0.395
$\widetilde{k}$ (10^3kN/m)	-	4.823	192.9	-	78.0
T (sec)	0.344	0.324	0.062	-	0.225
A_a(m/sec²)	-	0.833g	0.651g	-	0.833g
d_{max} (mm)	45.0	45.2	1.01	45.2	-
V_B (kN)	437.4	454.8	323.6	558.2	814.5
M_B (kNm)	3465.4	3661	1211	3856	3962
P_i (kN)	-	229.3	244.7	335.3	537.2
M_i (kNm)	-	1317.1	1156	1752.5	2256

8.4.2 Shallow Tank

1. The total inertial mass of concrete tank wall is M_w= 2300 kg/m³ x 0.6m x 6m x 1.0m=8.28x10³ kg. For the first mode shape, the generalized mass $\widetilde{m}_w$=2.07x10³ kg is 25% of M_w and the effective mass is m_w = 3.23x10³ kg is 39% M_w.

2. The total mass of liquid considered in the dynamic analysis is M_L= 1000 kg/m³ x 15m x 5.5m x 1.0m=82.5x10³ kg. For L_x/H_W = 2.5 and H_L/H_W = 0.917, $\widetilde{M}_{L-rigid}/M_L$ = $M_{L-rigid}/M_L$=0.2 obtained from Table 8.1 and $\widetilde{f}_{mass}$=0.07 and f_{mass}=0.22 obtained from

Tables 8.4 and 8.5. Therefore, the generalized and effective added mass of liquid due to the impulsive hydrodynamic pressure $\tilde{m}_L = 0.2 \times 0.07 \times M_L = 1.137 \times 10^3$ kg and $m_L = 0.2 \times 0.22 \times M_L = 3.65 \times 10^3$ kg

3. The generalized stiffness per meter is

$$\tilde{k} = \frac{E_c}{4} \cdot (\frac{t_W}{H_W})^3 = \frac{2.664 \times 10^4 MPa}{4}(\frac{0.5m}{6m})^3 = 6610 kN/m/m.$$

4. The combined natural frequency of vibration of the containment structure and the impulsive component of the stored liquid for rectangular tanks is

$$\omega_1 = \sqrt{\frac{\tilde{k}}{\tilde{m}}} = \sqrt{\frac{6610 kN/m}{2.07 \times 10^3 kg + 1.137 \times 10^3 kg}} = 45.4 Hz$$

   The corresponding natural period of vibration, T_1 is 0.138sec

5. From the earthquake response spectrum, the maximum response accelerations $A_a = 0.833g$ for $T_i = 0.138$sec

6. Calculate $\hat{q} = \hat{p}/\tilde{m} = \frac{m_W + m_L}{\tilde{m}_W + \tilde{m}_L} = 2.145$

7. Calculate the maximum displacement $d_{max} = (\hat{q}/\omega_i^2) \times A_a = 8.5$mm

8. Calculate the maximum base shear $V_{max} = \hat{q} \times (m_w + m_L) \times A_a = 120.5$kN

9. The effective height of tank wall is $h_w = 0.75 \times 6m = 4.5m$. The effective height of the effective added mass of liquid due to impulsive hydrodynamic pressure is $h_i = 0.456 \times 6.0m = 2.74m$ which is obtained from Table 8.6. The effective height of dynamic force is h=3.88m calculated from Eq.8.26.

10. Calculate the base moment M= V_{max}xh=120.5kNx3.88m=467.0kNm.

11. The calculation results for the shallow tank in terms of the first two modes and the combination using the SRSS method are shown in Table 8.7.

The calculations using ACI 350.3 Code and Model 4 proposed in Chapter 3 are also presented in this study for comparison. The consistent mass for both tank wall and added mass of liquid due to impulsive hydrodynamic pressure are considered in Model 4. The calculation results using Model 4 are summarized in Tables 8.6 and 8.7 for the tall and the shallow tank, respectively. A comparison of the results obtained using Model 4 and

the proposed generalized SDOF system show good agreement. However, the base shears obtained using ACI 350.3 Code are about 46% and 54% higher than those obtained using the proposed generalized SDOF system for the tall and the shallow tanks, respectively. The differences of base moment between ACI 350.3 Code and the proposed Generalized SDOF system are about 2.7% and 3.3% for the tall and the shallow tanks, respectively. It is concluded that the current design standards and codes are overly conservative in base shear. Since the effective height calculated based on ACI 350.3 is lower than that of proposed method, the difference in base moment is not significant.

Table 8.7 Summaries of Dynamic Response – Shallow Tank

Method	Model 4	Proposed Model			ACI 350.3
		1st Mode	2nd mode	SRSS	
$\widetilde{m}_W$ (10^3kg)	-	2.07	2.07	-	-
% of $\widetilde{M}_W$	-	25	25	-	-
m_W (10^3kg)	-	3.229	1.822	-	8.28
% of M_W	-	39	22	-	100
h_w (m)	-	4.5	1.26	-	3
h_w / H_w	-	0.75	0.21	-	0.5
$\widetilde{m}_L$ (10^3kg)	-	1.137	2.667	-	-
% of $\widetilde{M}_L$	-	1.4	0.32	-	-
m_L (10^3kg)	16.3	3.648	6.266	-	17.5
% of M_L	-	4.4	7.6	-	21.2
h_i (m)		2.739	2.275	-	2.063
h_i / H_L	-	0.498	0.414	-	0.375
h (m)		3.876	1.831	-	2.364
h/ H_w		0.646	0.305	-	0.394
$\widetilde{k}$ (10^3kN/m)		6.61	259.6	-	108.1
T (sec)	0.149	0.138	0.027	-	0.097
A_a (m/sec^2)	-	0.833g	0.469g	-	0.833g
d_{max} (mm)	8.7	8.5	0.143	8.5	-
V_B (kN)	116.0	120.5	63.5	136.2	210.3
M_B (kNm)	432.9	467.0	116.3	481.3	497.1
P_i (kN)	-	63.9	49.2	80.6	142.7
M_i (kNm)	-	175.0	111.9	207.7	294.2

8.5. Conclusions

In this chapter, a structural analysis model using the generalized SDOF system is proposed for seismic design of LCS. The theory and procedure for dynamic analysis of LCS are summarized. The proposed model can consider the consistent mass and the effect of flexibility of tank wall in design. The conceptual procedure for this methodology is similar to that of Housner's model adopted in the current design codes and standards. However, the generalized and effective added mass of liquid due to impulsive hydrodynamic pressure and the corresponding effective heights are introduced in the proposed model.

The design charts and tables for the added mass of liquid due to impulsive hydrodynamic pressure and the corresponding effective height are presented and compared with those adopted in the current design codes and standards. Two sets of calculations for a tall and a shallow tank are presented and compared with the results obtained using the current practice and Model 4 proposed in Chapter 3. The comparison shows that the results obtained from Model 4 and the generalized SDOF system are in good agreement. However, the results obtained using the current practice are overly conservative. It is recommended to use the generalized SDOF system for seismic design of concrete rectangular LCS. The proposed model can provide fairly accurate results for the structural design while still maintaining the simplicity.

CHAPTER 9 SUMMARY, CONCLUSIONS AND RECOMMENDATIONS

9.1 Summary

Dynamic response of concrete rectangular liquid storage tanks subjected to earthquakes is investigated in this study. Different analysis techniques and models are applied for dynamic analysis. The main purpose of this research is to develop a simplified method for dynamic analysis of concrete rectangular liquid containing structures (LCS).

An extensive literature review on dynamic analysis of liquid storage tanks is carried out. Damage to liquid storage tanks due to past major earthquakes and associated failure modes are discussed. The lessons learned from these earthquakes have had a major impact on the development of design codes for liquids storage tanks. The current design codes and standards for seismic design of liquid storage tanks are reviewed and the major differences are discussed.

Only the impulsive hydrodynamic pressure is considered in this research. The impulsive hydrodynamic pressure is calculated based on two different analytical methods, namely the laminar fluid method and the velocity potential method. The lamina fluid theory is used in Housner's model (Housner, 1957 and 1963) which is adopted in the current design codes and standards. In order to consider the effect of flexibility of tank wall, the velocity potential method is introduced to calculate the impulsive hydrodynamic pressure. The velocity potential method is used in the dynamic analysis based on both the sequential coupling analysis procedure and the generalized SDOF system. It is worth noting that one objective of this investigation is to study the effect flexibility of tank wall on dynamic response of rectangular liquid storage tanks which is ignored in the current design practice. Since the flexibility of tank wall does not affect the convective

component, the effect of convective hydrodynamic pressure is ignored in this investigation. However, the effect of convective pressure should be considered in design.

The analytical models that have been developed for dynamic analysis of LCS are reviewed in this thesis. The analytical - finite element models are used for dynamic analysis of liquid containing structures. The tank wall is modeled using the finite element method, while the analytical method is used to calculate the hydrodynamic pressure in liquid domain. The direct and sequential coupling analysis procedures are used for coupling analysis of fluid structure interaction.

In the direct coupling analysis procedure, the hydrodynamic pressure is normally treated as added mass. The added mass of liquid is treated the same way as that of inertial mass of tank wall in dynamic analysis. Therefore, the response of liquid storage tanks can be directly solved through the equation of motion including the added mass of liquid.

The sequential coupling analysis procedure is a coupling technique in which the two fields of fluid and structure are coupled by applying results from the first analysis as loads or boundary conditions for the second analysis. As compared to the direct coupling analysis procedure using the added mass, the effect of flexibility of tank wall in determining hydrodynamic pressure can be considered using time history analysis.

The general purpose finite element analysis software ANSYS® is used to verify the results of analyses obtained using the analytical – finite element models and the generalized SDOF system. In ANSYS®, the dynamic response of concrete liquid storage tanks can be defined as a multi-physics problem including the structural transient analysis of tank walls and fluid dynamic analysis of liquid inside tank. ANSYS® CFX analysis system based on the fluid flow theory is used to simulate the dynamic response of liquid

inside tank subjected to earthquake ground motions. The coupling analysis is executed through a sequence of multi-field time steps, each of which consists of one or more "stagger" (or coupling) iterations. The results obtained using ANSYS$^{®}$ are consistent with those obtained using the analytical - finite element models and the generalize SDOF system.

A simplified method using the generalized single degree of freedom (SDOF) system is proposed for seismic analysis of concrete rectangular liquid storage tanks. In the proposed method, the consistent mass approach and the effect of flexibility of tank wall on hydrodynamic pressure are considered. Compared with the results obtained using the analytical - finite element models and full finite element model using ANSYS$^{®}$, the results obtained using the generalized SDOF system is fairly accurate which can be used in the structural design of liquid containing structures.

A series of parametric studies on seismic analysis of concrete rectangular LCS using the generalized SDOF system are carried out. Five prescribed vibration shape functions representing the first mode shape of fluid structure interaction system are used to study the effect of flexibility of tank wall and the boundary conditions. The effect of flexibility of tank wall, the amplitude of hydrodynamic pressure, the added mass of liquid due to hydrodynamic pressure, the effective heights for liquid containing system and the effect of higher modes on dynamic response of LCS are investigated. The effect of variable tank sizes and liquid depth are also studied.

A design procedure based on the structural model using the generalized SDOF system is then proposed. The proposed structural model can overcome the deficiencies of analysis models in which the rigid boundary condition and the lumped mass approach are used. The design charts and tables for the added mass of liquid due to impulsive hydrodynamic

pressure and the corresponding effective height are presented and compared with those adopted in the current design codes and standards. The contribution of higher modes to dynamic response of LCS is also included in the proposed model. The SRSS method is used for the combination of the first two modes.

9.2 Conclusions

In this study, dynamic response of concrete rectangular liquid storage tanks is investigated. Based on the results of investigation, the following conclusions can be made:

1. The impulsive hydrodynamic pressure increases significantly due to the effect of flexibility of tank wall. Therefore, the effect of flexibility of tank wall should be considered in dynamic analysis of liquid storage tanks.

2. The effect of flexibility of tank wall can be considered in dynamic time history analysis using the sequential coupling analysis procedure. If the time interval specified in the dynamic analysis is small enough, the analysis results can appropriately reflect the actual dynamic behavior of liquid storage tanks.

3. The generalized SDOF system proposed in this study can consider the consistent mass and the effect of flexibility of tank wall on hydrodynamic pressure. The advantage of the proposed method over the finite element method is that it provides fairly accurate results while simplicity in analysis is maintained.

4. The use of an appropriate shape function is critical to determine the response of liquid storage tanks using the generalized SDOF system. Basically, for rectangular tanks with any configuration, the generalized SDOF system can be applied provided that the proper mode shape function is used in the analysis.

5. The ratio of the added mass of liquid for the n-th mode to the total mass of liquid in the container does not reflect the added mass of liquid due to this mode in participation of dynamic response of LCS. However, the participation of added mass

of liquid due to the n-th mode can be more directly reflected using the added mass of liquid based on the rigid wall condition.

6. With the increase in the flexibility of tank wall, there is increase in the participation of the added mass of the liquid due to impulsive hydrodynamic pressure in dynamic analysis of LCS.

7. When $L_x/H_L>1$, the ratio of the added mass of liquid due to impulsive hydrodynamic pressure to that in the rigid wall condition in participation of dynamic analysis is constant. A similar trend is observed in the amplification factor due to mode shape A_{flex}.

8. The effective heights considering the flexibility of tank wall are higher than those of the rigid wall condition.

9. For the empty tank condition, the use of only the first mode of response is appropriate. However, the second mode should be considered in the full tank condition, especially for tall tanks.

10. Instead of a single parameter which is commonly used for dynamic analysis of rectangle LCS, two parameters, i.e. the ratio of length of tank to the height of tank wall L_x/H_w and the ratio of height of liquid to the height of wall H_L/H_w, should be used to consider the size effect of tanks and the variable depth of liquid inside the tank, respectively. The design tables and charts based on these two parameters are presented in this study and can be used in the seismic design of LCS.

11. The natural frequencies of LCS are within a band of natural frequencies between the full level of liquid H_L and empty tank. As a result, it is recommended to use the frequency which may cause the maximum dynamic response of LCS.

12. When the length of tank is relatively large, the increase in the length of tank has no significant effect on dynamic response of LCS.

13. By keeping other parameters constant, the natural frequencies reduce with the increase in the length of tank.

14. With the increase in flexibility of tank wall, the overall effective height of LCS increases and the fundamental natural frequency reduces.

15. The results of analyses obtained using the analytical – finite element models, full finite element model based on ANSYS$^{®}$ and the generalized SDOF system are consistent.

9.3 Recommendations for Further Research

Based on this investigation, some recommendations for further research on dynamic response of concrete rectangular liquid storage tanks are made as follows:

1. The simplified method proposed in this study can be further developed for different wall boundary conditions.

2. As an extended application of the two-dimensional model presented in this study, the use of three-dimensional model can be considered for future research. As a result, the effect of sidewalls on dynamic response of liquid containing structures can be considered in the generalized SDOF system.

3. More case studies using sophisticated analysis methods such as the finite element method or the boundary element method can be carried out to verify the effects of tank size and liquid depth on dynamic response of liquid storage tanks.

4. More sophisticated computational fluid dynamic (CFD) analysis techniques such as nonlinear analysis can be carried out to determine dynamic response of liquid containing structures subjected to earthquakes.

5. The effect of damping on dynamic response of liquid storage tanks can be studied. In this study, only a constant value for damping was assumed.

REFERENCES

American Concrete Institute, ACI 350.3, 2006. Seismic design of Liquid Containing Concrete structures, Farmington Hills, MI.

American Concrete Institute, ACI 371, 1998. Design and Construction of Concrete Pedestal Water Towers, Farmington Hills, MI.

American Petroleum Institute, API 650, 1998. Welded Storage Tanks for Oil Storage, American Petroleum Institute Standard, Washington D.C.

American Society of Civil Engineers (ASCE), 2005. Minimum Design Loads for Buildings and Other Structures, ASCE 7, ASCE Standard, SEI/ASCE 7-02, Reston, VA.

American Water Works Association (AWWA), 2005. Welded Steel Tanks for Water Storage, AWWA D-100, CO.

American Water Works Association (AWWA), 1995. Wire- and Strand-Wounded Circular, Prestressed Concrete Water Tanks, AWWA 110, Denver, CO.

American Water Works Association (AWWA), 1995. Circular Prestressed Concrete Water tanks with Circumferential Tendons, AWWA 115, Denver, CO.

ANSYS Inc. (2009) ANSYS Help Manual. Canonsburg, PA 15317.

American Society of Civil Engineers (ASCE), 1998. ASCE 4-98 Seismic Analysis of Safety-Related Nuclear Structures and Commentary, Reston, Virginia.

ASCE Committee on Seismic Analysis of the Committee on Nuclear Structures and Materials of the Structural Division, American Society of Civil Engineers. 1984. Fluid/Structure Interaction During Seismic Excitation ISBN 0-87262-392-0.

American Society of Civil Engineers (ASCE), 1980. ASCE Manuals and Reports on Engineering Practice No.58 – Structural Analysis and Design of Nuclear Plant Facilities, New York, New York.

Ahari, M.N., Eshghi, S. and Ashtiany, M.G. 2009. The tapered beam model for bottom plate uplift analysis of unanchored cylindrical steel storage tanks. Journal of Engineering Structures, 31, 623-632.

Almazan, J.L., Cerda, F.A., Llera, J.C.D.L. and Lopez-García, D. 2007. Linear isolation of stainless steel legged thin-walled tanks. Journal of Engineering Structures, 29, 1596–1611.

Amano, K., Iwano, R. and Sibata, Y. 1993. Three-dimensional analysis method for sloshing behavior and its application to FBRs. Journal of Nuclear Engineering and Design, 140, 297-308.

Balendra, T., and Nash, W. A. 1978. Earthquake Analysis of Cylindrical Liquid Storage Tank with a Dome by the Finite Element Method. Engineering Research Institute, Department of Civil Engineering, University of Massachusetts, Amherst.

Balendra, T., Ang, K. K., Paramasivam, P. and Lee, S. L. 1982. Seismic Design of Flexible Cylindrical liquid Storage Tanks. Earthquake Engineering and Structural Dynamics, 10, 477-496.

Bathe, K. J., Wilson, E. L. and Peterson, F. E. 1974. SAP IV – A Structural Analysis Program For Static and Dynamic Response of Linear System, College of Engineering, University of California, Berkeley, EERC 73-11.

Bathe, K. J. 1996. Finite Element Procedures. Englewood Cliffs, N. J., Prentice Hall, ISBN 0133014584.

Berahman, F. and Behnamfar, F. 2007. Seismic Fragility Curves for Un-Anchored On-Grade Steel Storage Tanks: Bayesian Approach. Journal of Earthquake Engineering, 11, 166–192.

Chang, Y.W., Ma, D.C., Gvildys, J. and Liu, W.K. 1988. Seismic analysis of LMR reactor tanks. Journal of Nuclear Engineering and Design, 106, 19-33.

Chatterjee, P. and Basu, B. 2001. Non-stationary seismic response of tanks with soil interaction by wavelets. Journal of Earthquake Engineering and Structural Dynamics, 30, 1419–1437.

Chatterjee, P. and Basu, B. 2004. Wavelet-based non-stationary seismic rocking response of flexibly supported tanks. Journal of Earthquake Engineering and Structural

Dynamics, 33, 157-181.

Chen, J.Z. 2003. Dynamic analysis of concrete rectangular liquid storage tanks. M.A.Sc. thesis, Ryerson University, Toronto, Ontario, Canada.

Chen, J.Z. and Kianoush, M.R. 2004. Response of concrete rectangular liquid storage tanks in different seismic zones. Proceedings of the 13th World Conference on Earthquake Engineering, Vancouver, B.C.

Chen, J.Z. and Kianoush M.R. 2005. Seismic response of concrete rectangular tanks for liquid containing structures. Canadian Journal of Civil Engineering, 32, 739–752.

Chen, J.Z. and Kianoush, M.R. 2009. Generalized SDOF system for seismic analysis of concrete rectangular liquid storage tanks. Journal of Engineering Structures, 31, 2426-2635.

Chen, J.Z. and Kianoush, M.R. 2010. Generalized SDOF system for dynamic analysis of concrete rectangular liquid storage tanks: effect of tank parameters on response. Canadian Journal of Civil Engineering, 37, 262-272.

Chen, W., Haroun, M.A. and Liu, F. 1996. Large amplitude liquid sloshing in seismically excited tanks. Journal of Earthquake Engineering and Structural Dynamics, 25, 653-669.

Chen, Y.H., Hwang, W.S. and Ko, C.H. 2007. Sloshing behaviours of rectangular and cylindrical liquid tanks subjected to harmonic and seismic excitations. Journal of Earthquake Engineering and Structural Dynamics, 36, 1701–1717.

Chopra, N. K., 2001. Dynamic of Structures –Theory and Applications to Earthquake Engineering, Second Edition, Prentice Hall.

Choun, Y.S. and Yun, C.B. 1996. Sloshing characteristics in rectangular tanks with a submerged block. Journal of Computers and Structures, 61(3), 401-413.

Choun, Y.S. and Yun, C.B. 1999. Sloshing analysis of rectangular tanks with submerged structure by using small-amplitude water wave theory. Journal of Earthquake Engineering and Structural Dynamics, 28, 763-783.

Chwang, A. T. and Housner, G. W. 1978. Hydrodynamic Pressures on Sloping Dams During Earthquakes, Part 1. Momentum Method. Journal of Fluid Mechanics, 87(2), 335 – 341.

Clough, D. P. 1977. Experimental evaluation of seismic design methods for broad cylindrical tanks. University of California, Berkeley, EERC Report UCB/EERC-77/10, May.

Clough, R. W. and Niwa, A. 1979. Static tilt tests of a tall cylindrical liquid storage tank. Earthquake Engineering Research Center, University of California, Berkeley, Report No. UCB/EERC, 79-06, Feb.

Currie, I. G. 2002. Fundamental Mechanics of Fluid, 3rd edition. CRC Press, New York, N.Y.

Dogangun, A., Durmus, A. and Ayvaz, Y. 1996. Static and dynamic analysis of rectangular tanks using the Lagrangian fluid finite element. Journal of Computers and Structures, 59(3), 547-552.

Dutta, S.C., Dutta, S. and Roy, R. 2009. Dynamic behavior of R/C elevated tanks with soil-structure interaction. Journal of Engineering Structures, 31, 2617-2629.

Earthquake Engineering Research Center (EERC). 1994. Preliminary Report on the Seismological and Engineering Aspects of the January 17, 1994 Northridge Earthquake. UCB/EERC-94/01.

El-Bkaily, M. and Peek, R. 1998. Plastic Buckling of Unanchored Roofed Tanks under Dynamic Loads. ASCE-Journal of Engineering Mechanics, 124(6), 648-657.

El Damatty, A.A., Korol, R.M. and Mirza, F. A. 1997A. Stability of elevated liquid-filled conical tanks under seismic loading, Part I-theory. Journal of Earthquake Engineering and Structural Dynamics, 26, 1191-1208.

El Damatty, A.A., Korol, R.M. and Mirza, F. A. 1997B. Stability of elevated liquid-filled conical tanks under seismic loading, Part II-application. Journal of Earthquake Engineering and Structural Dynamics, 26, 1209-1229.

Ellsworth, W.L., 1990, Earthquake history, 1769-1989, chap. 6 of Wallace, R.E., ed., The San Andreas Fault System, California: U.S. Geological Survey Professional Paper 1515, p. 152-187.

Epstein, H. I. 1976. Seismic Design of Liquid-Storage Tanks. Journal of the Structural Division, Proceedings of the American Society of Civil Engineers, Vol. 102, No. ST9, September.

European Committee for Standardization (ECS), 1998. Design Provisions for Earthquake Resistance of Structures, Part I – General Rules and Part 4 – Silos, Tanks and Pipelines, Eurocode 8, Brussels, Belgium.

Faltinsen, O. M., Rognebakke, O. F. and Timokha, A.N. 2003. Resonant three-dimensional nonlinear sloshing in a square-base basin. Journal of Fluid Mechanics, 487, 1–42.

Faltinsen, O.M., Rognebakke, O.F. and Timokha, A.N. 2005. Classification of three-dimensional nonlinear sloshing in a square-base tank with finite depth. Journal of Fluids and Structures, 20, 81-103.

Fan, S. C. and Li, S. M. 2008. Boundary Finite-Element Method Coupling Finite-Element Method for Steady-State Analyses of Dam-Reservoir Systems. ASCE-Journal of Engineering Mechanics, 134(2), 133-142.

Flügge, W. 1960. Stress in shells. Springer-Verlag, Berlin.

Ghaemmaghami, A. 2010. Seismic response of concrete rectangular liquid tank using finite element method. Ph.D. thesis, Ryerson University, Toronto, Ontario, Canada

Ghaemian, M. and Ghobarah, A. 1998. Staggered solution schemes for Dam-reservoir interaction. Journal of Fluids and Structures, 12, 933-948.

Gupta, R. K. and Hutchinson, G. L. 1991. Effects of wall flexibility on the dynamic response of liquid storage tanks. Journal of Engineering Structures, 13(7), 253-267.

Gupta, R.K. 1995. Free vibrations of partially filled cylindrical tanks. Journal of Engineering Structures, 17(3), 221-230.

Haroun, M. A. and Housner, G. W. 1981. Seismic Design of Liquid Storage Tanks. Journal of the Technical Councils of ASCE.

Haroun, M. A. and Ellaithy, H. M. 1983. Seismically Induced Fluid Forces on Elevated Tanks. ASCE-Journal of Technical Topics in Civil Engineering, 111(1).

Haroun, M. A. 1983. Vibration Studies and Tests of Liquid Storage Tanks. Earthquake Engineering and Structural Dynamics, 11.

Haroun, M. A. 1984. Stress Analysis of Rectangular Walls Under Seismically Induced Hydrodynamic Loads. Bulletin of the Seismological Society of America, 74(3).

Haroun, M. A. and Ellaithy, H. M. 1985. Model for flexible tanks undergoing rocking. ASCE-Journal of Engineering Mechanics, 111(2), 143-157.

Haroun, M. A. and Tayel, M. A. 1985. Axisymmetrical vibrations of tanks – Analytical. ASCE-Journal of Engineering Mechanics, 111(3), 346-358.

Haroun, M. A. and Tayel, M. A. 1985. Axisymmetrical vibrations of tanks – Numerical. ASCE-Journal of Engineering Mechanics, 111(3), 329-345.

Haroun, M. A. and Tayel, M. A. 1985. Response of Tanks to Vertical Seismic Excitations. Earthquake Engineering and Structural Dynamic, 13, 583-5895.

Haroun, M. A. and Abou-Izzeddine, W. 1992A. Parametric Study of Seismic Soil-Tank Interaction. I: Horizontal Excitation. ASCE-Journal of Structural Engineering, 118(3), 783-797.

Haroun, M. A. and Abou-Izzeddine, W. 1992B. Parametric Study of Seismic Soil-Tank Interaction. II: Vertical Excitation. ASCE-Journal of Structural Engineering, 118(3), 798-812.

Housner, G. W. 1957. Dynamic Pressures on Accelerated Fluid Containers. Bulletin of the Seismological Society of American, Vol.47, No.1, 15 – 37.

Housner, G. W. 1963. The Dynamic Behavior of Water Tanks. Bulletin of the Seismological Society of American, Vol. 53, No. 2.

Housner, G. W. and Haroun, M. A. 1979. Vibration Tests of Full Scale Liquid Storage

Tanks. Earthquake Engineering Research Institute from Proceedings of the Second U.S. National Conference on Earthquake Engineering, Stanford, California, 137 – 145.

Housner, G. W. and Haroun, M. A. 1980. Dynamic Analyses of Liquid Storage Tanks. The Turkish National Committee on Earthquake Engineering from Proceedings of 7th Conference on Earthquake Engineering, Istanbul, Turkey, vol. 8, 431 – 438.

Hernandez-Barrios, H. Heredia-Zavoni, E and Aldama-Rodrıguez, A.A. 2007. Nonlinear sloshing response of cylindrical tanks subjected to earthquake ground motion. Journal of Engineering Structures, 29, 3364-3376.

Ibrahim, R.A. (2005) Liquid Sloshing Dynamics – Theory and Applications. Cambridge University.

Isaacson, M. and Ryu, C. S. 1998A. Earthquake-Induced Sloshing in Vertical Container of Arbitrary Section. ASCE-Journal of Engineering Mechanics, 124(2), 158-166.

Isaacson, M. and Ryu, C.S. 1998B. Directional effects of earthquake-induced sloshing in rectangular tanks. Canadian Journal of Civil Engineering, 25, 376-382.

Isaacson, M. and Premasiri, S. 2001. Hydrodynamic damping due to baffles in a rectangular tank. Canadian Journal of Civil Engineering, 25, 608-616.

Jacobson, L. S. and Ayre, R.S. 1949. Impulsive Hydrodynamics of Fluid Inside a Cylindrical Tank. Bulletin of the Seismological Society of America, Vol.39, pp.189-203.

Kachadoorian, R. 1965. Effects of the Earthquake of March 27, 1964 at Whitterier, Alaska. U.S. Geological Survey Professional Paper 542-B.

Kana, D. D. 1979. Seismic response of flexible cylindrical liquid storage tanks. Journal of Nuclear Engineering and Design, 52, 185-199.

Kana, D. D. 1982. Status and research needs for prediction of seismic response in liquid containers. Journal of Nuclear Engineering and Design, 69, 205-221.

Kennedy, R.P. and Kassawara, R.P. 1990. Seismic evaluation of large flat-bottomed tanks.

Journal of Nuclear Engineering and Design, 123, 205-216.

Kianoush, M. R. and Chen, J. Z., 2006. Effect of Vertical Acceleration on Response of Concrete Rectangular Liquid Storage Tanks, Engineering Structures 28, 704-715.

Kianoush, M.R., Mirzabozorg, H. and Ghaemian, M. 2006. Dynamic analysis of rectangular liquid containers in three-dimensional space. Canadian Journal of Civil Engineering, 33, 501–507.

Kim, J. K., Koh, H. M. and Kwahk, I. J. 1996. Dynamic Response of Rectangular Flexible Fluid Containers. ASCE-Journal of Engineering Mechanics, 122(9), 807-817.

Kim, N.S. and Lee, D.G. 1995. Pseudodynamic test for evaluation of seismic performance of base isolated liquid storage tanks. Journal of Engineering Structures, 17(3), 198-208.

Koh, H.M., Kim, J.K. and Park, J.H. 1998. Fluid-structure interaction analysis of 3-D rectangular tanks by a variation ally coupled BEM-FEM and comparison with test results. Journal of Earthquake Engineering and Structural Dynamics, 27, 109-124.

Kruntcheva, M.R. 2007. Free Vibrations of Cylindrical Storage Tanks:Finite-Element Analysis and Experiments. ASCE-Journal of Engineering Mechanics, 133(6), 728-733.

Lau, D. L., Tang, A. and Pierre, J.R. 1995. Performance of lifelines during the 1994 Northridge earthquake. Canadian Journal of Civil Engineering, 22, 438-451.

Lawson, A.C. 1908. The California Earthquake of April 18, 1906: Report of the State Earthquake Investigation Commission: Carnegie Institution of Washington Publication 87, 2 vols.

Lay, K.S. 1993. Seismic coupled modeling of axisymmetric tanks containing liquid. ASCE-Journal of Engineering Mechanics, 119(9), 1747-1761.

Leon, G. S. and Kausel E.A.M. 1986. Seismic analysis of fluid storage tanks. ASCE Journal of Structural Engineering, 112(1): 1-18.

Lepelletier, T. G. and Raichlen, F. 1988. Nonlinear oscillations in rectangular tanks. ASCE-Journal of Engineering Mechanics, 114(1), 1-23.

Li, J., Chen, H.M., and Chen, J.B. 2007. Studies on seismic performances of the prestressed egg-shaped digester with shaking table test. Journal of Engineering Structures, 29, 552-566.

Liu, W. K. 1981. Finite element procedures for fluid-structure interactions and applications to liquid storage tanks. Journal of Nuclear Engineering and Design, 65, 221-238.

Liu, W. K. and Lam, D. 1983. Nonlinear analysis of liquid-filled tank. ASCE-Journal of Engineering Mechanics, 109(6), 1344-1357.

Liu, W. K. and Uras, R. A. 1989. Transient failure analysis of liquid-filled shells part I: theory. Journal of Nuclear Engineering and Design, 117, 107-140.

Liu, W. K. and Uras, R. A. 1989. Transient failure analysis of liquid-filled shells part II: applications. Journal of Nuclear Engineering and Design, 117, 141-157.

Livaoglu, R. and Dogangun, A. 2006. Simplified seismic analysis procedures for elevated tanks considering fluid–structure–soil interaction. Journal of Fluids and Structures, 22, 421–439.

Luft, R. W. 1984. Vertical accelerations in prestressed concrete tanks. ASCE Journal of Structural Engineering, 110(4): 706-714.

Ma, D.C., Gvildys, J., Chang, Y.W. and Liu, W.K. 1982. Seismic behavior of liquid-filled shells. Journal of Nuclear Engineering and Design, 70, 437-455.

Maleki, A. and Ziyaeifar, M. 2007. Damping enhancement of seismic isolated cylindrical liquid storage tanks using baffles. Journal of Engineering Structures, 29, 3227–3240.

Malhotra, P. K. and Veletsos, A. S. 1994A. Uplifting response of unanchored liquid-storage-tanks. ASCE Journal of Structural Engineering, 120(12): 3525-3547.

Malhotra P. K. and Veletsos, A. S. 1994B. Uplifting analysis of base plates in cylindrical tanks. ASCE Journal of Structural Engineering, 120(12): 3489-3505.

Malhotra, P. K. and Veletsos, A. S. 1994C. Beam model for base-uplifting analysis of cylindrical tanks. ASCE Journal of Structural Engineering, 120(12): 3471-3488.

Malhotra, P. K. 1997. Seismic response of soil-supported Unanchored Liquid-Storage Tanks. ASCE Journal of Structural Engineering, 123(4): 440-450.

Malhotra, P. K. 1997. Method for seismic base isolation of liquid-storage tanks. ASCE Journal of Structural Engineering, 123(1): 113-116.

Malhotra, P. K. 1997. New method for seismic isolation of liquid-storage tanks. Journal of Earthquake Engineering and Structural Dynamics, 26, 839-847.

Malhotra, P. K. 1998. Seismic strengthening of liquid-storage tanks with energy-dissipating anchors. ASCE Journal of Structural Engineering, 124(4): 405-414.

Malhotra, P.K., Wenk, T. and Wieland, M. 2000. Simple Procedure for Seismic Analysis of Liquid-Storage Tanks. Structural Engineering International, 3, 197-201.

Manos, G. C. and Clough, R. W. 1982. Further study of the earthquake response of a broad cylindrical liquid-storage tank model Report No. UCB/EERC-82/07. Earthquake Engineering Research Center, University of California, Berkeley, CA.

Manos, G. C. 1986. Earthquake tank-wall stability of unanchored tanks. ASCE Journal of Structural Engineering, 112(8): 1863-1880.

Mordini, A. and Strauss, A. 2008. An innovative earthquake isolation system using fibre reinforced rubber bearings. Journal of Engineering Structures, 30, 2739–2751.

Munshi, J. A. 2002. Design of Liquid-Containing Concrete Structures for Earthquake Forces, Portland Cement Association.

Murphy, L. M. 1973. San Fernando, California, Earthquake of February 9. National Oceanic and Atmospheric Administration, U.S. Department of Commerce.

Nachtigall, I., Gebbeken, N., Urrutia-Galicia, J.L. 2003. On the analysis of vertical circular cylindrical tanks under earthquake excitation at its base. Journal of Engineering Structures, 25, 201–213.

New Zealand Standards Association. 1986 and 2010. NZS3106: The New Zealand Code of Practice for Concrete Structures for the Storage of Liquids.

Nielsen, R. and Kiremidjian, A. S. 1986. Damage to oil refineries from major earthquakes. ASCE Journal of Structural Engineering, 112(6): 1481-1491.

Niwa, A. 1978. Seismic behavior of tall liquid storage tanks Report No. UCBI EERC-78/04, Feb. Earthquake Engineering Research Center, University of California, Berkeley, CA.

Niwa, A. and Clough, R. W. 1982. Buckling of cylindrical liquid storage tanks under earthquake loading. Earthquake Engineering and structural dynamics, 10, 107-122.

Pal, N. C., Bhattacharyya, S. K. and Sinha, P. K. 1999. Coupled slosh dynamics of liquid-filled, composite cylindrical tanks. ASCE-Journal of Engineering Mechanics, 125(4), 491-495.

Panchal, V.R. and Jangid, R.S. 2008. Variable friction pendulum system for seismic isolation of liquid storage tanks. Journal of Nuclear Engineering and Design, 238, 1304–1315.

Park, J. H., Koh, H. M., and Kim, J. 1990. Liquid-Structure Interaction Analysis by Coupled Boundary Element-Finite Element Method in Time Domain. Proc., 7th International Conference on Boundary Element Technology, BE-TECH/92, Computational Mechanics Publication, Southampton, England, 89-92.

Park, J. H., Koh, H.M. and Kim, J.K. 2000. Seismic isolation of pool-type tanks for the storage of nuclear spent fuel assemblies. Journal of Nuclear Engineering and Design, 199, 143-154.

Paz, M. 1997. Structural Dynamics: Theory and Computation, New York, Chapman & Hall.

Peek, R. 1986. Analysis of unanchored liquid storage tanks under seismic loads. Report No. EERL 86-01, California Institute of Technology, Pasadena, California.

Peek, R., Jennings, P.C. and Babcock, C. D. 1988. Preuplift method to "anchor" liquid

storage tanks. ASCE Journal of Structural Engineering, 114(2): 475-486.

Peek, R. and Jennings, C. 1988. Simplified analysis of unanchored tanks. Journal of Earthquake Engineering and Structural Dynamics, 16, 1073-1085.

Peek, R. and El-Bkaily, M. 1997. Mechancial Analogies for Liquid Storage Tanks and Action of Eccentric Gravity Loads. ASCE-Journal of Engineering Mechanics, 123(6), 561-567.

Prato, C. A. and Godoy L. A. 1989. Bending of multi-bin RC Cylindrical silos. ASCE Journal of Structural Engineering, 115(12): 3194-3200.

Priestley, M. J. N., Hood, J. H. and Davidson, B. J. 1986. Seismic Design of Storage Tanks. Bulletin of the New Zealand National Society for the Earthquake Engineering, 19(4).

Rogowsky, R, A., D. M. and Elwi, A. E. 2000. Tests on reinforced partially prestressed concrete tanks walls. ASCE Journal of Structural Engineering, 126(6): 675-683.

Sameer, U. S. and Jain, S. K. 1994. Lateral-load analysis of frame stagings for elevated water tanks. ASCE Journal of Structural Engineering, 120(5): 1375-1394.

Schiff, A.J. 1998. The Loma Prieta, California, Earthquake of October 17, 1989-Lifelines. U.S. Geological Survey Professional Paper 1552-A.

Sezen, H., Livaoglu.R. and Dogangun, A. 2008. Dynamic analysis and seismic performance evaluation of above-ground liquid-containing tanks. Journal of Engineering Structures, 30, 794-803.

Sezen, H., Elwood, K.J., Whittaker, A.S., Mosalam, K.M., Wallace, J.W. and Stanton, J.F. 2000. Structural Engineering Reconnaissance of the August 17, 1999, Kocaeli (Izmit), Turkey, Earthquake. PEER Report 2000/09.

Shaaban, S. H. and Nash, W. A. 1975. Response of an Empty Cylindrical Ground Supported Liquid Storage Tank to Base excitation. Engineering Research Institute, Department of Civil Engineering, University of Massachusetts, Amherst, August.

Shekari, M.R., Khaji, N. and Ahmadi, M.T. 2009. A coupled BE–FE study for evaluation

of seismically isolated cylindrical liquid storage tanks considering fluid–structure interaction. Journal of Fluids and Structures, 25, 567–585.

Shenton H. W. III. and Hampton, F. P. 1999. Seismic Response of isolated elevated water tanks. ASCE Journal of Structural Engineering, 125(9): 965-976.

Shrimali, M.K. and Jangid, R.S. 2002A. Non-linear seismic response of base-isolated liquid storage tanks to bi-directional excitation. Journal of Nuclear Engineering and Design, 217, 1-20.

Shrimali, M.K. and Jangid R.S. 2002B. Seismic response of liquid storage tanks isolated by sliding bearings. Journal of Engineering Structures, 24, 909-921.

Shibata, H. and Akiyama, H. (1985). "Seismic capacity testing of a thin wall 500 ton cylindrical tank." Bulletin of the Earthquake Resistant Structure Research Center, 18, Institute of Industrial Science, University of Tokyo.

Sweedan, A. M. I. and El Damatty, A. A. 2003. Experimental identification of the vibration modes of liquid-filled conical tanks and validation of a numerical model. Journal of Earthquake Engineering and Structural Dynamics, 30, 1407–1430.

Sweedan A. M. I. and El Damatty, A. A. 2005. Equivalent Models of Pure Conical Tanks under Vertical Ground Excitation. ASCE Journal of Structural Engineering, 131(5): 725-733.

Tang, Y. 1994A. Computing response of tanks with two liquids. ASCE Journal of Structural Engineering, 120(12): 3668-3674.

Tang, Y. 1994B. Rocking response of tanks containing two liquids. Journal of Nuclear Engineering and Design, 152, 103-115.

Tang, Y. 1994C. Free vibration analysis of tank containing two liquids. ASCE-Journal of Engineering Mechanics, 120(3), 618-636.

Tang, Y. 1996. Laterally Excited Flexible Tanks with Nonuniform Density Liquid. ASCE-Journal of Engineering Mechanics, 122(10), 948-956.

Taniguchi, T. 2004. Rocking behavior of unanchored flat-bottom cylindrical shell tanks

under action of horizontal base excitation. Journal of Engineering Structures, 26, 415–426.

Tsang, S.K. and Harding, J.E. 1987. Ring-Stiffened Cylinders under Interactive Loading. ASCE Journal of Structural Engineering, 113(9).

Tung, A. T. Y. and Kiremidjian, A. S. 1991. Seismic Relibality analysis of elevated liquid-storage vessels. ASCE Journal of Structural Engineering, 117(5): 1372-1392.

U.S. Atomic Energy Commission. 1963. Nuclear Reactors and Earthquakes TID-7024.

Veletsos, A. S., 1984. Seismic Response and Design of Liquid Storage Tanks. Guidelines for the Seismic Design of Oil and Gas Pipeline Systems, Tech, Council on Lifeline Earthquake Engineering, ASCE, New York, N.Y.

Veletsos, A. S. and Tang, Y. 1986. Dynamics of vertically excited liquid storage tanks. ASCE Journal of Structural Engineering, 112(6): 1228-1246.

Veletsos, A. S. and Tang, Y. 1987. Rocking response of liquid storage tanks. ASCE-Journal of Engineering Mechanics, 113(11), 1774-1792.

Veletsos, A. S. and Tang, Yu. 1990. Soil-Structure Interaction Effects for Laterally Excited Liquid Storage Tanks. Earthquake Engineering and Structural Dynamics, 19, 473-496.

Veletsos, A. S., Tang, Y. and Tang, H. T. 1992. Dynamic response of flexibly supported liquid-storage tanks. ASCE Journal of Structural Engineering, 118(1): 264-283.

Veletsos, A. S. and Shivakumar, P. 1996. Dynamic Response of Tanks Containing Liquids or Solids. Computer Analysis and Design of Earthquake Resistant Structures, Computational Mechanics Publications Earthquake Engineering Series, Vol. 2.

Virella, J.C., Godoy, L.A. and Suarez L.E. 2003. Influence of the roof on the natural periods of empty steel tanks. Journal of Engineering Structures, 25, 877–887.

Virella, J.C., Godoy, L.A. and Suarez L.E. 2006. Fundamental modes of tank-liquid systems under horizontal motions. Journal of Engineering Structures, 28, 1450–1461.

Virella, J.C., Suarez, L.E. and Godoy, L.A. 2008. A Static Nonlinear Procedure for the Evaluation of the Elastic Buckling of Anchored Steel Tanks Due to Earthquakes. Journal of Earthquake Engineering, 22, 999–1022.

Wang, Y.P., Teng, M.C. and Chung, K.W. 2001. Seismic isolation of rigid cylindrical tanks using friction pendulum bearings. Journal of Earthquake Engineering and Structural Dynamics, 30, 1083–1099.

Warnitchai, P. and Pinkaew, T. 1998. Modelling of liquid sloshing in rectangular tanks with flow-dampening   devices. Journal of Engineering Structures, 20(7), 593-600.

Wei Yi and Natsiavas, S. 1992. Seismic Response of Unanchored Fluid-Filled Tanks Using Finite Elements. Journal of Pressure Vessel Technology, Transaction of ASME, 114, 74-79.

Westergaard, H. M. 1933. Water Pressures on Dams During Earthquakes. Transaction, American Society of Civil Engineers, Vol. 98.

Whittaker, D. and Jury, R.D. 2000. Seismic Design Loads for Storage Tanks. Proceedings 12th World Conference on Earthquake Engineering, Paper Number 2376.

Wozniak, R. S., and Mitchell, W. W. 1978. Basis of Seismic Design Provisions for Welded Steel Oil Storage Tanks. Proceedings American Petroleum Institute, Refining Department.

Yang, J. Y. 1976. Dynamic Behavior of Fluid-Tank System. Ph.D. Thesis, Civil Engineering, Rice University Houston, Texas.

Younan, A. H. and Veletsos, A. S. 1998A. Dynamics of solid-containing tanks. I Rigid tanks. ASCE Journal of Structural Engineering, 124(1): 52-61.

Younan, A. H. and Veletsos, A. S. 1998B. Dynamics of solid-containing tanks. II flexible tanks. ASCE Journal of Structural Engineering, 124(1): 62-70.

Yu, B. Q., Nash, W. A. and Kirchhoff, R. H. 1987 Finite Element-Perturbation Analysis of A Cylindrical Liquid Storage Tank With Dome. Department of Civil Engineering,

University of Massachusetts, Amherst.

Zhang, Z, He, S., and Xu, M. 2007. Seismic analysis of liquid storage container in nuclear reactors. Journal of Nuclear Engineering and Design, 237, 1325–1331

Ziari, A. and Kianoush, M.R. 2009. Investigation of flexural cracking and leakage in RC liquid containing structures. Journal of Engineering Structures,, 31, 1056-1067.